# Analysis of the Interactome and Membrane Insertion of VAPB, a Tail-Anchored Protein at the Inner Nuclear Membrane

**Dissertation**

for the award of the degree

**"Doctor of Philosophy"**

Division of Mathematics and Natural Sciences

of the Georg-August-Universität Göttingen

within the Göttingen Graduate School for Neurosciences, Biophysics and Molecular Biosciences (GGNB),

of the Georg-August University School of Science (GAUSS)

Submitted by

**Christina James**

from Kerala, India

Göttingen, April 2020

**Members of the Thesis Committee and Examination Board:**

| | |
|---|---|
| **Supervisor:** | **Prof. Dr. Ralph Kehlenbach**<br>Department of Molecular Biology<br>University Medical Center Göttingen |
| **Thesis committee:** | **Prof. Dr. Stefan Jakobs**<br>Department of NanoBiophotonics<br>Max-Planck-Institute for Biophysical Chemistry<br>University Medical Center Göttingen |
| **Thesis committee:** | **Dr. Ricarda Richter-Dennerlein**<br>Department of Cellular Biochemistry<br>University Medical Center Göttingen |
| **Examiner:** | **Prof. Dr. Henning Urlaub**<br>Bioanalytical Mass Spectrometry<br>Max-Planck-Institute for Biophysical Chemistry<br>University Medical Center Göttingen |
| **Examiner:** | **Prof. Dr. Michael Thumm**<br>Department of Cellular Biochemistry<br>University Medical Center Göttingen |
| **Examiner:** | **PD Dr. Sven Thoms**<br>Department of Child and Adolescent Health<br>University Medical Center Göttingen |

Date of oral examination: 10th June 2020

## Affidavit

I, Christina James, hereby declare that I have written this PhD thesis independently with no other sources and aids than quoted.
A part of this thesis was submitted in the same version for publication in the Journal of Biological Chemistry.

Göttingen, April 2020 Christina James

## Acknowledgements

This thesis would not have been possible without the guidance and help of several individuals who have contributed their valuable assistance in the preparation and completion of this study. First and foremost, I would like to earnestly thank Prof. Ralph Kehlenbach for giving me the opportunity to work on this project, his support and guidance and giving me possibilities to attend conferences. I can't thank him enough for motivating me during the whole phase of my Ph.D. journey.

I would also like to sincerely thank my thesis committee members Prof. Stefan Jakobs and Dr. Ricarda Richter-Dennerlein for their helpful discussions.

I thank all the current (Birgit Caspar, Floriane Lagadec, Ines Rodriguez Gonzalez, Marius Pörschke, Mohamed Hamed, Ulrike Möller) and former members (Christiane Spillner, Imke Baade, Janine Pfaff, Marina Blenski, Marret Müller) of the lab for providing a warm and conducive atmosphere to work in. I would like to extend my gratitude specially to Christiane Spillner for helping me with the project. Special thanks to Imke for being my travel companion all these years here.

I would like to sincerely thank my collaborators Prof. Martin Goldberg, Prof. Henning Urlaub, Dr. Christof Lenz, Christine Richardson, Thierry Wasselin and Lisa Neuenroth.

I like to extend my thanks to Dr. Imke Baade, Dr. Anisa Banu Abdul Rahim, and Dr. Jens Kretschmer for proofreading parts of the thesis. Thanks to Dr. Erik Arakel, Dr. Francisco Javier Coy Vergara and Dr. Jhon Rivera-Monroy for helpful scientific discussions and reagents.

I thank the whole Department of Molecular Biology for the positive and friendly working environment. I would also like to thank the Göttingen Graduate School for Neurosciences, Biophysics, and Molecular Biosciences (GGNB) and SFB1190 for all the support extended during my Ph.D.

I take this opportunity to thank Dr. Leah Vardy for her quality training and instilling passion in me to grow as a better scientist.

Last but not least, I would like to thank my family for supporting and encouraging me throughout my entire life.

# Contents

## Abstract

Tail-anchored (TA) proteins are a group of integral membrane proteins defined by the presence of a single transmembrane domain (TMD) at the C-terminal domain and are involved in functionally diverse cellular processes. Since the C-terminal TMD of TA proteins emerges from the ribosome tunnel only after termination of translation, insertion of these proteins to target membrane occurs mostly by post-translational pathways. Two model TA proteins used in this study are VAPB and emerin.

VAPB (vesicle-associated membrane protein-associated protein B) is an integral endoplasmic reticulum (ER) protein that is present at several contact sites of the ER. To understand the mechanism of insertion of VAPB into the ER, *in vitro* insertion assays were performed using rough microsomes and semi-permeabilized cells. VAPB was shown to be post-translationally inserted into the ER membrane independently of the TRC40 pathway. Apart from its ER-localization, immunoelectron microscopy and a rapamycin-based dimerization assay showed that VAPB also localizes to the inner nuclear membrane (INM).

The engineered ascorbate peroxidase (APEX2) has been effectively employed in mammalian cells to identify protein-protein interactions. Using a modified APEX2-approach with rapamycin-dependent targeting of the peroxidase to a protein of interest, proteins that are in close proximity to VAPB were identified in the ER and the INM. In combination with stable isotope labeling with amino acids in cell culture (SILAC), followed by co-immunoprecipitation assays, many well-known interaction partners of VAPB at the ER were confirmed and also novel proximity partners at the INM were identified. Hence, rapamycin-APEX2-mediated proximity labeling of VAPB neighboring proteins provide insights into the VAPB interactome at the ER and the INM.

Emerin is one of the best-characterized tail-anchored proteins of the INM but also localizes to the ER and the outer nuclear membrane (ONM). To better understand the dynamics of emerin at the nuclear envelope (NE), FRAP assays were performed at the NE on intact and permeabilized cells. The addition of cytosol to the permeabilized cells increased the diffusion of emerin to the NE and addition of a Ran deficient mutant, RanQ69L, a lectin wheat germ agglutinin (WGA) and a dominant-negative fragment of Importinβ (Impβ (45-462)) impaired the diffusion of emerin from the ER to the NE. These data suggest that diffusion of emerin to the NE is dependent on soluble components and thus may underscore a role of soluble factors in diffusion and retention mechanism for targeting of INM proteins.

# Chapter 1:
# Introduction

# Chapter 1 : Introduction

## 1.1. The nuclear envelope

The eukaryotic nucleus is enclosed by the nuclear envelope (NE) made up of two lipid bilayers: an inner nuclear membrane (INM) and an outer nuclear membrane(ONM). These two lipid bilayers are separated by a 30-50 nm lumen or perinuclear space. Nuclear pore complexes (NPCs) reside at regions of the NE, where the INM and ONM merge (Figure 1; Lusk et al., 2007). The ONM is contiguous with the rough endoplasmic reticulum (ER) with ribosomes scattered on its surface. In metazoans, the INM is lined with an underlying filamentous protein meshwork called nuclear lamina that consists of nuclear intermediate filament proteins, lamins (Dwyer and Blobel, 1976; Gruenbaum et al., 2005; Stewart et al., 2007) and several INM proteins that interact with the lamins (Schirmer et al., 2003). Lamins regulate genome organization and chromatin structure and mediate structural linkages between the nucleus and the cytoplasm (Dittmer and Misteli, 2011; Simon and Wilson, 2011; Stewart et al., 2007). The ONM contains unique membrane proteins and shares many of its functions with the ER (Stewart et al., 2007). Thus, the NE consists of discrete interconnected regions; the INM, the ONM continuous with the ER and NPCs with the perinuclear space being an extension of the ER lumen.

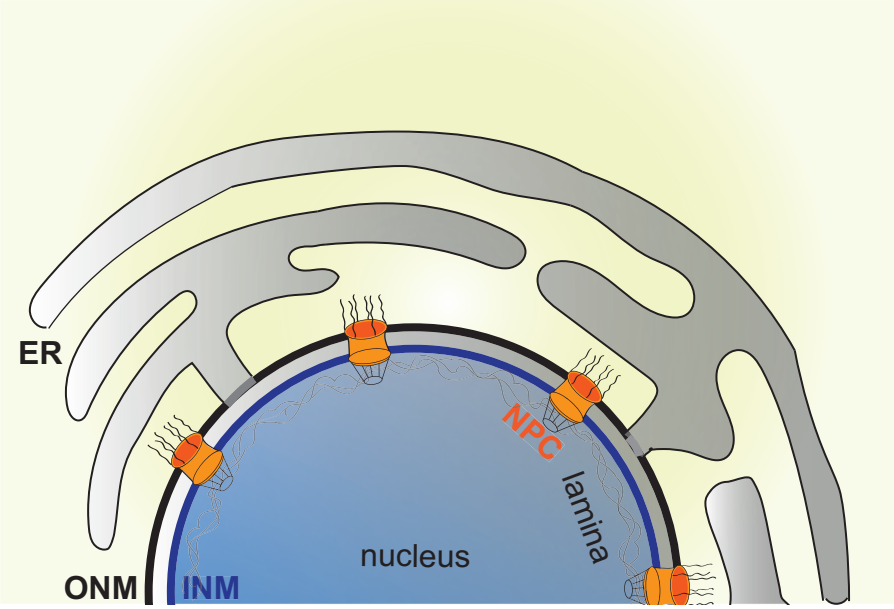


**Figure 1. Overview of the nuclear envelope.**
The nuclear envelope consists of inner nuclear membrane (INM) and outer nuclear membrane (ONM). The nuclear pore complexes (NPCs) are embedded into the INM and ONM. The ONM is continuous with the endoplasmic reticulum (ER). The nuclear lamina underlies the INM consisting of lamins and lamina associated proteins.

## 1.2. The gatekeepers of the nucleus: the nuclear pore complex

Nuclear pore complexes (NPCs) are large multiprotein complexes consisting of multiple copies of ~30 distinct protein subunits called nucleoporins (Nups) (Figure 2; Cronshaw et al., 2002). NPCs function as gatekeepers at the NE and restrict entry and exit of macromolecules into and out of the nucleus (Aitchison and Rout, 2012; Grossman et al., 2012). In addition to their best-characterized function to mediate passive exchange of small molecules and active transport of macromolecules, NPCs also regulate genome organization and expression, transcriptional regulation of many genes and the organization of complexes that control DNA damage repair and chromatin silencing (Akhtar and Gasser, 2007; Kalverda et al., 2010; Nakano et al., 2010; Towbin et al., 2009).

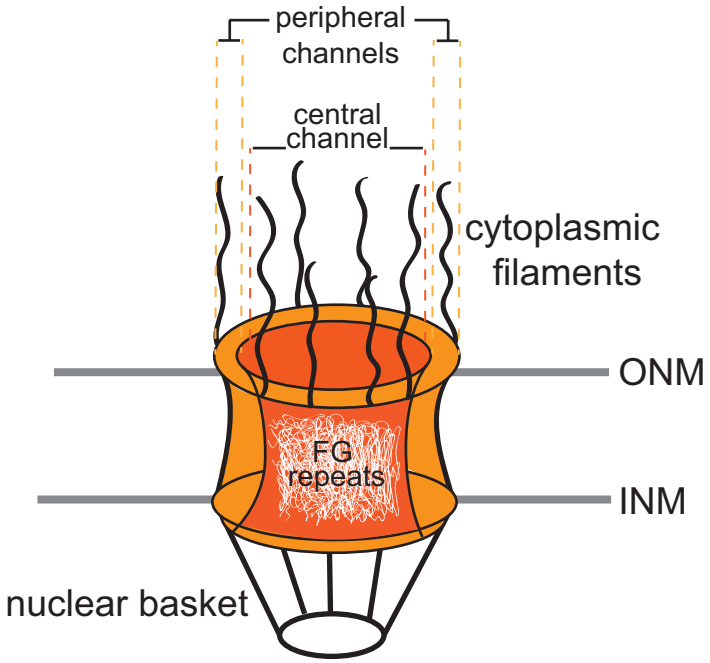


**Figure 2. The nuclear pore complex.**
Schematic of the nuclear pore complex (NPC) embedded between the inner and outer nuclear membrane. The NPC scaffold consists of a central channel lined by phenylalanine-glycine (FG) repeats. The nuclear basket faces the nucleoplasm and cytoplasmic filaments emanate to the cytoplasmic side. Peripheral channels are also present and allow for passive diffusion of small molecules.

The NPC shows an eight-fold symmetric, cylindrical assembly and is anchored within the NE by a core scaffold consisting of coaxial inner and outer ring structures. The core scaffold surrounds a central channel containing nucleoporins characterized by phenylalanine-glycine (FG) repeats that contribute to its selectivity barrier function (Dickmanns et al., 2015). On the nucleoplasmic side, the nuclear basket is present consisting of eight extended filaments connected to a distal ring (Allen et al., 2000). The cytoplasmic side is also decorated with eight cytoplasmic filaments (Kim et al., 2018; Knockenhauer and Schwartz, 2016).

## 1.3. Nucleocytoplasmic transport through the NPC

A bidirectional exchange exists between the nucleus and the cytoplasm through highly regulated nucleocytoplasmic transport. The exchange of molecules through the NPC occurs either by passive transport or by active transport. Typically, macromolecules smaller than 5 nm in diameter or 40 kDa in size diffuse through the NPC (Hülsmann et al., 2012; Mohr et al., 2009), whereas larger molecules like proteins, RNAs and RNPs are transported actively (Kutay et al., 1998).

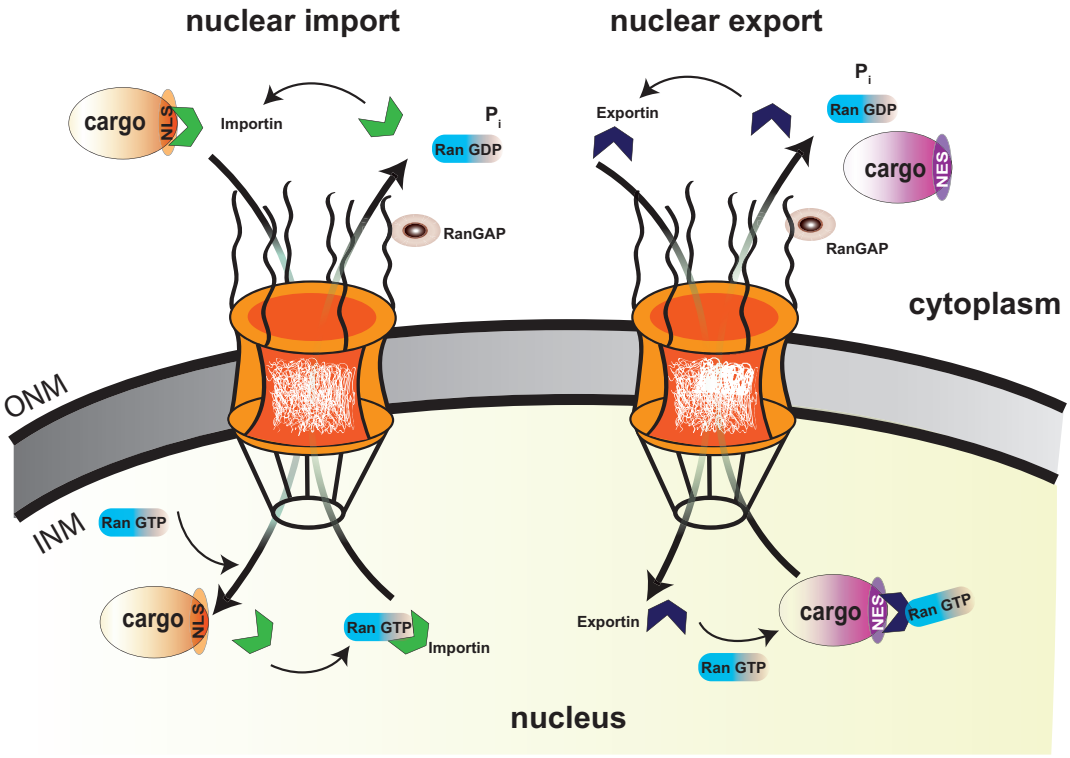


**Figure 3. Nucleocytoplasmic transport through the NPC.**
During import, importins bind to cargo in the cytoplasm and are transported to the nucleus, where the cargo is released upon RanGTP binding. The importin-RanGTP complex is recycled back to the cytoplasm for the next round of import. Nuclear export requires the binding of exportins and RanGTP to the cargoes to form a trimeric complex in the nucleus that is exported via the NPC. In the cytoplasm, this complex is disassembled by RanGAP mediated hydrolysis of GTP-bound Ran. The free exportin re-enters back into the nucleus for the next round of export.

Active transport of soluble cargoes requires very specific interactions with the NPC. It is typically mediated by soluble nuclear transport receptors (NTRs), which bind the cargo molecules and the RanGTPase system that determines the directionality of transport (Figure 3). NTRs are classified into importins and exportins, based on the direction in which they carry their cargo (Görlich and Kutay, 1999), although some of them mediate both export and import (Aksu et al., 2018; Gontan et al., 2009; Mingot et al., 2001; Yoshida and Blobel, 2001). They bind cargoes on one side, translocate through the NPC barrier and release cargoes on the other side. Next, they return to the original compartment to mediate another round of transport (Görlich and Kutay, 1999; Schmidt and Görlich, 2016; Weis,

2003). Cargo binding and release of importins and exportins is regulated by the two different nucleotide states of Ran, which cycles between a GTP- and GDP-bound form (Izaurralde et al., 1997). The Ran guanine nucleotide exchange factor (RanGEF) RCC1 catalyzes the nucleotide exchange in the nucleus (Bischoff and Ponstingl, 1991) and RanGTP hydrolysis is stimulated by the RanGTPase activating protein RanGAP in the cytoplasm (Bischoff et al., 1994). The compartmentalized distribution of RCC1 and RanGAP results in a RanGTP gradient across the NE with a high RanGTP concentration in the nucleus and low levels in the cytoplasm (Görlich and Kutay, 1999; Weis, 2003).

Cargoes destined for import contain a nuclear localization sequence (NLS), which is recognized by importins. This facilitates movement through the central NPC channel and the cargo-importin complex is released in the nucleus upon binding to RanGTP (Izaurralde et al., 1997; Rexach and Blobel, 1995). The importin-RanGTP complex then returns to the cytoplasm, and a Ran binding protein (RanBP) dissociates RanGTP from importin to allow binding of another import cargo and and RanGAP stimulates hydrolysis of RanGTP (Görlich et al., 1996; Hieda et al., 1999; Izaurralde et al., 1997). Exportins, on the other hand, bind to cargoes containing a nuclear export sequence (NES) and RanGTP in the nucleus to form a trimeric export complex. The complex is then exported to the cytoplasm through the NPC, where it is disassembled upon hydrolysis of RanGTP to RanGDP (Arts et al., 1998; Kutay et al., 1997b; Kutay et al., 1998). The free exportin re-enters the nucleus to allow the export of the next cargo. RanGAP together with RanBP1 and Nup358 (RanBP2) stimulates conversion of RanGTP to RanGDP (Bischoff and Görlich, 1997; Kehlenbach et al., 1999). RanGDP is imported into the nucleus by nuclear transport factor 2 (NTF2) (Paschal and Gerace, 1995; Ribbeck et al., 1998), where RCC1 facilitates conversion of RanGDP to RanGTP (Coutavas et al., 1993).

## 1.4. Integral membrane proteins

The mechanisms that regulate the nuclear transport of soluble proteins are well studied, however, much less is known about the mechanism by which integral membrane proteins of the INM reach their final destination (Katta et al., 2014; Laba et al., 2014). The targeting process of an INM protein involves its biogenesis, followed by trafficking to the INM, during which the proteins may engage in multiple distinct protein interactions.

### 1.4.1. Biogenesis of integral membrane proteins

Integral membrane proteins have single (bitopic) or multiple (polytopic) transmembrane domains. Transmembrane domains (TMDs) help the protein to anchor to the membrane. They are further classified based on their topology into type I (single pass; C-terminus oriented to the cytoplasm), type II (single-pass; N-terminus oriented to the

cytoplasm), type III (multi-pass with several transmembrane domains) (Chou and Cai, 2005; Ott and Lingappa, 2002) and type IV (single-pass; tail-anchored (TA)). TA proteins are a distinct class of integral membrane proteins with a single TMD at the C-terminus (Kutay et al., 1995) that contains targeting information for membrane insertion and proper delivery to its final destination (Borgese et al., 2007; Hegde and Keenan, 2011).

Newly synthesized membrane proteins are targeted to the membranes by two well-characterized insertion systems, the co-translational pathway and the post-translational pathway.

#### 1.4.1.1. Co-translational membrane insertion

Secretory proteins and integral membrane proteins can be translocated or inserted into membranes co-translationally i.e., during their synthesis (Cross et al., 2009). This mode of transport depends on a signal recognition particle (SRP) system, which consists of a cytosolic SRP and its membrane-bound receptor (SR) (Grudnik et al., 2009; Rapoport, 2007). The signal or a hydrophobic N-terminal sequence of a nascent polypeptide chain emerging from the ribosome is recognized by the SRP (Figure 4 step1; Grudnik et al., 2009). Subsequently, the ribosome nascent-chain complex (RNC)-SRP is recruited to the SRP receptor in the ER membrane (Figure 4 step2).

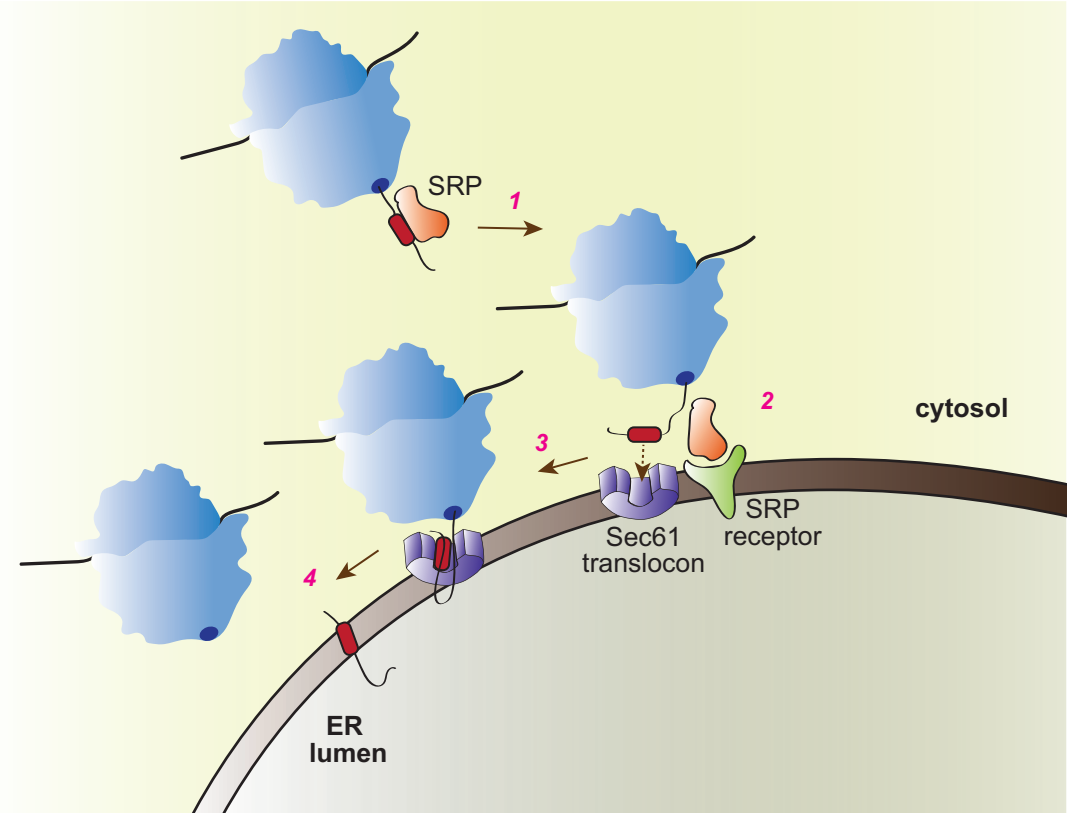


**Figure 4. Co-translational membrane targeting by the SRP system.**
SRP interacts with the signal sequence of the polypeptide chain as soon as it emerges from the ribosome exit tunnel (step 1). The RNC-SRP complex is then targeted to the ER membrane, where it binds to the SRP receptor under GTP hydrolysis (step 2). The RNC is then transferred to the Sec61 translocon (step 3) and subsequently integrated into the ER lipid bilayer (step 4) (scheme adapted from Reid and Nicchitta, 2015).

The SRP receptor consists of two proteins, which are both GTPases: SRα and SRγ (Gilmore et al., 1982a; Gilmore et al., 1982b). As a result of GTP hydrolysis in SRP and SR, the RNC is then transferred to the Sec61 translocon in the membrane (Wild et al., 2004). Translation is resumed and the TMD interacts with the translocon channel (Figure 4 step3; Rapoport, 2007). After termination of translation, the mature membrane protein is laterally integrated into the lipid bilayer of the ER from the Sec61 translocon (Figure 4 step4).

#### 1.4.1.2. Post-translational membrane insertion of TA proteins

Targeting and insertion of membrane proteins by post-translational pathways occur after the complete synthesis of the proteins. The post-translational pathways generally use TMD selective cytosolic chaperons for targeting and an ER-localized receptor for insertion (Mateja and Keenan, 2018). For TA proteins, the TMD remains sequestered inside the ribosome exit tunnel until the translation is complete and hence uses post-translational membrane insertion (Kutay et al., 1993).

Multiple pathways have been identified over the past decade for post-translational TA protein biogenesis at the ER. The guided entry of tail-anchored proteins (GET) pathway described in yeast or the homologous mammalian transmembrane domain recognition complex of 40kDa (TRC40) pathway (Schuldiner et al., 2008; Stefanovic and Hegde, 2007) targets TA proteins with highly hydrophobic TMDs (Table 1). In the TRC40 pathway (Figure 5), BCL2-associated athanogene cochaperone 6 (BAG6) interacts with the ribosome, forms a heterotrimeric complex with transmembrane domain recognition complex 35 (TRC35) and ubiquitin-like 4A (UBL4A) and binds to nascent TA substrates after their release from the ribosome (Mariappan et al., 2010; Mock et al., 2015; Mock et al., 2017). Then, the cytosolic chaperone small glutamine-rich tetratricopeptide repeat-containing protein alpha (SGTA) binds to either BAG6, or UBL4A (Figure 5 step 1; Darby et al., 2014; Leznicki et al., 2013). This pre-targeting complex binds to TRC40 in an ATP-bound conformation and delivers the TA protein to TRC40 (Figure 5 step2; Hegde and Keenan, 2011; Mariappan et al., 2010). The resulting TA-protein-TRC40 complex is targeted to the ER, where the membrane receptors tryptophan-rich basic protein (WRB) (Vilardi et al., 2011) and calcium-modulating cyclophilin ligand (CAML) (Vilardi et al., 2014; Yamamoto and Sakisaka, 2012) act as insertases for inserting TA proteins to the ER membrane (Figure 5 step 3 and 4).

**Table 1. Homologous proteins of the Get/TRC pathways in mammalian and yeast cells.**

| Organism | Pre-targeting complex | | | ATPase effector | ER receptor | |
|---|---|---|---|---|---|---|
| **mammals** | BAG6 | SGTA | UBL4A | TRC35 | TRC40 | CAML | WRB |
| **yeast** | - | Sgt2 | Get5 | Get4 | Get3 | Get2 | Get1 |

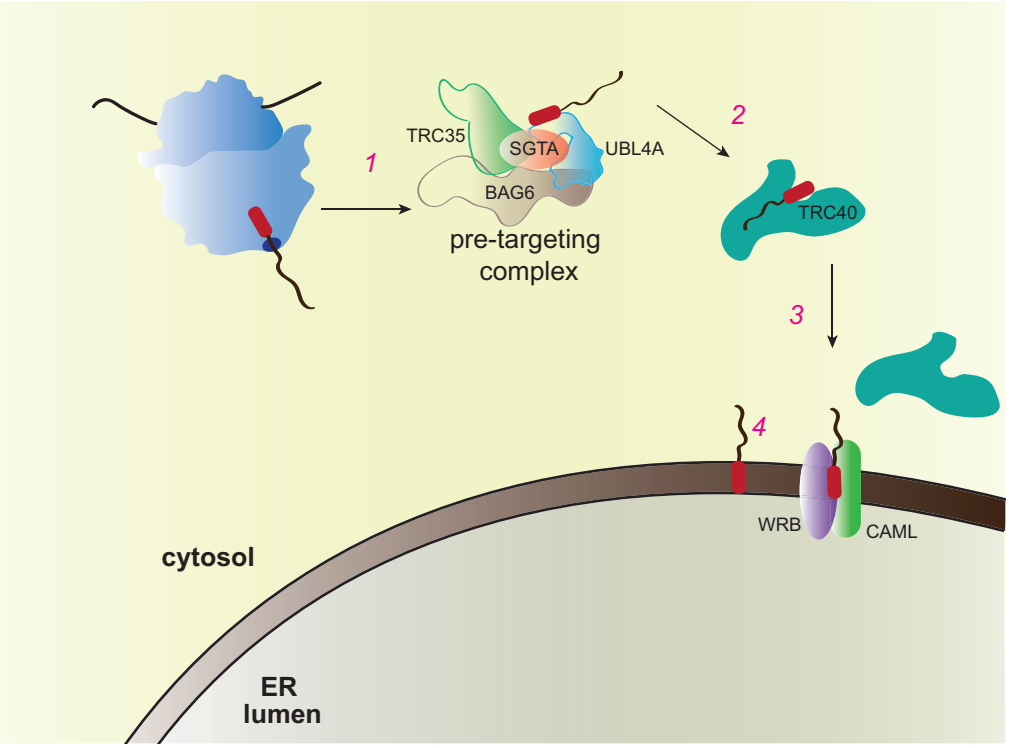


**Figure 5. TRC40 pathway of protein insertion to the ER membrane.**
After emerging from the ribosome exit tunnel, the TA-protein is bound via its TMD by a pre-targeting complex consisting of SGTA, BAG6, TRC35 and Ubl4A (step 1). Subsequently, the pre-targeting complex binds to TRC40 (step 2). After dissociation of the pre-targeting complex, TRC40 delivers the TA protein to the ER membrane. The ER receptors WRB and CAML bind to the protein under ATP hydrolysis (step 3) and integrate the protein into the ER membrane (step4).

Although TRC40 is proposed to be the canonical factor for post-translational delivery of TA proteins, several studies have reported the existence of other post-translational insertion pathways into the ER membrane (Casson et al., 2017) (also discussed in section 6.1.3). Abell et al., 2004 showed by chemical crosslinking that the SRP could interact with TA proteins and facilitate SR dependent membrane insertion *in vitro.* It was suggested that binding of the SRP to TA proteins might occur in a post-translational, but ribosome dependent manner (Abell et al., 2004; Abell et al., 2007; Berndt et al., 2009).

Another alternative pathway that was recently described in yeast and later in human cell lines, is the SRP-independent targeting (SND) pathway (Aviram et al., 2016; Haßdenteufel et al., 2017). The SND pathway was shown to function as backup targeting system for proteins that are not entirely dependent on either the SRP pathway or the GET pathway (Aviram et al., 2016; Haßdenteufel et al., 2017). The SND pathway in yeast consists of ribosome-associated Snd1 and two ER-resident transmembrane proteins Snd2 and Snd3 that form a complex with the Sec61 translocon (Aviram et al., 2016). In mammals, hSnd2, also known as TMEM208, which is the human orthologue of Snd2, has been shown to insert proteins with a C-terminal TMD (Haßdenteufel et al., 2017).

The insertion of less hydrophobic TA proteins and some SRP-dependent membrane proteins were reported to use an ER membrane protein complex (EMC) pathway (Guna et

al., 2018). The TA proteins are shielded in the cytosol by Calmodulin (CaM) and, after release from CaM, are inserted by EMC (Guna et al., 2018). On the contrary, CaM was also reported to inhibit the insertion of the TA proteins Cytochrome b5 and Synaptobrevin 2 *in vitro* (Hassdenteufel et al., 2011). Some proteins also showed partial dependence on both EMC and TRC40 pathways (Guna et al., 2018).

Studies have also shown the involvement of Hsp40/Hsc70 in membrane insertion of TA proteins with a low hydrophobic TMD (Abell et al., 2007; Rabu et al., 2008). Furthermore, an unassisted pathway has been reported for the insertion of some TA proteins like Cytochrome b5 (Brambillasca et al., 2006). Cytochrome b5 can be inserted into liposomes in an unassisted manner (Brambillasca et al., 2005; Brambillasca et al., 2006).

### 1.4.2. Integral membrane proteins of the INM

The INM is considered to be molecularly distinct from the ONM, which is contiguous with the ER, harboring more than 100 unique transmembrane proteins according to proteomic analysis, of which only a few have been further characterized (Cheng et al., 2019; Korfali et al., 2010; Korfali et al., 2012; Schirmer et al., 2003; Schirmer et al., 2005; Strambio-de-Castillia et al., 1995; Wilkie et al., 2011). The INM proteins are involved in maintaining nuclear structure, genome organization and positioning of chromosomal domains (Mekhail and Moazed, 2010; Rothballer and Kutay, 2013; Starr and Fridolfsson, 2010). The INM proteins from the SUN family connect the nucleus to the cytoskeleton (Starr and Fridolfsson, 2010). Several LEM (Lap2, emerin, Man1) domain-containing proteins and SUN proteins are involved in transcriptional control and DNA repair (Akhtar and Gasser, 2007; Mekhail and Moazed, 2010).

Mutations in genes encoding INM components and lamins are associated with several human diseases like tissue-specific diseases of the brain, muscle and fat disorders like laminopathies and progeria (Méndez-López and Worman, 2012; Schirmer et al., 2003; Schreiber and Kennedy, 2013; Stewart et al., 2007). Many transmembrane proteins of the INM are involved in multiple protein interactions (Bengtsson and Wilson, 2004). Moreover, these transmembrane proteins have different expression levels between different cell types (Korfali et al., 2012; Schirmer and Gerace, 2005; Wilkie et al., 2011).

The integral membrane proteins of the INM harbor several single-pass and multi-pass membrane proteins (Figure 6). The lamin B receptor (LBR) contains eight TMDs and binds to B-type lamins (Worman et al., 1988). It was also reported to bind to heterochromatin protein1 (HP1) and DNA (Mattout-Drubezki and Gruenbaum, 2003). LBR is essential for cholesterol synthesis (Tsai et al., 2016), and mutations in LBR are implicated in Pelger-Huet anomaly (Hoffmann et al., 2002) and Greenburg skeletal dysplasia (Waterham et al., 2003). The lamina associated polypeptide (Lap2$\beta$) is a single pass TA

protein, belongs to the Lap2 (thymopoietin) family of proteins that is involved in maintaining chromatin and nuclear architecture and transcriptional repression (Nili et al., 2001). *Emerin* was identified as a gene responsible for Emery-Dreifuss muscular dystrophy (Bione et al., 1994). It is a well-characterized, single-pass, tail-anchored, membrane protein of the INM. MAN1, another integral-membrane protein, has two hydrophobic segments and a C-terminal tail (Wu et al., 2002) and is related to several bone disorders (Hellemans et al., 2004). The three proteins, Lap2, MAN1 and emerin, belong to a family of nuclear proteins with a ~40-residue LEM-domain (Wolff et al., 2001) and bind to the conserved chromatin protein barrier-to-autointegration factor (BAF) (Lee et al., 2001; Shumaker et al., 2001).

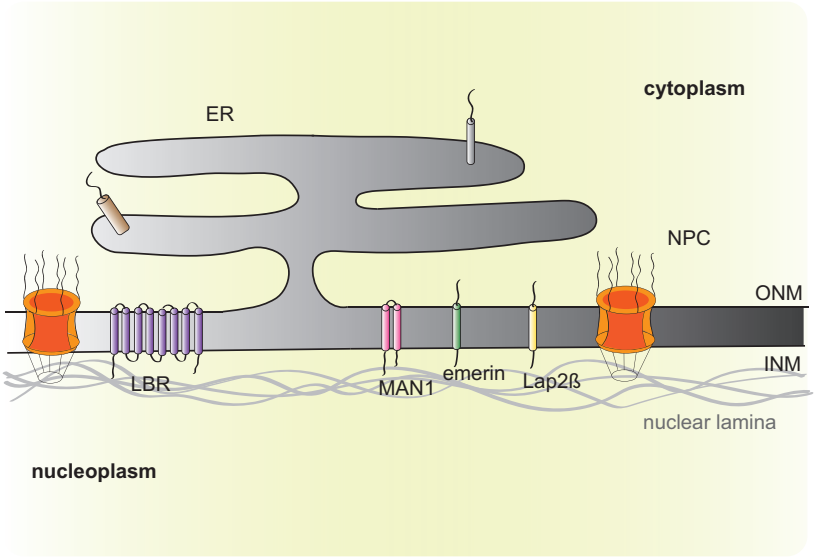


**Figure 6. Schematic view of integral membrane proteins anchored to the nuclear envelope.**
INM proteins including LBR, MAN1, emerin and Lap2β are depicted in the diagram based on their number of TMDs. All of them are associated with the underlying nuclear lamina.

## 1.5. Traffic of integral membrane proteins to the INM

Newly synthesized integral INM proteins are integrated into the ER membrane and afterwards traverse through the ONM to the INM via the NPC. To pass the central channel of the NPC, the nucleoplasmic domains of INM proteins would have to extend to the central channel from the membrane surface (Antonin et al., 2011). A size dependency of ~60 kDa for the nucleoplasmic domain for the passage through the central channel has been demonstrated. (Ohba et al., 2004; Soullam and Worman, 1995). Peripheral channels adjacent to the pore complex might also allow passage of membrane proteins (Maimon et al., 2012).

Four models of INM targeting have been proposed: transport-factor mediated targeting, localization based on diffusion and retention, targeting via an INM signal sequence (sorting-motif) and transport through the NPC with the help of FG-motifs (Katta et al., 2014; Ungricht et al., 2015). In the transport-factor mediated model (Figure 7), INM proteins containing a NLS interact with a nuclear transport factor in the cytoplasm. The

cargo-transport factor complex then passes through the NPC either through the central channel or via the peripheral channel. After reaching the nucleus, the transport factor is released from the cargo by Ran-GTP (Katta et al., 2014; Laba et al., 2014).

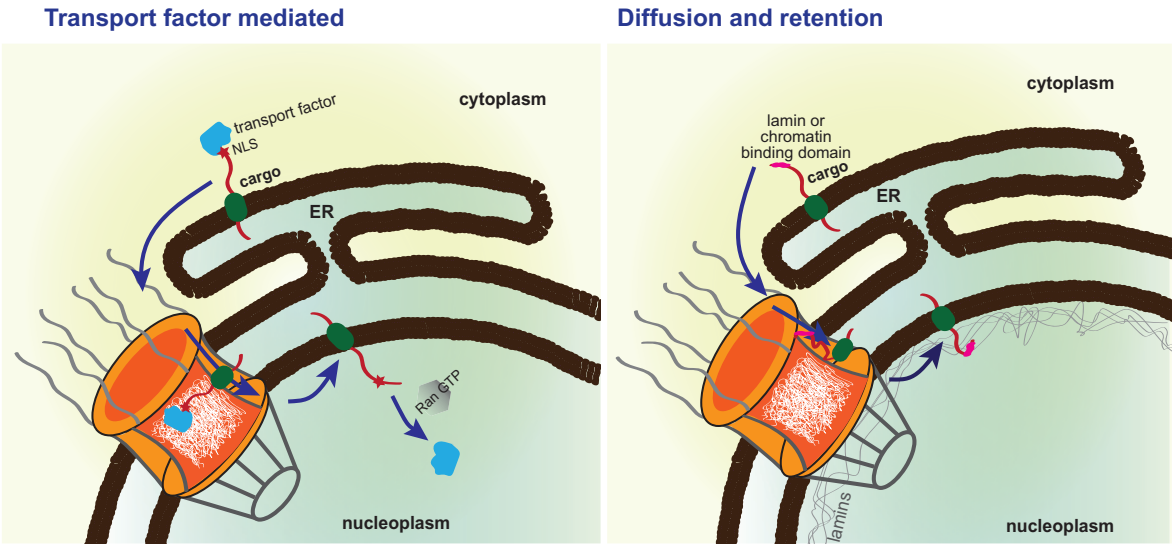


**Figure 7. Major models of membrane protein trafficking to the INM.**
The transport factor-mediated model uses similar principles of transport as those established for soluble proteins. Cargo proteins containing an NLS bind to transport factors and are transported through interaction with nucleoporins of the central channel. After reaching the nucleus, dissociation of the cargo-transport factor is mediated by RanGTP. The diffusion and retention model suggests that INM proteins laterally diffuse through the peripheral channel of the NPC, from the ER via the ONM to the INM. The proteins are retained at the INM by interacting with nuclear lamins or chromatin.

It was previously reported that the yeast LEM-domain containing proteins Heh1 and Heh2 require active transport using karyopherin-α (Kap60) and karyopherin-β (Kap95), and also the RanGTPase cycle (King et al., 2006). An NLS was identified in Heh2 that binds to karyopherins, which was important for its INM localization (Liu et al., 2010; Meinema et al., 2011). Many of the INM proteins may contain a putative NLS in their extraluminal domains, suggesting that this could be a widely used mechanism for INM targeting (Lusk et al., 2007). A possibility to consider with this targeting mechanism is whether INM proteins extend their NLSs through sideward openings of peripheral channel to provide a handle for transport-factor mediated translocation through the central NPC channel (Turgay et al., 2010). Therefore, the functional and mechanistic contributions of these NLSs to the INM protein targeting process needs to be further investigated. A variant of transport factor mediated model was also described suggesting that INM proteins bind to soluble NLS-containing cargoes and 'piggyback' on their transport factor-mediated transport to reach the INM (Gardner et al., 2011).

In the diffusion and retention model (Figure 7), INM proteins diffuse from the ER to the ONM, and from the ONM to the INM through the peripheral channels of the NPC. After reaching the INM, the proteins are retained by tethering to nuclear components like lamins or chromatin (Powell and Burke, 1990; Smith and Blobel, 1993; Soullam and Worman,

1995). This peripheral channel imposes a size limit of less than 40 kDa for the extraluminal domain of the INM proteins (Soullam and Worman, 1995). In line with this model, photobleaching studies performed on several INM proteins showed rapid diffusion from the ER to the INM (Ellenberg et al., 1997; Ostlund et al., 1999; Shimi et al., 2004; Ungricht et al., 2015; Wu et al., 2002; Zuleger et al., 2011). The mobility of the tested proteins was reduced at the INM compared to the ER, suggesting that they are associated with relatively immobile lamins or chromatin (Ungricht et al., 2015; Zuleger et al., 2011).

The signal sequence or sorting motif model relies on small, charged motifs on the INM proteins that are recognized by membrane-associated, short isoforms of karyopherins (for example, Importin $\alpha$-16). The transport occurs through the peripheral channel of the NPC and after reaching the nucleus, the protein release is stimulated by Nup50/Nup2, as reported for the yeast protein Heh2 (Braunagel et al., 2004; Braunagel et al., 2007; Saksena et al., 2004; Saksena et al., 2006). The fourth model is based on a systematic study performed on 15 different INM proteins suggesting that many INM proteins are enriched in FG-repeats that possibly allow for direct translocation of these proteins through the NPC and could use multiple overlapping pathways to reach INM (Katta et al., 2014; Zuleger et al., 2011). The transport models as well as the membrane-insertion pathways established for some well-characterized INM proteins are listed in Table 2.

**Table 2. Models of targeting of well-characterized INM proteins.**

| Protein | ER membrane insertion | Nuclear import machinery | Number of TMDs | References |
|---|---|---|---|---|
| LBR | co-translational | diffusion and retention, mobility dependent on RanGTP and Nup35 | 8 | (Braunagel et al., 2007; Smith and Blobel, 1993; Soullam and Worman, 1993; Ungricht et al., 2015; Zuleger et al., 2011) |
| Lap2$\beta$ | post-translational | diffusion and retention | 1 | (Furukawa et al., 1995; Furukawa et al., 1998; Ohba et al., 2004; Zuleger et al., 2011) |
| emerin | post-translational | diffusion and retention, mobility requires ATP | 1 | (Berk et al., 2013a; Zuleger et al., 2011) |
| Man1 | co-translational | diffusion and retention | 2 | (Wu et al., 2002) |
| Heh1 (yeast) | co-translational | transport factor mediated | 2 | (King et al., 2006; Meinema et al., 2011) |

| Protein | ER membrane insertion | Nuclear import machinery | Number of TMDs | References |
|---|---|---|---|---|
| Heh2 (yeast) | co-translational | transport factor mediated | 2 | (King et al., 2006; Liu et al., 2010; Meinema et al., 2011) |

## 1.6. Tools developed for assessing the molecular requirements of INM targeting

Several tools have been developed in the past decade to elucidate the molecular requirements of INM protein translocation from the ER to the INM. The trafficking of 15 integral INM proteins was compared by using FRAP (fluorescence recovery after photobleaching) assays (Zuleger et al., 2011). This study revealed that ATP and Ran dependence for translocation through the NPC are distinct for different proteins and are not essential for all INM proteins (Zuleger et al., 2011).

An assay developed by Ohba et al. 2004 was used to analyze movement of membrane proteins from the ER to the INM in living cells. In this assay, constructs tagged to an FKBP (FK506 binding protein) and FRB ((FKBP12/rapamycin-binding) domain of human mTOR (mechanistic target of rapamycin)), which dimerize upon addition of rapamycin are used. The first component of the assay is a reporter protein consisting of the FRB domain, the membrane insertion domain of Lap2β and a GFP-moiety. The second one is a 'trap' consisting of FKBP domain and the lamin-binding domain of Lap2β. Upon treatment with rapamycin, the reporter accumulates at the NE. This reporter and trap system was used to monitor energy and temperature dependent targeting of Lap2β and demonstrated an impaired targeting of Lap2β with reduced temperature and ATP-depletion (Ohba et al., 2004).

An INM protein targeting reporter system was developed in living mammalian cells. In this system, a pool of fluorescently tagged INM proteins is released from the ER by a self-cleaving retention domain (Boni et al., 2015). An inducible reporter system consisting of the Hepatitis C Virus NS3 protease (Soullam and Worman, 1995), a CMPK (chicken muscle pyruvate kinase) ER-retention domain and an NS3-cleavage site construct is tagged at the N-terminus of a minimal LBR (N-terminus and the first TMD, Ellenberg et al., 1997). The NS3 protease is induced by washout of its inhibitor, which removes the retention domain, releasing the protein from the ER and targeting it to the INM (Boni et al., 2015). Requirements of targeting of LBR were studied using this reporter in a siRNA gene-screening platform, coupled with automated high resolution microscopy. This reporter system was further used for Lap2β and suggested that both LBR and Lap2β use diffusion and retention mechanism for localization to the INM (Boni et al., 2015).

Using human LBR, SUN2 and Lap2β as model substrates, a visual *in vitro* INM targeting assay was developed by Ungricht et al, 2015. In this system, two RFP-moieties are appended to the nucleoplasmic domain of the INM proteins, separated by a Tev (tobacco etch virus) protease site and a GFP-moiety at the C-terminus of the INM protein. Addition of TEV-protease or co-expression of CFP-Tev cleaves the two RFPs, releasing the much smaller protein from the ER to the INM (Ungricht et al., 2015). Using this targeting assay, it was shown that INM targeting is energy-dependent and that INM accumulation of proteins depends on a highly interconnected ER network and retention at the INM (Ungricht et al., 2015). In addition, an artificial reporter (AR) system was developed to recapitulate diffusion and retention-based INM targeting using the FKBP-FRP dimerization by rapamycin approach (Ungricht et al., 2015). Using the AR system, it was observed that energy depletion affected the INM accumulation of reporter protein containing an artificial TMD domain, WALP17 (Ungricht et al., 2015).

Another approach to assess the requirements for targeting of INM proteins is the RUSH (retention using selective hooks) system, which was originally designed to study kinetics of proteins in the secretory pathway (Boncompain et al., 2012). This system was modified by Pawar et al, 2017, to trap INM proteins in the ER by using a SBP (streptavidin binding peptide) tag and STIM1-NN (a microtubule binding deficient mutant of ER protein STIM1) (Boncompain et al., 2012). By addition of biotin, release and accumulation of INM proteins at the NE was monitored (Pawar et al., 2017). Using the RUSH system together with INM targeting assays (Ungricht et al., 2015), it was reported that Atlastins, a family of membrane-bound GTPases of the ER, influence the efficient targeting of proteins to the INM (Pawar et al., 2017).

## 1.7. The tail anchored protein emerin

Emerin is predominantly anchored at the INM, where it binds to components of the nuclear lamina (Laba et al., 2014; Ostlund and Worman, 2003). Emerin belongs to the family of LEM-domain proteins, and mutations in the gene lead to an X-linked form of Emery-Dreifuss muscular dystrophy, characterized by muscle weakness and cardiomyopathic abnormalities (Bione et al., 1994). Human emerin is a serine-rich protein of 254 amino acids, consisting of an N-terminal domain and a single TMD of 21 residues followed by 11 residues at the C-terminus (Bione et al., 1994). Emerin and another LEM- domain containing protein, Lap2β, are homologous at their TMDs, and both are known to interact with the DNA-bridging protein BAF (Furukawa et al., 1998; Lee et al., 2001). A significant fraction of emerin was also observed in the ONM and peripheral ER, where it interacts with the centrosome (Salpingidou et al., 2007).

Even though emerin is not essential for cell viability in humans (Harborth et al., 2001), diverse functional roles have been implicated in gene regulation, mRNA splicing, signaling pathway regulation and maintaining the nuclear architecture (Holaska and Wilson, 2007). Emerin occurs in four different phosphorylated forms, three of which play a role in cell-cycle dependent events (Ellis et al., 1998). Emerin was also reported to play a role in nuclear calcium transients and nuclear invagination (Shimojima et al., 2017).

Emerin is inserted into the ER membrane post-translationally, mediated by the TRC40 pathway (Pfaff et al., 2016). Once inserted, emerin diffuses through the ER to the INM as shown by fluorescence loss in photobleaching (FLIP) and FRAP studies, since its cytoplasmic domain is small (25 kDa) (Ostlund et al., 1999). Emerin also lacks FG-repeats, and its predicted NLS (residues 35-47) does not seem to be required for nuclear import (Berk et al., 2013a; Tsuchiya et al., 1999). At the INM, emerin is retained and accumulated by binding to lamins, and knocking down lamin A redistributes emerin to the ER, further suggesting that lamin A serves as an emerin receptor at the INM (Sullivan et al., 1999). Accordingly, the diffusional mobility of emerin at the NE was observed to be three times slower than at the ER by FRAP assays (Ostlund et al., 1999). In the absence of lamin A, emerin was more mobile and was evenly distributed over the NE and ER, supporting the diffusion and retention model for emerin (Ostlund et al., 1999; Ostlund et al., 2006). It was also reported that the mobility of emerin required ATP both at the level of ER and also INM (Zuleger et al., 2011).

## 1.8. The tail anchored protein VAPB

The human vesicle associated membrane protein-associated protein (VAP) family was initially identified as homologous to the protein VAP33 from *Aplysia californica* (Skehel et al., 1995). Two protein coding VAP genes were identified in humans, *VAPA* and *VAPB,* the latter with an alternative splice variant (*VAPC*). The resulting proteins are shown in Figure 8A. VAPA and VAPB are ~60 % identical in sequence. They contain an N-terminal major-sperm protein domain (MSP), a coiled-coil domain and a single TMD defining it a TA protein (Figure 8A; Nishimura et al., 1999; Nishimura et al., 2004). VAPC lacks the coiled-coil domain and the TMD (Nishimura et al., 1999). The MSP domain consists of seven-stranded immunoglobulin-like β-sheet domains (Figure 8B; Shi et al., 2010). A mutation in this domain, P56S, leads to a familial form of amyotrophic lateral sclerosis (ALS) disease, which causes the death of motor neurons and muscular atrophy (Nishimura et al., 2004). A second mutation in this gene resulting in a T46I mutation was also reported to cause ALS in a mutation screen of genes responsible for familial ALS (Figure 8B) (Chen et al., 2010).

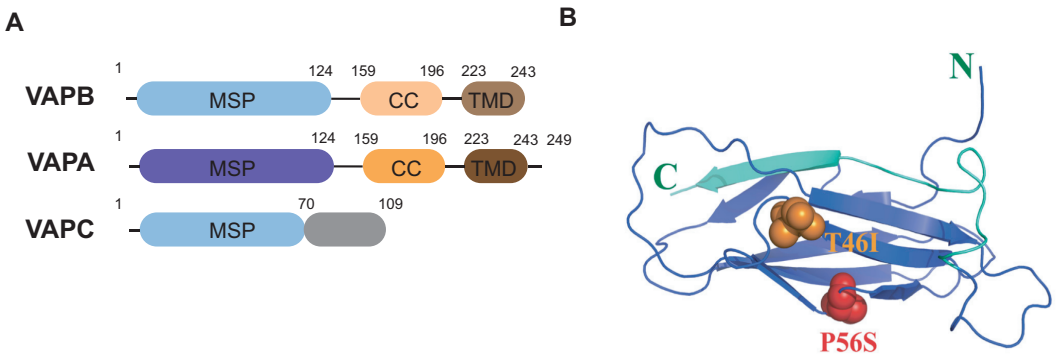


**Figure 8. Domain organization of the VAPs and crystal structure of the MSP domain.**
(A) Schematic representation of the proteins VAPB, VAPA and the protein resulting from the alternative splice variant of the gene *VAPB*, VAPC. The major sperm domain (MSP), coiled-coil (CC) and transmembrane domain (TMD) are indicated. (B) Crystal structure of the MSP domain of human VAPB (modified from Song, 2013). The P56S and T46I mutations causing ALS are represented as spheres. The seven Immunoglobulin β-strands are represented as arrows. The last 20 residues at the C-terminus represented in turquoise are absent in VAPC (Song, 2013).

The MSP domain is known to mediate interactions with the FFAT motif (two-phenlyalanines in an acidic tract) of lipid binding proteins (Loewen and Levine, 2005; Murphy and Levine, 2016). The coiled-coil domain mediates oligomerization of VAPB and a GXXXG dimerization motif in the TMD mediates self-association of the TMD (Kim et al., 2010).

VAPB has been implicated in the regulation of diverse cellular processes (Lev et al., 2008). These include membrane trafficking (Skehel et al., 1995; Soussan et al., 1999), regulation of lipid transport and metabolism (Kagiwada and Zen, 2003; Kawano et al., 2006), the unfolded protein response (Kanekura et al., 2006; Kanekura et al., 2009; Walker and Atkin, 2011) and autophagosome biogenesis (Zhao et al., 2018), microtubule organization (Amarilio et al., 2005; Pennetta et al., 2002; Skehel et al., 2000), calcium homeostasis (De Vos et al., 2012; Mórotz et al., 2012), synaptic activity (Gómez-Suaga et al., 2019; Pennetta et al., 2002), ephrin-induced signaling modulation (Mórotz et al., 2012; Tsuda et al., 2008) and cardiac and neuronal pacemaker channel function (Silbernagel et al., 2018). Furthermore, the P56S mutation in VAPB has been reported to cause nuclear envelope defects and block the transport of nucleoporins and emerin to the NE (Tran et al., 2012). Recently, VAPB has also been connected to the nuclear egress stage of the replication of the Herpes Simplex virus (Saiz-Ros et al., 2019).

Due to its main localization in the ER, VAPB acts as receptor for many cytoplasmic proteins (Murphy and Levine, 2016). The interactome of VAPB is very diverse, with components of many cellular pathways binding it to access the ER. So far nearly 100 proteins have been identified as interacting partners of VAPB and/or VAPA, of which ~50% interact via the MSP-FFAT domains (Huttlin et al., 2015; Murphy and Levine, 2016; Slee and Levine, 2019). VAPB is involved in forming ER contacts with multiple organelles by membrane contact sites (MCSs; Figure 9; De Vos et al., 2012; Johnson et al., 2018; Zhao et al., 2018). VAPB was reported to interact with voltage-gated $K^+$-channels (Kv2) at the

plasma membrane in brain neurons via a non-canonical FFAT motif present in C-terminus of the channel (Johnson et al., 2018; Kirmiz et al., 2018). The late-endosomal membrane-anchored protein StAR related lipid transfer domain 3 (STARD3) interacts with VAPB by its FFAT domain at the ER-endosome junction (Alpy et al., 2013). VAPB also interacts with multiple autophagy proteins, focal adhesion kinase family-interacting protein of 200 kDa (FIP200) and Unc-51-like autophagy-activating kinase 1 (ULK1) through FFAT motifs for autophagosome biogenesis (Zhao et al., 2018). Tyrosine phosphatase-interacting protein 51 (PTPIP51) and VAPB form a mitochondria-ER tethering complex to regulate association between the two organelles (De Vos et al., 2012; Stoica et al., 2014), whereas VAPB interacts with Acyl-CoA-binding domain proteins 5 and 4 (ACBD5 and ACBD4) to mediate membrane association between the ER and peroxisomes (Costello et al., 2017a; Costello et al., 2017b). The ER-Golgi recycling proteins YIF1A and YIF1B were reported to interact with VAPB to regulate membrane delivery into dendrites (Kuijpers et al., 2013) and the association of oxysterol-binding proteins (OSBPs) with VAPB mediates coordinated lipid transfer at the ER-Golgi junctions (Moustaqim-Barrette et al., 2014; Peretti et al., 2008; Venditti et al., 2019).

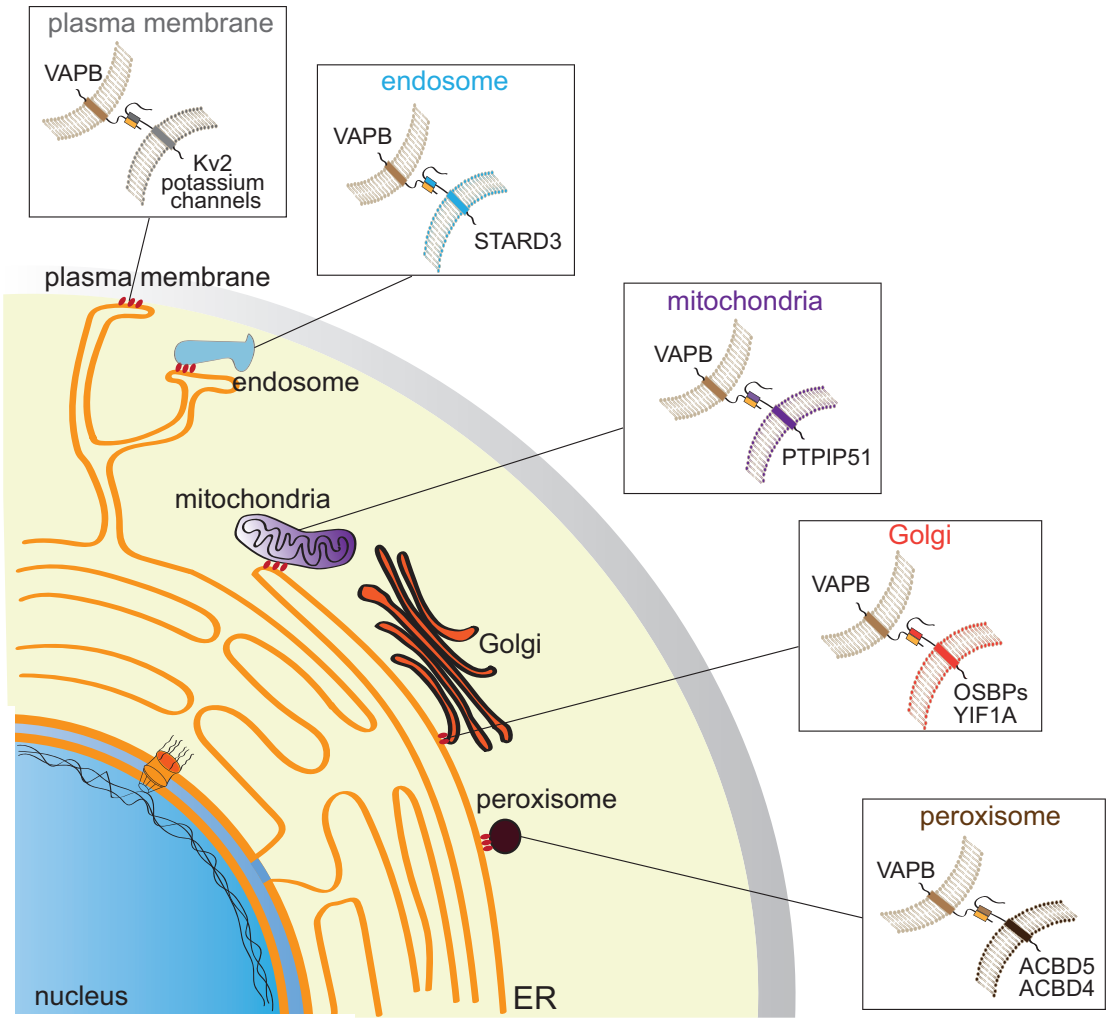

**Figure 9. Intracellular membrane contact sites formed by VAPB.**
(previous page) Schematic representation of membrane-contact sites formed between VAPB and other membrane proteins. VAPB mediates association with the plasma membrane (Kv2 channel), late endosome (STARD3), mitochondria (PTPIP51), Golgi (OSBPs, YIF1A) and peroxisomes (ACBD5, ACBD4).

## 1.9. Proximity based labeling methods for interactome mapping

Various methods have been developed for mapping protein-protein interactions. Complementary to affinity purification of protein complexes, proximity-based labeling approaches combined with mass-spectrometry have emerged as a powerful technique to map the interactomes of proteins. These techniques are based on the fusion of an enzyme, either a biotin ligase or a peroxidase, to a protein of interest, followed by addition of an enzyme-substrate (biotin or a phenolic biotin derivative) to enable covalent labeling of proteins in proximity to the protein of interest. These biotinylated proteins are then isolated by affinity purification using immobilized streptavidin and subjected to quantitative proteomic approaches (Gingras et al., 2019; Kim and Roux, 2016; Trinkle-Mulcahy, 2019). Proximity labeling methods have several key advantages over affinity purification approaches. The labeling can be performed *in vivo* and it helps to detect transient interactions that are not captured by standard co-affinity purification approaches. In addition it helps to study interactions among membrane proteins that are difficult to be identified using pull-down approaches. It also helps to avoid post-lysis artifacts usually associated with biochemical purification steps (Gingras et al., 2019).

Biotin ligases and peroxidases belong to the two main classes of enzymes used for proximity-dependent labeling (Table 3). Based on the enzyme used in proximity labeling approaches, protein associations over time or a snapshot of protein associations can be studied *in vivo* (Martell et al., 2012; Roux et al., 2012).

### 1.9.1. Biotin ligase-based proximity labeling

The best studied biotin ligase is *E. coli* derived BirA, which facilitates biotinylation of a single protein, BCCP (AccB) subunit of acetyl-CoA carboxylase, on a lysine residue of acetyl-CoA carboxylase. When the protein is incubated with BirA, biotin and ATP, biotinylation occurs, which involves reactive biotinyl-5'-AMP (bioAMP). BioAMP is retained at the active site by BirA and mediates transfer to a lysine on the substrate protein (Choi-Rhee et al., 2004). A proximity-dependent biotinylation approach termed 'proximity-dependent biotin identification' (BioID) that uses a mutant form of BirA (BirA*; mutation in biotin- and bioAMP-binding domain of BirA) was developed. The BirA* was tagged to a protein of interest, resulting in biotinylation of neighboring proteins (Choi-Rhee et al., 2004; Roux et al., 2012). The labeling time of BioID-fusion protein is 15-18 hours, induced by addition of biotin, with a labeling radius of less than 20 nm (Kim et al., 2014). Biotinylated proteins are captured on a streptavidin based affinity matrix and analyzed by mass

spectrometry (Kim and Roux, 2016; Roux et al., 2012; Roux et al., 2013) (Figure 10A). BioID was first applied to study interactions of insoluble lamin A, revealing interactions with proteins of the INM and NPC (Roux et al., 2012).

One of the limitations of BioID is the size of the biotin ligase, which is 35 kDa. Such a large domain might affect the localization or function when fused to the protein of interest. To overcome this, a smaller ligase (27 kDa) from *Aquifex aeolicus* was used in an improved assay termed as BioID2 (Kim et al., 2016). It was found that BioID2 required less biotin for efficient labeling and the biotinylation range of BioID2 could be modulated by using flexible linkers (Kim et al., 2016). The Khavari lab engineered a new mutant of BirA (28kDa) from *Bacillus subtilis* termed as BASU that was used to detect RNA-protein interaction in living cells (Ramanathan et al., 2018). Three mutations were introduced in the bioAMP-binding domain of BirA* that resulted in >1000-fold faster kinetics and >30-fold increased signal-to-noise ratio compared to BioID2 (Ramanathan et al., 2018).

Another drawback of the BioID method is its long labeling time (15-18 hours), which was circumvented by the development of TurboID and miniTurbo in yeast (Branon et al., 2018). The biotin ligase used in TurboID is the same as in BioID but has 14 mutations in the bioAMP-binding domain that greatly increase its labeling efficiency. MiniTurbo has 12 mutations in the bioAMP-binding domain of BirA* and a deletion of N-terminal DNA-binding domain that reduced the size of the tag to 28 kDa. Both tags enable a labeling time of 10 minutes and greater efficiency than BioID and BioID2 (Branon et al., 2018). As an extension of the biotin ligase based proximity labeling, split-BioID was developed (De Munter et al., 2017; Schopp et al., 2017). BirA* was split into two fragments that are compatible with protein-complementation assays and the N- and C-terminal fragments fused to two different proteins. Only if the two proteins associate, the activity of the ligase is regained by the reconstitution of both fragments (De Munter et al., 2017; Schopp et al., 2017). Split-BioID was used to map the interactome of protein phosphatase complexes (De Munter et al., 2017) and miRISC (microRNA-induced silencing complex) (Schopp et al., 2017). More recently, the 2C-BioID method was developed, in which a rapamycin analogue is used to initiate the dimerization of the biotin protein ligase and the protein of interest (Chojnowski et al., 2018).

Though mutations in BirA have improved the efficiency of tagging, biotin-based proximity has certain limitations. Biotin used in the method may not be accessible to the secretory pathway even though it is actively imported into the cytoplasm and freely diffuses into the nucleus (Zempleni, 2005). Moreover, the BioID methods have long labeling times in general, which prevent the analysis of events that have a short time duration, and the long labeling time may affect the function of the protein. As for all proximity labeling

approaches, BioID detects proteins in close proximity that may not necessarily be the direct interacting partners.

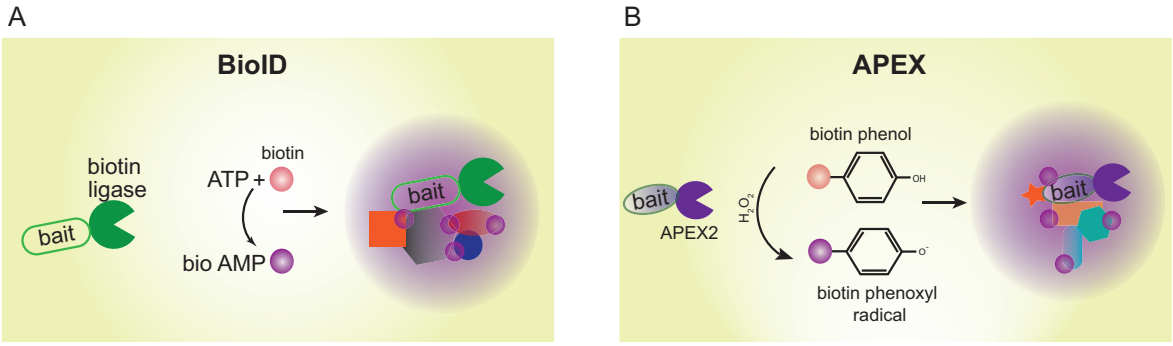


**Figure 10. Proximity based labeling approaches to study protein interactions.**
(A) BioID uses biotin ligase fused to a protein of interest (bait). The ligase catalyzes the conversion of biotin to biotinyl-5'-AMP (bioAMP), which leads to covalent tagging of lysine residues in the proteins in proximity to the bait. (B) The APEX approach is based on the expression of ascorbate peroxidase fused to the protein of interest (bait). The peroxidase catalyzes the conversion of biotin-phenol to the biotin-phenoxyl radical, which in the presence of $H_2O_2$ covalently labels tyrosine residues of proteins in close proximity.

### 1.9.2. Peroxidase based proximity labeling

Instead of biotin ligases, a more rapid approach of proximity labeling was obtained using the enzymatic activity of peroxidases. Peroxidases generate short-lived free radicals from molecules such as phenolic derivatives and $H_2O_2$ (Rhee et al., 2013a; Gross and Sizer, 1959). An engineered monomeric ascorbate peroxidase (APEX) from plants was developed, which was initially used in electron microscopy (EM) studies (Martell et al., 2012). APEX, used as an EM tag, is fused to a protein of interest and expressed in cells, which were fixed and overlaid with a solution of DAB (diaminobenzidine). When $H_2O_2$ is added, APEX catalyzes the polymerization of DAB and recruits electron-dense osmium tetroxide generating EM contrast (Martell et al., 2012). For studying protein-protein interactions *in vivo*, cells expressing a version of APEX, either fused to a protein of interest or directly targeted to a cellular organelle, are treated with biotin-phenol for 30 minutes, followed by labeling with $H_2O_2$ for one minute. APEX catalyzes the conversion of biotin-phenol to the biotin-phenoxyl radical that covalently tags tyrosine residues of endogenous proteins that are within a range of ~20 nm to APEX (Rhee et al., 2013a; Figure 10B). The biotinylated proteins are later enriched using streptavidin beads and identified using mass spectrometry (Rhee et al., 2013a). The enzyme tag can be fused to the N- or C-terminus of the protein of interest and is active in different cellular compartments.

**Table 3. Overview of enzyme tags developed for BioID and APEX-based proximity labeling methods.**

| Method | Enzyme | Source | Labeling time | Tag size (kDa) | Reference |
|---|---|---|---|---|---|
| BirA* | Biotin ligase | *E. coli* | 15-18 hours | 35 | (Roux et al., 2012) |
| BioID2 | Biotin ligase | *A. aeolicus* | 15-18 hours | 27 | (Kim et al., 2016) |
| TurboID | Biotin ligase | *E. coli* | 10 minutes | 25 | (Branon et al., 2018) |
| Mini Turbo | Biotin ligase | *E. coli* | 10 minutes | 28 | (Branon et al., 2018) |
| 2C-BioID | Biotin ligase | *E. coli* | 15-18 hours | 35 | (Chojnowski et al., 2018) |
| BASU | Biotin ligase | *B. subtilus* | 15-18 hours | 28 | (Ramanathan et al., 2018) |
| APEX | Ascorbate peroxidase | Pea | 1 minute | 28 | (Martell et al., 2012; Rhee et al., 2013a) |
| APEX2 | Ascorbate peroxidase | Soybean | 1 minute | 28 | (Hung et al., 2017; Lam et al., 2015) |

A catalytically more active version of APEX, called APEX2 was developed (Lam et al., 2015). APEX-based methods are capable of generating a snapshot of interacting proteins with a rapid labeling time of one minute in contrast to BioID that requires 15-18 hours of labeling. The APEX or APEX2 based methods have been used to map proteomes of the mitochondrial matrix and intermembrane space in mammalian cells (Hung et al., 2014; Hung et al., 2017; Lam et al., 2015; Rhee et al., 2013b), primary cilia (Mick et al., 2015), ER-PM junction (Jing et al., 2015), proteins engaged by G-protein coupled receptors (Lobingier et al., 2017; Paek et al., 2017) and also high resolution interactome mapping by EM (Lam et al., 2015; Martell et al., 2012). Similar to the split-BioID approach, a fragment complementation of APEX2-based proximity labeling called spilt-APEX2 was developed (Han et al., 2019; Xue et al., 2017). Two inactive fragments of APEX2, an N- and a C-terminal fragment, reconstitute to an active peroxidase only upon co-localization of both fragments. The split-APEX2 reconstitution was demonstrated on engineered RNA motifs and at mitochondria-ER contact sites (Han et al., 2019).

As an alternative to APEX, expression of horseradish peroxidase (HRP) fusion proteins or HRP-conjugated antibodies called ‘enzyme-mediated activation of radical source’ (EMARS) was also employed for proximity labeling (Jiang et al., 2012). In the presence of biotin and $H_2O_2$, active radical species are generated by HRP and proteins are

labeled within a radius of ~200 nm. Since HRP is a larger tag (44 kDa), it has been used primarily to study cell surface proteins like glycosylphosphatidylinositol-anchored proteins and receptor tyrosine kinases (Jiang et al., 2012). Another HRP-based approach termed 'selective proteomic proximity assay using tyramide' (SPPLAT) uses ligand or antibody conjugated HRP with a biotin-tyramide compound and $H_2O_2$ to label neighboring proteins on the cell surface (Li et al., 2014). Very recently, HRP was used to study intracellular antibody-based proteomic labeling in fixed cells and tissues. In this approach, biotin-phenol and $H_2O_2$ were added to cells stained with primary and HRP-coupled secondary antibody to induce biotinylation. This has the advantage of avoiding fusion and overexpression artifacts but requires a monospecific primary antibody (Bar et al., 2018).

APEX-based methods are advantageous in studying compartmental proteomics with faster kinetics. However, even with these advantages, there are certain limitations. The use of $H_2O_2$ in labeling could induce oxidative damage on some signal transduction pathways and organelle dynamics (Gerich et al., 2009; Lam et al., 2015). It also has to be noted that peroxidase based labeling is specific to electron rich amino acids like tyrosine, which are of low abundancy and might not be exposed to the surface and thus not be available for labeling (Echols et al., 2002). These limitations could be circumvented by designing more specific control experiments or by physically separating the enzyme from the protein of interest as performed by 2C-BioID (Chojnowski et al., 2018). Like any other proximity labeling approaches, APEX and APEX2 detects only proximate proteins and not necessarily direct protein-protein interactions. Standard biochemical approaches could be used for validating protein interactions with the possible caveat of losing interactions under harsh buffer conditions or due to insolubility. The use of methods like immunofluorescence assays, fluorescence complementation assays (Cooper et al., 2015; Snider et al., 2013), or proximity ligation assays (Chen et al., 2014) could also validate the results obtained even though these also provide proximity not direct interactions between proteins.

## 1.10. Aim of this work

Most of the integral membrane proteins specific to the INM have been identified by proteomic approaches, including a few proteins that belong to a specific class known as TA proteins. Some of these proteins are known to localize in the ER and are also enriched in the INM. However, how these proteins are inserted into the ER after their synthesis in the cytoplasm and targeted to the INM is less studied. Furthermore, the interactome of these proteins is poorly defined. The aim of this thesis is to study the biogenesis of TA proteins, the molecular requirements of targeting of TA proteins to the INM and finally to map the interaction repertoire of these proteins in different cellular compartments.

Two model TA proteins were used in this study: an ER protein, VAPB, and a well-established INM protein, emerin. The first part of this study focuses on the membrane biogenesis of VAPB, concentrating on TRC40-mediated membrane insertion. Emerin was used as a positive control for insertion studies.

In the second part of this thesis, the localization of VAPB and its interactome was studied in detail. VAPB is a protein that is involved in interactions at different contact sites. To study the interactome of VAPB at different intracellular localizations, a proximity based labeling approach was developed.

The third part of the thesis focuses on the diffusional mobility of different integral membrane proteins of the INM. Fluorescence recovery after photobleaching (FRAP) assays were used to study the molecular requirement of targeting of INM proteins, focusing on emerin as a model protein. Together, this work should provide a better understanding of the journey of TA proteins from the ER to the INM after their synthesis in the cytoplasm. Deciphering the interactome of these proteins may further help to understand their physiological functions.

# Chapter 2:
# Materials and Methods

# Chapter 2 : Materials and Methods

## 2.1. Materials

### 2.1.1. Software

| Software | Company |
|---|---|
| Adobe Illustrator CC 2020 | Adobe |
| Axiovision (LE) Rel 4.5 | Carl Zeiss |
| Cell Profiler 2.2 | Broad Institute |
| GraphPad Prism 5.03 | GraphPad Software Inc. |
| Image Reader LAS-3000 | Fujifilm |
| ImageStudioLite 5.25 | LI-COR |
| Lasergene | DNASTAR |
| LSM Image Browser | Carl Zeiss |
| Mendeley Desktop | Mendeley |
| NanoDrop 2000 | Thermo Scientific |
| Perseus | Max Plank Institute of Biochemistry |
| Zen 3.1 (blue edition) | Carl Zeiss |

### 2.1.2. Equipment

| Equipment | Company |
|---|---|
| Agarose gel documentation GelSTICK touch | INTAS Science Imaging Instruments |
| Autoclave DX-200 | Systec |
| CASY 1 | Schärfe System |
| Cell culture hood Herasafe™ KS | Thermo Scientific |
| Cell culture incubator Heracell™ 150i | Thermo Scientific |
| Centrifuge 5415R | Eppendorf |
| Centrifuge 5424 | Eppendorf |
| Centrifuge Allegra® X-15R with rotor SX475 | Beckman Coulter |
| Centrifuge Avanti™ J-30I , rotor JA30.50Ti | Beckman Coulter |
| Centrifuge J6-MI, rotor JS 4.2 | Beckman Coulter |
| Confocal microscope LSM 510 | Carl Zeiss |
| Dual gel caster for mini vertical units | Hoefer |
| Emulsiflex-C3 | Avestin |
| Fluorescence microscope Axioscope 2 | Zeiss |
| Incubator Heraeus function line | Heraeus |
| Incubator shaker INNOVA 4430 | New Brunswick Scientific |
| LAS-3000 documentation system | Fujifilm |
| Mini Trans-Blot® Cell | Bio-Rad |
| Odyssey® Sa Infrared Imaging System | LI-COR |
| Olympus CK40 Culture Microscope | Olympus |
| Spectrophotometer NanoDrop 2000c | Thermo Scientific |
| Thermocycler FlexCycler$^2$ | Analytik Jena AG |
| Thermocycler Tprofessional | Biometra |
| Thermomixer comfort | Eppendorf |
| Thermomixer compact | Eppendorf |
| UV sterilizer | Biometra |
| Vertical Electrophoresis unit | Hoefer |
| Vortexer MS2 Minishaker | IKA |

### 2.1.3. Consumables

| Consumable | Company |
|---|---|
| 5 ml Polystyrene Round-Bottom Tubes | BD Biosciences |
| Amersham Hybound Nitrocellulose Blotting Membrane | GE Healthcare |
| Amersham Protran 0.45 µm NC | GE Healthcare |
| Cell culture consumables | Sarstedt,Nalge Nunc International, greiner bio-one |
| Cell culture plastic ware | Sarstedt, greiner bio-one |
| Dual gel caster for Mini vertical units | Hoefer |
| Lab Tek chambered coverglass 8-well | Thermo Scientific |
| Microscope cover slips (12 mm Ø) | Marienfeld |
| Microscope slides (76x26 mm) | Glaswarenfabrik Karl Hecht GmbH & Co KG |
| Minisart RC 15 single use syringe filters (0.45 µm, 0.20 µm) | Sartorius Stedim Biotech |
| NuPAGE® Novex® 4-12% Bis-Tris Protein Gels | Thermo Scientific |
| Parafilm ‘‘M‘‘ | Bemis Company Inc. |
| Reaction tubes (1.5, 2 mL) | Sarstedt, greiner bio-one |
| Spectra/Por® Dialysis Membrane | Spectrum Laboratories |
| Syringes (5 ml) and needles(27G X 4/5’’) | B. Braun, BD Discardit™ II |
| Whatman gel blotting paper | GE Healthcare |

### 2.1.4. Kits

| Kit | Company |
|---|---|
| Duolink® In Situ Detection Reagents Red | Sigma-Aldrich |
| Duolink® In Situ Kit | Sigma-Aldrich |
| NucleoBond™ Xtra Midi | Macherey-Nagel |
| NucleoSpin® Gel and PCR Clean-up | Macherey-Nagel |
| NucleoSpin® Plasmid | Macherey-Nagel |
| Pierce® BCA Protein Assay Kit | Thermo Scientific |
| T7 TnT® Quick Coupled Transcription/Translation System | Promega |

### 2.1.5. Chemicals and reagents

All standard chemicals and solvents not listed here were purchased from AppliChem GmbH (Darmstadt), Carl Roth GmbH + Co. KG (Karlsruhe), Serva Electrophoresis GmbH (Heidelberg), Sigma-Aldrich (Taufkirchen) or Merck (Darmstadt).

| Chemical | Company |
|---|---|
| β-Mercaptoethanol | Roth |
| Acrylamide 4K Solution (30%) | AppliChem |
| Adenosine 5’-triphosphate disodium salt hydrate (A3377) | Sigma-Aldrich |
| Amylose Resin High Flow | New England Biolabs |
| Biotin-phenol | Iris Biotech |
| Bovine Serum Albumin (BSA) (20 mg/ml) | Thermo Scientific |
| Coomassie Plus™ Protein Assay Reagent | Thermo Scientific |
| D-Maltose | Serva Electrophoresis GmbH |
| DAPI (D9542) | Sigma-Aldrich |

| Chemical | Company |
|---|---|
| Desthiobiotin | Sigma-Aldrich |
| Digitonin | Calbiochem |
| dNTP Set, 100 mM Solutions | Thermo Scientific |
| Dithiobis[succinimidyl propionate] (DSP) | Thermo Scientific |
| FBS Superior | Biochrom |
| GeneRuler 100bp DNA Ladder | Thermo Scientific |
| GeneRuler 1kb DNA Ladder | Thermo Scientific |
| Gibco® DMEM (1x) | Thermo Scientific |
| Gibco® DMEM for SILAC, without L-Glu, L-Arg, L-Lys | Thermo Scientific |
| Gibco® Opti-MEM® (1x) | Thermo Scientific |
| Gibco® Penicillin Streptomycin (Pen Strep) | Thermo Scientific |
| Glutathione Sepharose 4 Fast Flow | GE Healthcare |
| Guanosine-5'-triphosphate sodium salt hydrate (51120) | Sigma-Aldrich |
| HeLa cell Cytosol | Ipracell |
| Hydrogen peroxide (35%) | Sigma-Aldrich |
| Imidazole | Roth |
| Immobilon™ Western Chemiluminescent HRP Substrate | Millipore |
| Isopropyl-ß-D-1-thiogalactopyranoside (IPTG) | Thermo Scientific |
| L-Arginine | Sigma-Aldrich |
| L-Arginine.HCl $^{13}C^{15}N$-labeled | Silantes |
| L-Glutamine 200 mM | Thermo Scientific |
| L-Lysine | Sigma-Aldrich |
| L-Lysine.HCl $^{13}C^{15}N$-labeled | Silantes |
| Lipofectamine® 2000 RNAiMAX | Thermo Scientific |
| MOWIOL® 4-88 | Calbiochem |
| NeutrAvidin® Agarose Resin | Thermo Scientific |
| Ni-NTA Agarose | Qiagen |
| NuPAGE® MES SDS Running Buffer (20x) | Thermo Scientific |
| PageRuler Plus Prestained Protein Ladder | Thermo Scientific |
| PageRuler Unstained Protein Ladder | Thermo Scientific |
| Paraformaldehyde solution (16%) EM grade | Electron Microscopy Sciences |
| Pierce® 660 nm Protein Assay Reagent | Thermo Scientific |
| Poly-L-lysine solution 0.1% (w/v) | Sigma-Aldrich |
| Protease Inhibitor cocktail tablets | Sigma-Aldrich |
| Protein A-Agarose | Roche |
| Phenyl Sepharose® 6 Fast Flow | Sigma-Aldrich |
| Rapamycin 2.5 mg/ml in DMSO | Sigma-Aldrich |
| SafeView™ Classic nucleic acid stain | Applied Biological Materials Inc. |
| Trolox (6 Hydroxy 2,5,7,8 tetramethyl chromane 2 carboxylic acid) | Sigma-Aldrich |

### 2.1.6. Enzymes

| Enzyme | Company |
|---|---|
| Benzonase | Sigma-Aldrich |
| FastAP Thermosensitive Alkaline phosphatase | Thermo Scientific |
| Pfu Ultra II polymerase | Agilent |
| Phusion High-Fidelity DNA Polymerase | Thermo Scientific |

| Enzyme | Company |
|---|---|
| PNGase F | New England Biolabs |
| Restriction digestion enzymes | Thermo Scientific |
| T4 DNA ligase | Thermo Scientific |
| Trypsin/ EDTA 0.25% (1X) | Thermo Scientific |

### 2.1.7. Stock solutions

| Stock solution | Composition |
|---|---|
| 1,4-Dithiothreitol (DTT) | 1 M in $H_2O$ |
| Ammonium persulfate (APS) | 10% APS (Sigma) in $H_2O$ |
| Ampicillin | 100 mg/ml in $H_2O$ |
| Adenosine triphosphate (ATP) | 100 mM ATP in 100 mM $Mg(OAc)_2$, 20 mM HEPES pH7.4 |
| $CaCl_2$ buffer | 250 mM $CaCl_2$ $H_2O$ |
| Creatine phosphokinase | 2000 U/ml in 50% glycerol, 20 mM HEPES pH 7.4 |
| Creatine phosphate | 80 mg/ml in $H_2O$ |
| Cytosol | 14.321 mg/ml in Transport buffer |
| Digitonin | 10% (w/v) in DMSO |
| Isopropyl-β -D-1-thiogalactopyranoside (IPTG) | 1 M in $H_2O$ |
| Kanamycin | 50 mg/ml in $H_2O$ |
| Leupeptin/Pepstatin | 1 mg/ml each, in DMSO |
| Phenylmethylsulfonyl fluoride (PMSF) | 100 mM in 2-propanol |
| WGA (wheat germ agglutinin/lectin) | 2 mg/ml in Transport buffer |

### 2.1.8. Buffers

| Buffer | Composition |
|---|---|
| 1X TBST | 50 mM Tris, pH 7.5, 150 mM NaCl, 0.05% (v/v) Tween-20 |
| Coomassie de-staining solution | 10% acetic acid |
| Coomassie fixation solution | 40% ethanol, 10% acetic acid |
| Coomassie staining solution | 5% aluminum sulfate-(14-18)-hydrate, 10% ethanol, 2% ortho-phosphoric acid, 0.02% CBB-G250 |
| Cross-linking quenching buffer | 20 mM Tris-HCl, pH 7.4 |
| DNA loading buffer (6X) | 0.2% bromophenol blue, 0.2% xylene cyanole, 60% glycerol, 60 mM EDTA |
| GST buffer | 50 mM Tris, pH 6.8, 300 mM NaCl, 1 mM $MgCl_2$, 2 mM DTT, 0.1 mM PMSF, 1 µg/mL of each AP and LP |
| HEPES (2X) buffer | 50 mM HEPES, 250 mM NaCl, 1.5 mM $Na_2HPO_4$, pH 6.98 |
| His lysis buffer | 50 mM Tris HCl, pH 7.5, 500 mM NaCl, 20 mM imidazole, 5 mM β-Mercaptoethanol |
| Homogenization buffer | 10 mM HEPES, pH 7.8, 10 mM KCl, 1.5 mM $MgCl_2$ 0.1 mM EGTA containing 1 mM DTT, 1 mM PMSF, 1 µg/ml each of pepstatin, leupeptin and aprotinin. |
| IP lysis buffer | 0.5% sodium deoxycholate, 50 mM Tris-HCl, pH 7.4, 150 mM NaCl, 0.25% SDS, and 0.5% Triton X-100 with Complete protease inhibitor mixture |

| Buffer | Composition |
|---|---|
| IP wash buffer | 10 mM HEPES, 150 mM NaCl, 1 mM EGTA, 0.1 mM $MgCl_2$, 0.1% Triton X-100, and Complete protease inhibitor mixture |
| Laemmli running buffer (10X) | 250 mM Tris, 1.92 M glycine, 0.5% SDS |
| LB agar plates | LB supplemented with 1.5% (w/v) bacto-agar |
| LB-medium | 1% (w/v) bacto-tryptone, 0.5% (w/v) yeast extract, 1% (w/v) NaCl, pH 7.0 |
| NP-40 lysis buffer | 1% NP-40, 50 mM Tris HCl, pH 8, 5 mM EDTA, 5 mM EGTA, 15 mM $MgCl_2$, 60 mM ß-glycerolphosphate, 0.1 mM $NaVO_4$, 200 mM NaCl, 2 mM DTT, and aprotinin, leupeptin, PMSF (1 µg/ml) |
| PBS (10X) | 1.37 M NaCl, 27 mM KCl, 100 mM $Na_2HPO_4$, 18 mM $KH_2PO_4$, pH 7.5 |
| PLA Wash Buffer A | 0.01 M Tris, pH 8.0, 0.15 M NaCl, 0.05% Tween-20 |
| PLA Wash Buffer B | 0.2 M Tris, pH 7.5, 0.1 M NaCl |
| PonceauS staining solution | 0.5% PonceauS in 1% acetic acid |
| RAPIDS quenching buffer | 5 mM Trolox, 10 mM $NaN_3$, and 10 mM sodium ascorbate in PBS |
| RAPIDS wash buffer 1 | 50 mM HEPES, pH 7.4, 0.1% (w/v) sodium deoxycholate, 1% (v/v) Triton X-100, 500 mM NaCl, 1 mM EDTA |
| RAPIDS wash buffer 2 | 50 mM Tris HCl, pH 8.0, 250 mM LiCl, 0.5% (v/v) Nonidet P-40, 0.5% (w/v) sodium deoxycholate, 1 mM EDTA |
| RAPIDS wash buffer 3 | 50 mM Tris HCl, pH 7.4, 50 mM NaCl |
| RIPA buffer | 50 mM Tris HCl, pH 7.4, 5 mM Trolox, 0.5% (w/v) sodium deoxycholate, 150 mM NaCl, 0.1% (w/v) sodium dodecyl sulfate (SDS), 1% (v/v) Triton X-100, 1 mM phenylmethanesulfonyl fluoride, 10 mM $NaN_3$, 10 mM sodium ascorbate, aprotinin, leupeptin, and pepstatin (1 µg/ml) |
| SDS sample buffer (4X) | 125 mM Tris, pH 6.8, 4% SDS, 0.02% Bromophenol blue, 10% glycerol |
| SOC-medium | 2% (w/v) tryptone, 0.5% (w/v) yeast extract, 10 mM NaCl, 2.5 mM KaCl, 10 mM $MgCl_2$, 10 mM $MgSO_4$, 0.36% (w/v) glucose, pH 7.0 |
| TA protein high salt buffer | 50 mM HEPES, 500 mM KOAc, 5 mM $Mg(OAc)_2$, 10% glycerol, 1 mM PMSF, 1 mM DTT, pH 7.0, 20 mM imidazole |
| TA protein low salt buffer | 50 mM HEPES, 150 mM KOAc, 5 mM $Mg(OAc)_2$, 10% glycerol, 1 mM PMSF, 1 mM DTT, pH 7.0, 20 mM imidazole |
| TAE buffer (50X) | 2 M Tris, 0.05 M EDTA, 5.71% acetic acid |
| Transport buffer (TB) (10x) | 200 mM HEPES, 1.1 M KOAc, 20 mM $Mg(OAc)_2$, 10 mM EGTA, pH 7.3 |
| Western blot transfer buffer (10X) | 250 mM Tris, 1.93 M glycine, 0.2% SDS |
| Western blot transfer buffer (1X) | 10% Western blot transfer buffer (10X), 20% methanol |

### 2.1.9. Cell lines and bacterial strains

| Cell line | Specification |
|---|---|
| HeLa P4 (P4 MAGI CCR5+ Cells) | Human adenocarcinoma cell line that expresses CD4; derived from cervix of a 31-year-old woman, NIH AIDS Reagent program, (Charneau et al., 1994) |

| Bacterial Strain | Genotype |
|---|---|
| BL21AI | F- ompT hsdSB (rB– mB–) gal dcm araB::T7RNAP tetA |
| DH5α | F- Φ80lacZΔM15 Δ (lacZYA-argF) U169 recA1 endA1 hsdR17 (rK-,mK+) phoA supE44 λ- thi-1 gyrA96 relA1 |
| M15pREP4 | F- Φ80ΔlacM15 thi lac- mtl- recA+ KmR |

### 2.1.10. Antibodies

**Table 4. Primary antibodies**

| Name | Species | Origin | Application | Dilution |
|---|---|---|---|---|
| α-ACBD5 | rabbit | #21080-1-AP, Proteintech | Western blotting<br>IP: Western blotting<br>Immunofluorescence<br>PLA | 1:1000<br>1:500<br>1:100<br>1:100 |
| α-ELYS | rabbit | #ab14431, Abcam | Western blotting, IP | 1:500 |
| α-ELYS | rabbit | #HPA031658, Sigma-Aldrich | Immunofluorescence<br>PLA | 1:500<br>1:300 |
| α-emerin | rabbit | #10351-1-AP, Proteintech | Immunofluorescence<br>PLA | 1:1000<br>1:1000 |
| α-emerin | mouse | #AMAb90562, Sigma-Aldrich | IP: Western blotting | 1:500 |
| α-emerin* | rabbit | raised by Genosphere Biotechnologies | Western blotting | 1:1000 |
| α-GAPDH | rabbit | #10494-1-AP, Proteintech | Western blotting | 1:5000 |
| α-GFP | rat | #3H9, ChromoTek | Western blotting | 1:1000 |
| α-GM130 | mouse | # 610823, BD Biosciences | Immunofluorescence | 1:200 |
| α-Imp11 | rabbit | #PA1-41600, Invitrogen | Western blotting | 1:1000 |
| α-Imp13* | rabbit | Baade et al. (2018) | Western blotting | 1:1000 |
| α-Imp7* | rabbit | A. Nath | Western blotting | 1:2000 |
| α-Impβ* | rabbit | Frohnert et al. (2014) | Western blotting | 1:1000 |
| α-lamin B1 | rabbit | # ab16048, Abcam, | Western blotting | 1:1000 |
| α-laminA/C | rabbit | #2032, Cell signaling Technology | Western blotting | 1:1000 |
| α-laminA/C | mouse | #ab40567, Abcam | PLA | 1:100 |
| α-$Na^+/K^+$-ATPase | mouse | #sc-21712, Santacruz Biotechnology | Western blotting | 1:1000 |
| α-NUP153 | rabbit | # HPA027897, Sigma-Aldrich | Western blotting | 1:200 |
| α-Nup62 | rabbit | #HPA005435, Sigma-Aldrich | Western blotting | 1:1000 |
| α-opsin | mouse | Adamus et al. (1991) | Western blotting | 1:1000 |

| Name | Species | Origin | Application | Dilution |
|---|---|---|---|---|
| α-OSBPL9 | rabbit | #11879-1-AP, Proteintech | Western blotting<br>IP: Western blotting<br>Immunofluorescence<br>PLA | 1:1000<br>1:500<br>1:100<br>1:100 |
| α-PMP70 | mouse | # SAB4200181, Sigma-Aldrich | Immunofluorescence | 1:300 |
| α-POM121 | rabbit | #SAB2700248, Sigma-Aldrich | Western blotting | 1:1000 |
| α-SEC22b (29-F7) | mouse | #sc-101267, Santacruz Biotechnology | Western blotting | 1:250 |
| α-SP1 | rabbit | #1860528, Thermo Scientific | Western blotting | 1:1000 |
| α-Stt3B | mouse | Laboratory of Stephen High (Manchester, UK) | Western blotting | 1:1000 |
| α-TMEM43 | rabbit | #ab184164, Abcam, | Western blotting<br>IP: Western blotting | 1:1000<br>1:500 |
| α-TMPO | rabbit | #14651-1-AP, Proteintech | Western blotting | 1:1000 |
| α-TNPO1 | mouse | Clone D45, Sigma Aldrich | Western blotting | 1:1000 |
| α-TOR1AIP1 | rabbit | #HPA050546, Sigma-Aldrich | Western blotting | 1:1000 |
| α-TRC40 | rabbit | Favaloro et al. (2010) | Western blotting | 1:1000 |
| α-Tubulin | rabbit | #11224-1-AP, Proteintech | Western blotting | 1:2000 |
| α-VAPB | rabbit | #14477-1-AP, Proteintech | Western blotting<br>Immunofluorescence | 1:1000<br>1:200 |
| α-VAPB | mouse | #66191-1-Ig, Proteintech | Immunofluorescence<br>PLA<br>EM | 1:200<br>1:100<br>/ |

*Kehlenbach lab

**Table 5. Secondary antibodies**

| Name | Species | Origin | Application | Dilution |
|---|---|---|---|---|
| Duolink® In Situ PLA® probe Anti-mouse PLUS | donkey | Sigma-Aldrich | PLA | 1:5 |
| Duolink® In Situ PLA® probe Anti-Rabbit MINUS | donkey | Sigma-Aldrich | PLA | 1:5 |
| α-mouse 680 | donkey | LI-COR | Western blotting | 1:10,000 |
| α-mouse 800 | donkey | LI-COR | Western blotting | 1:10,000 |
| α-mouse IgG, 10 nm gold | goat | EM.GMHL10, BBI Solutions, Cardiff, UK | EM | / |
| α-mouse-Alexa Fluor 488 | donkey | #A-21202, Thermo Fisher Scientific, Waltham, MA, USA | Immunofluorescence | 1:1000 |
| α-rabbit 680 | donkey | LI-COR | Western blotting | 1:10,000 |
| α-rabbit 800 | donkey | LI-COR | Western blotting | 1:10,000 |

| Name | Species | Origin | Application | Dilution |
|---|---|---|---|---|
| α-rabbit-Alexa488 | donkey | #A-21206, Molecular Probes, Eugene, OR, USA | Immunofluorescence | 1:1000 |
| α-rabbit-HRP | donkey | #711-035-152,Jackson ImmunoResearch Laboratories, West Grove, PA, USA | Western blotting | 1:5000 |
| α-rat 800 | donkey | LI-COR | Western blotting | 1:10,000 |
| α-rat-HRP | goat | #112-035-003, Jackson ImmunoResearch Laboratories, West Grove, PA, USA | Western blotting | 1:10,000 |

### 2.1.11. Oligonucleotides

Oligonucleotides were purchased from Sigma-Aldrich with a concentration of 100 µM, a synthesis scale of 0.025 µmol and purification grade desalted. Restriction sites were added to the 5' end of the oligonucleotides and a 5' end overhang was added to ensure high efficiency of cleavage of the restriction enzyme. A melting temperature between 68-72°C was used for a two-step protocol using the Phusion DNA polymerase.

| Number | Name | Sequence (5'-3')* |
|---|---|---|
| G1268 | Lap2β-fwd-KpnI | TTTGGTACCACCGGAGTTCCTAGAG |
| G1269 | Lap2β-rev-SpeI | TTTACTAGTGAGATGTGGCATGAAGGC |
| G1386 | VAPB-rev-BamHI | GGATGGATCCCTACAAGGCAATCTTCCCAAT |
| G1390 | VAPB-fwd-KpnI | TTTGGTACCAGCGAAGGTGGAGCAGGTC |
| G1394 | VAPB-opsin-rev-BamHI | TTTGGATCCTCAGCCCGTCTTGTTGGAGAAAGGCACGTAGAAGTTTGGGCCCAAGGCAATCTTCCCAATAAT |
| G1395 | PTP1B-fwd-KpnI | TTTGGTACCCATGGAGATGGAAAAGGAGTTC |
| G1396 | PTP1B-rev-BamHI | TTTGGATCCCTATGTGTTGCTGTTGAACAG |
| G1424 | LBR-fwd-XhoI | TTTCTCGAGTTATGCCAAGTAGGAAATTTGCC |
| G1425 | LBR-rev-BamHI | TTTGGATCCCTAGTAGATGTATGGAAATATACG |
| G1511 | VAPB-fwd-SpeI | TTTACTAGTCTACAAGGCAATCTTCCCAAT |
| G1512 | VAPB-fwd-EcoRI | TTTGAATTCAATGGCGAAGGTGGAGCAGGTC |
| G1562 | FKBP12-fwd-AflII- | GCCTTAAGATGGCTAGCGGAGTGCAGGTGG |
| G1563 | FKBP12-rev-BamHI | GCGGATCCTTCCAGTTTTAGAAGCTCCAC |
| G1571 | APEX2-rev-BcuI | TTTACTAGTAAGGCATCAGCAAACCCAAG |
| G1573 | APEX2-fwd-BcuI | TTTACTAGTATGGGAAAGTCTTACCCAACTGT |
| G1854 | APEX2-fwd-EcoR1 | GCGAATTCTGGAAAGTCTTACCCAACTGTGAG |
| G1855 | APEX2-rev-BamH1 | GCGGATCCGGCATCAGCAAACCCAAGCTC |
| G2065 | Impβ (45-462)-fwd-NcoI | AAAACCATGGGCAAATCCAGGAAACA |
| G2066 | Impβ (45-462)-rev-BglII | TTTAGATCTAGCACTGAGACCCTCAATCAG |

*restriction sites are underlined

### 2.1.12. siRNAs

| siRNA | Sequence (5'-3') | Target | Source |
|---|---|---|---|
| siRNA non-targeting | UGGUUUACAUGUCGACUAA | non-targeting | Dharmacon |
| siVAPB | GCUCUUGGCUCUGGUGGUUUU | VAPB | Sigma-Aldrich |

### 2.1.13. Vectors

**Table 6. Available vectors**

| Number | Name | Tag | Resistance | Application | Source |
|---|---|---|---|---|---|
| - | pET28 | His, ZZ | amp | *in vitro* TnT | Pfaff et al. 2016 |
| 30 | pEGFP-C1 | EGFP | kan | transfection | Clontech |
| 49 | pEF-HA | HA | amp | transfection | - |
| 51 | pcDNA 3 | - | amp | transfection | Invitrogen |
| 66 | pmCherry-C1 | mCherry | kan | transfection | Clontech |

### 2.1.14. Plasmids

**Table 7. Available plasmids**

| Number | Name | Tag | Resistance | Application | Source |
|---|---|---|---|---|---|
| 552 | pEF-myc-Impβ | myc | amp | transfection | S. Hutten |
| 1051 | pmCherry-emerin | mCherry | kan | transfection | R. Kehlenbach |
| 1052 | pET328-HZZ-tev-emerin-opsin | His, ZZ, opsin | amp | *in vitro* TnT | R. Kehlenbach |
| 1232 | pmCherry-FRB-emerin | mCherry | kan | transfection | K. Rajanala |
| 1233 | pmCherry-FRB-Lap2β | mCherry | kan | transfection | J. Pfaff |
| 1237 | pQE80L-MBP-tev-TRC40-HZZ-tev-emerin-opsin | MBP, His, ZZ, tev | amp | expression | J. Pfaff |
| 1487 | pmCherry-FRB-VAPB | mCherry | kan | transfection | J. Pfaff |

| Number | Name | Tag | Resistance | Application | Source |
|---|---|---|---|---|---|
| 1495 | pmCherry-FRB-PTP1B | mCherry | kan | transfection | J. Pfaff |
| 1503 | pQE80L-MBP-tev-TRC40-His-ZZ-tev-VAPB-opsin | MBP, His, ZZ, tev | amp | expression | C. Spillner |
| 1573 | pmCherry-FRB-LBR | mCherry | kan | transfection | C. Spillner |
| 1584 | pEF-HA-FRB-VAPB | HA | amp | transfection | J. Pfaff |
| 1595 | pcDNA3 Connexin43-GFP-APEX2 | GFP | amp | transfection | Addgene |
| 1604 | pcDNA3-VAPB-opsin28 | opsin | amp | *in vitro* TnT | Fasana et al. (2010) |
| 1610 | pcDNA3-FKBP12-EGFP-APEX2 | GFP | amp | transfection | M. Müller |
| 1631 | pdEGFP-APEX2-cNLS-FKBP12 | GFP-GFP | kan | transfection | M. Müller |
| 1878 | pAPEX2-emerin | - | kan | transfection | M. Müller |

**Table 8. Generated plasmids**

| Number | Name | Tag | Resistance | Application | Cloning |
|---|---|---|---|---|---|
| 2063 | pQE60-His-Impβ (45-462) | His | amp | expression | Impβ (45-462) from #552 (G2065, G2066) in vector #31 (NcoI/BglII) |
| 2101 | APEX2-VAPB | - | amp | transfection | Apex2 from #1878 (Nhe1/Xho1) and VAPB from #1487 (G1512, G1386) in vector #66 (EcoRI/BamHI) |

## 2.2. Molecular biology methods

### 2.2.1. Polymerase chain reaction (PCR)

PCR reactions (Mullis KB, 1990) were performed using Phusion High-Fidelity DNA Polymerase according to the manufacturer's instructions. The reaction volume was set to 50 µl. The annealing temperature chosen was generally 5°C below the primer melting temperature. Elongation time was adjusted based on the size of the PCR product.

After the PCR reaction, a 6X DNA sample buffer was added. Based on the expected size of the PCR products, the sample was loaded onto agarose gels (2.2.2). PCR products were cut from agarose gels with a scalpel and purified with the NucleoSpin® Gel and PCR Clean-up kit (Macherey-Nagel). Purified DNA was eluted in 20 µl water. The concentration and purity of DNA were measured using NanoDrop 2000c.

### 2.2.2. Agarose gel electrophoresis

DNA fragments were separated using 1% agarose gels. The agarose was dissolved in 1X TAE buffer and boiled in a microwave oven until completely dissolved. 2 µl of Safe View Classic nucleic acid stain per 60 ml gel was added to the dissolved agarose solution.

The gel electrophoresis was performed in 1X TAE buffer at 100 V for 30 to 50 minutes, depending on the size of the product.

The GeneRuler 100 bp DNA Ladder or 1 kb DNA Ladder were used as molecular weight markers. The bands were cut on a UV transilluminator with a scalpel. Gels were documented with the GelSTICK "touch" system.

### 2.2.3. Restriction digestion

Restriction digestion was performed using Fast Digest restriction enzymes as per manufacturer's instructions. The total reaction volume was 20 µl for plasmids and PCR products. Agarose gel electrophoresis (2.2.2) was used to separate the digested DNA. Heat inactivation of the enzymes was performed as per manufacturer's instructions.

### 2.2.4. Dephosphorylation of digested vectors

Dephosphorylation of the digested vector was performed using FastAP Thermosensitive Alkaline Phosphatase that catalyzes the release of 5' phosphate from the DNA to prevent re-circularization of the linear vector. 1U of the enzyme was used per µg of the vector in 1X FastAP reaction buffer at 37°C for 10 minutes. The reaction was inactivated at 75°C for 5 minutes.

### 2.2.5. Ligation of DNA

Ligation of the linearized vector and DNA fragment was performed using the T4 DNA ligase. A molar ratio of 3:1 to 5:1 of insert DNA to vector was used with 100 ng of vector, 1U of the enzyme, 1X T4 DNA ligase buffer for a reaction volume of 10 µl. The reaction mix was incubated at room temperature for 1 hour, after which the enzyme was inactivated at 65°C for 10 minutes.

### 2.2.6. Transformation into *E. coli*

5 µl of ligation mix was added to 50 µl of chemically competent DH5$\alpha$ cells. The cells were incubated on ice for 20 minutes, followed by a heat shock at 42°C for 1 minute. The cells were then incubated on ice for 2 minutes and 300 µl of SOC medium was added. The mixture was shaken at a speed of 800 rpm at 42°C for 1 hour. After an hour, the cell suspension was centrifuged at 840 g for 3 minutes and the pellet was suspended in fresh 50 µl SOC-medium and plated on LB-agar plate with the respective antibiotic. The plates were incubated at 37°C overnight.

### 2.2.7. Purification of plasmid DNA

Mini preparation of plasmid DNA and midi preparation of plasmid DNA was performed depending on the scale of DNA purification. For mini preparation, a single colony picked from the agar plate was inoculated in 5 ml of LB medium containing the selective antibiotic. The culture was incubated at 180 rpm at 37°C overnight. Plasmid DNA was purified from the overnight culture using the NucleoSpin® Plasmid kit according to the manufacturer's instructions, and the purified DNA was eluted in 50 µl water. The isolated DNA was subjected to restriction digestion (2.2.3) to check for the correct insert DNA and sequenced (2.2.8).

For midi preparation, a pre-culture was made from a single colony picked from the agar plate inoculated in 5 ml of LB medium with the respective antibiotic and incubated at 180 rpm at 37°C for 8 hours. 2 ml of the pre-culture was added to 200 ml LB medium with the respective antibiotic and incubated at 180 rpm at 37°C overnight. The NucleoBond™ Xtra Midi kit was used to purify plasmid DNA according to the manufacturer's instructions and the purified DNA was eluted in water. The concentration of purified DNA was measured using Nanodrop 2000c and the concentration was adjusted to 1 µg/ml.

### 2.2.8. DNA sequencing

The plasmid DNA isolated was sequenced by GATC Biotech, a sub-company of Eurofins. Primers for sequencing were selected from the standard sequencing primer list available from GATC Biotech (https://eurofinsgenomics.eu).

## 2.3. Biochemical methods

### 2.3.1. SDS-PAGE

Separation of the proteins based on their molecular weight was performed by SDS-PAGE (Laemmli, 1970; Smith, 1994). Depending on the molecular weight of the proteins, separating gels of 10-12% acrylamide and 4% stacking gel were used. The gels were cast using Dual gel caster for mini vertical units. In addition to self-made gels, pre-cast gradient NuPAGE® Novex® 4-12% Bis-Tris gels were used. Samples were mixed with a 4X SDS sample buffer and heated at 95°C for 5 minutes. Samples, as well as the Page Ruler Plus pre-stained or unstained protein ladder, were loaded onto the gels. The self-made gel run was performed using 1X Laemmli buffer in Mighty Small II Mini Vertical Electrophoresis Units, and pre-cast gel run run using 1X NuPAGE® MES SDS running buffer. After electrophoresis, proteins were visualized with Coomassie staining (2.3.2) or subjected to Western blotting (2.3.3).

### 2.3.2. Coomassie staining

After SDS-PAGE, the proteins were visualized after Coomassie staining (Fazekas de St Groth et al., 1963). Gels were washed with water, fixed with Coomassie fixation solution for 10 minutes and washed again with water. The gels were then stained overnight using a Coomassie staining solution. For destaining, the gels were washed with water. Finally, they were imaged using Image reader LAS-3000. The images were analyzed and quantified by ImageStudioLite 5.25 software.

### 2.3.3. Western blotting

To visualize proteins after SDS-PAGE, Western blotting (Burnette, 1981) was performed. The proteins were transferred to an Amersham Protran 0.45 µm NC Nitrocellulose Blotting Membrane under wet conditions in 1X Western blot transfer buffer using Mini Trans-Blot® Cell of Bio-Rad. The transfer was performed at 100 V and 350 mA for 1.5 hours.

To check for uniform transfer and equal loading in all the lanes, a reversible Ponceau S staining was performed. The membrane was washed with 0.1% acetic acid and incubated with Ponceau S staining solution for 1-3 minutes. The membrane was then destained using a 1X TBST solution.

For immunodetection of proteins, the membrane was blocked with 4% milk in 1X TBST solution at room temperature for 1 hour followed by primary antibodies (Table 4) incubation at 4°C overnight. The membrane was then washed thrice with 1X TBST for 10 minutes, followed by incubation with either LICOR specific or HRP-coupled secondary

antibodies (Table 5) at room temperature for 1 hour. The membrane was washed thrice with 1X TBST for 10 minutes each and developed using Odyssey® Sa Infrared Imaging System of LI-COR or Image reader LAS-3000 depending on the secondary antibodies used. The images were analyzed and quantified by ImageStudioLite 5.25 software.

### 2.3.4. Protein purification

**MBP-tev-TRC40/His-ZZ-tev-VAPB-opsin**

Expression and purification of the TA protein in complex with TRC40 were performed as previously described (Favaloro et al., 2010; Pfaff et al., 2016). For protein expression, the plasmid coding for MBP-tev-TRC40/His-ZZ-Tev-VAPB-opsin was transformed (2.2.6) into BL21AI *E. coli* strain and plated on LB-ampicillin agar plate. A preculture was prepared by inoculating a single colony into 100 ml of LB medium supplemented with ampicillin by shaking at 37°C overnight. 5% of the preculture was used per liter of LB medium supplemented with ampicillin to scale up the culture to 3-6 liters and shaken at 130 rpm at 30°C until an $OD_{600}$ of 0.6 was reached. 0.05mM IPTG was added to induce the expression of MBP-tev-TRC40 at 30°C for 1 hour, and 0.25% (w/v) of L-Arabinose was added to induce the expression of His-ZZ-Tev-VAPB-opsin at 30°C for 4 hours. After the induction, cells were pelleted by centrifugation at 4500 g for 30 minutes.

The pelleted bacterial cells were resuspended in TA protein low salt buffer supplemented with protease inhibitors (1µg/ml each of aprotinin, leupeptin-pepstatin), 1 mM PMSF, 20 mM imidazole and 10 µg/ml DNase I. The cell suspension was then lysed using an Emulsiflex-C3 and subjected to centrifugation at 100,000 g for 30 minutes using an Avanti$^{TM}$ J-30I centrifuge with JA 30.50Ti rotor. The supernatant was collected and incubated with pre-equilibrated Ni-NTA agarose resin at 4°C for 1 hour in a rotating wheel to bind the His-tagged VAPB. The resin was centrifuged later at 250 g for 2 minutes and washed with low salt buffer containing 5 mM ATP to remove bacterial heat shock proteins. Next, the resin was washed with a TA protein high salt buffer followed by washing with low salt buffer. The protein was eluted from the resin using the low salt buffer containing 300mM imidazole by loading the resin into an empty column. The protein content of the eluted fractions was monitored using a Bradford assay solution. The protein containing fractions were pooled and incubated with a pre-equilibrated amylose resin at 4°C for 1 hour in a rotating wheel to bind the MBP-tagged TRC40, in complex with VAPB. The washing steps were followed, as described before. The recombinant MBP-tev-TRC40/His-ZZ-Tev-VAPB-opsin protein was eluted in low salt buffer containing 20 mM D-maltose. The purified protein was then dialyzed overnight at 4°C against transport buffer (TB) containing protease

inhibitors and 2 mM DTT. After dialysis, the proteins were frozen in liquid nitrogen and stored at -80°C.

**MBP-tev-TRC40/His-ZZ-tev-emerin-opsin**

MBP-tev-TRC40/His-ZZ-tev-emerin-opsin was purified as described before (Pfaff et al., 2016) and following the same procedure as described for MBP-tev-TRC40/His-ZZ-tev-VAPB-opsin.

**His-Impβ (45-462)**

His-Impβ (45-462) was expressed and purified as previously described (Kutay et al., 1997a). The plasmid coding for His-Impβ (45-462) was transformed in M15pREP4 *E. coli* and a single colony was inoculated in 100 ml LB medium supplemented with kanamycin and ampicillin and incubated by shaking at 37°C overnight. To scale up the cultures to 5 litres, 1% of the pre-culture was added per liter of LB medium and incubated by shaking at 110 rpm at 37°C until an $OD_{600}$ of 0.6 was reached. The cultures were induced for protein expression by adding 0.5 mM of IPTG and incubated at 16°C overnight, 110 rpm. The cultures were pelleted at 4500 g at 4°C for 30 minutes.

The pellet was resuspended in cold His lysis buffer supplemented with protease inhibitors (1µg/ml each of aprotinin, leupeptin-pepstatin), 1 mM PMSF, and the lysis was performed by using an Emulsiflex-C3. The suspension was centrifuged at 100,000 g at 4°C for 30 minutes using an Avanti$^{TM}$ J-30I centrifuge with JA 30.50Ti rotor. The supernatant was then incubated with pre-equilibrated Ni-NTA Agarose resin at 4°C for 2 hours in a rotating wheel. The sample was centrifuged at 250 g at 4°C for 3 minutes and the resin was washed with His lysis buffer containing 5 mM ATP to remove bacterial heat shock proteins. The resin was then loaded on to a column and eluted with His lysis buffer supplemented with 400 mM imidazole. Protein containing fractions were pooled and dialyzed overnight against a buffer containing 50mM Tris-HCl, pH 7.4 and 250 mM sucrose. The dialyzed proteins were frozen in liquid nitrogen and stored at -80°C.

**Ran and Ran Q69L**

Expression and purification of Ran and Ran Q69L was performed as described by (Melchior et al., 1995). The stocks used were prepared by C. Spillner (Kehlenbach lab).

### 2.3.5. *In vitro* membrane integration assay

*In vitro* membrane integration assays were performed as described before (Favaloro et al., 2010; Pfaff et al., 2016; Vilardi et al., 2011; Yamamoto and Sakisaka, 2012). These

assays were performed either using rough microsomes or cell-derived membranes as sources of ER membranes.

#### 2.3.5.1. Membrane integration into rough microsomes

*In vitro* transcribed and translated membrane proteins with an opsin tag, that gets glycosylated upon insertion into ER membranes were inserted into canine rough microsomes (Gilmore et al., 1982a; Gilmore et al., 1982b). The glycosylation of the protein was observed by a shift in molecular weight that can be detected by Western blotting. 200 ng of the constructs coding for proteins with a C-terminal opsin tag (pcDNA3 VAPB-opsin 28, pET328-HZZ-tev-emerin-opsin) were used for expression. The transcription and translation was performed using an *in vitro* TnT® T7 Quick Coupled Transcription/Translation System kit. The reaction mixture consisted of 8.8 µl rabbit reticulocyte lysate supplemented with 0.2 µl of 1 mM methionine. The reaction mix was incubated at 30°C for 90 minutes, after which 1 µl of canine rough microsomes was added and incubated for an additional 60 minutes. The reaction was stopped by the addition of 50 µl 4X SDS sample buffer and heated at 95°C for 5 minutes. The samples were subjected to SDS-PAGE and Western blotting. The glycosylated and non-glycosylated proteins were detected using an anti-opsin antibody.

To validate post-translational membrane integration, the same assay was performed with the addition of puromycin at a final concentration of 2.5 mM at the start of reaction (at 0 minutes) and after the first 90 minutes incubation step at 30°C for 10 minutes.

The canine rough microsomes were a gift from the lab of Prof. Blanche Schwappach.

### Deglycosylation of membrane inserted proteins using PNGase F

To confirm for N-glycosylation of opsin tagged protein, a deglycosylation reaction using peptide-N-glycosidase F (PNGase F) was performed as described (Pfaff et al., 2016). 10% of the reaction mix was incubated with 1 µl glycoprotein-denaturing buffer at 99°C for 10 minutes. The denatured mixture was then incubated with 1 µl PNGase F or water as a control, 2 µl G7 reaction buffer (0.5 M sodium phosphate buffer, pH 7.5) and 2 µl NP40 (10% stock) with a final volume of 20 µl with water. The deglycosylation reaction was performed at 37°C for 1.5 hours. 4X SDS sample buffer was added to the reaction, and samples were analyzed by SDS-PAGE (2.3.1) and Western blotting (2.3.3).

#### Membrane integration assay in the presence of MBP-WRBcc or GST-CAML-N

To assess the membrane insertion via receptors of the TRC40 pathway, WRB and CAML, two inhibitory fragments WRBcc (Blenski and Kehlenbach, 2019; Pfaff et al., 2016;

Vilardi et al., 2011) and CAML-N (Blenski and Kehlenbach, 2019; Pfaff et al., 2016; Yamamoto and Sakisaka, 2012) were used in insertion assays. After the transcription and translation step, 5 or 10 µM of purified MBP-WRBcc or GST-CAML-N was added to the reaction mixture and the sample was incubated at 30°C for 10 minutes prior to the addition of rough microsomes. The reaction was further processed as in section 2.3.5.1.

The WRBcc and CAML-N fragments were a gift from the lab of Prof. Blanche Schwappach.

**Immunodepletion of TRC40 from rabbit reticulocyte lysate**

The immunodepletion of TRC40 from rabbit reticulocyte lysate was performed using antibodies against rabbit TRC40 as previously described (Favaloro et al., 2010; Leznicki et al., 2010; Pfaff et al., 2016). Protein A Sepharose 4 Fast flow beads (20µl) were washed withl cold PBS and centrifuged at 500 g at 30°C for 2 minutes. 1.5 µg of rabbit anti-TRC40 or rabbit IgG antibodies were added to the beads in 500 µl PBS and incubated at 4°C for 1 hour in a rotating wheel. After binding of TRC40 or IgG antibodies, the beads were washed with cold PBS and centrifuged at 500 g at 30°C for 2 minutes. 120 µl rabbit reticulocyte lysate per condition was added to the immobilized beads and incubated at 4°C for 1 hour on a rotating wheel. The beads were centrifuged at 13,000 g at 4°C for 1 minute, and the supernatant was used for microsome integration assay as described above. To control for the efficiency of immunodepletion, 5ul of depleted lysates were analyzed by SDS-PAGE (2.3.1) and Western blotting (2.3.3) using antibodies against TRC40.

### 2.3.5.2. Membrane integration into semi-permeabilized cells

In addition to rough microsomes, semi-permeabilized or digitonin treated cells can be used as a source of ER membrane in membrane integration assays. HeLa cells were trypsinized and washed with PBS. The cells were counted using an automated cell counter (CASY 1). 10,000 cells/µl of TB containing protease inhibitors (1 µg/ml each of aprotinin, leupeptin-pepstatin) were permeabilized with 0.01% digitonin on ice for 5 minutes. Permeabilization efficiency was controlled by trypan blue staining. The cells were washed thrice with TB and resuspended again in TB. For the membrane integration assay, 200 ng of TA protein in complex with TRC40, permeabilized cells. (20,000 cells), and 1 mM ATP was mixed and added up to a volume of 100 µl in TB. The reaction mixture was incubated either at 30°C or at 4°C for 1 hour and was centrifuged at 16,000 g at 4°C for 10 minutes, and the pellet was washed in TB and pelleted again. 50 µl 4X SDS sample buffer was added to the pellet and heated at 95°C for 5 minutes. The samples were subjected to SDS-PAGE (2.3.1) and Western blotting (2.3.3). The glycosylated and non-glycosylated proteins were detected using an anti-opsin antibody.

### 2.3.6. Subcellular fractionation

Subcellular fractionation was performed as described previously (Cheng et al., 2019) and as explained in James et al., 2019 (Supplementary Figure 1). HeLa cells were lysed by douncing in homogenization buffer (HB) containing protease inhibitors (1µg/ml each of aprotinin, leupeptin-pepstatin) and 1 mM PMSF. The whole-cell lysate was layered on top of 2.5 ml shelf of 0.8 M sucrose in HB and centrifuged in a JS4.2 rotor at 2,000 rpm at 4°C for 10 minutes yielding the pellet and the cytoplasmic fraction. The pellet was resuspended in 1.8 M sucrose and layered on top of a 2 ml 2 M sucrose cushion. The gradient was then centrifuged at 35,000 rpm at 4°C for 1 hour in an SW40 Ti rotor. The nuclear pellet was resuspended in HB containing 500 mM NaCl, 1 mM $CaCl_2$ and 25 U/ml benzonase, incubated for 15 minutes at 37°C, layered on top of 2 ml 0.8 M sucrose and centrifuged at 4,000 rpm at 4°C for 10 minutes in a JS4.2 rotor. The layer above the sucrose cushion (nuclear content fraction) and the pellet (nuclear envelope fraction) were collected.

### 2.3.7. Cross-linking and co-immunoprecipitation

Cross-linking and co-immunoprecipitation assays that were performed to validate interaction of proteins, are described in detail in James et al., 2019.

Co-immunoprecipitation using the nuclear envelope fraction obtained by subcellular fractionation (2.3.6) was performed as described in James et al., 2019 (supplementary Figure 1). Briefly, the nuclear envelope fraction was resuspended in NP-40 lysis buffer supplemented with protease inhibitors (1µg/ml each of aprotinin, leupeptin-pepstatin) and 1 mM PMSF. Immunoprecipitation of the proteins were done using antibodies against rabbit VAPB or rabbit IgG as a control. The proteins were detected using Western blotting (2.3.3).

### 2.3.8. Nuclear transport receptor depletion using phenyl sepharose

HeLa cytosol (Ipracell) was depleted of nuclear transport receptors, as described by Ribbeck and Görlich, 2002. 500 µl of cytosol was added to 80 µl of Phenyl-Sepharose 6 Fast flow resin and incubated at 4°C for 1 hour in a rotating wheel. The mixture was centrifuged at 800 g at 4°C for 2 minutes, and the depleted supernatant was tested for the efficiency of the depletion of various nuclear transport receptors by Western blotting.

## 2.4. Cell biology methods

### 2.4.1. Culturing of mammalian cells

HeLa P4 cells (Charneau et al., 1994) were grown in Dulbecco's Modified Eagle Medium (DMEM) containing 10% fetal bovine serum (FBS), 2 mM L-glutamine, 100 U/ml penicillin and 100 µg/ml streptomycin at 37°C and 5% $CO_2$. Cells were passaged twice a

week for maintaining optimal cell growth and were tested regularly for *Mycoplasma* contamination.

### 2.4.2. Poly-L-Lysine coating of coverslips

Coverslips were coated with Poly-L-Lysine to enhance adhesion of cells. The coated coverslips were used for proximity ligation assay (PLA; 2.4.6) and *in vitro* import assay (2.4.7). Coverslips were washed with 100% ethanol, air-dried and coated with 0.1% Poly-L-Lysine at room temperature for 30 minutes. The coverslips were then washed once with water, air-dried and sterilized with UV at 0.12 J/cm$^2$ for 3 minutes.

### 2.4.3. Transfection of plasmid DNA and siRNA in mammalian cells

The transfection of plasmid DNA was performed according to the calcium-phosphate method (Chen and Okayama, 1987). 40,000 HeLa P4 cells were seeded per well of a 24-well plate on the day prior to transfection. The next day, plasmid DNA (0.5-0.7 µg) was mixed with 20 µl of 250 mM $CaCl_2$ and vortexed for 5 seconds. Then, 20 µl of 2X HEPES buffer was added to the mixture and vortexed for 10 seconds. The transfection mix was incubated at room temperature for 20 minutes and added to the cells, which were then grown as described in 2.4.1.

siRNA mediated knockdown of HeLa P4 cells was carried out using Lipofectamine RNAiMax based on the manufacturer's protocol. 65,000 cells were seeded per well of a 24-well plate on the day before transfection. 100 nM siRNA was added to 50 µl opti-MEM and 1 µl Lipofectamine RNAiMax to 50 µl opti-MEM in separate tubes and incubated at room temperature for 5 minutes. After 5 minutes, the solutions were mixed and incubated for another 15 minutes. The mixture was added to cells in DMEM medium (2.4.1) without antibiotic.

### 2.4.4. Indirect immunofluorescence

For the detection of endogenous or overexpressed proteins, indirect immunofluorescence was performed. Cells grown on coverslips were washed with PBS and fixed with 4% paraformaldehyde. Cells tagged with fluorescently labeled proteins were mounted directly using Mowiol containing 1 µg/ml DAPI. For immunofluorescence, fixed cells were permeabilized with 0.5% Triton X-100 for 5 minutes, followed by washing thrice with PBS. To reduce non-specific binding of the antibodies, the cells were blocked with 3% BSA in PBS (blocking buffer) for 20 minutes. After blocking, primary antibodies (Table 4) diluted in blocking buffer were added and incubated for 1 hour in a dark humidity chamber. The unbound antibodies were washed off with PBS, and the cells were then incubated with fluorescently labeled secondary antibodies (Table 5) diluted in blocking buffer for another

hour in the dark humidity chamber. Cells were washed with PBS, air-dried and mounted using Mowiol containing 1 µg/ml DAPI.

### 2.4.5. Confocal microscopy

Microscopic analysis of the fluorescently labeled proteins was done using a LSM 510 confocal laser-scanning microscope with a 63X/1.4 oil immersion lens. Depending on the fluorophores used, distinct filter sets with a combination of a maximum of four lasers were used for excitation. DAPI was excited using a Diode 405 nm laser, GFP and the AlexaFluor488 dye using the tunable Argon 458/477/488/514 nm laser, mCherry and the AlexaFluor594 dye using HeNe 594 nm laser and AlexaFluor647 dye using HeNe 633 nm laser. A multi-track image acquisition mode was used in the LSM software for acquiring images. Laser output was adjusted to reduce bleaching effects, and the pinhole was set to 1 airy unit. The image intensity was adjusted using the Detector gain and the Amplifier Offset. Low scanning speed was used to get a high-resolution image. The acquired images were analyzed using Zen 3.1 and LSM image browser software.

### 2.4.6. Proximity ligation assay and image analysis by cell profiler

To detect proteins in close proximity, the Duolink®*in situ* Proximity ligation assay kit was used. The assay was performed as described in James et al., 2019.

The images acquired were analyzed for PLA interactions using CellProfiler 2.2 (Carpenter et al., 2006). A pipeline was designed to quantify the number of PLA interactions in the whole-cell and the nucleus. Using the module “Identify Primary Object’’, cell nuclei were identified based on DAPI images. The diameter of primary objects was set to 70-140 pixels, and two-class Otsu adaptive thresholding was used. The whole-cell was identified using the “Identify Secondary Object’’ module with the Distance-N method based on the images of protein of interest and by expanding the nuclear area by 80 pixels. Cells touching the border of the image were excluded from the analysis. PLA interactions were identified with the “Identify Primary Object’’ module using PLA images and by setting a diameter of 2-10 pixels for the PLA interactions. A two-class Otsu adaptive thresholding with a minimum threshold value of 0.15 was set. With the module “Relate objects’’, the identified PLA interactions identified in the nucleus and whole cells were related back to the previously identified nucleus and whole cell. Data was exported with the module “Export to spreadsheet’’ and the number of PLA interactions was plotted and analyzed using GraphPad prism 5.03.

### 2.4.7. *In vitro* import assay

Import assay was essentially performed as described previously by Adam et al., 1990. HeLa P4 cells (65,000 cells/well) were seeded in 24-well plates. After 24 hours, the cells were washed twice with cold TB and permeabilized with 0.007% digitonin on ice for 5 minutes. The efficiency of permeabilization was monitored by trypan blue staining. The soluble proteins were washed out by washing three times with TB. The cells were then incubated with 40 µl import reaction mixture at 30°C for 25 minutes in a dark humidity chamber. The reaction mixture consisted of cytosol (0.125 µg/µl) or cytosol supplemented with either of the factors like Ran (1 µg/µl), Ran Q69L (1 µg/µl), WGA (0.2 µg/µl), Impβ (45-462) (1 µM) and Cy3-BSA-NLS (1:4 dilution in TB) and ATP regenerating system (1 mM ATP, 4 mM creatine phosphate, 100 U/ml creatine phosphokinase). After incubation, the cells were washed with TB and fixed with 4% paraformaldehyde and mounted using Mowiol containing DAPI.

### 2.4.8. Fluorescence loss after photobleaching (FRAP) assay

FRAP assays were performed using a confocal 510 laser scanning microscope with a HeNe 594 nm laser with a 63X/1.4 oil immersion lens. For transfection, HeLa cells (20, 000 cells /well) were seeded in 8-well Lab Tek chambered coverglass. 24 hours after transfection, cells were washed thrice with TB and subjected to FRAP assays directly. Alternatively, the cells were permeabilized with 0.007% digitonin, washed and 200 µl of transport reaction mix in TB was added before subjecting to FRAP assays. The reaction mixture consisted of either cytosol or cytosol supplemented with factors like Ran, Ran Q69L, WGA, Impβ (45-462) or TRC40 and nuclear transport factor depleted cytosol (2.3.8). The concentration of the different factors used was the same as that used for *in vitro* import assay (2.4.7). For the FRAP assays, 3 pre-bleach images were taken, followed by bleaching an area of 5 $\mu m^2$ at the NE or 10 $\mu m^2$ at the ER using 100% laser intensity with the number of iterations set to 80. After bleaching, fluorescence recovery was measured every 7.86 seconds for 25 cycles per cell with a laser intensity of 5%. The intensity value was collected for different time intervals using the LSM FRAP module for a region of interest in the bleached area, in an unbleached adjacent cell and the background. The region of interest was applied to each frame in a FRAP experiment. The intensity of the region of interest was normalized to the intensity of the adjacent cell and the background. The recovery curves were then plotted and analyzed using GraphPad prism 5.03.

### 2.4.9. Rapamycin-dependent dimerization assay

In order to monitor localization of a protein of interest to the inner nuclear membrane, a rapamycin-dependent dimerization assay was used as described previously (Blenski and

Kehlenbach, 2019; James et al., 2019; Ohba et al., 2004; Pfaff et al., 2016; Ungricht et al., 2015). In this assay, rapamycin binds to a 12-kDa FK506-binding protein (FKBP12) and an FKBP-rapamycin-binding (FRB) cassette, promoting rapid interaction of the appropriately tagged proteins (Chen et al., 1995). HeLa cells (40,000 cells/well) were seeded on coverslips in a 24-well plate and transfected the next day with plasmids coding for FKBP12 reporter and FRB cassette fused to protein of interest. After 24 hours of transfection, cells were washed with TB and permeabilized with 0.007% digitonin for 5 minutes on ice. The cells were washed thrice with TB and the efficiency of permeabilization was monitored by trypan blue staining. Then, the cells were treated with 200 nM rapamycin in TB and incubated for 10 minutes on ice to allow dimerization of FKBP12 and FRB domains. The cells were washed again and fixed using 4% paraformaldehyde and mounted using Mowiol containing DAPI.

### 2.4.10. Immunoelectron microscopy

Immunoelectron microscopy was performed in HeLa cells as described by James et al., 2019, by Prof. Martin W. Goldberg, Durham University.

## 2.5. Rapamycin and apex dependent identification of proteins by SILAC (RAPIDS)

RAPIDS uses APEX2 based proximity labeling with rapamycin-dependent targeting of the peroxidase to a protein of interest, to identify proteins that are in close proximity by SILAC and quantitative mass spectrometry (James et al., 2019; Müller et al., 2020).

### 2.5.1. FBS dialysis

FBS was dialyzed against sterile 1X PBS to remove detectable amounts of free amino acids present in the serum (Ong et al., 2002). The dialysis was performed using a Spectra/Por® Dialysis Membrane with a molecular weight cut-off of 6-8 kDa. PBS was changed after 1 hour, overnight and again after one hour of exchange at 4°C with constant stirring. The dialyzed FBS was frozen and stored at -20°C.

### 2.5.2. Stable isotope labeling of amino acids in cell culture (SILAC)

For SILAC, HeLa P4 cells were grown in DMEM without L-glutamine, L-arginine, L-lysine supplemented with 10% dialyzed FBS, 6 mM L-glutamine, 100 U/ml penicillin, 100 µg/ml streptomycin and heavy and light isotopes of amino acids arginine and lysine. For SILAC media with heavy isotopes, 0.4 mM L-[$^{13}C_6$,$^{15}N_2$] lysine and 0.2 mM L-[$^{13}C_6$,$^{15}N_4$] arginine were added and with light isotopes, 0.4 mM L-[$^{12}C_6$,$^{14}N_2$] lysine and 0.2 mM L-[$^{12}C_6$,$^{14}N_4$] arginine were added. Cells were passaged 5-7 times in the SILAC medium to

ensure sufficient incorporation of heavy amino acids. The incorporation rates were above 97% for all the experiments performed, which was confirmed by mass spectrometry.

### 2.5.3. Rapamycin-dependent biotinylation assay

The day prior to transfection, 2 x$10^6$ HeLa P4 cells (heavy or light amino acid labeled) per 10 cm dish were seeded. A total of eleven 10 cm dishes were used per experiment, 5 dishes for cells grown in medium with heavy amino acids (heavy SILAC medium) and 5 dishes for cells grown in medium with light amino acids (light SILAC medium). One extra dish was seeded with cells grown in heavy SILAC medium to control for incorporation of heavy amino acids. To control for transfection efficiency by indirect immunofluorescence, one coverslip per dish was added. The next day, cells were transfected with APEX tagged FKBP12 reporter and FRB tagged VAPB constructs using Calcium phosphate method of transfection (2.4.3). The plasmids used for transfection were mCherry-FRB-VAPB and pcDNA3-FKBP12-GFP-APEX2 or pEF-HA-FRB-VAPB and pAPEX2-dGFP-NLS-FKBP12. After 24 hours of transfection, cells were incubated with 500 µM biotin-phenol with or without 200 nM rapamycin at 37°C for 30 minutes. The experiment was performed in forward and reverse conditions. For forward condition, cells grown in light SILAC medium were treated with rapamycin, and cells grown in heavy SILAC medium were not. For reverse conditions, this labeling scheme was switched. After the addition of biotin-phenol and rapamycin, cells were treated with 1 mM $H_2O_2$ at room temperature for 1 minute. The medium was aspirated, cells were washed twice with RAPIDS quenching buffer and once with PBS. Cells on coverslips for fluorescence microscopy were fixed with 4% paraformaldehyde and further processed by indirect immunofluorescence (2.4.4).

### 2.5.4. Biotinylated protein enrichment and Western blotting

Cells from each dish were lysed with 1 ml RIPA buffer, scraped and incubated on ice for 5 minutes. The harvested cells were centrifuged at 16,000 g at 4°C for 10 minutes. The protein concentration of the cleared ‘heavy labeled’ and ‘light labeled’ lysates for both forward and reverse conditions was determined using Pierce 660 nm Protein Assay. For Western blotting, 2 ml of each lysate of equal concentrations was transferred to two 1.5 ml tubes. For mass spectrometric analysis, 3 ml of equal concentrations of heavy labeled and light labeled lysates were combined in 1:1 ratio and transferred to six 1.5 ml tubes for either forward or reverse condition. To each 1.5 ml tubes, 130 µl NeutraAvidin Agarose Resin was added and incubated at 4°C overnight in a rotating wheel to enrich for biotinylated proteins. The beads were centrifuged at 800 g, 4°C for 2 minutes. The beads were washed once with wash buffer 1, once with wash buffer 2 and twice with wash buffer 3 with a washing interval of 8 minutes each. After the last washing step, the proteins bound to the beads were eluted

with 90 µl of 4X SDS sample buffer supplemented with 5 mM desthiobiotin. To increase protein concentration, beads from three tubes were pooled for mass spectrometry analysis and beads from two tubes were pooled for Western blotting. The samples were analyzed using NuPAGE® Novex® 4-12% Bis-Tris Protein Gels and subjected to Western blotting (2.3.3).

### 2.5.5. Mass spectrometric analysis

The mass spectrometric analysis was performed as described in James et al., 2019 in collaboration with Dr. Christof Lenz and Prof. Dr. Henning Urlaub (Core Facility Proteomics, University Medical Center Göttingen).

For statistical evaluation of the data Perseus software (Tyanova et al., 2016) was used. The workflow used in Perseus for identification of proteins in close proximity is described in Table S1 (Appendix).

# Chapter 3:
# Membrane insertion of VAPB

# Chapter 3 : Membrane insertion of VAPB

## 3.1. Introduction

(see also 1.8)

Vesicle-associated membrane protein-associated protein B (VAPB) is an ER-resident, tail-anchored (TA) protein that belongs to a ubiquitously expressed family of proteins called VAPs. VAPB is involved in lipid metabolism and transport (Loewen et al., 2003; Rocha et al., 2009), membrane trafficking, organelle transport along microtubules (Foster et al., 2000; Kagiwada et al., 1998; Kawano et al., 2006; Peretti et al., 2008; Skehel et al., 1995) and unfolded-protein-response (Kanekura et al., 2006; Suzuki et al., 2009). VAPB has an N-terminal Major Sperm Protein (MSP) domain, a coiled-coil (CC) domain and a C-terminal transmembrane domain (TMD) at the very end of the tail, defining it a C-tail-anchored (TA) protein (Figure 11; Borgese et al., 2007).

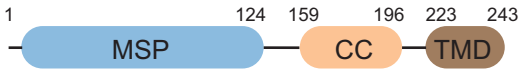


**Figure 11. Domain structure of VAPB.**
243-residue human VAPB consists of a major sperm protein (MSP) domain, a coiled-coil (CC) and a C-terminal transmembrane domain (TMD). See also Figure 8.

Interest in studying VAPB was heightened in the past decades because of the identification of dominant missense mutations in the *VAPB* gene in patients affected with a familial form of amyotrophic lateral sclerosis disease (ALS; Nishimura et al., 2004). The best characterized interaction of VAPB is the one, where its MSP domain interacts with the protein ligands bearing two phenylalanine in an acidic tract (FFAT motif; Loewen and Levine, 2005; Loewen et al., 2003).

Most TA proteins are known to integrate into the ER-membrane post-translationally. A conserved machinery for the post-translational insertion into the ER has been studied in yeast and mammalian cells (Aviram et al., 2016; Favaloro et al., 2008; Guna et al., 2018; Stefanovic and Hegde, 2007). One of the key players in the insertion mechanism of TA protein is the transmembrane domain recognition complex protein of 40 kDa (TRC40) also known as arsenical pump-driving ATPase protein (ASNA1) in mammals; guided entry of tail-anchored protein 3 (Get3) in yeast (Favaloro et al., 2008; Stefanovic and Hegde, 2007). Tryptophan-rich basic protein (WRB) and $Ca^{2+}$-mediating cyclophilin ligand (CAML) function as receptors of TRC40 in the ER-membrane (Vilardi et al., 2011; Vilardi et al., 2014; Yamamoto and Sakisaka, 2012). Being a TA protein, VAPB is predicted to insert into the ER membrane using the post-translational mechanism of insertion (see 1.4.1.2; Borgese et

al., 2007). Interestingly, VAPB was also reported to interact with TRC40 (Baron et al., 2014; Coy-Vergara et al., 2019).

This chapter investigates the requirements for ER-membrane insertion of VAPB, focusing on TRC40 mediated insertion using *in vitro* studies. Rough microsomes and semi-permeabilized cells were used as ER membrane sources for these studies. To study the insertion mechanism, either an opsin-tagged VAPB alone or in a complex with TRC40 was used. The N-glycosylation site (opsin tag) fused to the C-terminus of the protein of interest can be modified by luminal glycosyltransferase in the ER upon insertion (Pedrazzini et al., 2000).

## 3.2. Results

### 3.2.1. Membrane insertion mechanism of VAPB

VAPB is predicted to insert post-translationally into ER membrane because of its TA topology (Borgese et al., 2007). Since VAPB belongs to the class of TA-proteins, TRC40-mediated pathway for TA-protein targeting to the ER (Colombo et al., 2016) was addressed in an initial attempt to study the mechanism of insertion. VAPB interacts with TRC40 through its FFAT-like motif (Baron et al., 2014) and was shown to interact with TRC40 by using a 'trap' approach involving a dominant-negative ATPase-impaired mutant of TRC40 (Coy-Vergara et al., 2019).

#### 3.2.1.1. VAPB is inserted post-translationally into microsomal membranes

To determine whether VAPB can be inserted post-translationally into ER membrane, a rough microsome insertion assay (Abell et al., 2007; Favaloro et al., 2010; Vilardi et al., 2011) was performed. In this assay, microsomes were used as a source of ER-membrane and an opsin-tag fused to the C-terminus of the target protein was used to monitor membrane insertion. Emerin tagged with opsin was used as a positive control. The proteins of interest were synthesized in an *in vitro*-transcription/translation system. Insertion into rough microsomes was monitored by N-linked glycosylation of an opsin-tag at the very C-terminal end of the protein (Figure 12A). As shown in Figure 12B, VAPB-opsin and emerin-opsin were synthesized in reticulocyte lysates. A shift in molecular weight of the protein, indicating glycosylation, was observed after the addition of rough microsomes. To determine whether VAPB is post-translationally inserted into microsomes, the translation inhibitor puromycin was added 90 minutes after the start of the transcription/translation reaction. 10 minutes after the addition of puromycin, rough microsomes were added to initiate post-translational membrane insertion. Even after the addition of puromycin, a membrane inserted (glycosylated) form of VAPB was observed, suggesting that the protein is post-translationally inserted (Figure 12B). Note that puromycin added at the beginning of the reaction (t=0 min) completely inhibited protein synthesis. As reported before (Pfaff et al., 2016), emerin was also observed to be post-translationally inserted (Figure 12B). This result shows that both VAPB and emerin are post-translationally inserted into the ER membrane.

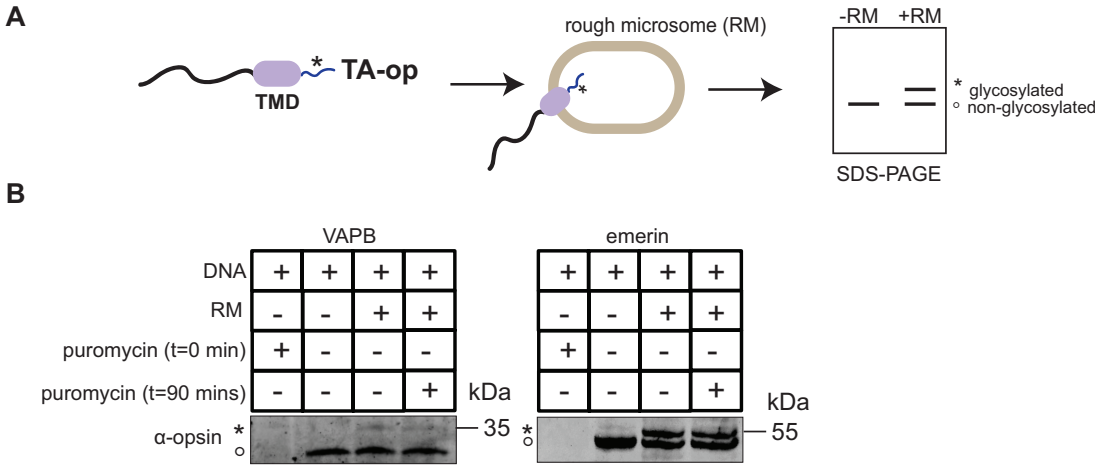


**Figure 12. VAPB and emerin are post-translationally inserted into microsomes.**
(A) Schematic depiction of *in vitro* membrane insertion assay. Tail-anchored-opsin (TA-op) proteins were synthesized in an *in vitro*-transcription/translation system and subsequent membrane insertion was carried out into rough microsomes. A shift in molecular weight occurs due to glycosylation of the opsin-tagged protein, which can be detected by Western blotting. (B) VAPB-opsin and emerin-opsin were synthesized by *in vitro*-translation/transcription system. Puromycin was added before translation/transcription step (t=0 min) or after for 10 minutes (t=90 mins) and the *in vitro* reaction mix was incubated in the presence of rough microsomes. After Western blotting the glycosylated bands were detected using an anti-opsin antibody. * indicates glycosylated protein and ° indicates non-glycosylated protein.

### 3.2.1.2. *In vitro* translated VAPB is inserted into microsomal membranes

To further confirm that the shift in molecular weight of the protein resulted from glycosylation, peptide-N-glycosidase F (PNGase F) was added to 10% of the reaction mix. As a control, PNGase buffer alone was added to another 10% of the reaction mix. Indeed, only a non-glycosylated form of the proteins was observed upon PNGase treatment, indicating deglycosylation of both VAPB-opsin and emerin-opsin compared to the samples treated with buffer alone (Figure 13). This result demonstrates that the proteins had originally been N-glycosylated and the opsin-tag with its N-glycosylation site have reached the microsomal lumen, confirming membrane insertion of VAPB and emerin.

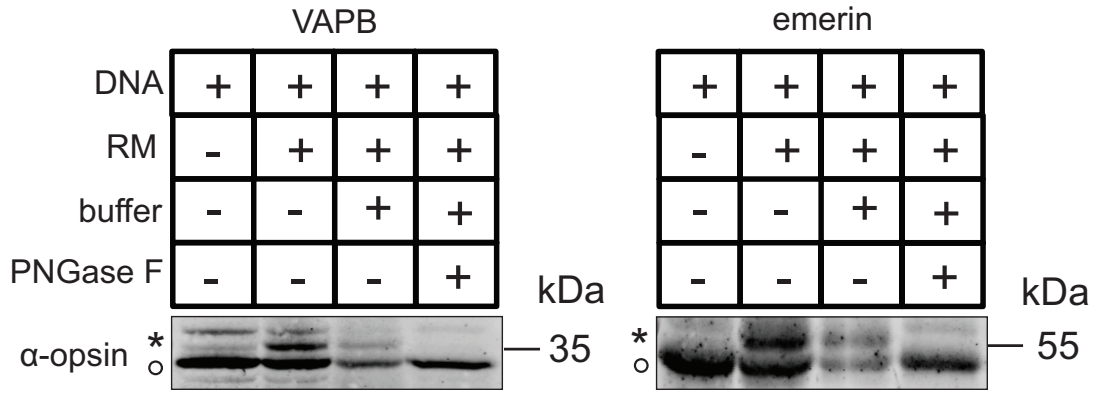


**Figure 13. Membrane insertion of *in vitro* translated VAPB-opsin and emerin-opsin.**
VAPB-opsin and emerin-opsin synthesized by *in vitro*-translation/transcription system was incubated in the presence of rough microsomes. 10% of each reaction mix with rough microsomes was taken and incubated either with PNGase buffer alone or with PNGase to facilitate deglycosylation. The samples were subjected to Western blotting and probed with an anti-opsin antibody to control for glycosylation. * indicates glycosylated protein and ° indicates non-glycosylated forms of VAPB or emerin.

### 3.2.1.3. Membrane insertion of recombinant TRC40/VAPB complex into semi-permeabilized cells

In order to characterize the association of VAPB with TRC40 in the context of membrane insertion, recombinant VAPB tagged with opsin was purified in a complex with TRC40.

#### Co-expression of VAPB with TRC40

VAPB was expressed in BL21AI *E. coli* strain that allows induction of protein expression using an arabinose-inducible promoter or IPTG inducible promoter, as a fusion protein carrying an N-terminal HZZ-tag (i.e. a His tag linked to an IgG-binding ZZ-domain) and a C-terminal N-glycosylation site (an 'opsin' tag), together with MBP (maltose-binding protein)-tagged TRC40 (Figure 14A). The two distinct bands obtained after amylose elution suggest that TRC40 and VAPB were co-purified successfully (Figure 14B). This confirms that VAPB can indeed form stable complexes with TRC40.

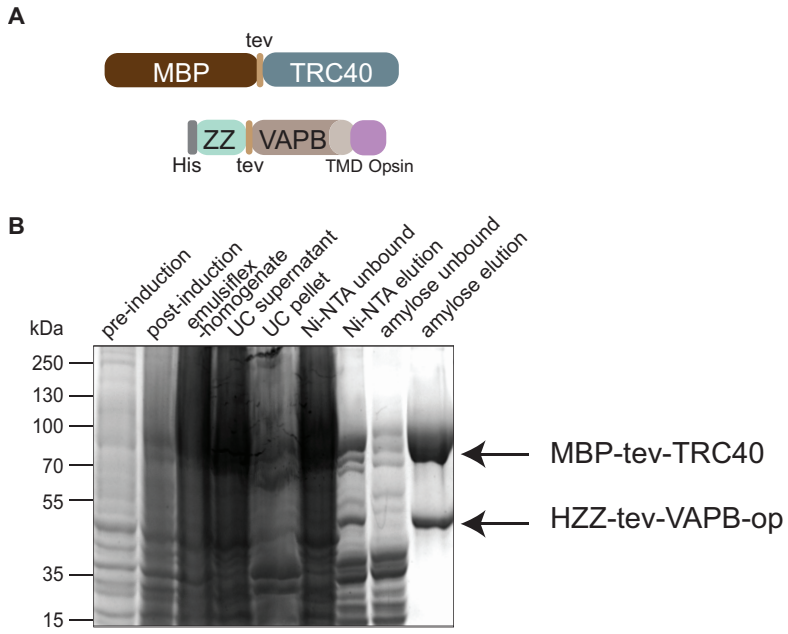


**Figure 14.When co-expressed VAPB exists as a complex with TRC40.**
(A) Schematic depiction of constructs used in expression and purification of VAPB in complex with TRC40. (B) Co-purification of soluble HZZ-VAPB-opsin/MBP-TRC40 complex by Ni-NTA and amylose resins. The proteins were separated by SDS-PAGE and stained by Coomassie Blue. (UC; ultracentrifugation).

### 3.2.1.4. TRC40/VAPB complex does not integrate into semi-permeabilized cells

To establish membrane integration of VAPB using TRC40/VAPB-opsin complex, a semi-permeabilized cell system was used as a source of ER membranes. An N-glycosylation site (opsin-tag) fused to the C-terminus of the protein of interest would help to monitor its insertion into the ER membranes. A shift in molecular mass indicates N-glycosylation of the reporter protein, a reaction that is specific for the ER. As an initial step, HeLa cells were treated with digitonin for selective permeabilization. To analyze the TRC40-

dependent membrane insertion of HZZ-VAPB-opsin, the purified HZZ-VAPB-opsin/TRC40 complex was incubated with the semi-permeabilized cells in the presence or absence of ATP for 1 hour at 4°C and 30°C respectively, as shown in Figure 15A. ATP was added to the reaction mix, since the TRC40-dependent membrane integration of TA proteins was shown to be an active, ATP-dependent process (Favaloro et al., 2008; Stefanovic and Hegde, 2007). As a control, emerin was co-expressed and co-purified with TRC40 since it is a well characterized TA INM protein that uses the TRC40 pathway for membrane insertion (Pfaff et al., 2016). After co-expression and incubation in semi-permeabilized cells as described above, the samples were analyzed by Western blotting using anti-opsin antibodies. Emerin, as previously shown (Pfaff et al., 2016), was inserted in an ATP and temperature-dependent manner into membranes of semi-permeabilized cells. As shown in Figure 15B, VAPB-opsin failed to integrate into semi-permeabilized cells suggesting that TRC40 is not essential for membrane insertion of VAPB, even if it forms a complex with VAPB.

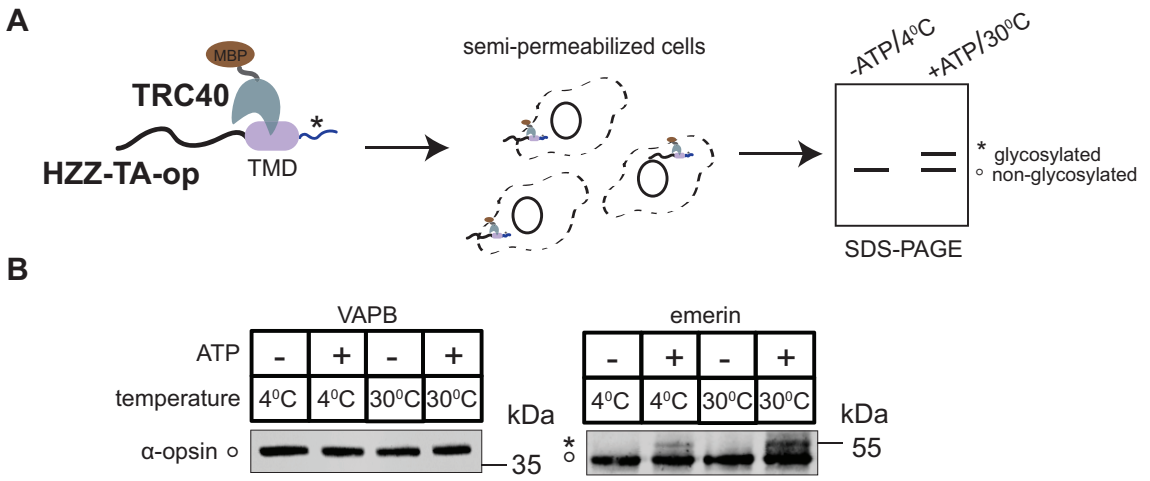


**Figure 15. Recombinant HZZ-VAPB-opsin in complex with TRC40 does not integrate into semi-permeabilized cells.**
(A) Schematic overview of membrane insertion using semi-permeabilized cells. Affinity purified protein complexes were added to HeLa cells permeabilized with digitonin and were incubated in the presence or absence of ATP at 4 and 30°C. (B) Semi-permeabilized cells were incubated with purified VAPB-opsin/TRC40 complex at 4 and 30°C, with or without ATP. Proteins were analyzed by SDS-PAGE and Western blotting. The glycosylated proteins were detected using an anti-opsin antibody. * indicates glycosylated and ° indicates non-glycosylated proteins. Purified emerin-opsin/TRC40 complex was used as positive control for insertion into permeabilized cells.

### 3.2.1.5. Insertion of VAPB into ER membranes does not require the TRC40-pathway receptors.

Next it was tested whether the receptors involved in TRC-40 pathway could assist in the post-translational insertion of VAPB. In order to investigate this, membrane insertion assays were performed in the presence of two inhibitory fragments of the pathway. TRC40 mediated insertion of TA proteins requires an ER receptor consisting of WRB protein along with CAML (Colombo et al., 2016; Favaloro et al., 2010; Vilardi et al., 2011; Vilardi et al.,

2014). A recombinant coiled-coil domain of WRB (WRB-CC) and an N-terminal domain of CAML (CAML-N) are known to interfere with TRC40 mediated insertion of TA proteins *in vitro* (Vilardi et al., 2011; Yamamoto and Sakisaka, 2012) (Figure 16A). To investigate whether the two dominant-negative fragments, WRB-CC and CAML-N, interfere with the insertion of VAPB-opsin into microsomes, insertion assay was performed using these fragments at two different concentrations, 5 µM and 10 µM. The insertion of emerin-opsin was strongly reduced as reported previously by Pfaff et al., 2016 in the presence of these fragments (Figure 16B and C). By contrast, membrane insertion of VAPB was marginally reduced by the addition of these fragments, indicating that membrane insertion of VAPB does not strictly require the receptors WRB and CAML (Figure 16B and C).

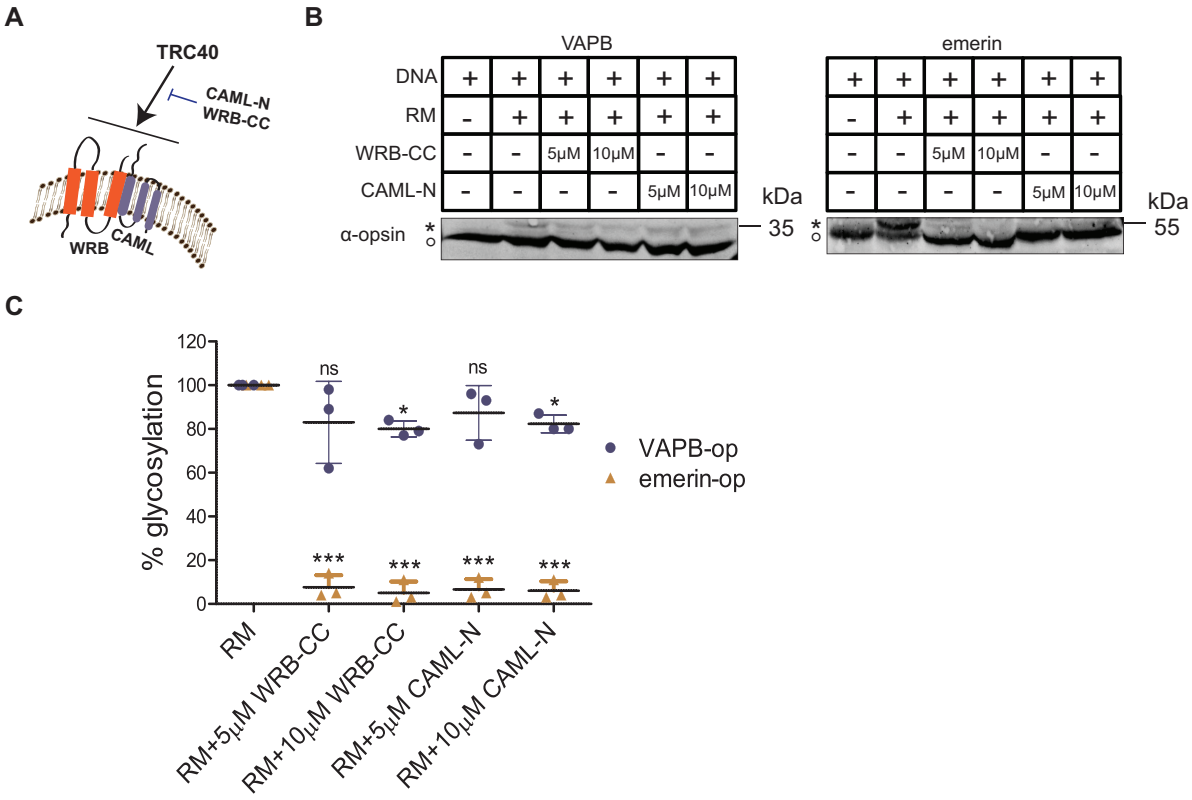


**Figure 16. VAPB does not require the receptors of the TRC-pathway for its insertion into microsomes.**
(A) Schematic representation of inhibition of TRC40 mediated insertion by dominant-negative fragments, WRB-CC and CAML-N. (B) *In vitro* translated VAPB-op and emerin-op were incubated with rough microsomes (RM) either in the presence or absence of 5 and 10 µM of WRB-CC or CAML-N. The glycosylated bands were detected using an anti-opsin antibody. * indicates glycosylated and º indicates non-glycosylated proteins. (C) Quantification of percentage (%) glycosylation for both VAPB-op and emerin-op into rough microsomes (RM) with and without the addition of WRB-CC and CAML-N. The relative amount of glycosylation (*) was quantified using Image-studio software and normalized to the maximum value. The graph represents the means ± SD of three independent experiments with $p < 0.001$(***), $p< 0.05$(*), ns; non-significant.

### 3.2.1.6. TRC40 depletion has no effect on VAPB membrane insertion

It was previously shown that the insertion of emerin could be inhibited by the depletion of TRC40 from reticulocyte lysate (Pfaff et al., 2016). To further address the

possibility of TRC40 dependent membrane insertion of VAPB into rough microsomes, immuno-depletion assays were performed. The reticulocyte lysate used for *in vitro* transcription/translation was immuno-depleted for TRC40. The efficiency of depletion of TRC40 was determined by Western blotting (Figure 17A). As shown in Figure 17B, TRC40-depletion affected the membrane insertion of emerin showing an increase in non-glycosylated form of emerin-opsin compared to the glycosylated protein, whereas VAPB remained unaffected.

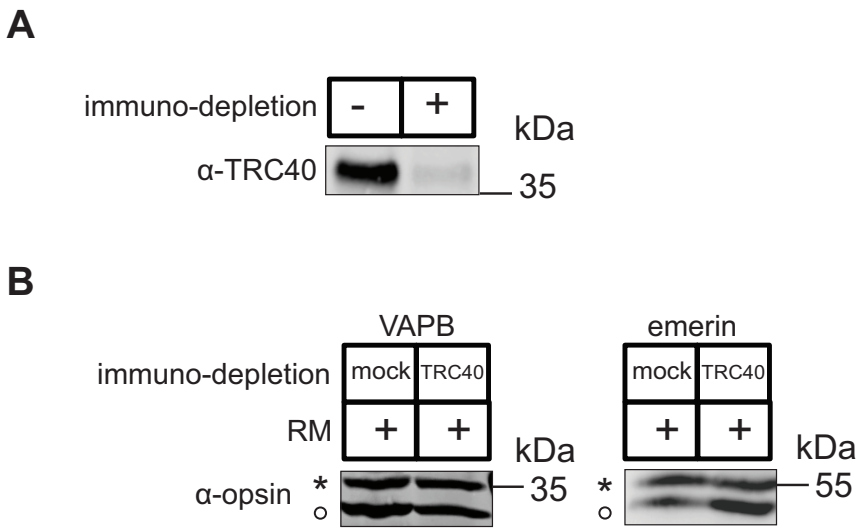


**Figure 17. Membrane insertion of VAPB in immuno-depleted lysates.**
(A) Lysates used for *in vitro* translation/transcription was depleted for TRC40 using Protein-A-agarose beads bound to antibodies against TRC40. As a control for depletion (mock (-)), rabbit IgG was used. The efficiency of depletion for TRC40 was detected by western blotting. (B) The glycosylated proteins were detected using an anti-opsin antibody. * indicates glycosylated protein and º indicates non-glycosylated protein.

Taken together, these results suggest that VAPB gets post-translationally inserted into the ER membrane but does not strictly require the TRC40 pathway for its insertion. Even though VAPB interacts with TRC40, this interaction may not help in the insertion into the ER membrane.

## 3.3. Discussion

This chapter investigated the requirements for membrane insertion of VAPB. The TRC40 pathway is the most studied route for post-translational membrane insertion of TA proteins, although alternative mechanisms using other factors like the ER membrane complex (EMC) (Guna et al., 2018), SRP-independent targeting (SND) (Aviram et al., 2016), signal recognition-particle (Abell et al., 2004; Abell et al., 2007; Casson et al., 2017) or HSC70/HSP40 (Rabu et al., 2008) have been previously described. Insertion can also occur through unassisted pathways (Brambillasca et al., 2006; Colombo et al., 2009). VAPB formed a stable complex with TRC40 upon co-expression in *E. coli* (Figure 14), confirming the previous findings that VAPB interacts with TRC40 (Baron et al., 2014; Coy-Vergara et al., 2019). Mass spectrometric analysis of VAPB immunoprecipitates had revealed that VAPB interacts with the TRC pathway subunits-TRC40, BAG6, UBL4A and GET4 (Baron et al., 2014; 1.4.1.2) and interaction with TRC40 was confirmed by co-immunoprecipitation of endogenous VAPB in the same study. An FFAT-like sequence close to the N-terminus of TRC40 was also identified that interacts with the MSP domain of VAPB (Baron et al., 2014). Additionally, using a dominant-negative ATPase impaired mutant of TRC40 that traps TA proteins in the cytoplasm, VAPB was reported to get trapped by the TRC40 mutant (Coy-Vergara et al., 2019).

Although a stable complex was formed with TRC40, integration assay using semi-permeabilized cells showed no membrane insertion (Figure 15). Given that the interaction of TA proteins with TRC40 for ER-membrane insertion occurs via their C-terminal TMD (Stefanovic and Hegde, 2007), it is interesting to investigate whether the interaction of VAPB via its N-terminus has other functions. It has been proposed that VAPB may serve as an alternative receptor for TRC40 whose ubiquitinated targets require the ATPase p97 and its cofactor FAF1 (Baron et al., 2014). Further studies will be needed to determine this function of VAPB.

Integration assays using WRB and CAML inhibitory fragments or TRC40 immunodepletion (Figure 16 and Figure 17) also suggested that VAPB does not strictly use the TRC40 pathway for its insertion into the ER. However, integration assays using microsomes confirmed the post-translational membrane insertion of VAPB (Figure 12). These observations suggest that alternative mechanisms might contribute to the post-translational insertion of VAPB (Abell et al., 2004; Abell et al., 2007; Aviram et al., 2016; Guna et al., 2018; Rabu et al., 2008; see also 6.1.3).

# Chapter 4:
# Proteomic mapping by rapamycin-dependent targeting of APEX2 identifies binding partners of VAPB at the INM

# Chapter 4 : Proteomic mapping by rapamycin-dependent targeting of APEX2 identifies binding partners of VAPB at the INM

**James C**, Müller M, Goldberg MW, Lenz C, Urlaub H, Kehlenbach RH (2019). Proteomic mapping by rapamycin-dependent targeting of APEX2 identifies binding partners of VAPB at the INM. J Biol Chem 294 (44):16241-16254

doi: 10.1074/jbc.RA118.007283
PMID: 31519755

**Table 9. Author contributions**

| Figures | Method | Experimental contributions |
|---|---|---|
| Figure 1 | Immunofluorescence and rapamycin assay | Christina James |
| Figure 1 | Electron microscopy | Dr. Martin W Goldberg |
| Figure 2 | Biotinylation experiment to compare the classic and new APEX approach | Christina James |
| Figure 3 | RAPIDS using mCherry-FRB-VAPB | Christina James |
| Figure 3 | Establishing the method, RAPIDS | Dr. Marret Müller |
| Figure 3 | Mass-spectrometric analysis of samples | Dr. Christof Lenz and Christina James |
| Figure 4 | RAPIDS using HA-FRB-VAPB | Christina James |
| Figure 4 | Mass-spectrometric analysis of samples | Dr. Christof Lenz and Christina James |
| Figure 5 | Cross-linking and immunoprecipitation assays | Christina James |
| Figure 6 | Proximity ligation assay of VAPB-emerin and VAPB-ELYS | Christina James |
| Figure S1 | Subcellular fractionation and immunoprecipitation assays | Christina James |
| Figure S2 | Western blotting to confirm biotinylation and check for transfection efficiency | Christina James |
| Figure S3 | Proximity ligation assay of VAPB-ACBD5 and VAPB-OSBPL9 | Christina James |

**Non-experimental contributions**

Data curation; C.J., M.M., M.W.G., C.L., H.U., and R.H.K. formal analysis; C.J., M.M., and M.W.G. investigation; C.J., M.M., M.W.G., C.L., and H.U. methodology; C.J., M.M., C.L., H.U., and R.H.K. writing-review and editing; C.L., H.U., and R.H.K. supervision; C.L., H.U., and R.H.K. project administration; H.U. and R.H.K. funding acquisition; R.H.K. conceptualization; R.H.K. writing-original draft.

# Proteomic mapping by rapamycin-dependent targeting of APEX2 identifies binding partners of VAPB at the inner nuclear membrane

Christina James[1], Marret Müller[1], Martin W. Goldberg[2], Christof Lenz[3,4], Henning Urlaub[3,4] and Ralph H. Kehlenbach[1,*]

[1]Department of Molecular Biology, Faculty of Medicine, GZMB, Georg-August-University Göttingen, Humboldtallee 23, 37073 Göttingen, Germany

[2]School of Biological and Biomedical Sciences, Durham University, Durham, DH1 3LE, UK

[3]Bioanalytics Group, Institute of Clinical Chemistry, University Medical Center Göttingen, Robert-Koch-Straße 40, 37075 Göttingen, Germany

[4]Bioanalytical Mass Spectrometry Group, Max Planck Institute for Biophysical Chemistry, Am Fassberg 11, 37077 Göttingen, Germany

* Corresponding author

Running title: Binding partners of VAPB at the inner nuclear membrane

* to whom correspondence should be addressed:
Tel. +49 551 395950; Fax: +49 551 395960; e-mail: rkehlen@gwdg.de

Keywords: APEX, emerin, nuclear envelope, proteomic proximity mapping, RAPIDS, VAPB, ELYS

**VAPB (vesicle-associated membrane protein-associated protein B) is a tail-anchored protein that is present at several contact sites of the endoplasmic reticulum (ER). We now show by immunoelectron microscopy that VAPB also localizes to the inner nuclear membrane (INM). Using a modified APEX2 (enhanced ascorbate peroxidase 2)-approach with rapamycin-dependent targeting of the peroxidase to a protein of interest, we searched for proteins that are in close proximity to VAPB, particularly at the INM. In combination with stable isotope labeling with amino acids in cell culture (SILAC), we confirmed many well-known interaction partners at the level of the ER with a clear distinction between specific and non-specific hits. Furthermore, we identified emerin, TMEM43 and ELYS as potential interaction partners of VAPB at the INM and the nuclear pore complex, respectively.**

The family of vesicle-associated membrane protein (VAMP/synaptobrevin) associated proteins (VAPs) includes VAPA and VAPB with described roles in the morphology and the function of the endoplasmic reticulum (ER) and the Golgi apparatus (1,2). VAPB is a tail-anchored protein, i.e. a protein containing a single transmembrane domain close to its C-terminus. Such proteins are typically inserted into the cellular membrane system in a post-translational manner (3,4). In its N-terminal region, VAPB contains a characteristic major sperm protein (MSP) domain. VAPB localizes largely to the ER and its binding to several partner proteins has been shown to mediate the association of the ER with other organelles. The acyl-CoA binding domain protein 5 (ACBD5), for example, interacts with VAPB and is involved in binding peroxisomes to the ER (5), whereas tyrosine phosphatase interacting protein 51 (PTPIP51) and VAPB form an ER-mitochondria tethering complex (6). In the secretory pathway, VAPB interacts with the Yip1-interacting factor homologue YIF1A, e.g. at the level of the ER-Golgi intermediate compartment (7). Furthermore, several oxysterol binding proteins (OSBPs), which play important roles in lipid transport,

interact with VAPB (8) and Kv2 potassium channels form ER-plasmamembrane junctions via interactions with VAPB (9). In total, >100 proteins have been reported to directly or indirectly interact with VAPB and/or the highly similar protein VAPA (10,11) (see also https://thebiogrid.org). A major binding motif, which is found in many VAPB-interacting proteins, is the "two phenylalanines in an acidic tract" (FFAT)-motif (11,12). Typically, the FFAT- (or FFAT-like) motif interacts with the MSP-domain of VAPB. One example for a protein containing the FFAT-motif that binds VAPB is the WD repeat-containing protein WDR44 (13). A mutation in VAPB (P56S) is involved in an autosomal dominant form of amyotrophic lateral sclerosis (ALS) (14) and blocks transport of nucleoporins and emerin, a major protein of the inner nuclear membrane (INM), to the nuclear envelope (15).

Several methods have been developed for the identification of proteins that are in close proximity to each other. They typically introduce biotin into unknown proteins as a tag that can be used for affinity capture with immobilized streptavidin and subsequent analysis by mass-spectrometry (for review see (16,17)). One prominent approach, proximity-dependent biotin identification (BioID), is based on a mutant form of the biotin ligase BirA, which can be fused to a protein of interest (the bait) whose neighboring proteins are to be analyzed (18). The enzyme part of the fusion protein releases reactive biotin, which can modify proteins (the prey) within a small spatial range. One drawback of this method is a rather long reaction time of >15 hours, although a faster method has been described very recently (19). As an alternative to biotin ligase dependent modifications, peroxidase-based methods have been introduced that allow short reaction times in the range of seconds to minutes (20). Ascorbate peroxidase (APEX) is a plant enzyme that generates biotin-phenoxyl radicals from biotin phenol in the presence of $H_2O_2$. These radicals have a very short half-life and, thus, can modify proteins within a range of ~20 nm, reacting with several amino acids with tyrosine as the primary site of biotinylation (21). Importantly, APEX can be fused to the N- or the C-terminus of proteins and may also reside internally. Furthermore, the enzyme has been shown to be active in several cellular compartments (20,22,23). Recently, APEX2 was introduced, which is far more active than the original enzyme (24). So far, APEX- or APEX2-based methods have mainly been used for the identification of proteins that reside in defined subcellular compartments, e.g. in primary cilia (23) or in the intermembrane space of mitochondria (25). As an alternative to APEX, horseradish peroxidase (HRP) can also be used as an enzyme to initiate the formation of biotin-phenoxyl radicals, and antibody-directed targeting of HRP to proteins of interest was recently described (26).

We previously characterized the post-translational insertion mechanisms of emerin into ER-membranes and analyzed targeting of the protein to the INM (27). For this, we applied a rapamycin-dependent dimerization method to monitor sequestration of a soluble nuclear reporter protein (dGFP-GST-NLS-FKBP12) to mCherry-tagged emerin (mCherry-FRB-emerin) at the INM. In this system, rapamycin binds to its two cognate binding regions, a 12-kDa FK506 binding protein (FKBP12) and an FKBP-rapamycin-binding (FRB)-cassette, promoting rapid interaction of the appropriately tagged proteins (28).

We now combine the APEX2-technology with the rapamycin-dependent dimerization approach. To this end, we target FKBP12-tagged APEX2 to FRB-tagged proteins in a rapamycin-dependent manner. SILAC, followed by quantitative mass spectrometry, then allows the comparison of proteins that get biotinylated by APEX2 in either the absence or the presence of rapamycin. Using this method (rapamycin- and APEX-dependent identification of proteins by SILAC or RAPIDS), we found RMDN3 (PTPIP51), ACBD5, YIF1A, OSBPL9 and other previously known interacting proteins of VAPB. Using a version of APEX2 that accumulates in the nucleus, we identified additional neighboring proteins of VAPB that reside at the nuclear envelope, e.g. emerin, TMEM43, lamins and the nucleoporin ELYS (embryonic large molecule derived from yolk

sac; AHCTF1). We further demonstrate the INM-localization of VAPB by immunoelectron microscopy and confirm the close proximity of endogenous VAPB with several of the newly identified proteins using proximity ligation assays and co-immunoprecipitation experiments.

## Results

*VAPB resides at the INM*

VAPB is typically described as an ER-resident protein, mediating interactions with multiple organelles. In addition, VAPB seems to play a role in the dynamics of the nuclear envelope and the nuclear pore complex. In this context, it was reported to affect transport of emerin to the INM (15). A localization of VAPB itself to the INM, however, has not been demonstrated so far. We therefore investigated the subcellular localization of VAPB in detail. First, we analyzed endogenous VAPB by indirect immunofluorescence using different buffers for the procedure. The specificity of the anti-VAPB antibody was confirmed by siRNA-mediated knockdown (compare Fig. 6). As shown before, VAPB localized to the endoplasmic reticulum (ER), with a clear rim around the nucleus visible in many cells (Fig. 1A). Interestingly, the ratio of the ER- and the nuclear envelope signal varied a lot, depending on the buffer used (compare (i) and (ii)). Similar to the endogenous protein, differently tagged versions of VAPB (mCherry-FRB-VAPB and HA-FRB-VAPB) were also found at the level of the ER and the nuclear envelope (Fig. 1B). We next tested if the nuclear rim could reflect targeting of VAPB not only to the outer, but also to the inner nuclear membrane. For readout, we used our established rapamycin-system (27). As shown before for emerin, the nuclear reporter protein dGFP-GST-NLS-FKBP12 was sequestered to the nuclear rim upon the addition of rapamycin in cells co-expressing mCherry-FRB-VAPB (Fig. 1C). This result suggested that at least a portion of the exogenously expressed VAPB reached the INM. To unequivocally demonstrate INM-localization of endogenous VAPB, we performed immunoelectron microscopy. As shown in Fig. 1D, immunoreactivity was detected at mitochondria, possibly reflecting the interaction of VAPB with PTPIP51. Furthermore, a significant number of gold dots were found at the level of the INM and also in close proximity to nuclear pores. In addition to these morphological studies, we also performed biochemical analyses. Obtaining pure INM-fractions is hardly possible, nevertheless, we subjected cell lysates to an established fractionation protocol (29). As shown in Fig. S1, VAPB was largely recovered in the same fraction as emerin and other proteins of the nuclear envelope, although other membrane proteins are certainly expected in this fraction as well. Together, our results clearly point to a localization of a fraction of the cellular VAPB-pool at the INM. They are in line with a recent study that was published during the review process of this paper, suggesting a role of VAPB in nuclear egress of Herpes Simplex viral particles (30).

*APEX2-dependent biotinylation of proteins*

A number of membrane proteins exposing binding regions to the cytoplasm have been shown to interact with the ER-form of VAPB (2). A portion of VAPB, however, localizes to the INM and we now set out to devise a method for the identification of neighboring partners of VAPB that allows to focus on either the cytoplasm (where the majority of VAPB is expected) or the nuclear compartment. Our approach is based on the APEX2-method for identification of proximity partners. In a “classic” approach, we first fused APEX2 directly to VAPB (Fig. 2A, left), as done before for many other proteins (9,20-23,25,31-35). HeLa cells were transfected with constructs coding for APEX2-VAPB or, for a control reaction, GFP-APEX2. Fig. 2B shows the subcellular localization of the APEX2-fusion proteins: as expected, GFP-APEX2 is found all over the cell and should promote unspecific biotinylation of many cellular proteins, whereas APEX2-VAPB localizes largely to the ER, very similar to other fusion proteins of VAPB (compare Fig. 1B). Next, the cells were subjected to the biotinylation protocol, including loading of cells with biotin-phenol and a short pulse with $H_2O_2$. For

analysis, biotinylated proteins were enriched using neutravidin beads and detected by Western-blotting. As shown in Fig. 2C, both fusion proteins were detected at similar levels in total cell lysates and in the protein fractions as bound to the neutravidin beads, indicating self-biotinylation. Furthermore, they led to a similar pattern of biotinylated proteins as detected by streptavidin-HRP. Next, we probed the blots with antibodies against proteins that had previously been identified as interaction partners of VAPB. Indeed, ACBD5 and OSBPL9 were clearly enriched when cells expressed APEX2-VAPB. In the control cells expressing GFP-APEX2, much lower levels of ACBD5 and OSBPL9 were detected (compare lanes 7 and 8). This result shows that the APEX-method is suited for the identification of interaction/proximity partners of VAPB at the level of the ER. We noted, however, that the difference between specific and unspecific biotinylation (i.e. modification in cells expressing APEX2-VAPB versus cells expressing GFP-APEX2) varied a lot, possibly resulting from different transfection efficiencies. We therefore modified our approach in a way that should allow a better control over specific versus unspecific biotinylation and combined APEX2-dependent biotinylation with the protocol for rapamycin-dependent targeting of proteins to a protein of interest (27). For a first proof-of-principle, we constructed a GFP-linked version of APEX2 with the rapamycin-interaction cassette FKBP12 (Fig. 2A, right). Cells were transfected with this construct, together with a construct coding for mCherry-FRB-VAPB. Transfected cells were treated with or without rapamycin and subjected to the biotinylation protocol. Fig. 2B shows the localization of mCherry-FRB-VAPB at the ER and the nuclear envelope and the recruitment of GFP-FKBP12-APEX2 to these sites upon addition of rapamycin. This treatment resulted in a pronounced overlap of the GFP- and the mCherry-signals, suggesting a tight interaction of FKBP12-GFP-APEX2 with mCherry-FRB-VAPB (compare Fig. 1C). As for the "classic" approach, cells were then subjected to the biotinylation protocol and biotinylated proteins were analyzed by Western-blotting. As shown in Fig. 2C, ACBD5 and OSBPL9 were detected as biotinylated proteins (i.e. in the bound fraction) when cells had been treated with the drug, indicating rapamycin-dependent targeting of APEX2 to mCherry-FRB-VAPB and biotinylation of the known VAPB-interaction partners. The levels of proteins that were recovered from the neutravidin beads were as high or higher than those found in the "classic" experiment using APEX2-VAPB as a fusion protein (compare lanes 4 and 8; compare also Fig. 3C). The added advantage of rapamycin-dependent targeting of APEX2 to our protein of interest, however, is twofold: first, a simple, single-parameter-change experiment (+/- rapamycin) can be performed for subsequent analysis of biotinylated proteins by quantitative mass spectrometry and discrimination between specific and unspecific hits. Second, the physical separation of APEX2 from the protein of interest allows an independent subcellular localization of the enzyme and, hence, a control over the population of cellular proteins that are potential targets for biotinylation. This is of particular importance for proteins like VAPB that can engage in interactions with different sets of proteins residing at distinct localizations.

*Rapamycin- and APEX-dependent identification of proteins by SILAC (RAPIDS)*

Based on the results described above, we decided to use the combined APEX2/rapamycin system for the identification of novel VAPB-proximity partners. The outline for an experiment with a version of APEX2 with the rapamycin-interaction cassette and identification of proteins by SILAC and quantitative mass-spectrometry is depicted in Fig. 3A. Briefly, cells are grown in media containing either light or heavy isotopes of the amino acids lysine and arginine and transfected with plasmids coding for mCherry-FRB-VAPB and FKBP12-GFP-APEX2. The two types of cells ("light" and "heavy") are then treated with or without rapamycin and subjected to the biotinylation procedure. Cellular lysates are combined and biotinylated proteins are enriched by binding to neutravidin beads. Mass-spectrometry of

eluted proteins then allows a direct comparison between plus- (i.e. specific biotinylation close to mCherry-FRB-VAPB) and minus- (i.e. background biotinylation) rapamycin conditions. A quantitative evaluation of heavy and light tryptic fragments of biotinylated proteins should immediately yield proteins that were in close proximity to mCherry-FRB-VAPB in the presence of rapamycin. Fig. S2A shows the controls for $H_2O_2$-dependent protein biotinylation. Prominent bands that are seen in the absence of $H_2O_2$ correspond to endogenously biotinylated proteins. Similar transfection efficiencies in the two sets of cells ("light" and "heavy") are controlled in Fig. S2B.

Fig. 3B shows the combined results of two independent experiments, each with forward (i.e. using light and heavy medium for the plus- and minus-rapamycin conditions) and reverse reactions (i.e. with changed conditions, as depicted in Fig. 3A). Proteins that are preferentially biotinylated in the presence of rapamycin in both forward- (X-axis) and reverse-reactions (Y-axis) are expected in the upper left quadrant of the plot. One prominent protein here is VAPB itself, indicating its modification by the APEX2-fusion protein. Many previously known cytoplasmic interaction partners of VAPB were also identified with high levels of significance, including PTPIP51 (RMDN3), YIF1A, WDR44, OSBPL9, OSBPL8 and ACBD5. GAPDH, by contrast, was found in the cloud of proteins that were hardly affected by rapamycin, close to the intersection of the x- and the y-axis. The list of identified proteins is presented in Table S1. Interestingly, the INM-protein emerin was also identified with a high significance. Another potential interaction partner is TMEM43, also known as LUMA, a membrane protein that interacts with emerin at the INM (36) and plays a role in certain forms of muscular dystrophies (37). Its localization is, however, controversial, since it was mainly found in zonula adhaerens and punctum adhaerens plaques in another study (38). Another nuclear protein that was identified is the AT-rich interactive domain-containing protein 4 A (ARID4A). This protein, also known as Rbbp1, is a retinoblastoma-binding protein (39) with functions in chromatin remodeling (40). The significance of the proximity and/or interaction of VAPB and ARID4A remains to be investigated.

Next, we performed Western-blotting to confirm the mass-spectrometry data. As shown in Fig. 3C, high levels of mCherry-FRB-VAPB, ACBD5, OSBPL9 and emerin were detected in the bound fraction when the cells had been treated with rapamycin, confirming rapamycin-dependent biotinylation. For GAPDH, by contrast, very similar levels were observed for rapamycin-treated and non-treated cells. Based on the successful identification of known interaction partners, we termed our approach "RAPID-SILAC" or "RAPIDS" (Rapamycin- and APEX-dependent identification of proteins by SILAC).

*RAPIDS using a nuclear version of APEX2*

The identification of emerin supported the notion that VAPB can reach the INM (compare Fig. 1), although emerin could also localize to other regions of the cell (41,42). Two parameters of the assay as performed above disfavor the identification of *bona fide* INM-proteins: first, FKBP12-GFP-APEX2 is found all over the cell and may preferentially interact with VAPB that localizes to the ER upon addition of rapamycin. Second, the version of VAPB in this experiment contains a large cytoplasmic mCherry-tag. Although the protein can reach the INM to some extent (Fig. 1C), the efficiency of diffusion of proteins from the ER via the outer nuclear membrane to the INM in general is clearly affected by the size of the cytoplasmic domain (43-47). We therefore modified our approach twofold (Fig. 4A). First, we used a version of APEX2, APEX2-dGFP-NLS-FKBP12, which strongly accumulates in the nucleus of transfected cells as a result of its nuclear localization signal. Hence, biotinylation of nuclear proteins or INM-proteins should be favored. Second, we designed a smaller version of VAPB, HA-FRB-VAPB, which we expect to diffuse more readily across the nuclear pore to the INM than the mCherry-tagged version. As shown in Fig. 4B, APEX2-dGFP-NLS-FKBP12 localized largely in the nucleus in the absence of rapamycin. Upon addition of the drug, the

reporter protein was sequestered to the nuclear envelope, suggesting binding to HA-FRB-VAPB at the INM. We then performed RAPIDS and could show that VAPB (i.e. HA-FRB-VAPB in this experiment) was prominently biotinylated in the presence of rapamycin (Fig. 4C, D). By quantitative proteomics, we identified at least 22 biotinylated proteins that were enriched on the neutravidin beads upon addition of rapamycin to the cells, suggesting their close proximity to HA-FRB-VAPB (Fig. 4C and Table S2). Strikingly, many of the proteins identified are known to reside on the nuclear side of the nuclear envelope. The proximity-candidates fall into three categories: first, proteins of the INM like emerin, the lamina-associated polypeptide 1 (LAP1 or TOR1AIP1, Torsin-1A-interacting protein 1; (48)) and LAP2β (TMPO, thymopoetin; (48,49)). Another protein in this category is TMEM43, which we also found with mCherry-FRB-VAPB as a bait (Fig. 3); second, proteins of the nuclear pore complex (NPC) like Nup153 (50), Tpr (51) and ELYS (AHCTF1; (52)) and third, components of the nuclear lamina like lamin A and lamin B (LMNA, LMNB; (53)). To confirm preferential biotinylation of candidates in the presence of rapamycin, we performed Western-blotting of proteins eluted from the neutravidin beads (Fig. 4D). Essentially all the tested protein showed increased recovery from neutravidin beads upon treatment of cells with rapamycin, including ELYS, lamin A/C, LAP1 (TOR1AIP1), LAP2β (TMPO) and emerin. Together, our results show that RAPIDS allows the identification of known interaction partners of VAPB and, possibly, of novel proximity- and/or interaction partners.

*Validation*

Proteins identified by RAPIDS could be direct or indirect binding partners of VAPB and occur in biochemically stable complexes or just reside in very close proximity to our protein of interest. As a first step to distinguish between these possibilities, we performed co-immunoprecipitation experiments, combined with a crosslinking approach to stabilize low-affinity interactions. First, we immunoprecipitated endogenous VAPB using a specific antibody and analyzed the precipitate for co-precipitating proteins. As a control, total IgG was used (Fig. 5A). For the established binding partners of VAPB, ACBD5 and OSBPL9, and also for emerin and TMEM43, specific co-precipitation with VAPB was observed when the cells had been treated with the cleavable bi-functional crosslinker dithiobis(succinimidyl propionate) (DSP). For OSBPL9 and TMEM43, co-precipitation above the IgG-background was also seen in the absence of the crosslinker, suggesting tight interactions. To corroborate these findings, we also used HA-FRB-VAPB-overexpressing cells for co-immunoprecipitation experiments, again with and without DSP as a crosslinking reagent. As shown in Fig. 5B, low levels of ACBD5 and OSBPL9 co-precipitated with overexpressed HA-FRB-VAPB. The levels of coprecipitated proteins strongly increased when the cells had been treated with DSP prior to cell lysis (compare lanes 5 and 7). For emerin and TMEM43 and, to some extent, for ELYS, co-precipitation was observed in the cross-linked samples, suggesting that the corresponding complexes exist in intact cells. Very low levels of co-precipitating proteins were observed when the cells had been transfected with a plasmid coding for HA-FRB (lanes 6 and 8). Together, these results show that VAPB indeed interacts with some of the proteins that were identified as proximity partners by RAPIDS. It remains to be investigated whether these interactions are direct or indirect.

Next, we performed proximity ligation assays (PLAs, (54)), which detect interactions (or at least proximity) of endogenous proteins and allow statements about the precise localization of the protein-protein interactions. These assays are based on the decoration of proteins in fixed cells, first with specific primary antibodies and subsequently with oligonucleotide-linked secondary antibodies. If the proteins of interest are in close proximity (i.e. within ~40 nm), subsequent ligation and amplification reactions lead to formation of a fluorescent product that can easily be detected by microscopy. We first analyzed VAPB with respect to its interaction with known binding partners that were also detected by RAPIDS,

namely ACBD5 and OSBPL9. To characterize our antibodies, we performed immunofluorescence analysis. As shown in Fig. S3A and B, ACBD5 co-localized with the peroxisomal marker protein PMP70, and OSBPL9 with the Golgi-marker GM130, indicating the specificity of the ACBD5- and the OSBPL9-antibodies. In PLAs, specific interactions of VAPB were observed with characteristic patterns of dots: for ACBD5 (Figs. S3C, D), dots were found scattered all over the cell, consistent with signals derived from ER-peroxisome interactions. For OSBPL9, the observed dots were largely found in an area corresponding to the Golgi compartment (Figs. S3E, F). The specificity of the signals was supported by single-antibody controls. These results show that our antibodies are suitable for a faithful detection of VAPB-protein interactions. Next, we performed PLAs with antibodies against VAPB and emerin or ELYS (Fig. 6). TMEM43 was not analyzed here due to lack of PLA-suitable antibodies. For emerin, PLA-dots were mostly observed at the nuclear rim, consistent with the major localization of emerin at the INM (Fig. 6A). For ELYS (Fig. 6B), PLA-dots were observed at the nuclear envelope, but also in the nuclear interior. For both proteins, the number of dots decreased significantly when VAPB had been depleted by specific siRNAs as well as in single-antibody-controls, demonstrating the specificity of the PLA. In summary, co-immunoprecipitation experiments and PLA-assays suggest that VAPB indeed forms complexes with proteins of the INM and/or the NPC. Figure 7 depicts the interactome of VAPB, as revealed by our analysis and by previous studies.

## Discussion

*RAPIDS*

The known binding partners of VAPB localize exclusively to the cytoplasm or to cytoplasmic membranes. The INM-localization of VAPB therefore prompted us to search for nuclear proteins that could interact with VAPB or are at least in close proximity to VAPB at the level of the INM or the NPC. For this, affinity-based methods that require an initial cell-lysis step were not very promising, since the lysis buffers must fulfill two conflicting criteria: they must be strong enough to solubilize protein complexes like the nuclear lamina or the NPC, yet maintain the interactions of interest. Indeed, validation of our candidate proteins by co-immunoprecipitation approaches required a careful choice of specific reaction conditions concerning the lysis buffer, the specific antibody and, importantly, the crosslinker used for stabilization of protein-protein interactions. As an alternative, proximity-based approaches like BioID and the APEX-system have the advantage of targeting proteins in their natural environment, the living cells. BioID, in fact, was initially developed to probe the nuclear lamina for interaction partners of lamin A (18). In the last couple of years, APEX-based biotinylation approaches have been used very successfully for the analysis of the interactome of many proteins (9,20-23,25,31-35). With RAPIDS, we now introduce a method that combines APEX2-dependent biotinylation, rapamycin-dependent targeting of the enzyme to proteins of interest, and quantitative proteomics using SILAC. The use of rapamycin to induce rapid targeting of APEX2 to a specific subcellular localization should facilitate the discrimination between proteins that are modified in a specific vs. a nonspecific manner. Furthermore, a careful choice of the tags used for APEX2- (here: +/- NLS) and the protein of interest (here: HA vs. mCherry) may strongly affect the spectrum of identified proteins. This is of particular importance for proteins of the INM, where the size and the nature of the tag may affect efficient targeting of proteins to their final destination. In general, the approach to physically separate the APEX2-enzyme from the protein of interest offers a tight control over the cellular proteins that are potential targets for biotinylation. This is a clear advantage for proteins like VAPB that can engage in interactions at different intracellular contact sites. Notably, a similar targeting approach using the rapamycin analogue AP21967 as a dimerizing agent was very recently described (55). In 2C-BioID, the authors used the rapamycin analogue AP21967 to initiate dimerization of a biotin-protein

ligase and a protein of interest to analyze the interactomes of LAP2β and lamins A and C as a proof of principle.

The feasibility of RAPIDS was demonstrated by the identification of many of the previously known binding partners of VAPB (Fig. 3). Furthermore, we identified several novel nuclear proximity partners of VAPB, consistent with the INM-localization of the protein. For this, usage of our nuclear version of APEX2 was important, as it favors the biotinylation of nuclear proteins. Fig. 7 summarizes our findings and also indicates some of the proteins that had previously been identified as binding partners of VAPB. Together, RAPIDS is a versatile method for the identification of proteins that are in close proximity to a protein of interest. This modification of the classic APEX-approach should be applicable to proteins residing at different subcellular localizations.

*VAPB at the INM*

To our knowledge, a nuclear localization of VAPB itself has not been documented so far, except in a very recent publication (30). Using our rapamycin-dependent dimerization assay as well as immunoelectron microscopy, we now unequivocally show that VAPB can indeed reach the INM and can also be detected in close proximity to NPCs (Fig. 1). At this point, we cannot say with certainty, which percentage of the entire cellular pool of endogenous VAPB resides at the INM. In immunofluorescence, the ratio of the nuclear envelope- and the ER-signal of VAPB is affected by the buffer conditions (Fig. 1A). In immunoelectron microscopy (Fig. 1D), epitope masking is a general issue and could affect nuclear and cytoplasmic immunoreactivity of VAPB differently. Hence, other, more quantitative methods are required for an accurate determination of VAPB-levels at different localizations within the cell.

VAPB has been described as a protein that localizes to ER-contact sites (2). Using RAPIDS under conditions that should favor the identification of cytoplasmic binding/proximity partners (i.e. with mCherry-FRB-VAPB and FKBP12-GFP-APEX2; Figs. 2 and 3), we found many of the previously known interaction partners of VAPB, including oxysterol binding proteins, PTPIP51 and ACBD5. Most of the identified proteins associate with membranes and many of them localize to the ER (see Table S1), consistent with the major localization of mCherry-FRB-VAPB. Nevertheless, we also identified emerin as a mainly nuclear protein using this approach, in agreement with the observation that mCherry-FRB-VAPB can reach the INM (Fig. 1C). A different picture emerged when we used FRB-VAPB with an HA-tag at the N-terminal end instead of an mCherry-tag and APEX2-dGFP-NLS-FKBP12 as a nuclear version of the biotinylating enzyme (Fig. 4 and Table S2). Under this condition, we identified significantly more nuclear proteins, including emerin and other membrane proteins of the INM, several nucleoporins and components of the nuclear lamina. This result is consistent with the observation that the efficiency of translocation of proteins from the outer to the inner nuclear membrane inversely correlates with the size of the cytoplasmic/nuclear region of the protein (43-47). Since the HA-tag is significantly smaller than the mCherry-tag, a larger proportion of the overexpressed protein is expected to reach the INM via passive diffusion (45), where, upon rapamycin treatment, the nuclear version of APEX2 can then initiate efficient biotinylation of neighboring proteins.

Importantly, interaction of endogenous VAPB or overexpressed VAPB with emerin and TMEM43 could be confirmed by co-immunoprecipitation experiments, where the novel binding partners behaved very similar to the established binding partners ACBD5 and OSBPL9 (Fig. 5). Interestingly, co-precipitation of TMEM43 with emerin has been described previously (36). For VAPB/emerin and VAPB/ELYS we also confirmed a close proximity *in situ*, using PLA-assays (Fig. 6). For emerin, PLA-dots were largely restricted to the nuclear envelope, consistent with the predominant localization of the protein. ELYS is a nucleoporin that can also localize to the nuclear interior in interphase cells (52) and plays a role in early steps of post-mitotic NPC-assembly (56,57). Hence, a role of VAPB in this process could be

envisaged. ELYS has previously been suggested to interact directly with VAPB based on an FFAT-like motif in its sequence (2,10). In our PLAs, we also observed intranuclear dots, suggesting that not only ELYS, but also VAPB might reside in the nucleoplasm. This seems counterintuitive, since VAPB is a membrane protein. Being a tail-anchored protein, however, a soluble pool of it must exist and a fraction could even reach the nuclear interior. At this point, we can only speculate about the functional significance of INM-localization of VAPB. VAPB has been implicated in the transport of emerin and nucleoporins to the INM and the NPC, respectively (15).

In summary, our findings suggest that the interaction repertoire of VAPB is even larger than previously thought. VAPB not only serves as a bridging factor at multiple contact sites of the ER with mitochondria, peroxisomes, the Golgi apparatus and the plasma membrane, but also localizes to the INM, where it may contact several nucleoporins, integral membrane proteins and components of the nuclear lamina.

## Experimental procedures

*Plasmids*

Standard procedures were used for cloning and the obtained constructs were confirmed by sequencing. To obtain pcDNA3-FKBP12-GFP-APEX2, the FKBP12 coding sequence was originally derived from pcDNA3-FKBP12 (27,58) using primers G1562 and G1563 and cloned into pcDNA3-Connexin43-GFP-APEX2 (Addgene plasmid #49385) through AflII and BamHI, thereby replacing the Connexin43 coding sequence (oligonucleotides are listed in Table S3). For APEX2-dGFP-NLS-FKBP12, the APEX2 coding sequence was amplified by PCR using pcDNA3-Connexin43-GFP-APEX2 as a template and primers G1573 and G1571. The PCR product was cloned into a pEGFP-C1 derivative encoding dGFP-cNLS-FKBP12 through BcuI. For pmCherry-FRB-VAPB, the VAPB coding sequence was amplified by PCR using primers G1390 and G1386 and pCAN-myc-VAPB (59) as a template. The PCR product was cloned into a pmCherry-C1 derivative coding for mCherry-FRB through KpnI and BamHI.

For pEF-HA-FRB-VAPB, the FRB coding sequence (as above) from mCherry-FRB was first inserted into a modified pEF-HA vector (60) via NcoI and EcoRI, generating pEF-HA-FRB. The VAPB coding sequence was amplified by PCR using primers G1512 and G1511 and pCAN-myc-VAPB (59) as a template. The PCR product was then inserted into pEF-HA-FRB plasmid through EcoRI and SpeI. To obtain pEGFP-APEX2, APEX2 was amplified from pcDNA3-FKBP12-GFP-APEX2 using primers G1854 and G1855 and cloned into pEGFP-C1 through EcoR1 and BamH1. For APEX2-VAPB, VAPB was amplified from pmCherry-FRB-VAPB using primers G1512 and G1386 and cloned via EcoR1 and BamH1 into pAPEX2-C1, which had been generated by exchanging the mCherry sequence of pmCherry-C1 for that of APEX2.

*Cell culture and transfection*

HeLa P4 cells (61) were obtained from the NIH AIDS Reagent Program. Cells were cultivated in DMEM (Life technologies, Carlsbad, CA, USA) supplemented with 10% (v/v) FBS (Life technologies, Carlsbad, CA, USA), 100 U $ml^{-1}$ penicillin, 100 µg $ml^{-1}$ streptomycin and 2 mM L-glutamine (Life technologies, Carlsbad, CA, USA) under 5% $CO_2$ at 37°C. They were tested regularly for contamination by mycoplasma.

For SILAC, cells were grown in medium containing heavy or light isotopes of arginine and lysine. For this purpose, DMEM (high glucose) lacking glutamine, lysine and arginine (Thermo Fisher Scientific, Waltham, MA, USA) was supplemented with 10% (v/v) dialyzed FBS (Life technologies, Carlsbad, CA, USA), 6 mM L-glutamine (Life technologies), 100 U $ml^{-1}$ penicillin and 100 µg $ml^{-1}$ streptomycin. To obtain SILAC media with heavy and light isotopes, either 0.4 mM $^{13}C_6{}^{15}N_2$-L-lysine (Silantes, Munich, Germany) and 0.2 mM $^{13}C_6{}^{15}N_4$-L-arginine (Silantes, Munich, Germany) or 0.4 mM $^{12}C_6{}^{14}N_2$-L-lysine (Sigma-Aldrich, St. Louis, MO, USA) and 0.2 mM $^{12}C_6{}^{14}N_4$-L-arginine (Sigma-Aldrich, St. Louis, MO, USA) were added,

respectively. To ensure sufficient incorporation of heavy amino acids, cells were passaged five to seven times in SILAC medium before the biotinylation experiment, and the incorporation rate was confirmed to be ≥97% by mass spectrometry.

Transfections were performed according to the calcium phosphate method (62). Briefly, the respective plasmids were mixed with 250 mM $CaCl_2$. After the addition of the same amount of HEPES buffer (50 mM HEPES, pH 6.98, 250 mM NaCl, 1.5 mM $NaHPO_4$) and 20 min incubation at room temperature, the mixture was added to the cells, which were then grown as above.

siRNA mediated knockdown of VAPB was carried out using Lipofectamine RNAiMAX (Thermo Fisher Scientific, Waltham, MA, USA) following the protocol of the manufacturer. VAPB siRNA (GCUCUUGGCUCUGGUGGUUUU, AAAACCACCAGAGCCAAGAGC; Sigma), and ON-Target plus non-targeting siRNA (Dharmacon, Lafayette, CO, USA, D-001810-01-50) were used at a final concentration of 100 nM.

*Rapamycin-dependent biotinylation assay*

HeLa P4 cells were grown in 10 cm dishes in SILAC medium as described above. Two sets of cells (in "light" or "heavy" medium) were transfected with pmCherry-FRB-VAPB and pcDNA3-FKBP12-GFP-APEX2 or pEF-HA-FRB-VAPB and pAPEX2-dGFP-NLS-FKBP12, using the same transfection mix to ensure similar expression levels, and grown to confluency. Cells were then incubated for 30 min with 500 µM biotin-phenol (Iris Biotech, Marktredwitz, Germany), with or without 200 nM rapamycin (Sigma Aldrich, St. Louis, MO, USA). For each experiment, forward and reverse reactions were performed. For forward reactions, cells grown in "light'' SILAC medium were treated with rapamycin and cells grown in "heavy" SILAC medium were not. For reverse reactions, this labeling scheme was switched. After incubation with biotin-phenol and rapamycin, 1 mM $H_2O_2$ was added at room temperature. After 1 min, the medium was aspirated and cells were washed twice with quenching buffer (5 mM Trolox, 10 mM $NaN_3$, 10 mM sodium ascorbate in PBS) and once with PBS. Cells used for fluorescence microscopy were fixed immediately.

For Western blot and SILAC analyses, cells from each dish were lysed with 1 ml RIPA buffer (50 mM Tris, pH 7.4, 5 mM Trolox, 0.5% (w/v) sodium deoxycholate, 150 mM NaCl, 0.1% (w/v) sodium dodecyl sulfate (SDS), 1% (v/v) Triton X-100, 1 mM phenylmethane sulfonyl fluoride (PMSF), 10 mM $NaN_3$, 10 mM sodium ascorbate, 1 µg $ml^{-1}$ aprotinin, 1 µg $ml^{-1}$ leupeptin and 1 µg $ml^{-1}$ pepstatin). The cell lysate was incubated for 5 min on ice and centrifuged for 10 min at 16,000 g and 4°C. The cleared cell lysate was used to enrich biotinylated proteins with neutravidin beads (Thermo Fisher Scientific, Waltham, MA, USA). For mass spectrometry, cell lysates derived from three 10 cm dishes were pooled, the protein concentration of the cell lysates was determined using the Pierce 660 nm Protein Assay (Thermo Fisher Scientific, Waltham, MA, USA) and equal protein amounts of samples treated with or without rapamycin were mixed prior to addition to neutravidin beads. For Western blot analyses, the samples were kept separately. For each forward or reverse experiment, six batches of 130 µl neutravidin beads were incubated with 1ml cell lysate overnight at 4°C on a rotor. The beads were washed once with washing buffer 1 (50 mM HEPES (pH 7.4), 0.1% (w/v) sodium deoxycholate, 1% (v/v) Triton X-100, 500 mM NaCl, 1 mM ethylenediaminetetraacetic acid (EDTA), once with washing buffer 2 (50 mM Tris (pH 8.0), 250 mM LiCl, 0.5% (v/v) Nonidet P-40, 0.5% (w/v) sodium deoxycholate, 1 mM EDTA) and twice with washing buffer 3 (50 mM Tris (pH 7.4) and 50 mM NaCl). For each washing step, the beads were incubated for 8 min at 4°C on a rotor. After the last washing step, the buffer was removed and bound proteins were eluted from the beads by incubation for 5 min at 95°C with 90 µl SDS sample buffer (4% (w/v) SDS, 125 mM Tris pH 6.8, 10% (v/v) glycerol, 0.02% (v/v) bromophenol blue, 10% (v/v) β-mercaptoethanol) supplemented with 5 mM desthiobiotin (Sigma-Aldrich, St. Louis, MO, USA). To increase the protein concentration,

three batches of beads were consecutively eluted in the same buffer.

*Mass spectrometric analyses*

Samples were separated on 4-12% NuPAGE Novex Bis-Tris Minigels (Invitrogen, Carlsbad, California). Gels were stained with Coomassie Blue, and each lane sliced into 11-12 equidistant bands. After washing, gel slices were reduced with dithiothreitol (DTT), alkylated with 2-iodoacetamide and digested with trypsin (sequencing grade, Promega, Madison Wisconsin) overnight. The resulting peptide mixtures were then extracted, dried in a SpeedVac, reconstituted in 2% acetonitrile/0.1% formic acid/ (v/v) and analyzed by nanoLC-MS/MS on a hybrid quadrupole/orbitrap mass spectrometer (Q Exactive, Thermo Fisher Scientific, Dreieich, Germany) as described previously (63). Raw data were processed using MaxQuant Software version 1.5.7.4 (Max Planck Institute for Biochemistry, Martinsried, Germany). Proteins were identified against the human reference proteome (v2017.02, 92.927 protein entries) along with a set of common lab contaminants. The search was performed with trypsine (excluding proline-proximal cleavage sites) as enzyme and iodoacetamide as cysteine blocking agent. Up to two missed tryptic cleavages were allowed for, as well as methionine oxidation and protein N-terminal acetylation variable modifications. Instrument type 'Orbitrap' was selected to adjust for MS acquisition specifics. Following an initial internal recalibration, this translated into an MS mass tolerance of 4.5 ppm and an MS/MS mass tolerance of 20 ppm. Protein and peptide results lists were thresholded at False Discovery Rates (FDR) of 0.01, using a forward-and-reverse decoy database approach. The Arginine R10 and Lysine K8 labels including the 'Re-quantify' option were specified for relative protein quantitation. Perseus Software version 1.5.6.0 (Max Planck Institute for Biochemistry, Martinsried, Germany) was used for statistical evaluation of relative protein quantitation values from the MaxQuant Software results and a two-sided Significance B test (64) was performed using normalized $\log_2$ ratios. For the analysis, a Benjamini-Hochberg correction was applied and a threshold value of 0.05 was chosen. Mass spectrometry experiments were performed twice, each with two biological and two technical replicates.

*Data availability*

The MS proteomics data have been deposited to the ProteomeXchange Consortium via the PRIDE (65) partner repository with the dataset identifier PXD012157 (username: reviewer27517@ebi.ac.uk; password: LrJXmV8h)

*Western blot analyses*

Western blotting was performed according to standard methods using HRP-coupled secondary antibodies. To detect biotinylated proteins, they were separated by SDS-PAGE using 4-12% NuPAGE Novex Bis-Tris Minigels (Invitrogen, Carlsbad, California). After transfer to nitrocellulose, the membranes were incubated in blocking buffer (3% BSA in TBS-T (24.8 mM Tris, pH 7.4, 137 mM NaCl, 2.7 mM KCl, 1% (v/v) Tween 20)) overnight at 4°C. Incubation with streptavidin-HRP (Jackson ImmunoResearch Laboratories, West Grove, PA, USA; diluted 1:5,000-1:40,000 in blocking buffer) for 1 h at room temperature was followed by three washing steps with TBS-T. For detection of proteins, Immobilon Western Chemiluminescent HRP Substrate (Millipore, Burlington, MA, USA) and a luminescent image analyzer (LAS-3000; Fuji, Tokyo, Japan) were used. Signal intensities were measured using Image Studio Lite (Ver. 5.2). Two-way analysis of variance (ANOVA) followed by Bonferroni post-test was used for statistical analysis and a confidence interval of 95% was set. Primary and secondary antibodies are listed in Table S4.

*Immunofluorescence and microscopy*

For fluorescence microscopy, cells were grown on coverslips and fixed with 4% (v/v) para formaldehyde. Cells expressing fluorescently labeled proteins were mounted directly with MOWIOL supplemented with 1 µg/ml DAPI. For immunofluorescence, fixed cells were permeabilized with 0.5% (v/v) Triton X-100 in PBS for 5 min at room temperature and

blocked with 3% (w/v) BSA in PBS for 20 min at room temperature. Staining was performed for 1 h at room temperature using appropriate primary antibodies and fluorescently labeled secondary antibodies (Table S4), which were diluted in 3% BSA in PBS. Afterwards, cells were embedded in MOWIOL-DAPI.
Microscopic analysis was performed using an LSM510 Confocal laser scanning microscope using a 63X /1.4 oil immersion lens (Zeiss, Oberkochen, Germany).

*Electron microscopy*
For immunoelectron microscopy, HeLa cells were fixed with 2% paraformaldehyde, 0.2% glutaraldehyde in PHEM buffer (60 mM Pipes, 25 mM Hepes, 2 mM $MgCl_2$, 10 mM EGTA, pH 6.9) for 1 h, washed with PHEM, and scraped off. Cells were pelleted (200 x g, 2 min) and resuspended in 0.1% glycine in PBS, pelleted (400 x g, 2 min), resuspended in 0.1% glycine in PBS (15 min), pelleted (400 x g, 2 min), resuspended in 1% gelatin (Dr. Oetker) at 37°C for 10 min, pelleted (400 x g, 2 min), resuspended in 10% gelatin for 10 min at 37°C, then replaced on ice. Pellets were immersed in 15% PVP (polyvinylpyrrolidone, 10 kDa, Sigma), 1.7 M sucrose in PBS overnight, then mounted and frozen in liquid nitrogen and sectioned on a cryo-ultramicrotome (Leica UC6 with FC6). Cryosections were thawed and placed at 37°C, washed in 0.1% bovine serum albumin (BSA, Sigma) in PBS, then 1% BSA in PBS for 3 min, followed by overnight incubation with undiluted primary antibody (mouse anti-VAPB mouse, Proteintech), washed in PBS, incubated with 10 nm colloidal gold-anti-mouse antibody (BBI solutions). Grids were washed in PBS, transferred to 1% glutaraldehyde in PBS (5 min), washed in $H_2O$, and embedded in 2% methyl cellulose containing 0.4% uranyl acetate (Agar Scientific). Imaging was done using a Hitachi H7600 TEM at 100 kV.

*Cross-linking and co-immunoprecipitation*
$2x10^6$ Hela P4 cells per 10 cm dish were transfected with plasmids coding for HA-FRB-VAPB or HA-FRB. After 24 hours, the cells were washed twice with cold PBS containing 0.1 mM $CaCl_2$ and 1 mM $MgCl_2$ and incubated with DSP (Dithiobis (succinimidyl propionate), Thermo Scientific) at a final concentration of 1 mM in DMSO for two hours on ice. For control reactions, DMSO alone was used. DSP was quenched by the addition of 20 mM Tris-HCl pH 7.4 for 15 min. The cells were then washed twice with cold PBS and lysed with 1 ml lysis buffer (0.5% Na-deoxycholate, 50 mM Tris-HCl pH 7.4, 150 mM NaCl, 0.25% SDS, 0.5% Triton X-100 with complete protease inhibitor cocktail (Roche)) for 30 min on ice. To reduce viscosity, the lysate was passed through a 27Gx3/4" needle and then centrifuged at 15,000g for 20 min at 4°C. For immunoprecipitation, 25 µl anti-HA-agarose beads (Sigma A2095) were washed with washing buffer (10 mM Hepes, 150 mM NaCl, 1 mM EGTA, 0.1 mM $MgCl_2$, 0.1% Triton X-100 and complete protease inhibitor cocktail). The lysate from $24x10^6$ cells was added to the beads and rotated for three hours at 4°C. The beads were then washed four times with washing buffer and proteins were eluted with sample buffer containing 50 mM DTT. For immunoprecipitation of endogenous protein complexes, 4 µg of rabbit-anti-VAPB, rabbit-anti-ELYS or IgG as a control were immobilized on 40 µl Protein A sepharose 4 Fast Flow beads (GE Healthcare) for three hours and incubated with lysates from $24x10^6$ cells that had or had not been subjected to cross-linking as described above.

*Proximity Ligation Assay (PLA)*
HeLa cells were seeded at a density of 40,000 cells/well in 24-well plates. After 48 hours, cells were fixed with 4% paraformaldehyde and permeabilized with 0.05% (v/v) Triton X-100. PLA assays were performed using the Duolink In Situ PLA kit (Sigma Aldrich, St. Louis, MO, USA, DUO 9200). Cells were blocked and incubated with mouse anti-VAPB and rabbit anti-emerin, rabbit anti-ELYS, rabbit anti-ACBD5 or rabbit anti-OSBPL9, respectively (see Table S4 for antibodies). After ligation and amplification using the corresponding PLA probes, the cells were counterstained for VAPB and mounted using Duolink mounting medium with DAPI. Images were acquired on an LSM510 Confocal laser

scanning microscope using a 63X /1.4 oil immersion lens. 450 cells over three independent experiments were analyzed for PLA interaction using CellProfiler 2.2 (66). One-way analysis of variance (ANOVA) followed by Bonferroni post-test was used for statistical analysis and a confidence interval of 95% was set.

**Acknowledgements**
The authors would like to thank Thierry Wasselin and Christiane Spillner (University Medical Center Göttingen, Germany) and Christine Richardson (School of Biological and Biomedical Sciences, Durham University, UK) for expert technical assistance, Drs. Eric Schirmer (Edinburgh), Nica Borgese (Milan, Italy) and Sima Lev (Rehovot, Israel) for valuable reagents and Dr. Eric Arakel (Göttingen) for advice. The work was funded by grants from the DFG to RHK and HU (SFB1190).

**Conflict of Interest**
The authors declare that they have no conflicts of interest with the contents of this article.

## References


1. Lev, S., Ben Halevy, D., Peretti, D., and Dahan, N. (2008) The VAP protein family: from cellular functions to motor neuron disease. *Trends Cell Biol* **18**, 282-290
2. Murphy, S. E., and Levine, T. P. (2016) VAP, a Versatile Access Point for the Endoplasmic Reticulum: Review and analysis of FFAT-like motifs in the VAPome. *Biochim Biophys Acta* **1861**, 952-961
3. Casson, J., McKenna, M., Hassdenteufel, S., Aviram, N., Zimmerman, R., and High, S. (2017) Multiple pathways facilitate the biogenesis of mammalian tail-anchored proteins. *J Cell Sci* **130**, 3851-3861
4. Kutay, U., Hartmann, E., and Rapoport, T. A. (1993) A class of membrane proteins with a C-terminal anchor. *Trends Cell Biol.* **3**, 72-75.
5. Costello, J. L., Castro, I. G., Hacker, C., Schrader, T. A., Metz, J., Zeuschner, D., Azadi, A. S., Godinho, L. F., Costina, V., Findeisen, P., Manner, A., Islinger, M., and Schrader, M. (2017) ACBD5 and VAPB mediate membrane associations between peroxisomes and the ER. *J Cell Biol* **216**, 331-342
6. Stoica, R., De Vos, K. J., Paillusson, S., Mueller, S., Sancho, R. M., Lau, K. F., Vizcay-Barrena, G., Lin, W. L., Xu, Y. F., Lewis, J., Dickson, D. W., Petrucelli, L., Mitchell, J. C., Shaw, C. E., and Miller, C. C. (2014) ER-mitochondria associations are regulated by the VAPB-PTPIP51 interaction and are disrupted by ALS/FTD-associated TDP-43. *Nat Commun* **5**, 3996
7. Kuijpers, M., Yu, K. L., Teuling, E., Akhmanova, A., Jaarsma, D., and Hoogenraad, C. C. (2013) The ALS8 protein VAPB interacts with the ER-Golgi recycling protein YIF1A and regulates membrane delivery into dendrites. *EMBO J* **32**, 2056-2072
8. Moustaqim-Barrette, A., Lin, Y. Q., Pradhan, S., Neely, G. G., Bellen, H. J., and Tsuda, H. (2014) The amyotrophic lateral sclerosis 8 protein, VAP, is required for ER protein quality control. *Hum Mol Genet* **23**, 1975-1989
9. Johnson, B., Leek, A. N., Sole, L., Maverick, E. E., Levine, T. P., and Tamkun, M. M. (2018) Kv2 potassium channels form endoplasmic reticulum/plasma membrane junctions via interaction with VAPA and VAPB. *Proc Natl Acad Sci U S A* **115**, E7331-E7340
10. Huttlin, E. L., Ting, L., Bruckner, R. J., Gebreab, F., Gygi, M. P., Szpyt, J., Tam, S., Zarraga, G., Colby, G., Baltier, K., Dong, R., Guarani, V., Vaites, L. P., Ordureau, A., Rad, R., Erickson, B. K., Wuhr, M., Chick, J., Zhai, B., Kolippakkam, D., Mintseris, J., Obar, R. A., Harris, T., Artavanis-Tsakonas, S., Sowa, M. E., De Camilli, P., Paulo, J. A., Harper, J. W., and Gygi, S. P. (2015) The BioPlex Network: A Systematic Exploration of the Human Interactome. *Cell* **162**, 425-440
11. Murphy, R., and Wente, S. R. (1996) An RNA-export mediator with an essential nuclear export signal. *Nature* **383**, 357-360
12. Loewen, C. J., Roy, A., and Levine, T. P. (2003) A conserved ER targeting motif in three families of lipid binding proteins and in Opi1p binds VAP. *EMBO J* **22**, 2025-2035
13. Baron, Y., Pedrioli, P. G., Tyagi, K., Johnson, C., Wood, N. T., Fountaine, D., Wightman, M., and Alexandru, G. (2014) VAPB/ALS8 interacts with FFAT-like proteins including the p97 cofactor FAF1 and the ASNA1 ATPase. *BMC Biol* **12**, 39
14. Nishimura, A. L., Mitne-Neto, M., Silva, H. C., Richieri-Costa, A., Middleton, S., Cascio, D., Kok, F., Oliveira, J. R., Gillingwater, T., Webb, J., Skehel, P., and Zatz, M. (2004) A mutation in the vesicle-trafficking protein VAPB causes late-onset spinal muscular atrophy and amyotrophic lateral sclerosis. *Am J Hum Genet* **75**, 822-831
15. Tran, D., Chalhoub, A., Schooley, A., Zhang, W., and Ngsee, J. K. (2012) A mutation in VAPB that causes amyotrophic lateral sclerosis also causes a nuclear envelope defect. *J Cell Sci* **125**, 2831-2836
16. Gingras, A. C., Abe, K. T., and Raught, B. (2018) Getting to know the neighborhood: using proximity-dependent biotinylation to characterize protein complexes and map organelles. *Curr Opin Chem Biol* **48**, 44-54

17. Kim, D. I., and Roux, K. J. (2016) Filling the Void: Proximity-Based Labeling of Proteins in Living Cells. *Trends Cell Biol* **26**, 804-817
18. Roux, K. J., Kim, D. I., Raida, M., and Burke, B. (2012) A promiscuous biotin ligase fusion protein identifies proximal and interacting proteins in mammalian cells. *J Cell Biol* **196**, 801-810
19. Branon, T. C., Bosch, J. A., Sanchez, A. D., Udeshi, N. D., Svinkina, T., Carr, S. A., Feldman, J. L., Perrimon, N., and Ting, A. Y. (2018) Efficient proximity labeling in living cells and organisms with TurboID. *Nat Biotechnol* **36**, 880-887
20. Rhee, H. W., Zou, P., Udeshi, N. D., Martell, J. D., Mootha, V. K., Carr, S. A., and Ting, A. Y. (2013) Proteomic mapping of mitochondria in living cells via spatially restricted enzymatic tagging. *Science* **339**, 1328-1331
21. Udeshi, N. D., Pedram, K., Svinkina, T., Fereshetian, S., Myers, S. A., Aygun, O., Krug, K., Clauser, K., Ryan, D., Ast, T., Mootha, V. K., Ting, A. Y., and Carr, S. A. (2017) Antibodies to biotin enable large-scale detection of biotinylation sites on proteins. *Nat Methods* **14**, 1167-1170
22. Lobingier, B. T., Huttenhain, R., Eichel, K., Miller, K. B., Ting, A. Y., von Zastrow, M., and Krogan, N. J. (2017) An Approach to Spatiotemporally Resolve Protein Interaction Networks in Living Cells. *Cell* **169**, 350-360 e312
23. Mick, D. U., Rodrigues, R. B., Leib, R. D., Adams, C. M., Chien, A. S., Gygi, S. P., and Nachury, M. V. (2015) Proteomics of primary cilia by proximity labeling. *Dev Cell* **35**, 497-512
24. Lam, S. S., Martell, J. D., Kamer, K. J., Deerinck, T. J., Ellisman, M. H., Mootha, V. K., and Ting, A. Y. (2015) Directed evolution of APEX2 for electron microscopy and proximity labeling. *Nat Methods* **12**, 51-54
25. Hung, V., Zou, P., Rhee, H. W., Udeshi, N. D., Cracan, V., Svinkina, T., Carr, S. A., Mootha, V. K., and Ting, A. Y. (2014) Proteomic mapping of the human mitochondrial intermembrane space in live cells via ratiometric APEX tagging. *Mol Cell* **55**, 332-341
26. Bar, D. Z., Atkatsh, K., Tavarez, U., Erdos, M. R., Gruenbaum, Y., and Collins, F. S. (2018) Biotinylation by antibody recognition-a method for proximity labeling. *Nat Methods* **15**, 127-133
27. Pfaff, J., Rivera Monroy, J., Jamieson, C., Rajanala, K., Vilardi, F., Schwappach, B., and Kehlenbach, R. H. (2016) Emery-Dreifuss muscular dystrophy mutations impair TRC40-mediated targeting of emerin to the inner nuclear membrane. *J Cell Sci* **129**, 502-516
28. Chen, J., Zheng, X. F., Brown, E. J., and Schreiber, S. L. (1995) Identification of an 11-kDa FKBP12-rapamycin-binding domain within the 289-kDa FKBP12-rapamycin-associated protein and characterization of a critical serine residue. *Proc Natl Acad Sci U S A* **92**, 4947-4951
29. Cheng, L. C., Baboo, S., Lindsay, C., Brusman, L., Martinez-Bartolome, S., Tapia, O., Zhang, X., Yates, J. R., 3rd, and Gerace, L. (2019) Identification of new transmembrane proteins concentrated at the nuclear envelope using organellar proteomics of mesenchymal cells. *Nucleus* **10**, 126-143
30. Saiz-Ros, N., Czapiewski, R., Epifano, I., Stevenson, A., Swanson, S. K., Dixon, C. R., Zamora, D. B., McElwee, M., Vijayakrishnan, S., Richardson, C. A., Dong, L., Kelly, D. A., Pytowski, L., Goldberg, M. W., Florens, L., Graham, S. V., and Schirmer, E. C. (2019) Host Vesicle Fusion Protein VAPB Contributes to the Nuclear Egress Stage of Herpes Simplex Virus Type-1 (HSV-1) Replication. *Cells* **8,** doi: 10.3390/cells8020120
31. Cho, I. T., Adelmant, G., Lim, Y., Marto, J. A., Cho, G., and Golden, J. A. (2017) Ascorbate peroxidase proximity labeling coupled with biochemical fractionation identifies promoters of endoplasmic reticulum-mitochondrial contacts. *J Biol Chem* **292**, 16382-16392
32. Han, S., Udeshi, N. D., Deerinck, T. J., Svinkina, T., Ellisman, M. H., Carr, S. A., and Ting, A. Y. (2017) Proximity Biotinylation as a Method for Mapping Proteins Associated with mtDNA in Living Cells. *Cell Chem Biol* **24**, 404-414
33. Hung, V., Lam, S. S., Udeshi, N. D., Svinkina, T., Guzman, G., Mootha, V. K., Carr, S. A., and Ting, A. Y. (2017) Proteomic mapping of cytosol-facing outer mitochondrial and ER membranes in living human cells by proximity biotinylation. *Elife* **6,** doi: 10.7554/eLife.24463

34. Lee, S. Y., Kang, M. G., Park, J. S., Lee, G., Ting, A. Y., and Rhee, H. W. (2016) APEX Fingerprinting Reveals the Subcellular Localization of Proteins of Interest. *Cell Rep* **15**, 1837-1847
35. Paek, J., Kalocsay, M., Staus, D. P., Wingler, L., Pascolutti, R., Paulo, J. A., Gygi, S. P., and Kruse, A. C. (2017) Multidimensional Tracking of GPCR Signaling via Peroxidase-Catalyzed Proximity Labeling. *Cell* **169**, 338-349 e311
36. Bengtsson, L., and Otto, H. (2008) LUMA interacts with emerin and influences its distribution at the inner nuclear membrane. *J Cell Sci* **121**, 536-548
37. Liang, W. C., Mitsuhashi, H., Keduka, E., Nonaka, I., Noguchi, S., Nishino, I., and Hayashi, Y. K. (2011) TMEM43 mutations in Emery-Dreifuss muscular dystrophy-related myopathy. *Annals of Neurology* **69**, 1005-1013
38. Franke, W. W., Dorflinger, Y., Kuhn, C., Zimbelmann, R., Winter-Simanowski, S., Frey, N., and Heid, H. (2014) Protein LUMA is a cytoplasmic plaque constituent of various epithelial adherens junctions and composite junctions of myocardial intercalated disks: a unifying finding for cell biology and cardiology. *Cell Tissue Res* **357**, 159-172
39. Defeo-Jones, D., Huang, P. S., Jones, R. E., Haskell, K. M., Vuocolo, G. A., Hanobik, M. G., Huber, H. E., and Oliff, A. (1991) Cloning of cDNAs for cellular proteins that bind to the retinoblastoma gene product. *Nature* **352**, 251-254
40. Wu, M. Y., Eldin, K. W., and Beaudet, A. L. (2008) Identification of chromatin remodeling genes Arid4a and Arid4b as leukemia suppressor genes. *J Natl Cancer Inst* **100**, 1247-1259
41. Cartegni, L., di Barletta, M. R., Barresi, R., Squarzoni, S., Sabatelli, P., Maraldi, N., Mora, M., Di Blasi, C., Cornelio, F., Merlini, L., Villa, A., Cobianchi, F., and Toniolo, D. (1997) Heart-specific localization of emerin: new insights into Emery-Dreifuss muscular dystrophy. *Hum Mol Genet* **6**, 2257-2264
42. Salpingidou, G., Smertenko, A., Hausmanowa-Petrucewicz, I., Hussey, P. J., and Hutchison, C. J. (2007) A novel role for the nuclear membrane protein emerin in association of the centrosome to the outer nuclear membrane. *J Cell Biol* **178**, 897-904
43. Ohba, T., Schirmer, E. C., Nishimoto, T., and Gerace, L. (2004) Energy- and temperature-dependent transport of integral proteins to the inner nuclear membrane via the nuclear pore. *J Cell Biol.* **167**, 1051-1062.
44. Soullam, B., and Worman, H. J. (1995) Signals and structural features involved in integral membrane protein targeting to the inner nuclear membrane. *J Cell Biol* **130**, 15-27
45. Ungricht, R., Klann, M., Horvath, P., and Kutay, U. (2015) Diffusion and retention are major determinants of protein targeting to the inner nuclear membrane. *J Cell Biol* **209**, 687-704
46. Zuleger, N., Kelly, D. A., Richardson, A. C., Kerr, A. R., Goldberg, M. W., Goryachev, A. B., and Schirmer, E. C. (2011) System analysis shows distinct mechanisms and common principles of nuclear envelope protein dynamics. *J. Cell Biol.* **193**, 109-123.
47. Blenski, M., and Kehlenbach, R. H. (2019) Targeting of LRRC59 to the Endoplasmic Reticulum and the Inner Nuclear Membrane. *Int J Mol Sci* **20,** doi: 10.3390/ijms20020334.
48. Foisner, R., and Gerace, L. (1993) Integral membrane proteins of the nuclear envelope interact with lamins and chromosomes, and binding is modulated by mitotic phosphorylation. *Cell.* **73**, 1267-1279.
49. Furukawa, K., Pante, N., Aebi, U., and Gerace, L. (1995) Cloning of a cDNA for lamina-associated polypeptide 2 (LAP2) and identification of regions that specify targeting to the nuclear envelope. *EMBO J.* **14**, 1626-1636.
50. Sukegawa, J., and Blobel, G. (1993) A nuclear pore complex protein that contains zinc finger motifs, binds DNA, and faces the nucleoplasm. *Cell* **72**, 29-38
51. Cordes, V. C., Reidenbach, S., Rackwitz, H. R., and Franke, W. W. (1997) Identification of protein p270/Tpr as a constitutive component of the nuclear pore complex-attached intranuclear filaments. *J Cell Biol* **136**, 515-529

52. Rasala, B. A., Orjalo, A. V., Shen, Z., Briggs, S., and Forbes, D. J. (2006) ELYS is a dual nucleoporin/kinetochore protein required for nuclear pore assembly and proper cell division. *Proc Natl Acad Sci U S A* **103**, 17801-17806
53. Gerace, L., and Blobel, G. (1980) The nuclear envelope lamina is reversibly depolymerized during mitosis. *Cell* **19**, 277-287
54. Söderberg, O., Gullberg, M., Jarvius, M., Ridderstrale, K., Leuchowius, K. J., Jarvius, J., Wester, K., Hydbring, P., Bahram, F., Larsson, L. G., and Landegren, U. (2006) Direct observation of individual endogenous protein complexes in situ by proximity ligation. *Nat Methods* **3**, 995-1000
55. Chojnowski, A., Sobota, R. M., Ong, P. F., Xie, W., Wong, X., Dreesen, O., Burke, B., and Stewart, C. L. (2018) 2C-BioID: An Advanced Two Component BioID System for Precision Mapping of Protein Interactomes. *iScience* **10**, 40-52
56. Franz, C., Walczak, R., Yavuz, S., Santarella, R., Gentzel, M., Askjaer, P., Galy, V., Hetzer, M., Mattaj, I. W., and Antonin, W. (2007) MEL-28/ELYS is required for the recruitment of nucleoporins to chromatin and postmitotic nuclear pore complex assembly. *EMBO Rep* **8**, 165-172
57. Gillespie, P. J., Khoudoli, G. A., Stewart, G., Swedlow, J. R., and Blow, J. J. (2007) ELYS/MEL-28 chromatin association coordinates nuclear pore complex assembly and replication licensing. *Curr Biol* **17**, 1657-1662
58. Belshaw, P. J., Ho, S. N., Crabtree, G. R., and Schreiber, S. L. (1996) Controlling protein association and subcellular localization with a synthetic ligand that induces heterodimerization of proteins. *Proc Natl Acad Sci U S A* **93**, 4604-4607
59. Fasana, E., Fossati, M., Ruggiano, A., Brambillasca, S., Hoogenraad, C. C., Navone, F., Francolini, M., and Borgese, N. (2010) A VAPB mutant linked to amyotrophic lateral sclerosis generates a novel form of organized smooth endoplasmic reticulum. *FASEB J* **24**, 1419-1430
60. Gasteier, J. E., Madrid, R., Krautkramer, E., Schroder, S., Muranyi, W., Benichou, S., and Fackler, O. T. (2003) Activation of the Rac-binding partner FHOD1 induces actin stress fibers via a ROCK-dependent mechanism. *J Biol Chem* **278**, 38902-38912
61. Charneau, P., Mirambeau, G., Roux, P., Paulous, S., Buc, H., and Clavel, F. (1994) HIV-1 reverse transcription. A termination step at the center of the genome. *J Mol Biol* **241**, 651-662
62. Chen, C., and Okayama, H. (1987) High-efficiency transformation of mammalian cells by plasmid DNA. *Mol Cell Biol* **7**, 2745-2752
63. Atanassov, I., and Urlaub, H. (2013) Increased proteome coverage by combining PAGE and peptide isoelectric focusing: comparative study of gel-based separation approaches. *Proteomics* **13**, 2947-2955
64. Cox, J., and Mann, M. (2008) MaxQuant enables high peptide identification rates, individualized p.p.b.-range mass accuracies and proteome-wide protein quantification. *Nat Biotechnol* **26**, 1367-1372
65. Vizcaino, J. A., Deutsch, E. W., Wang, R., Csordas, A., Reisinger, F., Rios, D., Dianes, J. A., Sun, Z., Farrah, T., Bandeira, N., Binz, P. A., Xenarios, I., Eisenacher, M., Mayer, G., Gatto, L., Campos, A., Chalkley, R. J., Kraus, H. J., Albar, J. P., Martinez-Bartolome, S., Apweiler, R., Omenn, G. S., Martens, L., Jones, A. R., and Hermjakob, H. (2014) ProteomeXchange provides globally coordinated proteomics data submission and dissemination. *Nat Biotechnol* **32**, 223-226
66. Carpenter, A. E., Jones, T. R., Lamprecht, M. R., Clarke, C., Kang, I. H., Friman, O., Guertin, D. A., Chang, J. H., Lindquist, R. A., Moffat, J., Golland, P., and Sabatini, D. M. (2006) CellProfiler: image analysis software for identifying and quantifying cell phenotypes. *Genome Biol* **7**, R100

## Figure legends

**Figure 1**
VAPB localizes to the INM.
(A) HeLa cells were grown on coverslips and subjected to indirect immunofluorescence using antibodies against VAPB. Cells were blocked (i) with 3% BSA or (ii) with Sigma Duolink blocking solution.
(B) HeLa cells were transfected with plasmids coding for mCherry-FRB-VAPB or HA-FRB-VAPB, as indicated.
(C) HeLa cells were co-transfected with plasmids coding for mCherry-FRB-VAPB and dGFP-GST-cNLS-FKBP12. After treatment with (+) or without (-) rapamycin, cells were fixed and analyzed by confocal microscopy. Scale bar, 10 μm.
(D) HeLa cells were analysed by immunoelectron microscopy, using antibodies against VAPB. C, cytoplasm; M, mitochondria; N, nucleus. The arrows indicate nuclear pore complexes. Scale bar, 100 nm.

**Figure 2**
Comparison of the classic and a new APEX-approach.
(A) Schemes of the "direct fusion (classic) approach" (left) and the "rapamycin (new) approach" (right).
(B) For the direct fusion and the rapamycin approach, cells were transfected with plasmids coding for GFP-APEX2 or APEX2-VAPB and FKBP12-GFP-APEX2 and mCherry-FRB-VAPB, respectively. Cells were analyzed directly (left) or upon incubation with or without rapamycin (right). Scale bar, 10 μm.
(C) Cells were transfected as in B and subjected to the biotinylation protocol. Biotinylated proteins were enriched using neutravidin beads and total and bound proteins were analyzed by SDS-PAGE followed by Western blotting. Note that GFP-APEX2 (lanes 5 and 7) and APEX2-VAPB (lanes 6 and 8) have very similar molecular weights.

**Figure 3**
Proximity mapping of mCherry-FRB-VAPB by RAPIDS.
(A) Experimental workflow. Cells grown in "light" or "heavy" medium are co-transfected with plasmids coding for FKBP12-GFP-APEX2 and mCherry-FRB-VAPB, and subjected to APEX2-dependent biotinylation in the absence or presence of rapamycin. Note that this labelling scheme reflects the reverse reaction. In the forward reaction, "light" and "heavy" media are used for cells treated with or without rapamycin, respectively. Proteins from cell lysates are bound to neutravidin beads and the total and the bound fractions are analyzed by LC-MS.
(B) The scatter plot resulting from two independent experiments shows normalized $\log_2$-ratios of proteins eluted from neutravidin beads in forward (heavy medium (H), without rapamycin; light (L) medium, with rapamycin; x-axis) and reverse (heavy medium (H), with rapamycin; light (L) medium, without rapamycin y-axis) experiments. The plot focuses on the upper left quadrant, because in the forward reaction, low H/L-ratios (i.e. negative $\log_2$-values) are expected for specific hits, whereas high ratios are expected in the reverse reaction. Known interacting partners of VAPB are underlined. Closed circles: proteins that were significant in all experiments; open triangles: proteins that were significant only in forward experiments; open squares: proteins that were significant only in reverse experiments.
(C) Total cell lysates (total) and proteins bound to neutravidin beads (bound) from one of the experiments depicted in (B) were analyzed by Western blotting, using antibodies against VAPB, ACBD5, OSBPL9 and emerin and GAPDH as a loading control.

**Figure 4**
RAPIDS using HA-FRB-VAPB.
(A) Experimental workflow. Cells are grown in "light" or "heavy" medium as indicated, co-transfected with plasmids coding for APEX2-dGFP-cNLS-FKBP12 and HA-FRB-VAPB, and subjected to RAPIDS as described in Fig. 3A.

(B) Transfected cells were treated with or without rapamycin as indicated, fixed and analyzed by fluorescence microscopy. Scale bar, 10 μm.
(C) The scatter plot resulting from two independent experiments shows normalized $log_2$-ratios of proteins eluted from neutravidin beads in forward (heavy medium (H), without rapamycin; light (L) medium, with rapamycin; x-axis) and reverse (heavy medium (H), with rapamycin; light (L) medium, without rapamycin y-axis) experiments. As in Fig. 3, the plot focuses on the upper left quadrant. Closed circles: proteins that were significant in all experiments; open triangles: proteins that were significant only in forward experiments; open squares: proteins that were significant only in reverse experiments.
(D) Total cell lysates (total) and proteins bound to neutravidin beads (bound) from experiments depicted in (C) were analyzed by Western blotting using antibodies against VAPB, ELYS, Lamin B1, Nup153, Lamin A/C, TMPO, TOR1AIP1, SEC22b, emerin and GAPDH as a loading control.

**Figure 5**
VAPB forms complexes with emerin, TMEM43 and ELYS.
(A) HeLa cells were treated with (+) or without (-; DMSO as a control) DSP and endogenous proteins from cell lysates were precipitated using rabbit-anti-VAPB and rabbit IgG as a control. *, IgG heavy chain.
(B) HeLa cells were transfected with constructs coding for HA-FRB-VAPB or HA-FRB and subjected to crosslinking with (+) or without (-; DMSO as a control) DSP. Proteins from cell-lysates were immunoprecipitated using anti-HA antibodies. Note that HA-FRB was expressed and precipitated to similar levels as HA-FRB-VAPBB (data not shown). (A, B) Precipitated proteins were analyzed by Western blotting, detecting VAPB, ACBD5, OSBPL9, emerin, TMEM43, ELYS, the HA-tag and, for control, $Na^+/K^+$-ATPase, as indicated.

**Figure 6**
VAPB is in close proximity to emerin and ELYS.
(A, B) Cells were treated with siRNAs against VAPB or non-targeting (nt) siRNAs as indicated and subjected to PLAs using antibodies against VAPB (A and B) and emerin (A) or ELYS (B), respectively. Indirect immunofluorescence was used to detect VAPB. The graphs show the quantification of PLA-results from three independent experiments, analyzing a total of 450 cells. The bars indicate mean values ± SD. Single antibody controls were performed to confirm the specificity of PLA interactions. ***, $P<0.001$. Scale bars, 10 μm.

**Figure 7**
The VAPB-interactome. Schematic representation of the protein network identified by RAPIDS using HA-FRB-VAPB (HA-VAPB) with APEX2-dGFP-cNLS-FKBP12 (NLS-APEX2) or mCherry-FRB-VAPB (mCherry-VAPB) with FKBP12-GFP-APEX2 (APEX2). Dotted lines indicate interactions that have also been found in previous studies.

Figure 1

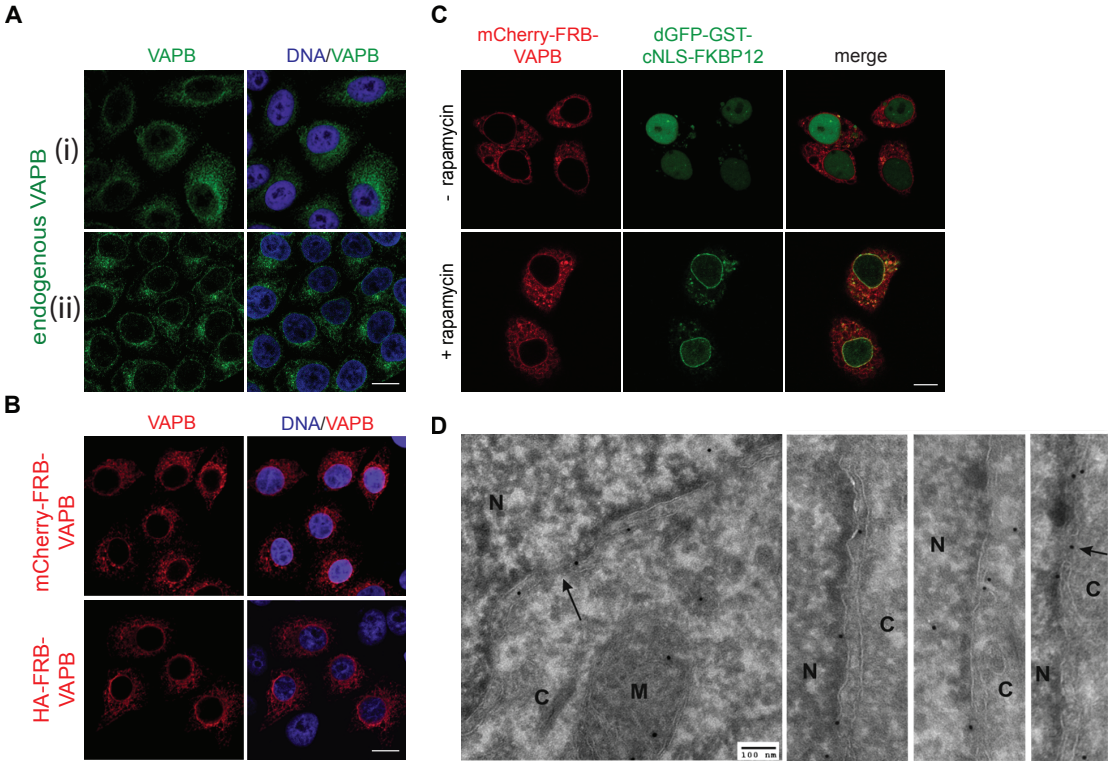
A
VAPB
DNA/VAPB
endogenous VAPB
(i)
(ii)
B
VAPB
DNA/VAPB
mCherry-FRB-VAPB
HA-FRB-VAPB
C
mCherry-FRB-VAPB
dGFP-GST-cNLS-FKBP12
merge
- rapamycin
+ rapamycin
D
N
C
M
100 nm

Figure 2

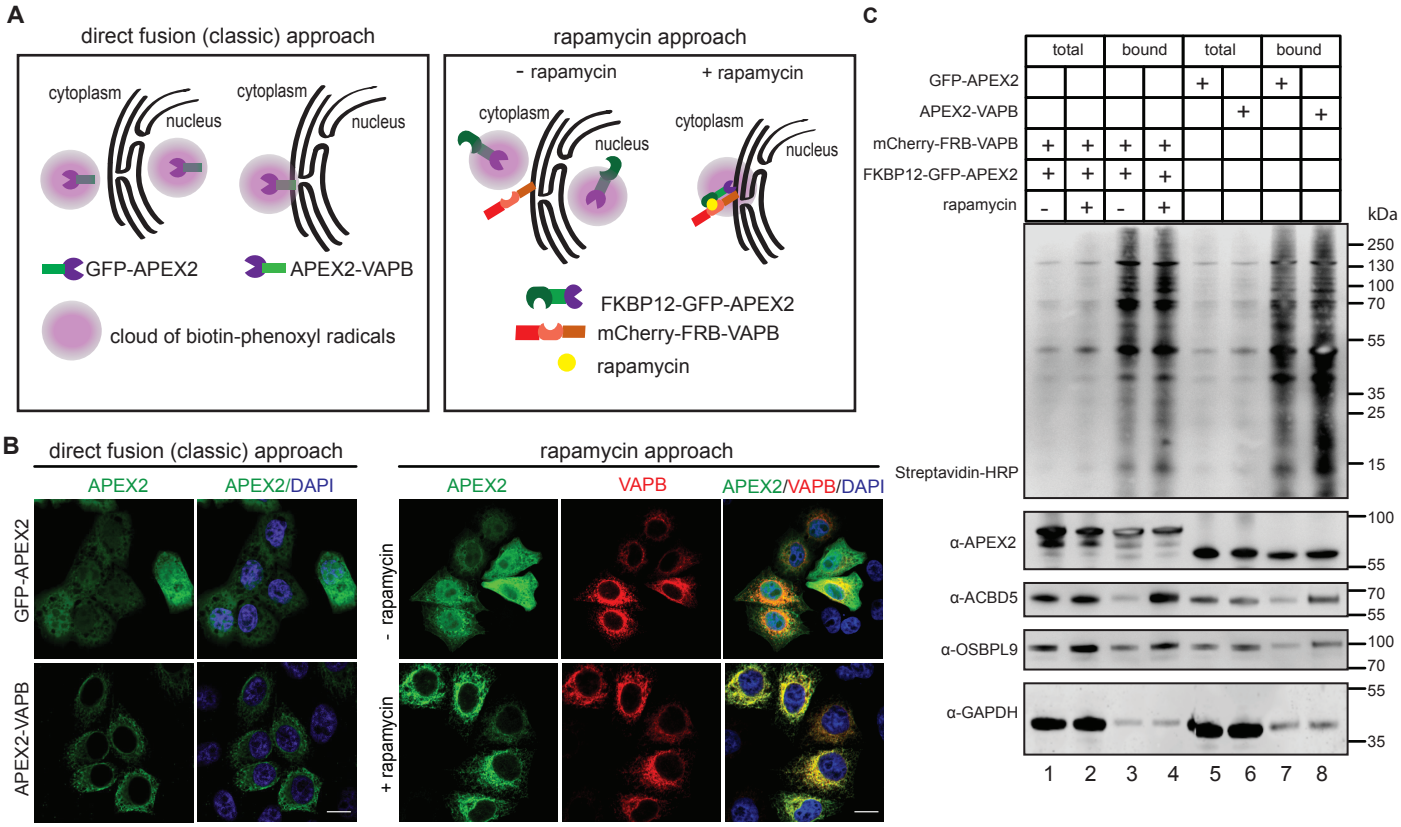
A
direct fusion (classic) approach
rapamycin approach
- rapamycin
+ rapamycin
cytoplasm
nucleus
GFP-APEX2
APEX2-VAPB
cloud of biotin-phenoxyl radicals
FKBP12-GFP-APEX2
mCherry-FRB-VAPB
rapamycin
B
direct fusion (classic) approach
rapamycin approach
APEX2
APEX2/DAPI
VAPB
APEX2/VAPB/DAPI
GFP-APEX2
APEX2-VAPB
- rapamycin
+ rapamycin
C
total
bound
GFP-APEX2
APEX2-VAPB
mCherry-FRB-VAPB
FKBP12-GFP-APEX2
rapamycin
kDa
Streptavidin-HRP
α-APEX2
α-ACBD5
α-OSBPL9
α-GAPDH
250
130
100
70
55
35
25
15
1 2 3 4 5 6 7 8

Figure 3

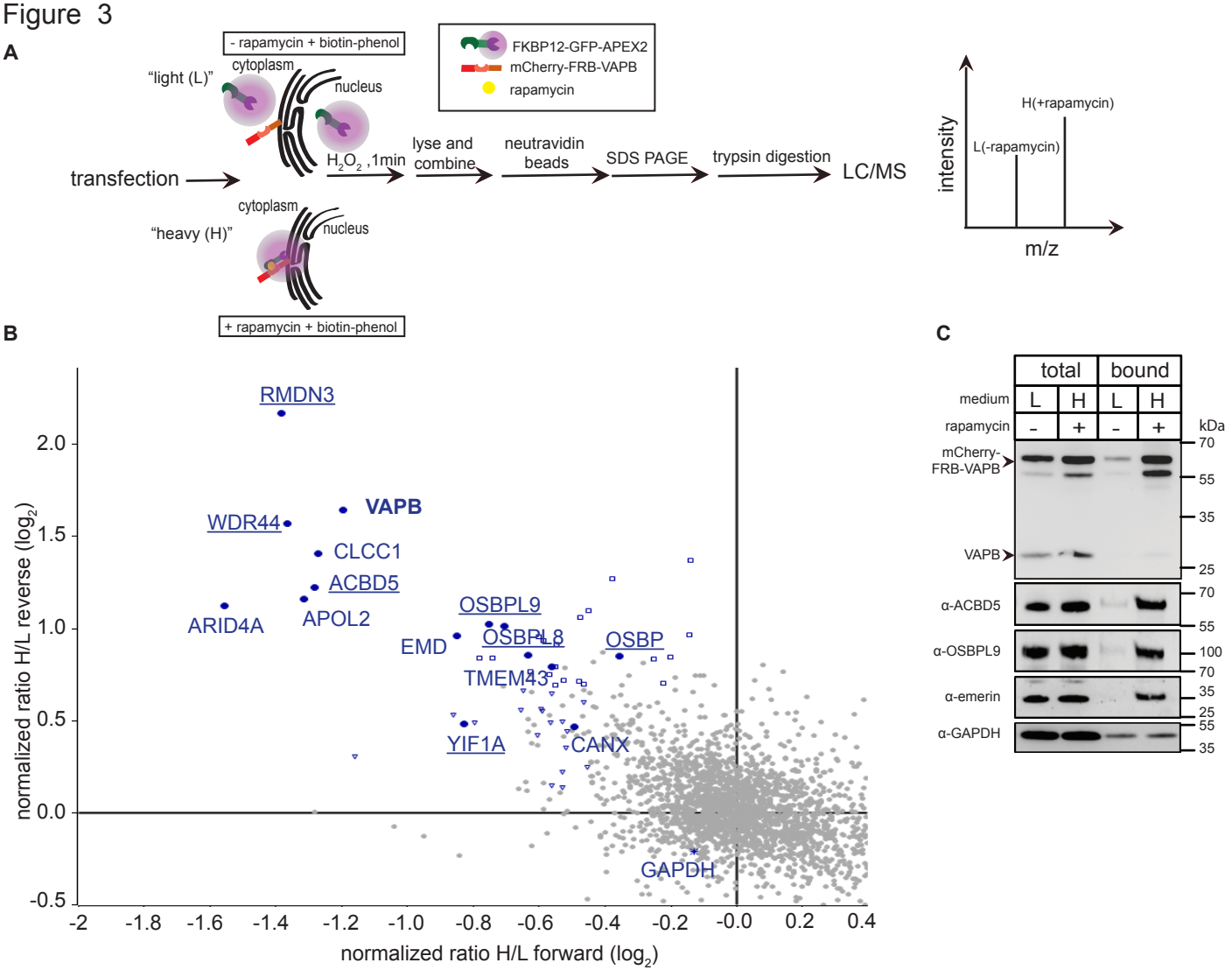
A
- rapamycin + biotin-phenol
FKBP12-GFP-APEX2
mCherry-FRB-VAPB
rapamycin
"light (L)"
cytoplasm
nucleus
transfection
$H_2O_2$ ,1min
lyse and combine
neutravidin beads
SDS PAGE
trypsin digestion
LC/MS
"heavy (H)"
+ rapamycin + biotin-phenol
intensity
H(+rapamycin)
L(-rapamycin)
m/z
B
RMDN3
VAPB
WDR44
CLCC1
ACBD5
ARID4A
APOL2
OSBPL9
EMD
OSBPL8
OSBP
TMEM43
YIF1A
CANX
GAPDH
normalized ratio H/L reverse ($log_2$)
normalized ratio H/L forward ($log_2$)
C
total
bound
medium
L
H
rapamycin
kDa
mCherry-FRB-VAPB
VAPB
α-ACBD5
α-OSBPL9
α-emerin
α-GAPDH

Figure 4

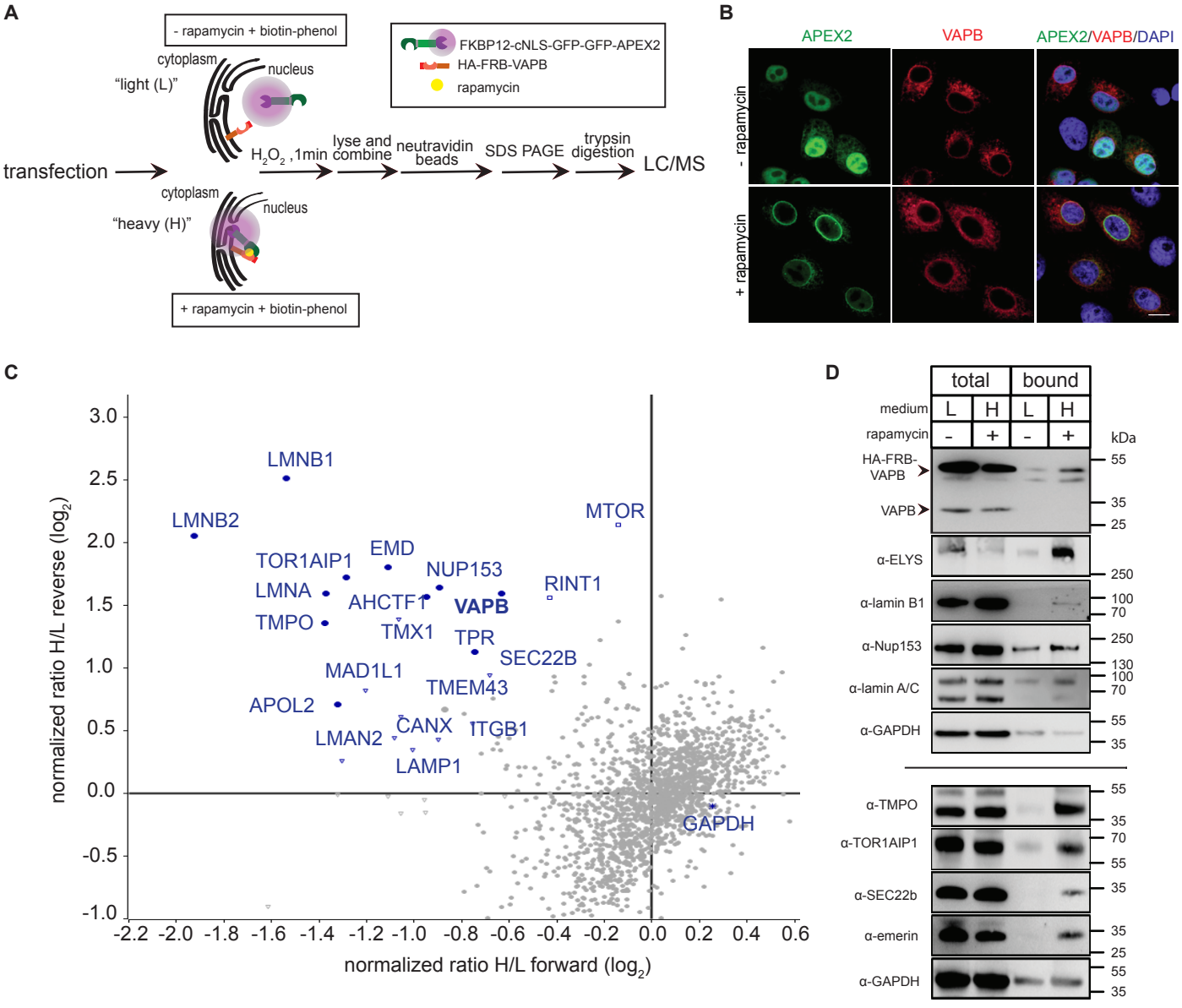
A
- rapamycin + biotin-phenol
cytoplasm
nucleus
"light (L)"
FKBP12-cNLS-GFP-GFP-APEX2
HA-FRB-VAPB
rapamycin
transfection
H2O2 ,1min
lyse and combine
neutravidin beads
SDS PAGE
trypsin digestion
LC/MS
cytoplasm
nucleus
"heavy (H)"
+ rapamycin + biotin-phenol
B
APEX2
VAPB
APEX2/VAPB/DAPI
- rapamycin
+ rapamycin
C
normalized ratio H/L reverse (log2)
normalized ratio H/L forward (log2)
LMNB1
LMNB2
MTOR
TOR1AIP1
EMD
NUP153
RINT1
LMNA
AHCTF1
VAPB
TMPO
TMX1
TPR
SEC22B
MAD1L1
TMEM43
APOL2
CANX
ITGB1
LMAN2
LAMP1
GAPDH
D
total
bound
medium
L
H
L
H
rapamycin
-
+
-
+
kDa
HA-FRB-VAPB
VAPB
α-ELYS
α-lamin B1
α-Nup153
α-lamin A/C
α-GAPDH
α-TMPO
α-TOR1AIP1
α-SEC22b
α-emerin
α-GAPDH

Figure 5

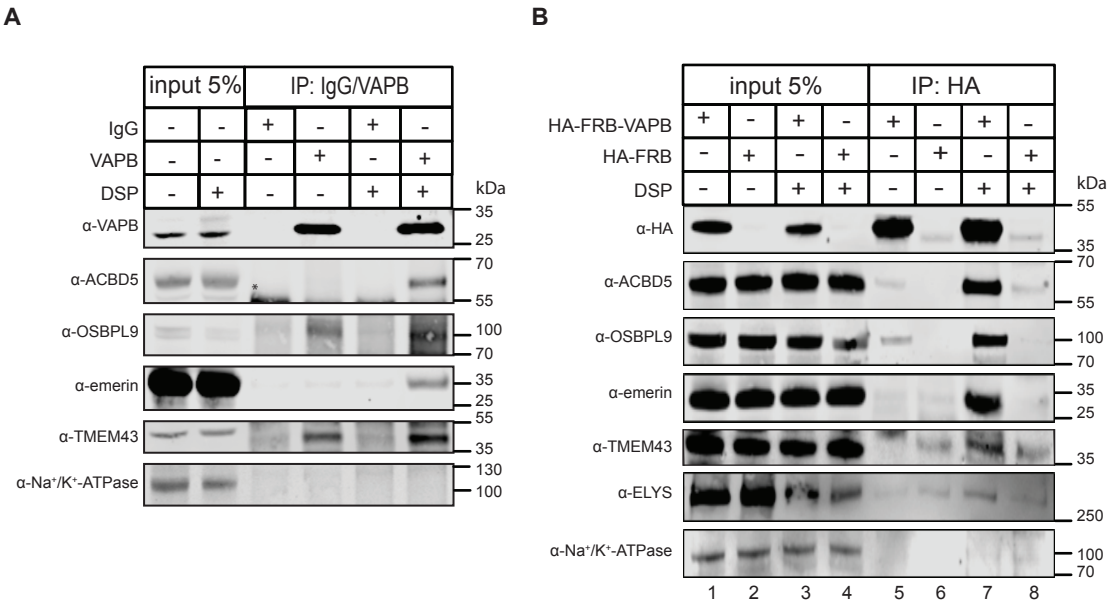
A
input 5%
IP: IgG/VAPB
IgG
VAPB
DSP
kDa
α-VAPB
α-ACBD5
α-OSBPL9
α-emerin
α-TMEM43
α-Na⁺/K⁺-ATPase
B
input 5%
IP: HA
HA-FRB-VAPB
HA-FRB
DSP
kDa
α-HA
α-ACBD5
α-OSBPL9
α-emerin
α-TMEM43
α-ELYS
α-Na⁺/K⁺-ATPase
1 2 3 4 5 6 7 8

Figure 6

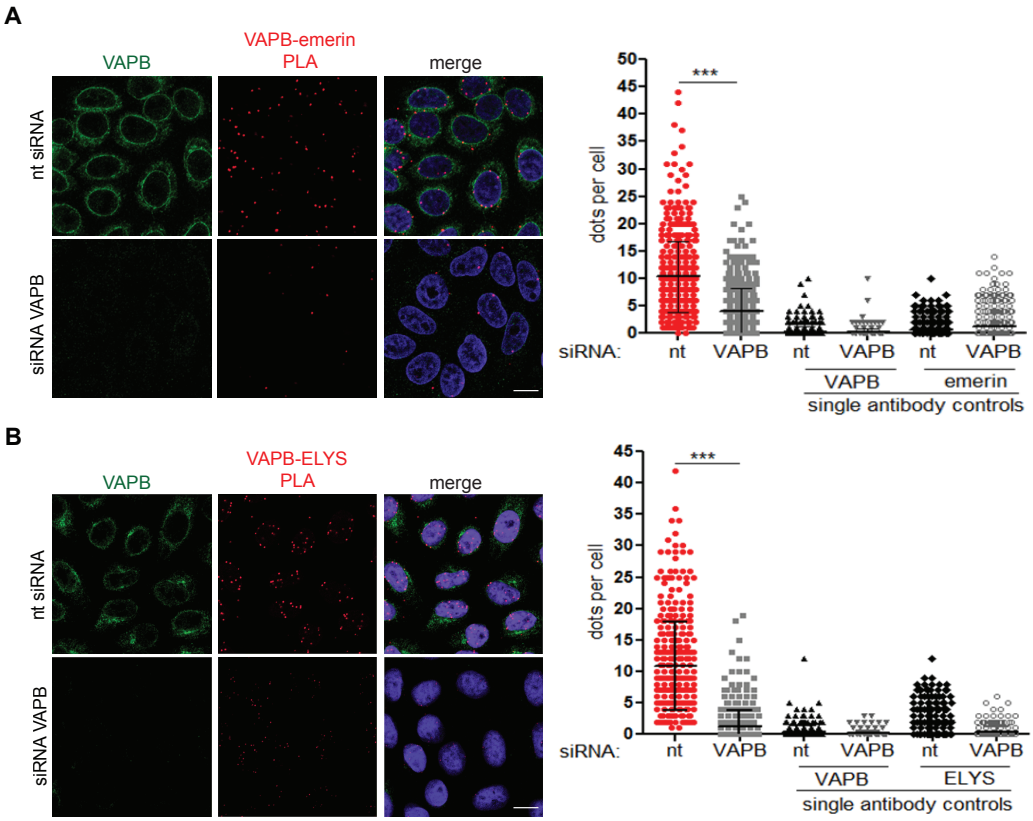
A
VAPB
VAPB-emerin PLA
merge
nt siRNA
siRNA VAPB
dots per cell
***
siRNA:
nt
VAPB
nt
VAPB
nt
VAPB
VAPB
emerin
single antibody controls
B
VAPB
VAPB-ELYS PLA
merge
nt siRNA
siRNA VAPB
dots per cell
***
siRNA:
nt
VAPB
nt
VAPB
nt
VAPB
VAPB
ELYS
single antibody controls

Figure 7

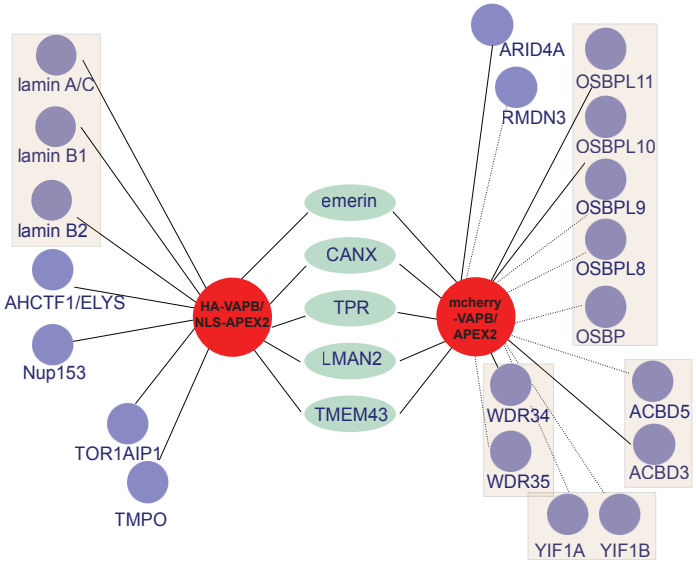
lamin A/C
lamin B1
lamin B2
AHCTF1/ELYS
Nup153
TOR1AIP1
TMPO
HA-VAPB/
NLS-APEX2
emerin
CANX
TPR
LMAN2
TMEM43
mcherry
-VAPB/
APEX2
ARID4A
RMDN3
OSBPL11
OSBPL10
OSBPL9
OSBPL8
OSBP
WDR34
WDR35
ACBD5
ACBD3
YIF1A
YIF1B

## Supporting Information

**Figure S1**
(A) Subcellular fractionation was performed as described by Cheng et al (29). Briefly, Hela cells from three 15 cm plates were lysed by douncing in homogenization buffer (HB, 10 mM HEPES pH 7.8, 10 mM KCl, 1.5 mM $MgCl_2$ 0.1 mM EGTA) containing 1 mM DTT, 1 mM PMSF, 1 ug/ml each of pepstatin, leupeptin and aprotinin. The total cell lysate (T) was layered on top of 2.5 ml sucrose (0.8 M) in HB and centrifuged at 2000 rpm for 10 min at 4° C in a JS4.2 rotor yielding the pellet and the cytoplasmic (C) fraction. The pellet fraction was resuspended in 1.8 M sucrose and layered on top of a 2 ml sucrose cushion (2 M). The gradient was then centrifuged at 35.000 rpm for 1 hr at 4° C in a SW40 Ti rotor. The nuclear pellet was resuspended in HB containing 500 mM NaCl, 1 mM $CaCl_2$ and 25 U/ml benzonase, incubated for 15 min at 37°C, layered on top of 2 ml sucrose (0.8 M) and centrifuged at 4000 rpm for 10 min at 4° C in a JS4.2 rotor. The layer above the sucrose cushion (nuclear content, NC) and the pellet (nuclear envelope, NE) were collected. (B) Equivalent amounts of each fraction were subjected to SDS-PAGE and Western blotting detecting SP1 (a nuclear transcription factor), ELYS and Nup62 (two nucleoporins) POM121 (a transmembrane nucleoporin), lamin A/C and B1, OSBPL9, TMEM43, emerin, VAPB, Stt3B (an ER-protein) and tubulin as a cytoplasmic marker.

**Figure S2**
(A) Cells were co-transfected with plasmids coding for mCherry-FRB-VAPB and FKBP12-GFP-APEX2 and subjected to APEX2-dependent biotinylation in the presence of biotin-phenol, and in the absence (-) or presence of (+) $H_2O_2$ and rapamycin, as indicated. Proteins from cell lysates were bound to neutravidin beads and the total and the bound fractions were analyzed by Western blotting. HRP-streptavidin was used for the detection of biotinylated proteins. (B) Cells were transfected as in A, grown in "light" (L) or "heavy" (H) medium and treated with or without rapamycin. Cells were subjected to APEX-dependent biotinylation in forward and reverse reactions. Proteins from cell lysates were analyzed as in A, detecting biotinylated proteins, FKBP12-GFP-APEX2 as a control for transfection efficiencies and GAPDH as a loading control.

**Figure S3**
HeLa cells were subjected to indirect immunofluorescence, detecting the peroxisomal protein PMP70 and ACBD5 (A) or the Golgi marker GM130 and OSBPL9 (B). Cells were subjected to PLAs using anti-VAPB (C,E) and anti-ACBD5 (C) or anti-OSBPL9 (E) antibodies. Indirect immunofluorescence was used to detect VAPB (C,E). Quantification of the PLA-results for VAPB-ACBD5 (D) and VAPB-OSBPL9 (F), showing the number of PLA-dots in a total of 450 cells that were analyzed. The bars indicate mean values ± SD. Single antibody controls were performed to confirm the specificity of PLA interaction. ***, $P<0.001$. Scale bars, 10 μm.

**Table S1**
RAPIDS using FKBP12-GFP-APEX2 and mCherry-FRB-VAPB

**Table S2**
RAPIDS using APEX2-dGFP-NLS-FKBP12 and HA-FRB-VAPB

**Table S3**
Oligonucleotides used for cloning

**Table S4**
Antibodies used in this study

Extended figure S1

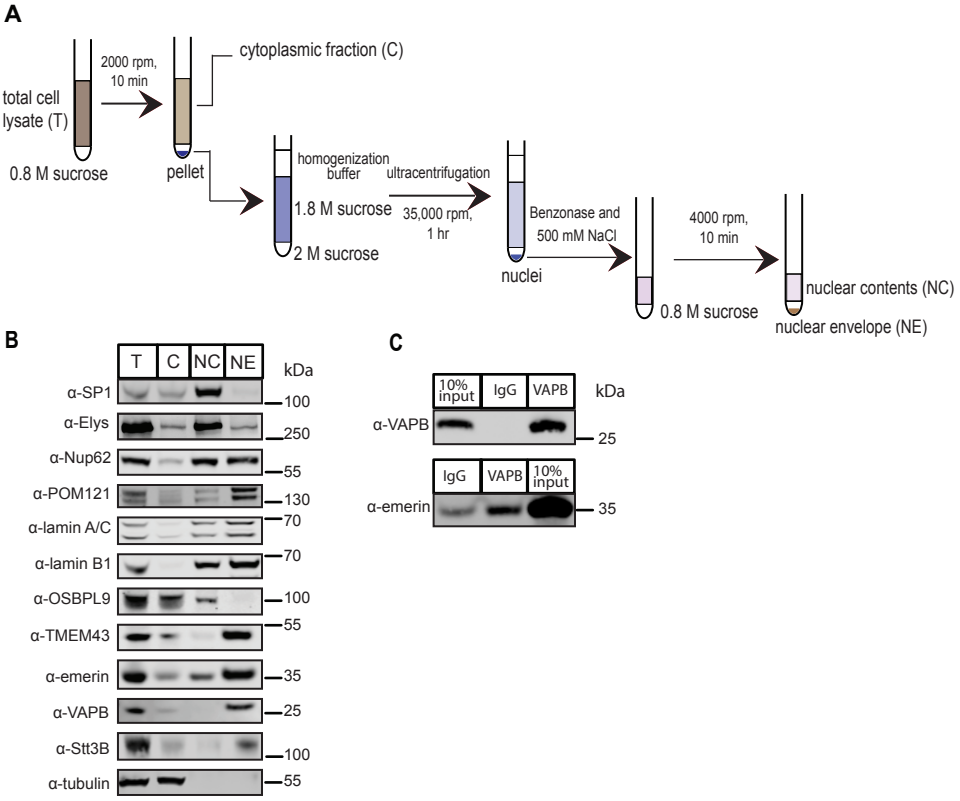


A,B: see legend to figure S1. C: The nuclear envelope fraction (NE) was resuspended in NP-40 lysis buffer (1% NP-40, 50 mM Tris HCl pH 8, 5 mM EDTA, 5 mM EGTA, 15 mM $MgCl_2$, 60 mM ß-glycerolphosphate, 0.1 mM $NaVO_4$, 200 mM NaCl, 2 mM DTT, and aprotinin, leupeptin, PMSF (1ug/ml) and then subjected to immunoprecipitation using antibodies against VAPB or IgG as a control.

Figure S2

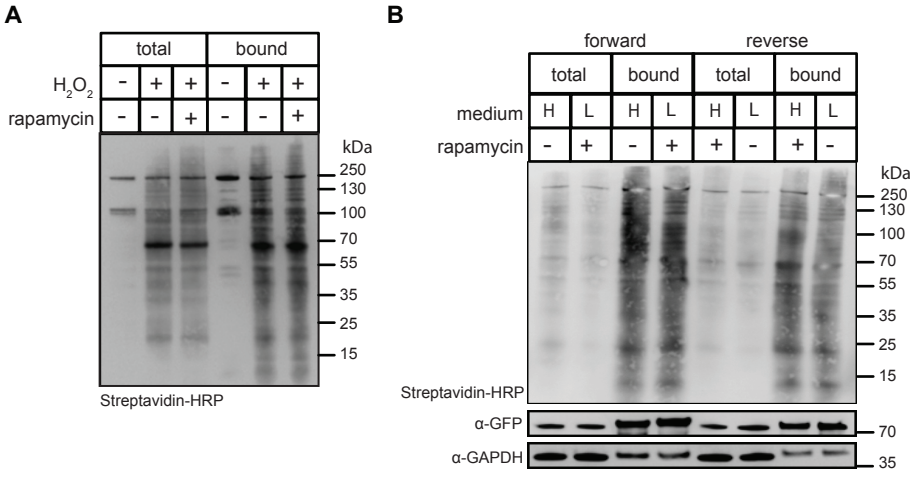
A
total
bound
H2O2
rapamycin
kDa
250
130
100
70
55
35
25
15
Streptavidin-HRP
B
forward
reverse
total
bound
total
bound
medium
H
L
rapamycin
kDa
250
130
100
70
55
35
25
15
Streptavidin-HRP
α-GFP
70
α-GAPDH
35

Figure S3

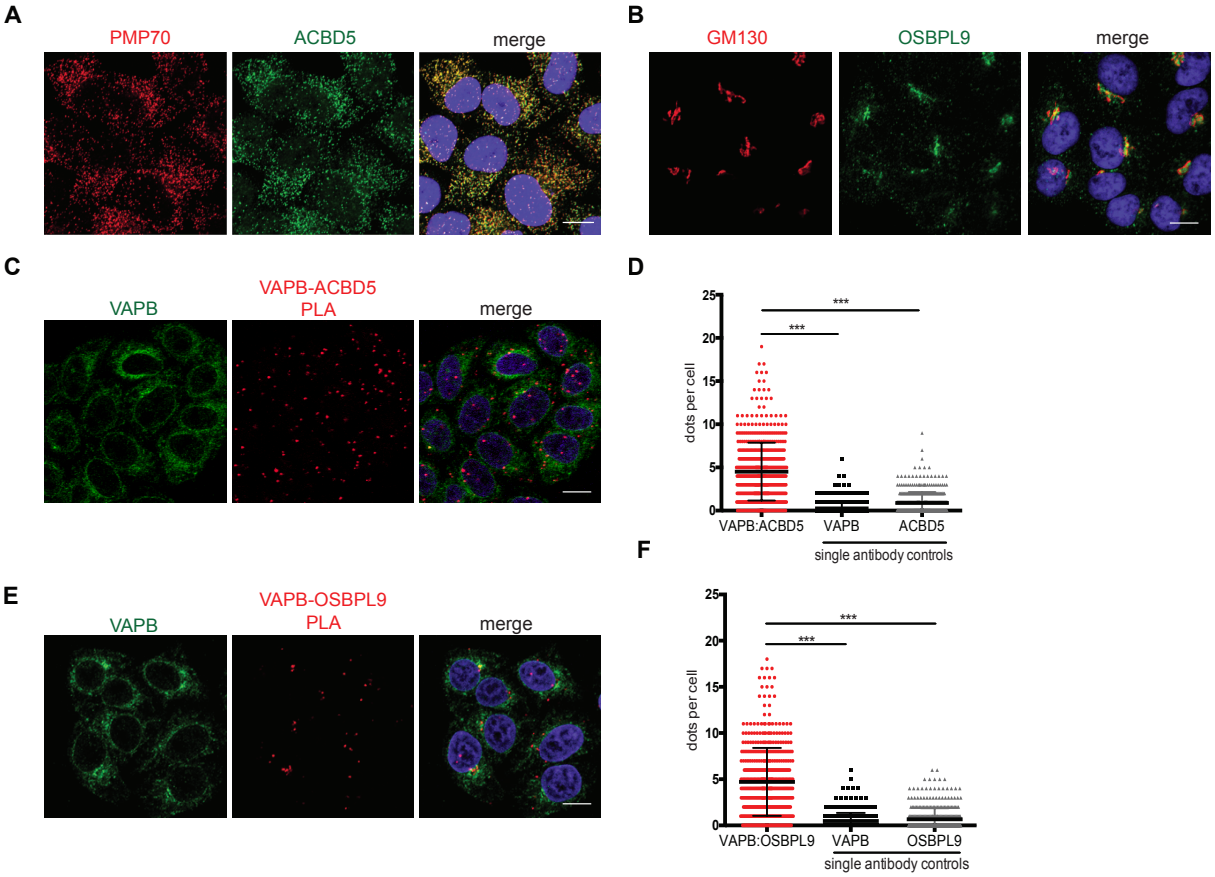
A
PMP70
ACBD5
merge
B
GM130
OSBPL9
merge
C
VAPB
VAPB-ACBD5
PLA
merge
D
dots per cell
***
***
VAPB:ACBD5
VAPB
ACBD5
single antibody controls
E
VAPB
VAPB-OSBPL9
PLA
merge
F
dots per cell
***
***
VAPB:OSBPL9
VAPB
OSBPL9
single antibody controls

# Chapter 5:
# Analysis of dynamics of inner nuclear membrane (INM) proteins by photobleaching-based techniques

# Chapter 5 : Analysis of dynamics of inner nuclear membrane (INM) proteins by photobleaching-based techniques

## 5.1. Introduction

(see also sections 1.5, 1.6, 1.7)

As detailed in Chapter 1, the integral membrane proteins move across the ONM, the NPC before finally reaching the INM. Lateral diffusion is proposed as the primary model for targeting of INM proteins that diffuse through the lipid bilayer of the ER to the ONM and through the NPC to the INM. Once the proteins reach the INM, they are retained there by interaction with nuclear components. (Katta et al., 2014; Smith and Blobel, 1993; Soullam and Worman, 1995; Ungricht et al., 2015). In contrast, a receptor-mediated active transport was described in yeast (King et al., 2006; Meinema et al., 2011; see section 1.5).

An accurate understanding of the dynamics of INM proteins has been achieved by studying them in living cells. The analysis of fluorescently tagged proteins of interest enables to study dynamics of proteins after being expressed in cells. Several techniques have been used to characterize the dynamics. One of the methods is the time-lapse imaging of the fluorescent proteins, while the second method is based on photobleaching technique that includes fluorescence recovery after photobleaching (FRAP) and the third based on fluorescence loss in photobleaching (FLIP) (reviewed in Lippincott-Schwartz et al., 2001). In FRAP, a portion of the fluorescently tagged protein is bleached with a high-intensity laser, and the fluorescence recovery in the bleached area is measured at different time intervals, whereas in FLIP, fluorescence loss is measured over time after bleaching in a region of interest. The mechanisms underlying transport to the INM have also been elucidated by several reporter systems that enable measurements of INM targeting kinetics (see section 1.6).

In this chapter, the dynamics of various INM proteins are studied by FRAP assays in both intact (living cells) and permeabilized cells. Previous FRAP studies on INM proteins have been performed on either intact cells or permeabilized cells. However, a comparative study on the dynamics of INM proteins under both conditions has not been performed before. The model proteins tested in this study are emerin, lamina-associated polypeptide 2 (Lap2β), lamin B receptor (LBR), protein tyrosine phosphatase 1B (PTP1B) and VAPB. Emerin, Lap2β and LBR are well characterized INM proteins. Both emerin and Lap2β have one TMD while LBR has eight TMDs. PTP1B and VAPB are TA proteins that are also reported to localize to the INM (James et al., 2019; Saiz-Ros et al., 2019; Yip et al., 2012). In addition, the molecular requirements for the transport of emerin to the INM were studied in detail in a permeabilized cell system.

# 5.2. Results

## 5.2.1. Fluorescence recovery after photobleaching (FRAP) of INM proteins at the NE

### 5.2.1.1. FRAP assays performed in intact cells reveals different mobilities for INM proteins

Fluorescence recovery after photobleaching (FRAP) is a versatile tool to monitor the dynamics of molecules in living cells, the movement between different organelles and the import and export of proteins through nuclear pores (Boni et al., 2015; Day et al., 2012; Ohba et al., 2004; Pawar et al., 2017; Shimi et al., 2004; Ungricht et al., 2015; Vijayaraghavan et al., 2018; Zuleger et al., 2011). FRAP assays were performed at the NE in cells overexpressing mCherry-emerin, mCherry-FRB-VAPB, mCherry-FRB-PTP1B, mCherry-FRB-LBR and mCherry-FRB-Lap2β. In this study, to analyze the diffusional properties of these INM proteins, HeLa cells were transiently transfected with the respective plasmids. After 24 hours of transfection, cells were subjected to FRAP experiments. Analysis of FRAP assays in intact cells showed that emerin and Lap2β recovered rapidly at the NE after photobleaching with a recovery rate of 60%, while VAPB, PTP1B and LBR recovered at the NE with 40% recovery (Figure 18A and B). These data suggest that all INM proteins tested had almost similar diffusional mobility at the NE with a higher recovery rate for emerin and Lap2β in comparison to VAPB, PTP1B and LBR.

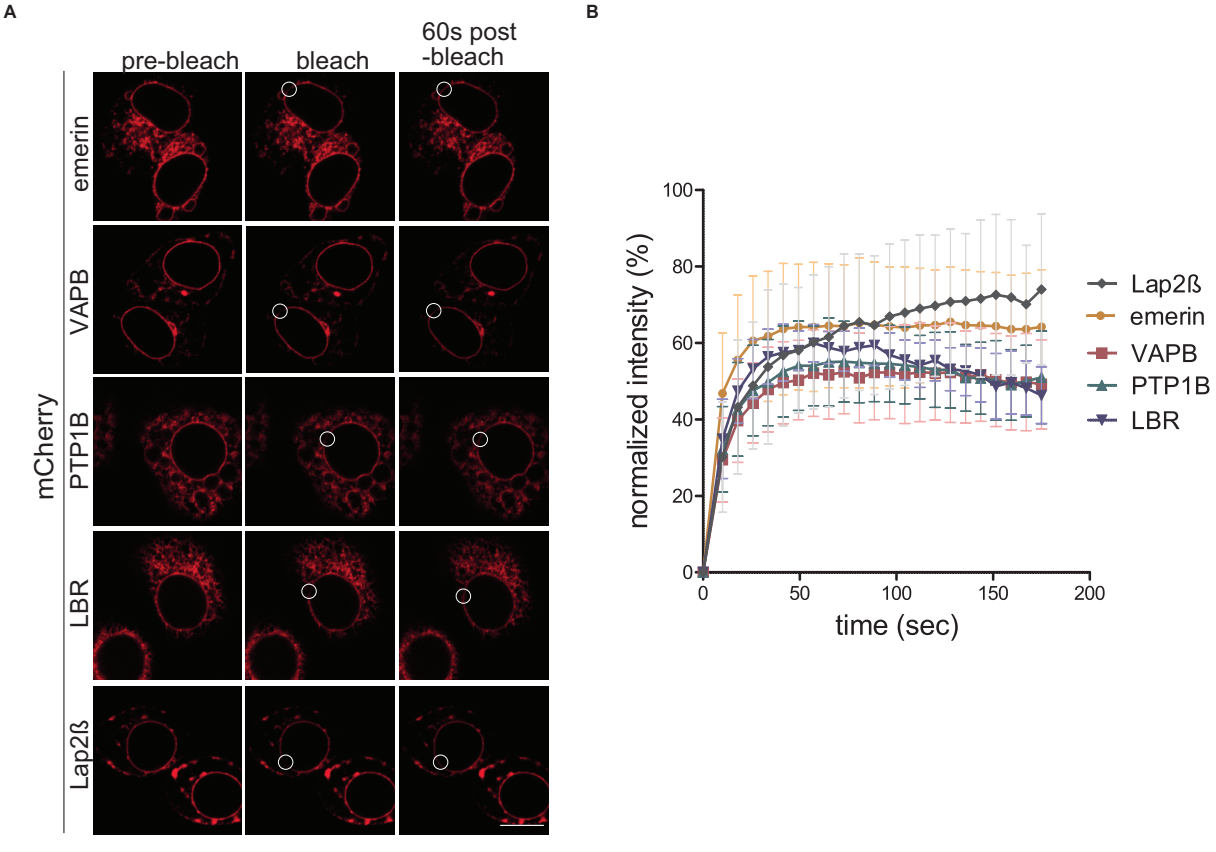

**Figure 18. Mobility of INM proteins emerin, VAPB, PTP1B, LBR and Lap2β at the NE in intact cells.** (previous page) (A) HeLa cells expressing mCherry-tagged versions of emerin, VAPB, PTP1B, LBR and Lap2β were subjected to FRAP assays. The bleached areas are represented by circles. Cells were imaged by a confocal microscope at different time points. The scale bar corresponds to 10 µm. (B) Fluorescence recovery was plotted over time. The curve shows the normalized fluorescence intensities with error bars indicating the standard deviation from the mean of a total of 12 cells from two independent experiments per condition.

#### 5.2.1.2. Digitonin treatment affects the diffusional mobility of proteins at the NE

To characterize the factors affecting diffusional mobility to the NE, a semi-permeabilized cell system was used. This has been previously established to study the molecular requirements of nuclear import of soluble factors (Adam et al., 1990). HeLa cells were transiently transfected with constructs coding for mCherry tagged versions of emerin, VAPB, PTP1B, LBR and Lap2β. The cells were then treated with digitonin, which selectively permeabilizes the plasma membrane leaving the NE intact and washed to remove soluble factors (Figure 19A). The diffusional mobility of the fluorescent proteins at the nuclear envelope (NE), in both intact and semi-permeabilized cells, were measured by FRAP. As observed before (5.2.1.1), the fluorescence recoveries of untreated or intact cells ranged from 40-60% for the tested INM proteins. Strikingly, the fluorescence recovery of emerin, VAPB, LBR and Lap2β at the NE in semi-permeabilized cells were low (20%) compared to intact cells (Figure 19B and C). The effect of permeabilization on the recovery rate of PTP1B was marginally lower than in intact cells (Figure 19C). This suggests that digitonin reduces the diffusional mobility of these proteins. Moreover, cytosolic factors that were removed upon digitonin treatment could affect the transport of these proteins to the NE and/or the diffusional mobility of the proteins.

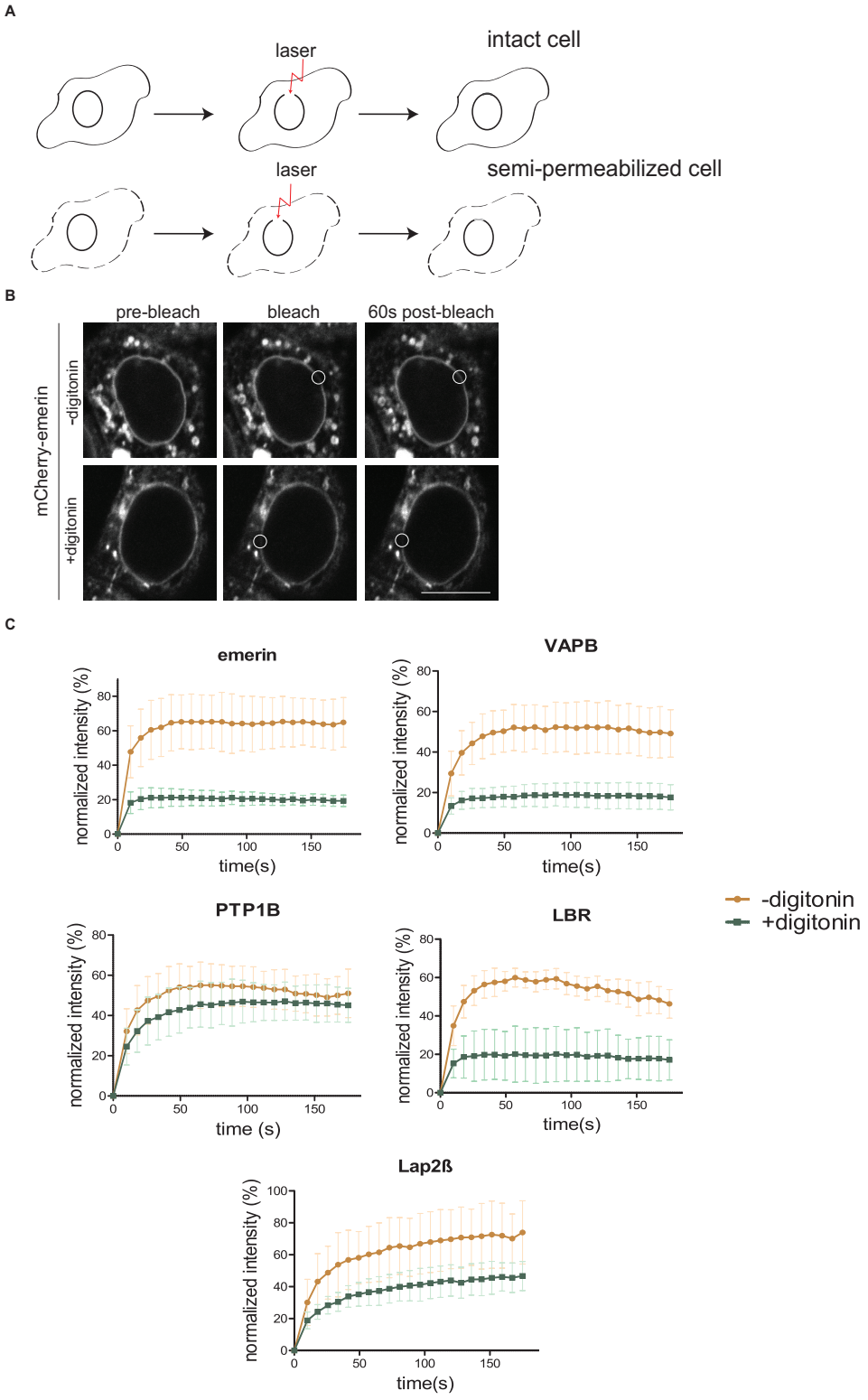


**Figure 19: Mobility of INM proteins emerin, VAPB, PTP1B, LBR and Lap2β at the NE in semi-permeabilized cells.**
(A) Schematic depiction of FRAP assays performed on both intact and semi-permeabilized cells. HeLa cells expressing INM proteins were permeabilized with digitonin and washed or left intact. FRAP assays were performed on both intact and semi-permeabilized cells. (B) Representative images of FRAP performed on cells over-expressing emerin with (+ digitonin) or without (- digitonin) permeabilization. The bleached areas are represented by circles. Cells were analyzed by a confocal microscope. The scale bar corresponds to 10 µm. (C) Fluorescence recovery (normalized intensity) was plotted over time. The curve shows the normalized fluorescence intensities under both conditions as mentioned in (A) for emerin, VAPB, PTP1B, LBR and Lap2β with error bars indicating the standard deviation from the mean of a total of 12 cells from two independent experiments per condition.

### 5.2.1.3. Diffusion of emerin to the NE is cytosol dependent

Semi-permeabilization and subsequent washing releases most of the soluble factors from the cells, thereby disrupting nucleocytoplasmic transport. However, addition of exogenous cytosol alleviates this effect by supplementing soluble factors (Adam et al., 1990; Kehlenbach et al., 1998). To assess whether the addition of cytosol to semi-permeabilized cells expressing INM proteins affects the fluorescence recovery at the NE, transiently transfected HeLa cells permeabilized with digitonin were supplemented with cytosol. FRAP assays were performed in intact cells and in semi-permeabilized cells with or without the addition of cytosol. Interestingly, emerin showed a partial recovery at the NE with a recovery rate of 30% after the addition of cytosol, compared to the untreated semi-permeabilized cells (20%) (Figure 20A and B).

In addition to emerin, the effect of cytosol supplementation on targeting of VAPB, PTP1B, LBR and Lap2β to the NE was also assessed using FRAP assay. The mobility of the three proteins, namely VAPB, PTP1B and LBR, was unaffected by the addition of cytosol, as shown by the confocal images and quantification in Figure 21. In contrast, Lap2β showed a minor recovery upon the addition of cytosol (Figure 22A and B), but not significant as compared to emerin.

Together, these data demonstrate that the efficient targeting of emerin and to a smaller extent, Lap2β, to the NE requires cytosolic factors, whereas the targeting of VAPB, PTP1B and LBR do not require additional cytosolic factors.

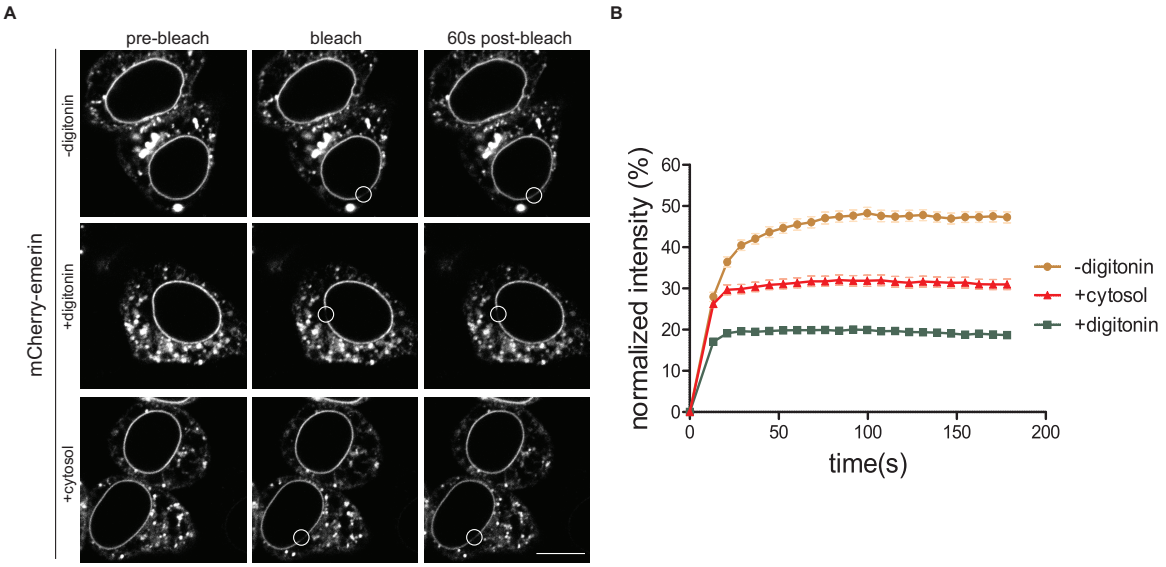


**Figure 20. Cytosol affects the diffusional mobility of emerin at the NE in semi-permeabilized cells.** (A) FRAP assays were performed on intact (- digitonin) and semi-permeabilized HeLa cells expressing mCherry-emerin in the presence or absence of cytosol (+ digitonin; + cytosol). The bleached areas are represented by circles. Cells were analyzed by a confocal microscope. The scale bar corresponds to 10 µm. (B) The curve shows the normalized fluorescence intensities under the three conditions as mentioned in (A) with error bars indicating the standard deviation from the mean of a total of 36 cells per condition from six independent experiments.

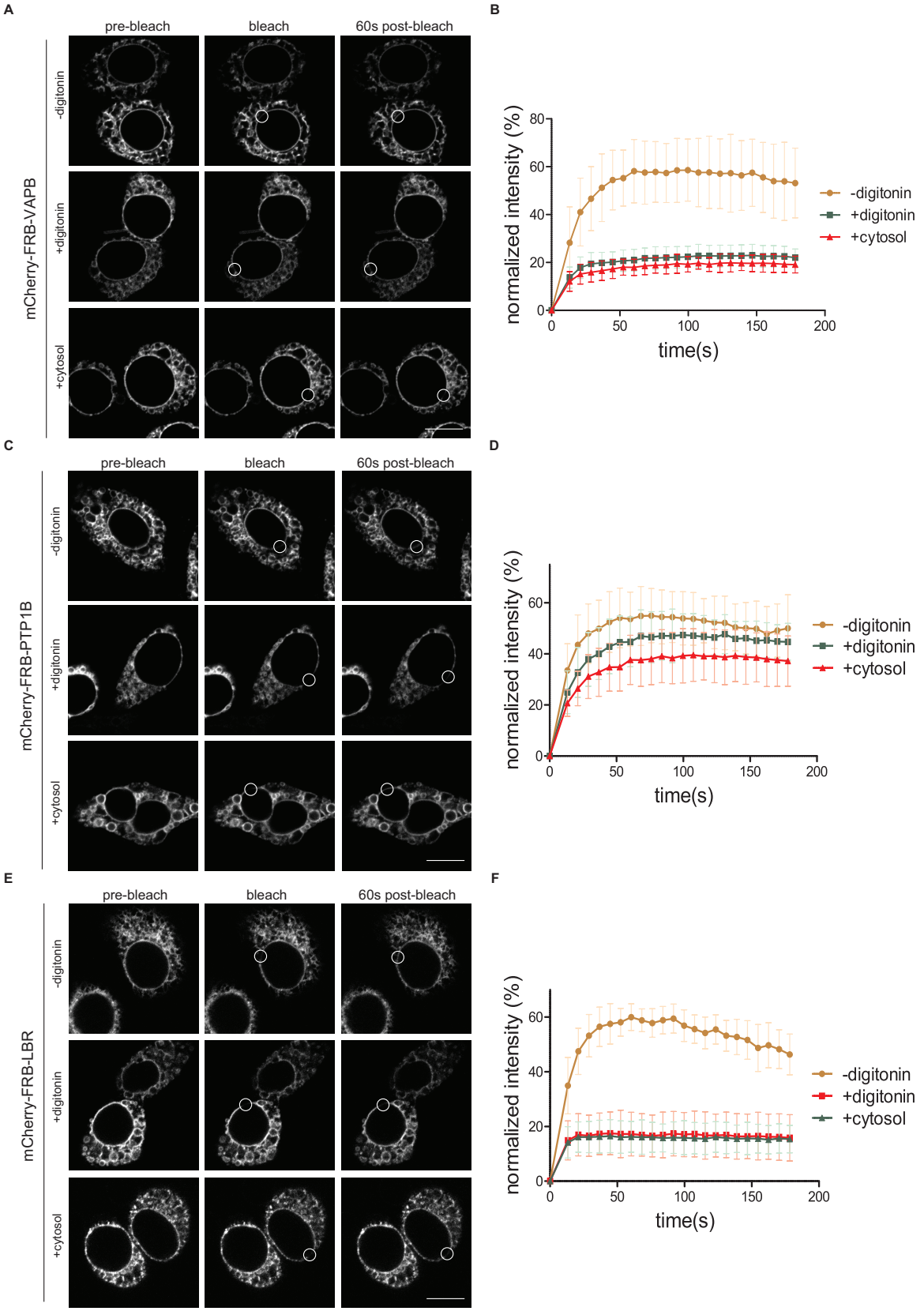


**Figure 21. Diffusional mobilities of VAPB, PTP1B and LBR are unaffected by cytosol supplementation.**
FRAP assays were performed on intact (- digitonin) and semi-permeabilized HeLa cells transfected with either mCherry-FRB-VAPB (A) or mCherry-FRB-PTP1B (C) or mCherry-FRB-LBR (E) in the presence or absence of cytosol (+digitonin; + cytosol). Representative images of FRAP performed in cells over-expressing VAPB, PTP1B and LBR (A, C and E). The bleached areas are represented by circles. The scale bars correspond to 10 µm. (B, D and F) The curve shows the normalized fluorescence intensities under the

three conditions as mentioned in (A, C and E) with error bars indicating the standard deviation from the mean of a total of 12 cells from two independent experiments.

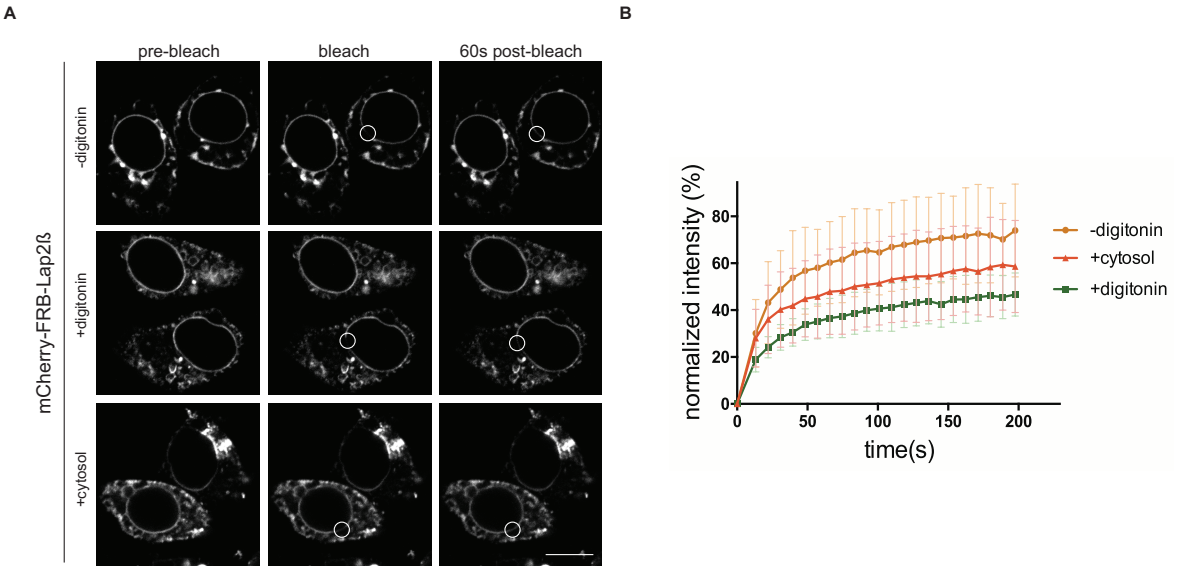


**Figure 22. Cytosol supplementation facilitates the mobility of Lap2β to the NE to a lesser extent in semi-permeabilized cells.**
(A) FRAP assays were performed on intact (- digitonin) and semi-permeabilized HeLa cells expressing mCherry-FRB-Lap2β in the presence or absence of cytosol (+digitonin; +cytosol). Representative images of FRAP performed in cells over-expressing Lap2β. The bleached areas are represented by circles. Images were acquired by a confocal microscope. The scale bar corresponds to 10 µm. (B) Quantification of normalized intensity at the NE under the three conditions as mentioned in (A) with error bars indicating the standard deviation from the mean of a total of 12 cells from two independent experiments.

### 5.2.1.4. *In vitro* import assay validates the functionality of cytosolic factors required for transport to the nucleus

Import into the nuclear envelope of semi-permeabilized cells depends on the addition of cytosol or cytosolic fraction (Adam and Adam, 1994; Adam et al., 1990; Moore and Blobel, 1992). Therefore, supplementing soluble fractions responsible for import, or impeding import by addition of inhibitory fractions is a plausible way to study translocation of proteins. To control for the efficacy of recombinant cytosolic factors, nuclear uptake of a soluble protein Cy3-BSA-NLS, was monitored in digitonin permeabilized cells in the presence of cytosol alone or cytosol supplemented with (1) Ran, which is essential for nuclear protein transport, (2) GTPase-deficient RanQ69L, a mutant of Ran, deficient in hydrolyzing Ran bound GTP (Klebe et al., 1995), (3) WGA (wheat germ agglutinin), a lectin that binds to nuclear pores and inhibits import by disturbing the interaction of importins with nucleoporins containing FG repeats (Finlay et al., 1987) and (4) a dominant-negative fragment of Importinβ (Impβ (45-462)) that binds to sites of the NPC from which it cannot be cleared (Kutay et al., 1997a).

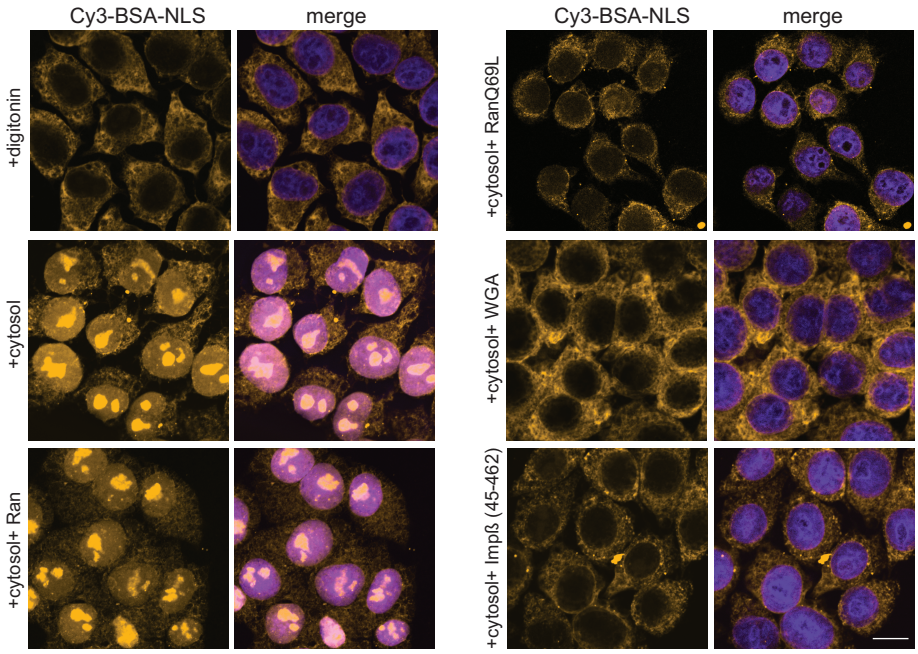


**Figure 23. *In vitro* import assay to validate the functionality of cytosolic factors.**
HeLa cells were permeabilized with digitonin and subjected to nuclear import reactions. The cells were treated with either cytosol or cytosol supplemented with Ran, RanQ69L, WGA or Impβ (45-462) and incubated with Cy3-BSA-NLS and an energy-regenerating system. Cells were washed and fixed. Images were analyzed using a confocal microscope. The scale bars correspond to 10 µm.

An *in vitro* nuclear import assay (Adam et al., 1990) was performed to confirm that the recombinantly purified cytosolic factors were fully functional. HeLa cells were permeabilized with digitonin, washed to remove soluble transport factors and incubated with Cy3-BSA-NLS and an energy-regenerating system (Kehlenbach and Gerace, 2002) in the absence or presence of cytosol or cytosol with the addition of recombinant Ran, RanQ69L, WGA or Impβ (45-462) at 30°C for 25 minutes. The presence of cytosol alone or with the addition of Ran favored transport in comparison to control cells treated with digitonin (Figure 23). However, nuclear import of Cy3-BSA-NLS was impaired in the presence of Ran Q69L, WGA and Impβ (45-462) respectively. This was in accordance with previously reported functions of these soluble factors in affecting nuclear transport (Finlay et al., 1987; Klebe et al., 1995; Kutay et al., 1997a), thereby further validating the functionality of these recombinant factors.

#### 5.2.1.5. A Ran mutant deficient in GTP hydrolysis inhibits targeting of emerin to the NE

To test whether additional soluble fractions enhance the targeting of emerin to the INM, the nuclear transport factor Ran was added to the cytosol. Cytoplasmic Ran GDP and GTP hydrolysis by Ran (Melchior et al., 1993; Moore and Blobel, 1992) is required for nuclear protein import. HeLa cells were transfected with mCherry-emerin. The diffusional mobility of emerin in semi-permeabilized cells in the presence of cytosol and Ran was measured by FRAP assays. The addition of cytosol resulted in an increase in the diffusional

mobility of emerin compared to permeabilized cells (also shown in Figure 20) while the addition of Ran to the cytosol did not further increase the mobility of emerin (Figure 24A and B).

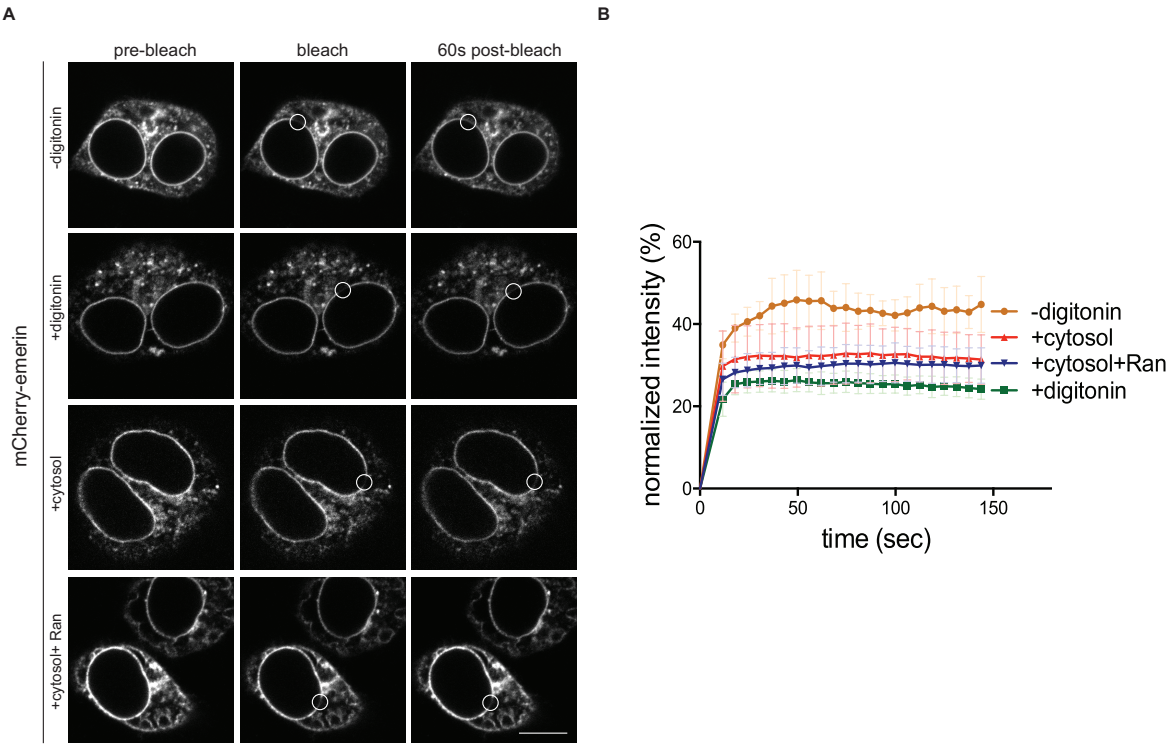


**Figure 24. Targeting of emerin to the NE is not affected by addition of Ran to the cytosol.**
(A) FRAP assays were performed on intact (- digitonin) and semi-permeabilized (+ digitonin) HeLa cells expressing mCherry-emerin in the presence or absence of cytosol (+ cytosol; +digitonin) and also in the presence of cytosol with Ran. The bleached areas are represented by circles. Images were analyzed by a confocal microscope. The scale bars correspond to 10 µm. (B) Quantification of normalized intensity at the NE under the conditions mentioned in (A) with error bars indicating the standard deviation from the mean of a total of 12 cells from two independent experiments.

RanQ69L is a dominant-negative mutant of Ran, which is deficient in the hydrolysis of Ran bound GTP (Dickmanns et al., 1996; Klebe et al., 1995). A recombinantly purified Ran mutant, Ran Q69L, whose functionality was already validated (Figure 23) was used in FRAP assays. In this assay, HeLa cells transfected with mCherry-emerin and semi-permeabilized were analyzed in the absence or presence of cytosol or cytosol with RanQ69L. Strikingly, the addition of RanQ69L reduced the mobility of emerin at the NE to 20% as compared to that observed in permeabilized cells without the addition of cytosol (Figure 25A and B). In summary, targeting of emerin to the NE is dependent on a functional Ran as observed by the reduction in recovery rate at the NE in the presence of RanQ69L.

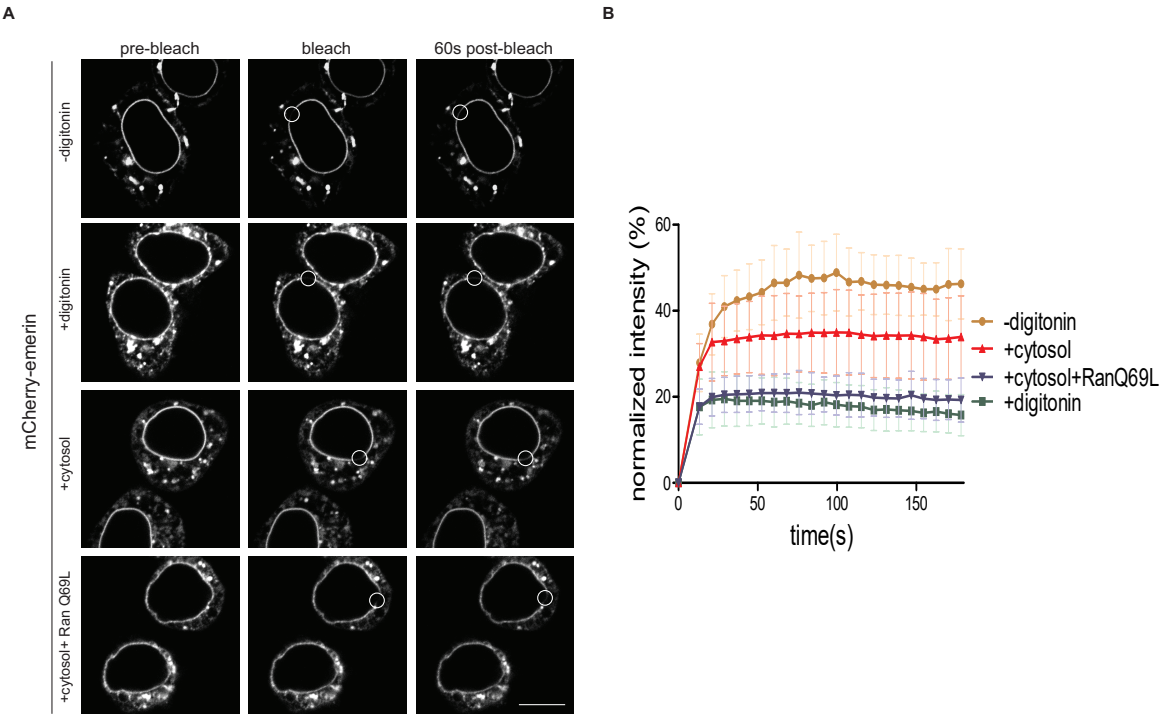


**Figure 25. GTPase deficient RanQ69L impairs the mobility of emerin at the NE.**
(A) FRAP assays were performed on intact (- digitonin) and semi-permeabilized HeLa cells (+ digitonin) expressing mCherry-emerin in the presence or absence of cytosol (+ cytosol; + digitonin) and cytosol in the presence of RanQ69L, as indicated, and images were analyzed by a confocal microscope. The bleached areas are represented by circles. The scale bar corresponds to 10 µm. (B) Quantification of normalized intensity at the NE under the conditions tested as in (A) with error bars indicating the standard deviation from the mean of a total of 12 cells from two independent experiments.

### 5.2.1.6. WGA inhibits the targeting of emerin to the NE

WGA was described as an inhibitor that impairs the nuclear transport of a fluorescently labeled nuclear protein, nucleoplasmin (Finlay et al., 1987). Using electron microscopy, WGA was found to bind to the cytoplasmic face of the nuclear pore. It inhibits import by disturbing the interaction of importins with nucleoporins containing FG repeats (Finlay et al., 1987). Since WGA was functional in inhibiting the import of soluble proteins (Figure 23), it was assessed whether the diffusion of emerin to the NE was impaired by WGA. To compare targeting kinetics in the presence and absence of WGA in addition to cytosol, FRAP assays were performed. Interestingly, the recovery rate of transiently expressed emerin at the NE was reduced from 30% to 20% upon addition of WGA to cytosol, i.e. almost to the level as observed in the absence of cytosol (Figure 26A and B). This suggests that transport of emerin to the NE is inhibited when nuclear pores are blocked by WGA.

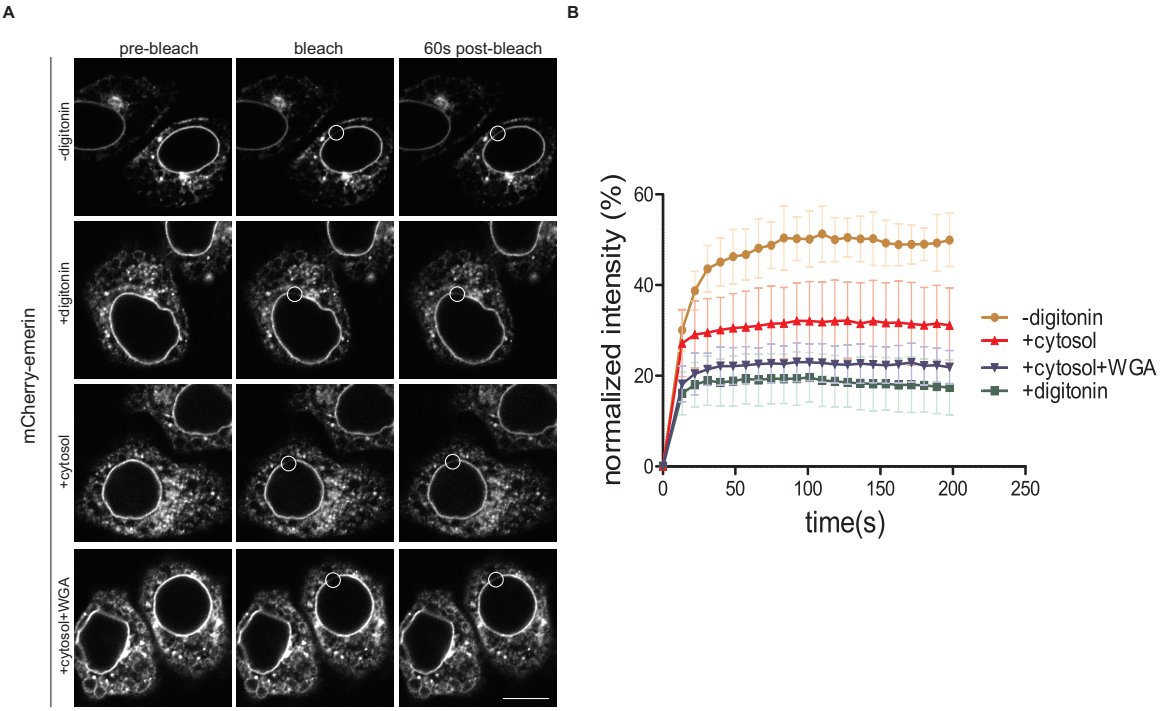


**Figure 26. WGA restricts passage of emerin to the NE.**
(A) FRAP assays were performed on intact (- digitonin) and semi-permeabilized HeLa cells (+ digitonin) expressing mCherry-emerin in the presence or absence of cytosol (+ cytosol; + digitonin) and cytosol in the presence of WGA. Images were analyzed by confocal microscopy. The bleached areas are represented by circles. The scale bar corresponds to 10 µm. (B) Quantification of normalized intensity at the NE under the conditions tested as in (A) with error bars indicating the standard deviation from the mean of a total of 12 cells from two independent experiments.

### 5.2.1.7. Targeting of emerin to the NE is inhibited by a dominant negative fragment of Importinβ (Impβ 45-462)

In addition to WGA, a fragment of Importinβ was also reported to impair nuclear import. Importinβ (45-462) inhibits protein import in a dominant negative manner by binding to sites at the NPC from which it cannot be cleared (Kutay et al., 1997a). To test whether this fragment could affect the targeting of emerin to the NE, it was bacterially expressed and purified and tested for its efficacy to inhibit transport by import assay. The purified Impβ (45-462) blocked the import of Cy3-BSA-NLS (Figure 23). FRAP assays were performed to compare targeting of emerin in the presence or absence of Impβ (45-462). As observed for RanQ69L and WGA, addition of the Impβ inhibitory fragment also reduced the recovery rate of emerin from 30% to 20% (Figure 27A and B). Thus, the dominant-negative Impβ (45-462) has an inhibitory effect on the diffusional mobility of emerin to the NE.

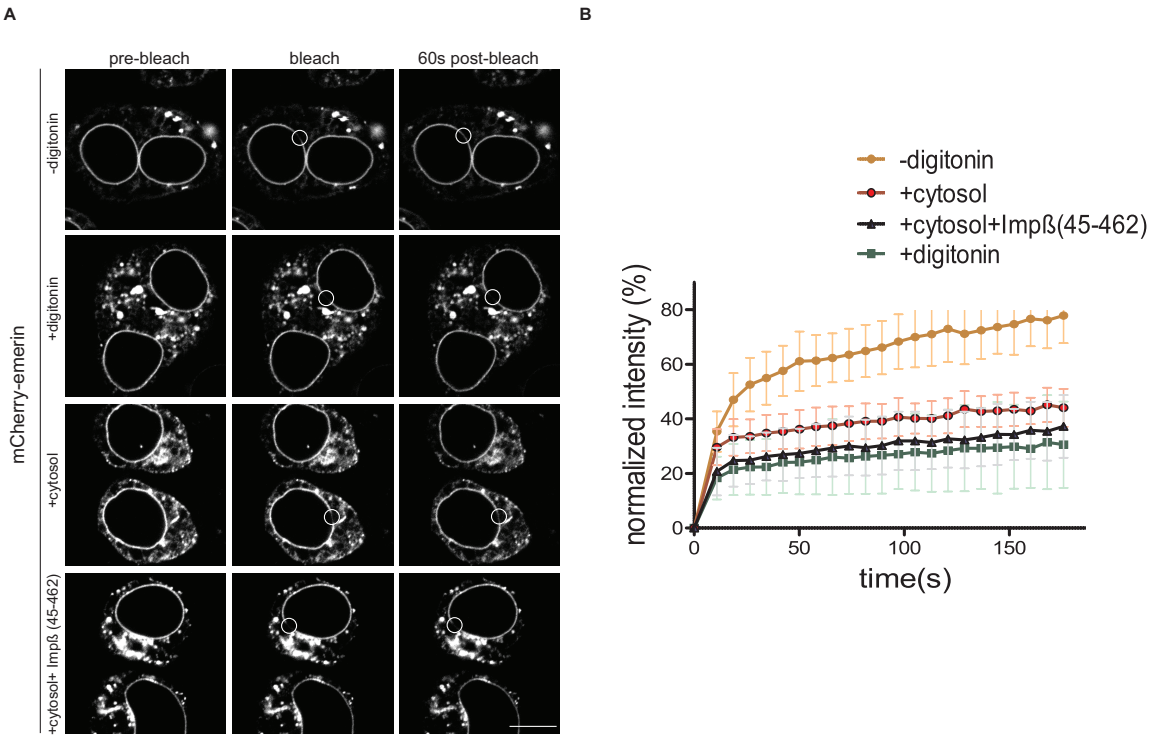


**Figure 27. Importinβ (45-462) fragment impairs the mobility of emerin at the NE.**
(A) FRAP assays were performed on intact (- digitonin) and semi-permeabilized (+ digitonin) HeLa cells expressing mCherry-emerin in the presence or absence of cytosol (+cytosol; +digitonin) and also in the presence of cytosol with Impβ (45-462). Images were analyzed by a confocal microscope. The bleached areas are represented by circles. The scale bar corresponds to 10 µm. (B) Quantification of normalized intensity at the NE under the conditions tested as in (A) with error bars indicating the standard deviation from the mean of a total of 12 cells from two independent experiments.

### 5.2.1.8. Nuclear transport receptors depleted cytosol marginally reduces the mobility of emerin in permeabilized cells

From the previous experiments, it was observed that RanQ69L and Impβ (45-462) had a significant effect on the diffusional mobility of emerin to the NE. Since both of these factors contribute to NTR (nuclear transport receptor)-mediated NPC translocation (Ribbeck and Görlich, 2002b), the effect of NTRs on the mobility of emerin was determined. NTRs have hydrophobic properties that assist them to pass through the NPCs. These can be enriched by a hydrophobic interaction column, phenyl-sepharose (Ribbeck and Görlich, 2002b). To deplete NTRs, HeLa cytosol was subjected to binding to phenyl-sepharose. The efficiency of depletion was monitored by Western blotting for Importins β, 11, 13, 7 and Transportin 1 (Figure 28A). FRAP assays were performed using cytosol depleted of NTRs in semi-permeabilized cells. As shown in (Figure 28B and C), the depleted cytosol showed a reduced effect (20%) compared to cytosol with no depletion (30%), but the mobility was not as low as that observed in digitonin treated cells (less than 20%). Thus, NTRs depletion only has a marginal effect on the mobility of emerin to the NE.

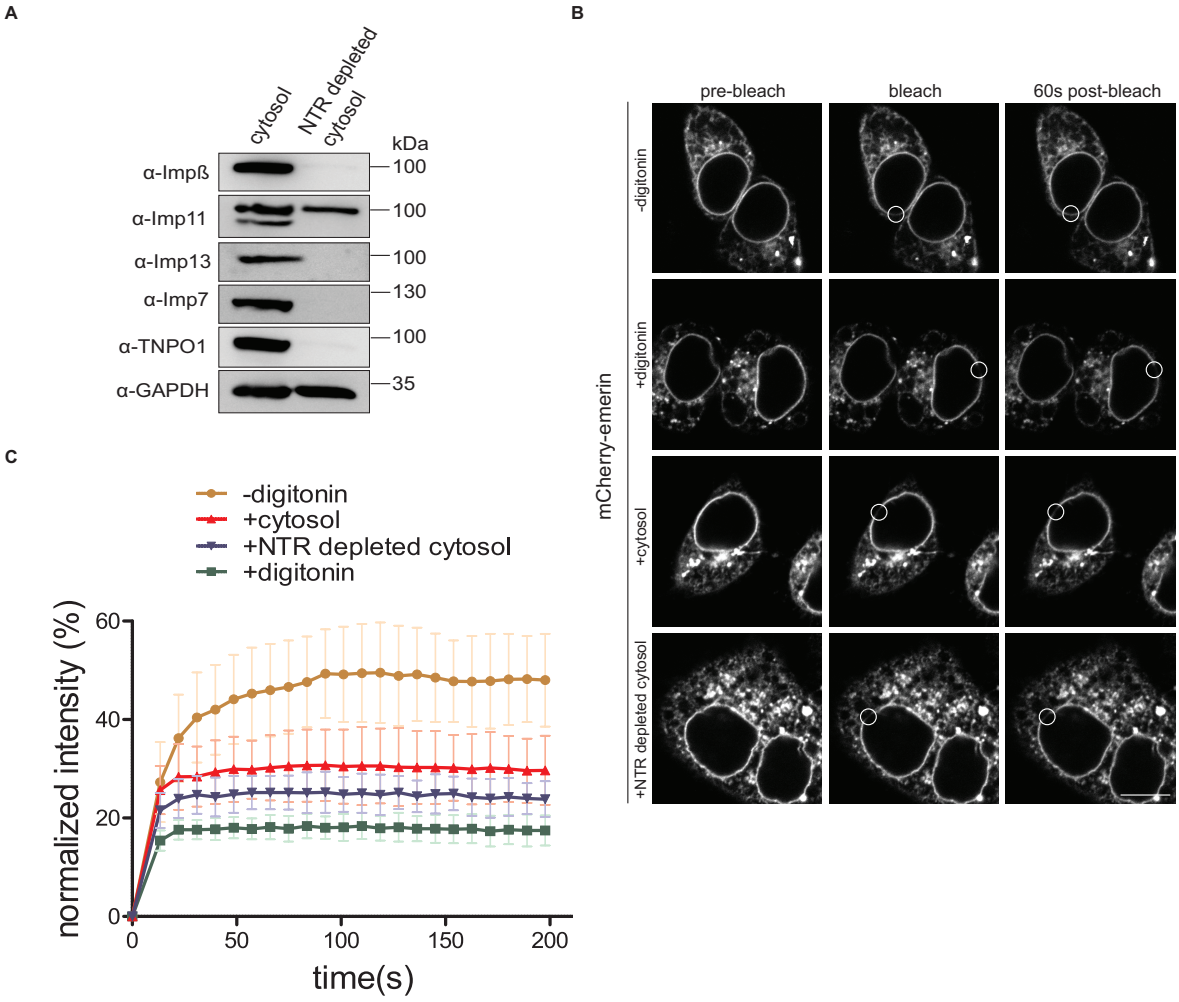


**Figure 28. NTRs depleted cytosol has a reduced effect on the diffusion of emerin to the NE.**
(A) Cytosol was depleted of nuclear transport factors (NTRs) by phenyl-sepharose. The efficacy of depletion was monitored by Western blotting using antibodies against Impβ, Imp11, Imp 13, Imp7 and TNPO1. GAPDH was used as a loading control. (B) FRAP assays were performed on intact (- digitonin) and semi-permeabilized (+ digitonin) HeLa cells expressing mCherry-emerin using this depleted cytosol or untreated cytosol (+cytosol; +digitonin). Images were analyzed by a confocal microscope. The bleached areas are represented by circles. The scale bar corresponds to 10 µm. (C) The curve shows the normalized fluorescence intensities with error bars indicating the standard deviation from the mean of a total of 12 cells from two independent experiments per condition.

### 5.2.2. Cytosol supplementation affects the diffusional mobility of emerin in the ER

The differences in the mobility of emerin in the NE upon addition of cytosol and cytosolic factors prompted us to check for its mobility in the ER. FRAP assays were performed on cells that were transiently transfected with mCherry-emerin, permeabilized and incubated in the presence or absence of cytosol. As shown in Figure 29, in intact cells recovery of nearly 60% was observed, whereas in semi-permeabilized cells only 20% recovery was obtained. This was in line with the NE targeting defect of emerin in semi-permeabilized cells. Next, cytosol was added to the permeabilized cells to assess changes in mobility of emerin in the ER. Interestingly, the addition of cytosol slightly increased the recovery rate in semi-permeabilized cells to 30%. This suggests that the addition of soluble

factors indeed affect the diffusional mobility of emerin in the ER. Additional experiments will have to be performed to monitor what factors in the cytosol are responsible for this effect.

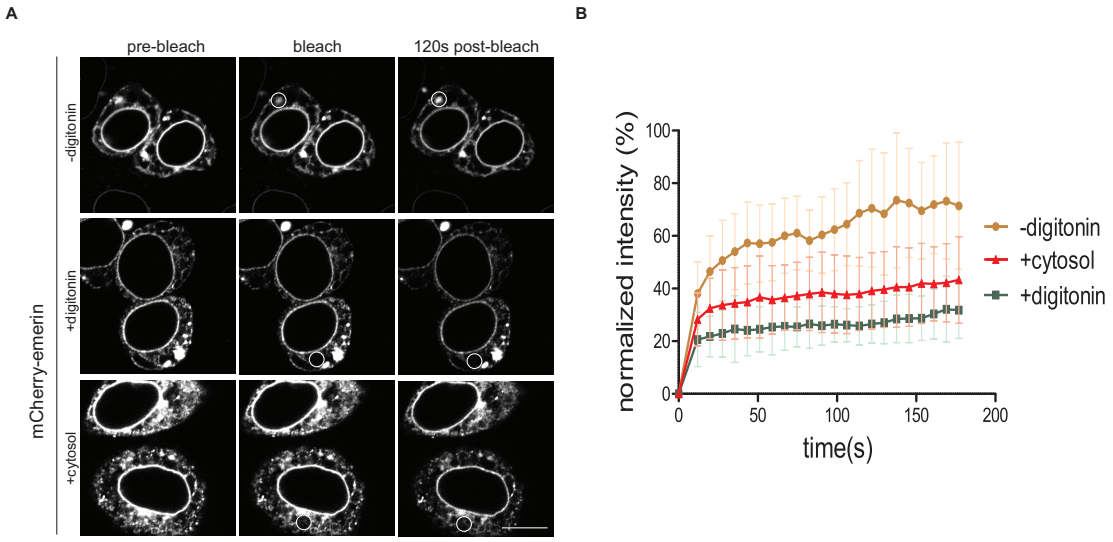


**Figure 29. Mobility of emerin in the ER measured by FRAP.**
(A) HeLa cells transfected with mCherry-emerin were subjected to FRAP assays in the ER. The regions that were bleached are represented by circles. The recovery of emerin was monitored over time in intact (-digitonin) and semi-permeabilized cells (+ digitonin), which were treated in the presence or absence of cytosol (+ cytosol; + digitonin). Images were analyzed by a confocal microscope. The scale bar corresponds to 10 µm. (B) Quantification of normalized intensity at the ER under the conditions as mentioned in (A) with error bars indicating the standard deviation from the mean of a total of 12 cells per experiment per condition.

## 5.3. Discussion

This chapter addresses the dynamics of several INM proteins with both single and multiple TMDs using FRAP assays. Under the experimental conditions used in this work, all the tested proteins showed a percentage recovery of 40 to 60% in intact cells (Figure 18). For emerin and Lap2β, similar percentages were observed, which were consistent with previous reports (Ostlund et al., 1999; Shimi et al., 2004; Wu et al., 2002). LBR had a lower percentage of recovery, possibly due to its binding to lamins and heterochromatin proteins (Ellenberg et al., 1997; Ostlund et al., 2006). Lower recovery rates were similarly observed for VAPB and PTP1B, suggesting that their mobility at the NE could also be affected by binding to proteins at the INM (James et al., 2019; Yip et al., 2012).

In contrast to the high percentage of recovery monitored in intact cells, a lower recovery was observed in permeabilized cells for all the proteins tested (Figure 19). The measured fluorescence recovery may not only result from the exchange of proteins within the NE but also from transport of proteins from the ER. The effect observed due to permeabilization could result from the loss of cytosolic factors. Alternatively, the reduction in recovery may also result from an effect that might alter the ER topology. The long-range diffusional mobility of proteins in the ER network, and the efficiency of targeting to the INM is reduced when ER-topology is altered (Pawar et al., 2017). Interestingly, the addition of cytosol partially increased the recovery of emerin but not for other proteins tested. This suggests that diffusion of emerin is dependent on the presence of cytosolic factors and/or on a proper ER-topology, whereas diffusion of other tested proteins might be dependent solely on proper maintenance of the ER network. However, further investigations have to be performed to monitor the effect of proper maintenance of ER-topology on the diffusion of the proteins tested in this work.

It has been previously reported that the mobility of emerin to the NE requires ATP (Zuleger et al., 2011) and that emerin also binds to cytoplasmic partners, which might affect its release from the ER (Lattanzi et al., 2000; Salpingidou et al., 2007; Zuleger et al., 2011). The observation that the addition of cytosolic factors led to an increase in fluorescence recovery at the NE may reflect an increase in the efficiency of diffusion of emerin. It was also observed that the addition of RanQ69L, WGA and Impβ (45-462) that block nuclear import, impaired the diffusion of emerin to the NE, further suggesting that the decrease in recovery observed in permeabilized cells was indeed due to a lower rate of diffusion of emerin from the ER to the NE. A cytosol dependence has also been observed for an INM protein SUN2 (Ungricht et al., 2015), further raising the question of whether additional molecular requirements add to the diffusion and retention model for efficient targeting of INM proteins.

# Chapter 6:
# Discussion

# Chapter 6 : Discussion

In eukaryotes, TA proteins with important roles in diverse processes can be found in different organelles like the mitochondria, peroxisome, ER, Golgi, plasma membrane, endosomes, lysosomes (Borgese et al., 2007) and also NE (Blenski and Kehlenbach, 2019; Pfaff et al., 2016). Two different TA proteins that localize to the INM were studied in this work. The first is VAPB, which is known as an ER-resident protein, and the second is emerin, which is a well-characterized INM protein.

The entry site for several TA proteins that reside in the membranes of the secretory pathway is the ER (Behrens et al., 1996; Kutay et al., 1995; Linstedt et al., 1995). Even though VAPB is well studied as an ER protein, the biogenesis of the protein is not entirely understood. To characterize the biogenesis of VAPB, the possible role of the TRC40 pathway in the membrane insertion of VAPB was analyzed.

In addition to its already established ER localization, localization of VAPB to the INM was observed for the first time. Moreover, the interactome of VAPB at the INM was established by a new proximity-based approach Rapamycin and APEX-dependent identification of proteins by SILAC (RAPIDS) and the interactome at the INM and ER was validated by this approach.

Requirements for targeting of newly synthesized TA proteins from the ER to the INM have been studied only for a few proteins. In this work, diffusional mobility of several INM proteins were assessed in intact and semi-permeabilized cells and emerin was one of the proteins that was studied further in detail.

## 6.1. ER membrane insertion of VAPB

### 6.1.1. The interaction of VAPB with TRC40 is not required for its insertion into the ER membranes

In this work, membrane insertion of VAPB via the TRC40 pathway was analyzed. Interaction of VAPB with TRC40 has been reported previously (Baron et al., 2014; Coy-Vergara et al., 2019). FFAT-like motif in TRC40 mediates its interaction with the MSP domain of VAPB (Baron et al., 2014). VAPB was also identified as a TRC40 interacting precursor TA protein, using a dominant-negative ATPase-impaired mutant of TRC40 in which an aspartate 74 was replaced by a glutamate residue to trap TA proteins in the cytoplasm (Coy-Vergara et al., 2019). Even though a stable complex was formed by TRC40 and VAPB (Figure 14), the complex, however, failed to get inserted into the ER membranes of semi-permeabilized cells (Figure 15). Neither the use of dominant-negative WRB/CAML-fragments (Figure 16) nor the immuno-depletion of TRC40 (Figure 17) impeded the

membrane insertion of VAPB, which further confirms that TRC40 is not essential for VAPB insertion. It is possible that the interaction of VAPB with TRC40 has another role, unrelated to protein targeting to the ER. It has to be taken into account that TRC40 does not bind to the TMD of VAPB (Baron et al., 2014), unlike other established TA proteins where the interaction occurs via a TMD-dependent manner (Stefanovic and Hegde, 2007). It has also been previously reported that VAPB interacts with ubiquitinated proteins, p97 ATPase and FAF1 (ubiquitin binding protein) and these proteins are recruited by TRC40 (Baron et al., 2014). Thus, it can be speculated that the TRC40-VAPB interaction may be required in the context of cellular quality control or proteasomal degradation.

### 6.1.2. Post-translational targeting of VAPB to ER membranes

The presence of a single transmembrane domain at the C-terminal end of VAPB suggests that the protein can be post translationally inserted into ER membranes. Even with the addition of a 13-amino acid length opsin tag at the C-terminal end, VAPB could be inserted into rough microsomes, in a post-translational manner (Figure 12 and Figure 13). It had also been observed previously that *in vitro* translated VAPB can be inserted into microsomes, and protease protection assay confirmed its post-translational membrane insertion (Fasana et al., 2010). There are generally two pathways for TA protein insertion; an assisted and a non-assisted mode of insertion (Borgese and Fasana, 2011; Brambillasca et al., 2005; Hegde and Keenan, 2011). As a general rule, the pathway that TA proteins use depends on their TMD hydrophobicity. Low or moderately hydrophobic proteins use an unassisted pathway of insertion, whereas highly hydrophobic ones require assistance from chaperones or membrane proteins (Borgese et al., 2007; Brambillasca et al., 2006). As shown in Table 10, the TMD of VAPB is hydrophobic and has a similar hydrophobicity as that of emerin, which favors an assisted pathway of insertion. VAPB was also shown to be unable to get inserted into liposomes ruling out the possibility of unassisted membrane integration (Fasana et al., 2010).

**Table 10. TMD hydrophobicity of VAPB and emerin.**

| Protein | TMD | TMD hydrophobicity* | C-tail sequence |
|---|---|---|---|
| VAPB | RLLALVVLFFIVGVIIGKIAL | 2.562 | - |
| emerin | VPLWGQLLLFLVFVIVLFFIY | 2.481 | HFMQAEEGNPF |

*TMD hydrophobicity score was calculated according to the GRAVY scale (Kyte and Doolittle, 1982).

### 6.1.3. Redundancy in post-translational membrane insertion

*In vivo* studies showed that TA proteins use several additional targeting options. Recently, calmodulin (CAM), a factor that recognizes hydrophobic domains in the cytosol (Shao and Hegde, 2011), was identified to interact with a TA protein of moderate hydrophobicity, squalene synthase (SQS) (Guna et al., 2018). CAM was reported to deliver these proteins to a transmembrane domain insertase, ER membrane complex (EMC), which aids in inserting them into the ER membrane (Guna et al., 2018; Shurtleff et al., 2018). An SRP-independent targeting (SND) pathway consisting of cytoplasmic Snd1 and ER-resident Snd2 and Snd3 was recently described in yeast (Aviram et al., 2016). The human ortholog, TMEM208 (hSnd2) was reported to provide an alternative pathway for the insertion of substrates with a single TMD at the C-terminus into the ER membranes (Haßdenteufel et al., 2017). It was also proposed that some TA proteins can utilize the SRP pathway post translationally (Abell et al., 2004; Abell et al., 2007; Casson et al., 2017). Additionally Hsp40/Hsc70 was reported to promote the membrane insertion of TA proteins of low hydrophobicity (Abell et al., 2007; Rabu et al., 2008). All these studies suggest that TA proteins can utilize multiple pathways for their delivery to the ER and there are also possibilities of other unidentified routes contributing to their biogenesis. It is also possible that these pathways may compensate for one another if one pathway is non-functional. Taken together, the post-translational membrane insertion of VAPB is TRC40-independent as VAPB neither required the TRC40-receptors, WRB and CAML, for insertion nor was it inserted into the ER membrane when TRC40 was depleted. Further studies will be needed to determine whether VAPB uses any of these alternative mechanisms as depicted in Figure 30.

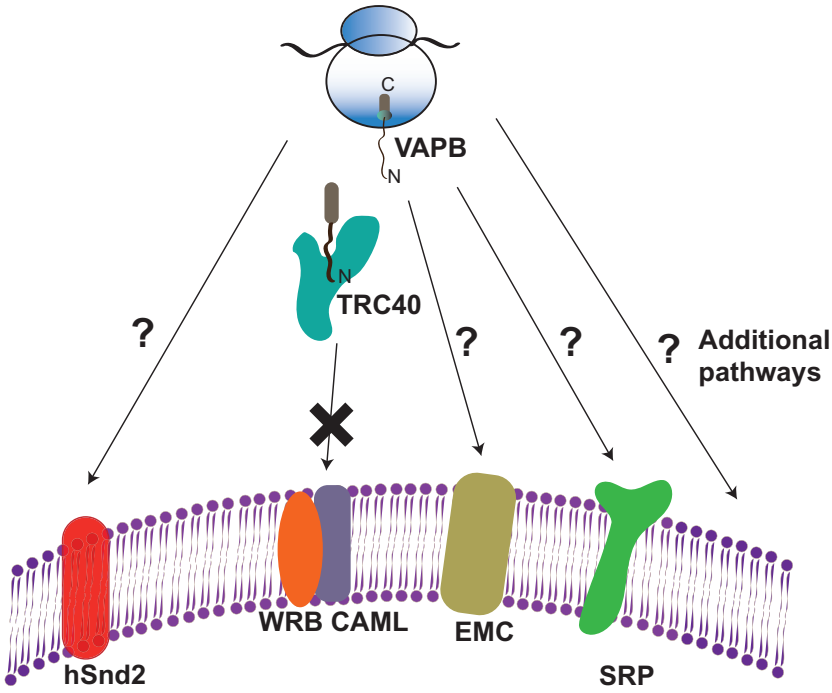


**Figure 30. Alternate mechanisms for post-translational insertion of TA proteins.**
Scheme depicting additional pathways reported for the insertion of TA proteins. VAPB could use any of the alternate pathways namely the SND pathway, the EMC pathway, the SRP pathway or additional, yet unidentified routes for its ER insertion.

## 6.2. VAPB localizes to the INM

VAPB is an integral membrane protein previously characterized in the ER. In this work, an INM localization of VAPB is demonstrated. By using a rapamycin based dimerization approach (Pfaff et al., 2016), VAPB was shown to be localized at the INM (Chapter 4; manuscript Figure 1C). Since the rapamycin approach uses over-expression of the protein of interest (in this case VAPB), the INM localization of endogenous VAPB was also demonstrated by immunoelectron microscopy (manuscript Figure 1D). VAPB was also recovered mostly in NE fraction similar to emerin, lamin A/C and other NE proteins (Chapter 4; manuscript Figure S1) by subcellular fractionation. Very recently, an INM localization of VAPB was demonstrated in which a role of VAPB in HSV-1 nuclear egress was reported (Saiz-Ros et al., 2019). Based on this study, a sub-population of VAPB was present in the INM, which was observed by immunoelectron microscopy and indirect-immunofluorescence assays. In the context of localization to the INM, VAPB knockdown was previously reported to affect the NE targeting of emerin and the nucleoporins, Nup214 and gp210 (Tran et al., 2012). P56S VAPB mutation, which causes ALS was also reported to cause a nuclear envelope defect (Tran et al., 2012).

A yeast homologue of VAPB, Scs2/Scs2p (Kagiwada and Zen, 2003; Kagiwada et al., 1998) was also reported to be a nuclear and ER membrane protein. There are also reports which mention that Scs2 mediates the activation of INO1, a target gene of the

unfolded protein response (UPR) at the nuclear membrane (Brickner and Walter, 2004). Scs2 binds at the nuclear membrane to an ER-associated transcription factor Opi1 which translocates to the nucleus upon reduction of phosphatidic acids (Loewen et al., 2004; Romanauska and Köhler, 2018).

Taken together, these studies favor the localization of a sub-population of VAPB to the INM. However, the percentage of the total VAPB pool residing at the INM still needs to be investigated. It is also possible that VAPB resides at the INM only for a short duration. Since the ER is continuous with the ONM and the ONM with the NPC, lateral diffusion of VAPB through the NPC is favorable, as it is a relatively small protein of 29 kDa. However, more quantitative methods are required to demonstrate the population of VAPB at different subcellular localizations. Further studies are needed to prove if VAPB is retained at the INM and has a distinct function there or if it shuttles in and out of the nucleus by lateral diffusion.

## 6.3. RAPIDS as an approach to detect protein-protein interactions

Proximity-based labeling has become an important approach in mapping protein-protein interactions. In this work, a method which was termed ‘RAPIDS’ (Rapamycin and APEX- dependent identification of proteins by SILAC) was used to identify the interactome of VAPB at the ER and INM (Chapter 4; manuscript Figures 3 and 4). In comparison to affinity purification based mass-spectrometry of proteins, which requires a careful selection of lysis buffers, and yeast-two hybrid methods, which detect interactions under non-physiological conditions, proximity labeling techniques coupled with quantitative proteomics approaches give a snapshot of stable and transient interactions in a physiologically relevant cellular environment. In recent years there has been an advancement in biotin-based proximity labeling techniques using BioID and APEX systems. The use of BioID for interactome analysis has been steadily rising since its initial attempt to probe nuclear lamina for identifying the interactome of lamin A (Roux et al., 2012). However, the long labeling time in BioID experiments for efficient biotinylation has restricted its use to some extent, even though recent advances in BioID with shorter labeling time have been developed (Branon et al., 2018). A functionally related method, APEX based proximity labelling, has also been extensively used for the past seven years, following its initial attempt to map the proteome of mitochondria (Cho et al., 2017; Han et al., 2017; Hung et al., 2014; Hung et al., 2017; Lee et al., 2016; Lobingier et al., 2017; Mick et al., 2015; Paek et al., 2017; Rhee et al., 2013b).

RAPIDS is a method, which involves the combination of APEX2-dependent biotinylation, rapamycin-dependent targeting of APEX2 to a protein of interest, and SILAC based mass spectrometry. The initial attempt in this work was to differentiate between the ‘classic’ approach, in which APEX2 is directly tagged to a protein of interest and RAPIDS.

This clearly showed an advantage for using the RAPIDS approach for known interactors of VAPB like ACBD5 and OSBPL9 (Chapter 4; manuscript Figure 2). There are mainly two limitations in using the 'classic' method; first, it requires the use of a protein (APEX2), with a size of 28 kDa, which could interfere with protein localization and function. Second, the additional requirement of a control reaction (GFP-APEX2 in this work) to compare for non-specific interactions. These problems are circumvented by using RAPIDS. The localization of a protein is not affected, since APEX2 is physically separated from the protein of interest, and the use of rapamycin to facilitate targeting of APEX2 to a specific subcellular compartment helps to discriminate between proteins that are modified in a specific versus a non-specific manner.

Additionally, by controlling the localization of tags used for APEX2, i.e., in the presence and absence of an NLS, it would be possible to map interactomes within specific cellular compartments. VAPB fused with a smaller tagged HA that diffuses freely to the INM or a 29 kDa mCherry-tag that is more restricted to the ER (Chapter 4; manuscript Figures 3 and 4), gives additional flexibility to the approach to map interactome of a protein that localizes both in ER and the INM. Very recently, a similar targeting approach named as 2C-BioID was described using the rapamycin analogue AP21967 as a dimerizing agent (Chojnowski et al., 2018). Using this approach, the dimerization of a biotin-protein ligase and a protein of interest was initiated by AP21967 to analyze the interactomes of LAP2ß and lamins A and C.

The significant advantages of using APEX based proximity approach over BioID are its smaller tag size (APEX; 28 kDa versus BioID; 35 kDa) and the speed of labeling (1 minute versus 18-24 hours) (Martell et al., 2012; Roux et al., 2012). Therefore, APEX2 detects a 'snapshot' of protein-protein interactions, whereas BioID provides the sum of interactions of a protein of interest over several hours. Recently several modified approaches have been established to reduce the labeling time required for BioID. For instance, BioID2 uses a smaller version of biotin ligase (27 kDa) with 16 hours of labeling (Kim et al., 2016). In yeast, a much faster BioID approach has been recently developed called TurboID (with a tag size 35 kDa) and miniTurboID (with a tag size 27 kDa), which enables labeling in 10 minutes (Branon et al., 2018).

### 6.3.1. RAPIDS validates the known VAPB interactome at the ER

VAPB is a protein that is present at several contact sites involving the ER (Murphy and Levine, 2016). Under conditions that should favor ER interacting partners using an mCherry-FRB-VAPB, which localizes mostly in the ER and FKBP12-GFP-APEX2, which has a cytoplasmic and nuclear localization, many previously known interaction partners of VAPB were identified (Chapter 4; manuscript Figures 2C and 3, Table 11).

**Table 11. ER/cytoplasmic VAPB interactors identified in this and in previous studies.**

| Protein name | Reference | Presence of FFAT motif | Function |
|---|---|---|---|
| PTPIP51 (RMDN3) | (De Vos et al., 2012; Stoica et al., 2014) | ✓ | signaling |
| ACBD5 | (Costello et al., 2017b) | ✓ | membrane tether |
| WDR44 | (Baron et al., 2014) | ✓ | - |
| OSBPL9 | (Mesmin et al., 2013; Moustaqim-Barrette et al., 2014) | ✓ | lipid transport |
| OSBPL8 | (Mesmin et al., 2013; Moustaqim-Barrette et al., 2014) | ✓ | lipid transport |
| OSBPL10 | (Mesmin et al., 2013; Moustaqim-Barrette et al., 2014) | ✓ | lipid transport |
| OSBPL11 | (Mesmin et al., 2013; Moustaqim-Barrette et al., 2014) | ✓ | lipid transport |
| OSBP | (Mesmin et al., 2013; Moustaqim-Barrette et al., 2014) | ✓ | lipid transport |
| YIF1A | (Kuijpers et al., 2013) | - | ER-Golgi membrane trafficking |

Most of the identified proteins localized to the ER or ER-associated membranes, consistent with the prime ER localization of mCherry-FRB-VAPB. Additionally, the majority of the proteins identified had an FFAT domain that binds to the cytoplasmic MSP domain of VAPB (Loewen and Levine, 2005). Proteins localized to the NE like emerin and TMEM43 were also identified using RAPIDS with the mCherry-tagged version of VAPB for which there were two possibilities; (1) mCherry-FRB-VAPB could also reach the INM (Chapter 4; manuscript Figure 1C) and (2) emerin and TMEM43 could also traverse through the ER before reaching their final destination. The ER interactome of VAPB identified in this study was also compared with two major VAPB interaction network studies (Huttlin et al., 2015; Murphy and Levine, 2016). Both studies were performed using the BioPlex network, an interaction network developed from affinity purification-mass spectrometry analysis for human proteins. Huttlin et al. identified 162 interactors for VAPB, and the identified proteins showed association with several OSBPs and other proteins linked with membrane trafficking or signaling. Murphy and Levine used the same BioPlex network to study VAPs-(VAPA and VAPB) FFAT interaction (also known as VAPome) and could show that nearly 50% of VAPome binds directly or indirectly via the VAP-FFAT interactions. As shown in Figure 31, almost 5% of proteins were common in all three approaches. The overlapping candidates mostly belonged to the FFAT motif- containing proteins.

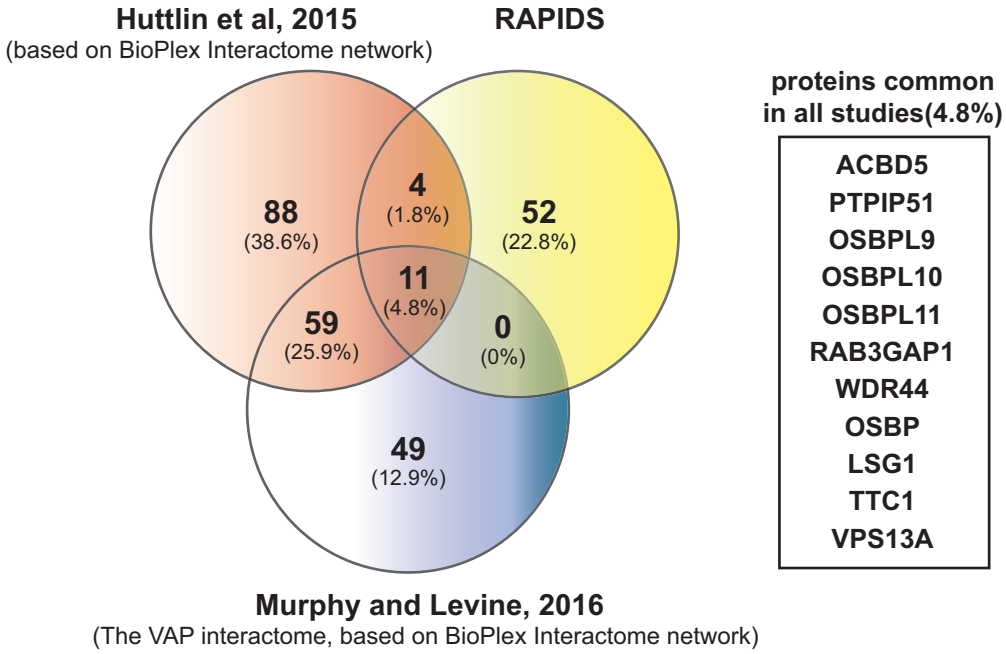


**Figure 31. Comparison of VAPB interactome reported by Huttlin et al, Murphy and Levine and by RAPIDS.**
Venn diagram depicts the overlap between proteins identified by the three approaches. Proteins common in all the studies are listed on the right. Note that the high degree of overlap between the two studies reported by Huttlin et al. and Murphy and Levine et al, is due to the use of the same BioPlex Interactome network.

### 6.3.2. RAPIDS identifies novel INM interactors of VAPB

Since VAPB localized to the INM as well, RAPIDS was also used to identify nuclear binding partners of VAPB. RAPIDS was advantageous to identify nuclear partners compared to affinity-based methods since the latter requires strong lysis buffers for cell lysis in order to solubilize nuclear lamina, while keeping the interactions intact. The NPC imposes a size limit on the trafficking of membrane proteins between the outer and inner nuclear membranes (Blenski and Kehlenbach, 2019; Lusk et al., 2007; Soullam and Worman, 1995; Ungricht et al., 2015; Zuleger et al., 2011). Using a HA-tag instead of an mCherry-tag at the N-terminal end for VAPB, facilitated a smooth passage of VAPB to the INM. Besides, a nuclear version of APEX2, APEX2-dGFP-NLS-FKBP12 that predominantly localizes in the nucleus, favored the detection of proteins from the nuclear side. Significantly more nuclear proteins, including proteins of the nuclear lamina (lamin A and C, lamin B1), nucleoporins (Tpr, Nup153 and ELYS) and proteins of the INM (emerin, TMEM43, Tnpo1 and TOR1AIP1) were identified by this approach (Chapter 4; manuscript Figure 4).

Like any other proximity labeling methods, RAPIDS identifies neighboring partners of a protein of interest. To test whether the neighboring proteins identified are indeed binding partners, further validations to prove the interactions have to be performed. Interaction of both endogenous and over-expressed VAPB with its INM partners emerin and TMEM43 were confirmed by cross-linking followed by co-immunoprecipitation experiments (Chapter 4; manuscript Figure 6). For emerin, the interaction with endogenous VAPB was further confirmed by co-immunoprecipitation using NE fractions obtained by subcellular

fractionation (Chapter 4; manuscript supplementary Figure S1C). It has been reported previously that the VAPB function is essential for the transport of emerin to the NE (Tran et al., 2012). Very recently, interactome analysis of emerin using BioID proximity labeling approach also detected VAPB as a proximity partner of emerin (Moser et al., 2020). The results obtained by immunoprecipitation assays further confirm that VAPB indeed forms a complex with emerin. Interaction of TMEM43 (LUMA) with emerin and its effect in distribution at the INM has also been previously reported (Bengtsson and Otto, 2008). The interaction of VAPB with TMEM43 might be dependent on the association of emerin with TMEM43.

Proximity Ligation Assays (PLAs) were performed to detect the proximity of VAPB/emerin and VAPB/ELYS. The PLA interactions (dots) for emerin and VAPB were restricted to the NE, which was consistent with the INM localization of both proteins. In addition to PLA dots at the NE, intranuclear dots were also observed for VAPB/ELYS. ELYS is a nucleoporin required for nuclear pore assembly (Rasala et al., 2006). It also localizes to the nuclear interior during interphase. Since the dots were also observed inside the nucleus, VAPB might also reside in the nucleoplasm. However, this has to be further studied, since alternative splice variants of VAPB lacking the transmembrane domain are also present in human tissues and they localize to the nuclear interior (Nachreiner et al., 2010). ELYS was also reported to interact with VAPB through its predicted FFAT like-motif (Murphy and Levine, 2016). Even though single antibody controls and silencing of VAPB was performed as a control reaction to monitor specificity of PLA interaction, the use of an antibody against an organelle marker protein, which is not involved in interaction would further validate the specificity of the PLA signal.

### 6.3.3. The interaction repertoire of VAPB identified by RAPIDS

RAPIDS is an approach useful for assessing cell compartmental-specific protein interactions by the restriction of the enzyme to a specific compartment. The approach is also convenient when the protein of interest being investigated localizes to multiple cellular compartments. VAPB is an example of a protein that can be distributed between two different subcellular localizations, namely the ER and the INM. The Gene Ontology (GO) analysis performed on Cellular Compartment (CC) for the interactors of VAPB at the ER (Figure 32A) and the INM (Figure 32B) also clearly indicates the abundance of ER/ cytoplasmic proteins and NE proteins, respectively. GOCC enrichment score of VAPB interactome at the ER revealed a diverse list of ER and Golgi membrane compartment GO terms and a comparatively lower enrichment score for nuclear components. A stronger focus on the nuclear components was observed for VAPB interactome at the INM, such as ‘nuclear pore basket’, ‘nuclear lamina’ and ‘INM’ with a high enrichment score.

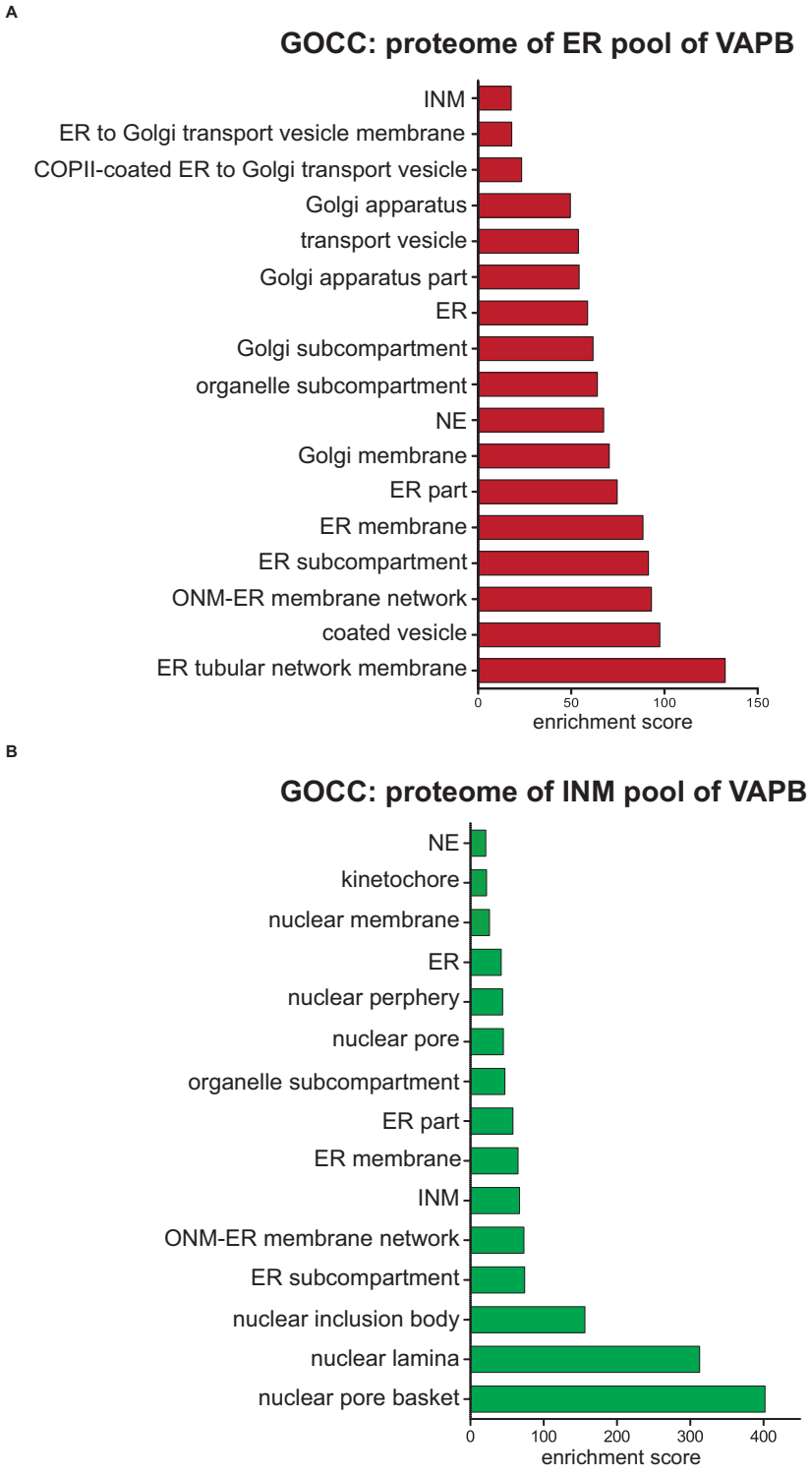


**Figure 32. GOCC analysis of VAPB interactome.**
Gene Ontology cellular compartment (GOCC) classification of all significant proteins identified using RAPIDS, which was used to enrich VAPB proteome in the ER (A) and in the INM (B). The x-axis shows the enrichment score of different cellular compartments.

Taken together, this work demonstrates that the interactome of VAPB not only confines to the ER/cytoplasmic compartment, but VAPB as a contact site protein also localizes to the INM, where it may contact the nuclear lamina, integral membrane proteins and proteins of the NPC. Figure 33 summarizes the entire interactome of VAPB identified using RAPIDS. At this point, it is only possible to speculate on the function of VAPB at the INM. The P56S mutation of VAPB and also knockdown of endogenous VAPB have been reported to affect the transport of emerin and nucleoporins to the nuclear envelope (Tran et al., 2012). VAPB also has been implicated as an important contributor to the HSV-1 life cycle and might facilitate HSV-1 nuclear egress. VAPB was reported to play a role in primary envelopment since it localizes to the NE in association with primary enveloped nucleoplasmic virions (Saiz-Ros et al., 2019). Further studies have to be performed to investigate the role of VAPB at the INM.

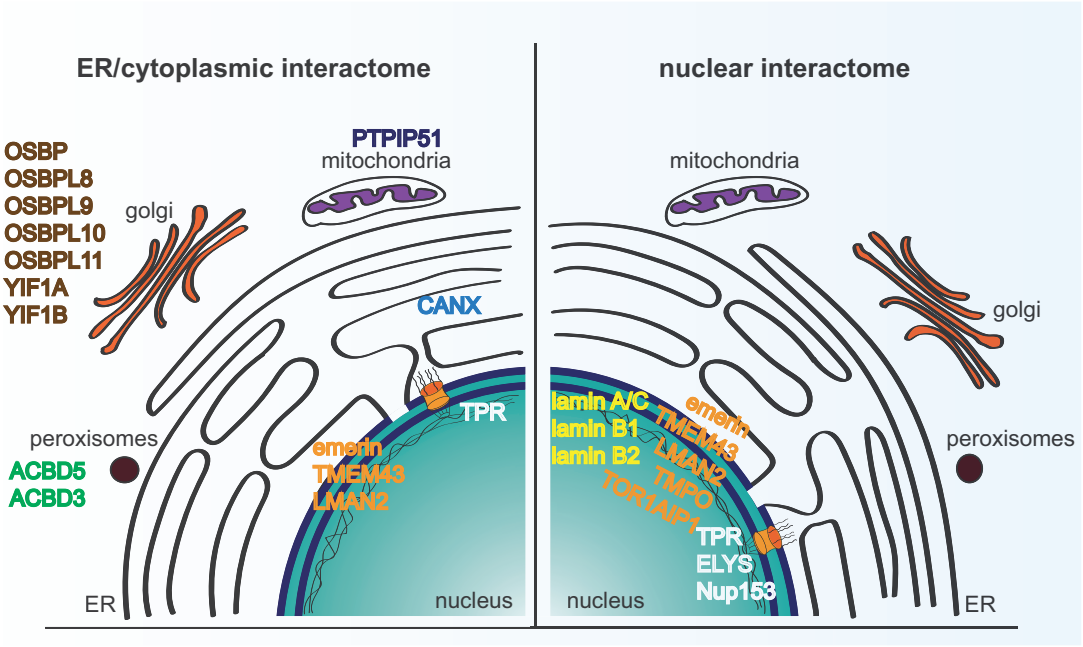


**Figure 33. The VAPB interactome.**
Schematic depiction of interactome of VAPB identified by RAPIDS from the ER/ cytoplasmic pool of VAPB and nuclear pool of VAPB.

### 6.3.4. Limitations of RAPIDS and other proximity labeling approaches

One of the advantages of RAPIDS over other proximity labeling approaches is that it reduces non-specific backgrounds to a larger extend compared to classic APEX2 or BioID approaches. The experimental setup in the absence of rapamycin serves as an internal control to identify non-specific interactors. Moreover, rapamycin treatment is performed in the same cellular context with the expression of the same fusion constructs. However, RAPIDS is a proximity labeling method, detecting neighbors, and therefore, the method as such cannot be used to demonstrate interactions of the proteins. It is crucial to validate the

candidates identified by independent approaches like immunoprecipitation approaches, super-resolution microscopy or bimolecular fluorescence complementation assays. Additionally, the impact that the addition of rapamycin and $H_2O_2$ may have on the interactome of proteins also needs to be considered. For instance, prolonged rapamycin treatment affects the mTOR signaling pathway (Sarbassov et al., 2006; Schreiber et al., 2015). Therefore, analogs of rapamycin that are non-toxic to the cells are an alternative. There are also reports that $H_2O_2$ treatment, though brief, might affect the cellular oxidative status and stress response (Schreiber et al., 2015). Another concern is the expression level of fusion constructs used in RAPIDS that can vary between different transient transfections. An effective approach would be to use stable cell lines for one of the fusion construct (FKBP12-APEX2) that could be transfected with the other (FRB-protein of interest) or vice versa. The use of HA-tag in RAPIDS could also affect proximity labeling, since APEX2 can cause oxidative damage to tyrosine residues in the tag (Martell et al., 2017). Alternate smaller epitope tags like FLAG-tag could be used instead. It has to be noted that VAPB was not a significant hit in our recent work on the interactome of emerin by using RAPIDS (Müller et al., 2020), even though the raw data set included VAPB. This could be due to the unavailability of appropriate sites for biotinylation on the surface of VAPB. Alternatively, the tag used for the overexpression of emerin could affect protein-protein interaction.

## 6.4. Kinetics of trafficking of integral proteins to the INM

Different models have been suggested for the targeting of INM proteins from the ER to the INM through the NPC. Diffusion retention (Boni et al., 2015; Ungricht et al., 2015) and receptor-mediated translocation (King et al., 2006; Meinema et al., 2011) models have been described as the major mechanisms of INM protein translocation. Diffusional mobilities of several INM proteins like LBR, SUN2, Lap2β, Man1 and emerin (Ellenberg et al., 1997; Ostlund et al., 1999; Ungricht et al., 2015; Wu et al., 2002) have been previously measured using FRAP. In this work, the diffusional mobilities of four different single pass TA proteins, namely, emerin, VAPB, Lap2β, PTP1B, and a multi-pass protein LBR were studied in live cells and semi-permeabilized cells by FRAP assays. All the proteins exhibited different rates of fluorescent recovery in living cells, measured at the NE, ranging from 40-60% (Figure 18). For emerin, the fluorescent intensity after recovery was 60% at the NE and it has been reported that emerin is less mobile in the NE compared to the ER (Ostlund et al., 1999). Ostlund et al. also suggest that emerin is not entirely immobile at the NE even though it binds to chromatin. Instead, it slowly diffuses as a complex by binding to non-chromatin nuclear proteins. In addition, export from the INM to the ER also might account for a 60% fluorescent intensity after recovery at the NE. Similar diffusional mobility was observed for Lap2β, consistent with the previous reports that emerin and Lap2β have similar half-time

(t½) recovery rate at the NE (Ostlund et al., 1999; Shimi et al., 2004; Wu et al., 2002). For LBR, the rate was rather low (40%), in accordance with its lower diffusional mobility at the NE due to extensive immobilization that occurs in the INM by binding to chromatin and lamins (Ellenberg et al., 1997). A similar observation was also made for the recovery rate of fluorescence for VAPB and PTP1B, suggesting that it could be either retained by interacting with other INM proteins or exported back to the ER. Using RAPIDS, VAPB showed an interaction with INM proteins emerin and TMEM43. It was also reported that PTP1B interacts with emerin at the INM (Yip et al., 2012).

### 6.4.1. Diffusion of emerin to the NE requires soluble cytoplasmic factors

FRAP assays analyzing protein dynamics have been performed either on intact or semi-permeabilized cells. A comparative analysis under both conditions has not been studied previously. Interestingly, a different picture emerged when the FRAP assays were performed in semi-permeabilized cells. All of the tested proteins showed a decreased diffusional mobility at the NE in semi-permeabilized cells compared to intact or living cells (Figure 19). Even though a complete absence in the fluorescent recovery was not observed, which could be attributed to the fact that diffusion occurs within the NE, the recovery rate was reduced by 50% or more for emerin, Lap2β, VAPB and LBR. For PTP1B, only a slight reduction in recovery was observed, suggesting that permeabilization does not have a strong effect on its diffusional mobility.

Since differential permeabilization with digitonin removes the cytosolic components leaving the NE intact, cytosol was added back to the permeabilized cells. Interestingly, the addition of cytosol significantly increased the fluorescent intensity after recovery of emerin (Figure 20) compared to the permeabilized cells with no cytosol addition, which was not the case for other INM proteins tested. The cytosol dependence of emerin might involve soluble components. This was also observed for another INM protein, SUN2, which was targeted to the INM efficiently in the presence of both cytosol and energy (Ungricht et al., 2015). Additionally, it was found that none of the three targeting signals of SUN2, a classical NLS, a Golgi retrieval signal and a lumenal SUN domain, were linked to its cytosol dependence for targeting to the NE (Ungricht et al., 2015). Further investigation is needed to determine whether the two INM retention signals present at the N-terminal of emerin (Ostlund et al., 1999) are linked to its cytosol dependence on diffusion to the NE. The INM localization of emerin and SUN2 was compromised by ATP depletion, suggesting that an energy dependent step could assist them in diffusion to the INM (Zuleger et al., 2011). Moreover, the translocation of LBR to the INM was shown to be dependent on RanGTPase (Zuleger et al., 2011). These reports suggest that, additional cytosolic factors also assist in diffusion of INM proteins through the NPC.

### 6.4.2. Molecular requirements for targeting of emerin to the NE in permeabilized cells

The dependence of emerin on cytosol for its diffusional mobility prompted us to study the requirements for targeting to the NE in semi-permeabilized cells. An initial attempt by testing the factors that affect nuclear import of soluble, NLS-containing cargo, led to the observation that RanQ69L, WGA and Impβ (45-462) impaired the diffusional mobility of emerin (Figure 25, Figure 26, Figure 27). The requirement of functional RanGTPase has also been reported for other INM proteins: the yeast proteins, Heh1 and Heh2 (King et al., 2006), and the mammalian protein LBR (Zuleger et al., 2011). For LBR, it was also observed that Nup35 residing in the peripheral channels of the NPC plays a role in Ran-mediated INM translocation (Zuleger et al., 2011). It has to be investigated whether knocking down Nup35 has an effect on the targeting of emerin to the INM. The reduction in diffusional mobility observed with WGA and Impβ (45-462), both of which bind to the NPC and inhibit protein import, also suggests that the diffusion of emerin through the NPC to the INM is dependent on a cytosolic factor that potentially contributes to importin-mediated NPC translocation. It has been previously reported that the higher mobility of exogenous emerin in the nuclear membrane depends on Samp1 and RanGTP. Ran regulates the interaction between Samp1 and emerin in the NE (Vijayaraghavan et al., 2018). Therefore, there is indeed an effect of functional Ran in the mobility of emerin at the NE. However, it has to be taken into account that NTR-depletion did not have a significant effect on the diffusional mobility of emerin to the NE (Figure 28). Recent studies have also suggested the involvement of components used for NPC transport of soluble proteins (King et al., 2006). Furthermore, soluble 'piggyback' proteins (Gardner et al., 2011) help in the targeting of INM proteins. Thus, further investigations are required to systematically determine the factor present in cytosol that promotes the diffusion of emerin to the NE.

Most of the recovery in fluorescence intensity observed in the FRAP assays performed at the NE likely comes from the protein exchange between the ER and NE, as confirmed by different factors that affect the transport from the ER to the NE (WGA, RanQ69L and Impβ (45-462)). WGA binds to cytosolically exposed O-glycosylated regions of FG repeat nucleoporins to inhibit transport (Finlay et al., 1987) to the NE. WGA could potentially bind to other glycosylated proteins as well. Emerin is reported to be O-glycosylated that regulates its association with barrier to autointegration factor (BAF) at the INM (Berk et al., 2013b). It has to be further investigated whether WGA binds to the glycosylated emerin which could inhibit its diffusion to the NE. It was also been reported that for many NETs (NE transmembrane proteins), binding in the INM is so stable that recovery after photobleaching depends more on diffusion of proteins between the ER and INM than on the mobility within the INM (Zuleger et al., 2011). However, the possibility of redistribution of the proteins within the NE cannot be ruled out as observed for the lower

mobility of all the tested INM proteins after permeabilization. Also, since targeting of INM proteins requires maintenance of ER topology (Pawar et al., 2017), FRAP assays performed at the ER, in the absence or presence of the factors tested in this study for NE, would provide better insights into the diffusion of emerin (Figure 29). Digitonin selectively permeabilizes the plasma membrane by binding to cholesterol that is more abundant in the plasma membrane than the ER membrane. It has to be further studied whether digitonin affects the ER topology of the cells and thereby the diffusion of proteins from the ER to the INM. It has also been demonstrated that Atlastins, a family of membrane-bound GTPases that preserve ER structure, are critical for efficient targeting of proteins to the INM (Pawar et al., 2017). Therefore, further investigation is needed to determine the importance of ER network topology on the targeting of emerin to the NE.

In summary, different explanations for the effect of cytosol on the diffusional mobility of emerin are possible. First, cytosol addition might have a direct effect on emerin transport. This could be due to the presence of 'piggyback' proteins present in the cytosol that could assist in the transport of emerin. For instance, nuclear import of yeast SUN protein, Mps3, was assisted by a soluble histone H2A.Z protein (Gardner et al., 2011). Second, addition of cytosol might affect NPC itself, since classic reagents that block transport of soluble cargoes through NPC (WGA, Impβ (45-462) and RanQ69L) also reduced the diffusional mobility of emerin. Third, cytosol addition might have assisted in an unhindered diffusion from the ER to the NE that could have been affected by the permeabilization of cells with digitonin. Figure 34 summarizes the requirements observed in this study for the diffusion of emerin to the NE in intact and permeabilized cells.

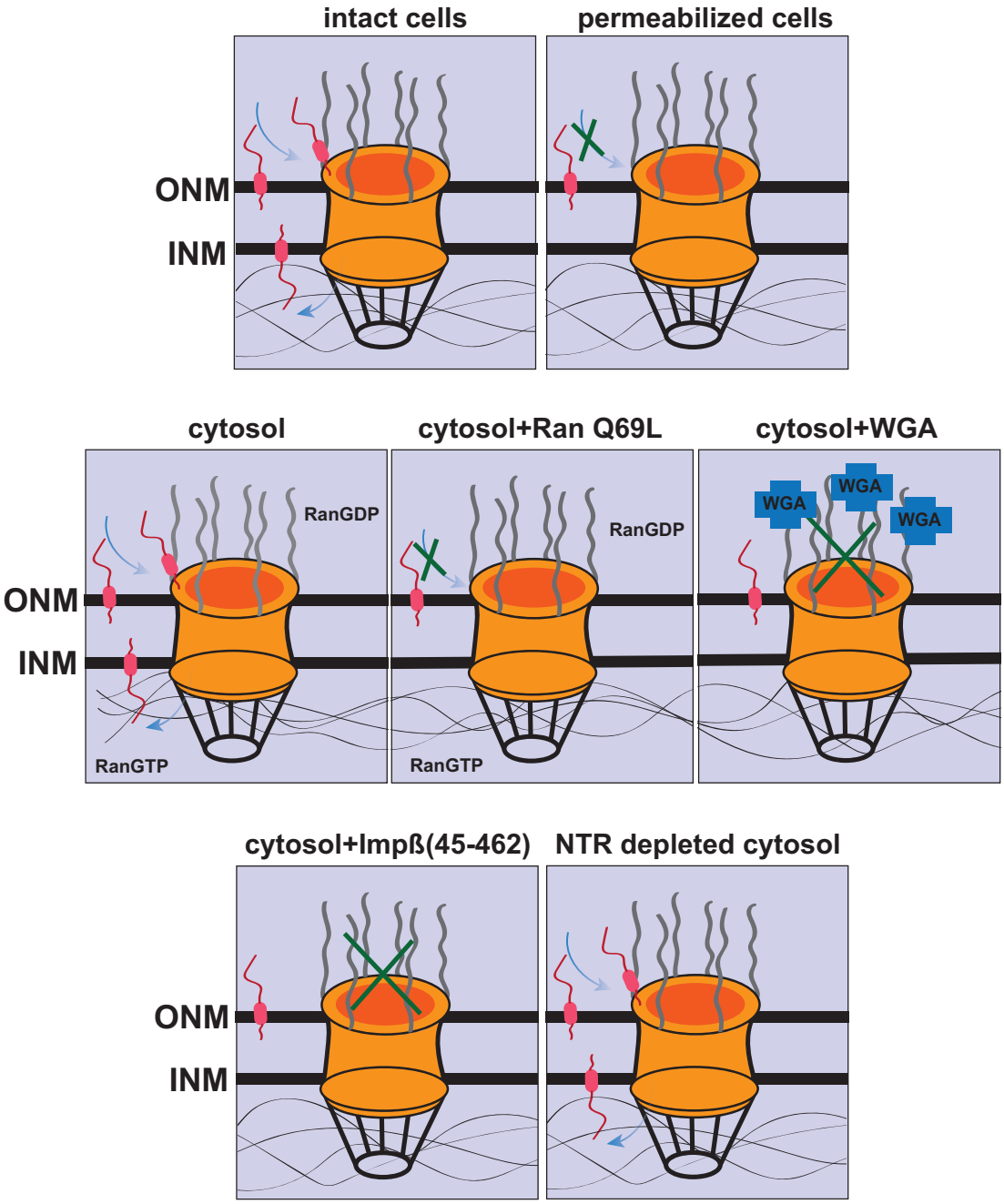


**Figure 34. Schematic depiction of factors affecting diffusion of emerin to the NE.**
Emerin diffuses readily from the ER to the NE in intact cells whereas the diffusional mobility decreases in permeabilized cells. Cytosol addition to permeabilized cells increase the diffusional mobility in permeabilized cells. Addition of RanQ69L, WGA and Impβ (45-462) impairs the diffusional mobility of emerin in semi-permeabilized cells whereas NTP depleted cytosol had no significant effect on the diffusion of emerin.

# Outlook

## ER membrane insertion of VAPB

In this study, it was shown that post-translational insertion of VAPB into ER membranes does not depend on the TRC40 system. Therefore, other possible pathways for ER insertions need to be investigated.

Knock down studies using components of the alternate pathways like ER membrane complex (EMC), hSnd2 and SRP targeting pathways could be performed in semi-permeabilized cell system followed by membrane insertion. The role of VAPB-TRC40 association could be studied using the ATPase-impaired trap mutants of TRC40 as described by Coy-Vergara et al., 2019.

## The VAPB interactome

Using RAPIDS, the ER and INM interactome of VAPB was established, proving it as a versatile approach to identify proximity partners of a protein of interest.

Using RAPIDS to identify the interactome of P56S VAPB, a mutant of VAPB that causes Amyotrophic Lateral Sclerosis (ALS) might shed light on the pathogenicity of the disease caused by P56S VAPB. RAPIDS could also be used to identify the interactome of VAPA, a related protein belonging to the VAP family. It will also be interesting to see whether both VAP proteins share the same interactome and whether VAPA also localizes to the INM. The functional characterization of VAPB at the INM could also be studied. For that, high-resolution ultrastructure imaging analysis of the NE obtained by electron microscopy performed on control, VAPB and VAPA knockdown cells could be useful to see whether the knockdown causes any NE defects. Additionally, the effect of VAPB and VAPA knockdown on its interaction partners could also be investigated. To overcome the caveats of RAPIDS, changes in experimental conditions like using a rapamycin analog that does not lead to any secondary toxic effects in cells or monitoring rapamycin based non-specific effects by performing a control experiment using only the APEX2 reporter could be performed.

## Kinetics of trafficking of emerin to the NE

In this study, it was observed that the diffusional mobility of emerin was affected by permeabilization of the cells by digitonin and was enhanced by the addition of cytosol to the cells. Addition of RanQ69L, WGA and Impβ (45-462) impaired the diffusion to the NE.

A tool for studying INM targeting of emerin as described by Ungricht et al., 2015, could be used to identify and validate the requirements of protein targeting to the INM. Moreover, FRAP assays performed at the ER and also FLIP assays performed at the ER could help to find out a role of ER topology in efficient targeting of emerin to the INM. Finally,

it is important to determine what cytosolic factors assist the diffusion of emerin to the NE This could be achieved by fractionating the cytosol and analyzing each fractions for its transport-stimulating activity (Moore and Blobel, 1992). This would provide new insights into the mechanism of targeting of emerin to the NE.

# References

**Abell, B. M., Pool, M. R., Schlenker, O., Sinning, I. and High, S.** (2004). Signal recognition particle mediates post-translational targeting in eukaryotes. *EMBO J.* **23**, 2755–64.

**Abell, B. M., Rabu, C., Leznicki, P., Young, J. C. and High, S.** (2007). Post-translational integration of tail-anchored proteins is facilitated by defined molecular chaperones. *J. Cell Sci.* **120**, 1743–51.

**Adam, E. J. and Adam, S. A.** (1994). Identification of cytosolic factors required for nuclear location sequence-mediated binding to the nuclear envelope. *J. Cell Biol.* **125**, 547–55.

**Adam, S. A., Marr, R. S. and Gerace, L.** (1990). Nuclear protein import in permeabilized mammalian cells requires soluble cytoplasmic factors. *J. Cell Biol.* **111**, 807–16.

**Aitchison, J. D. and Rout, M. P.** (2012). The yeast nuclear pore complex and transport through it. *Genetics* **190**, 855–83.

**Akhtar, A. and Gasser, S. M.** (2007). The nuclear envelope and transcriptional control. *Nat. Rev. Genet.* **8**, 507–17.

**Aksu, M., Pleiner, T., Karaca, S., Kappert, C., Dehne, H.-J., Seibel, K., Urlaub, H., Bohnsack, M. T. and Görlich, D.** (2018). Xpo7 is a broad-spectrum exportin and a nuclear import receptor. *J. Cell Biol.* **217**, 2329–2340.

**Allen, T. D., Cronshaw, J. M., Bagley, S., Kiseleva, E. and Goldberg, M. W.** (2000). The nuclear pore complex: mediator of translocation between nucleus and cytoplasm. *J. Cell Sci.* **113 ( Pt 1**, 1651–9.

**Alpy, F., Rousseau, A., Schwab, Y., Legueux, F., Stoll, I., Wendling, C., Spiegelhalter, C., Kessler, P., Mathelin, C., Rio, M.-C., et al.** (2013). STARD3 or STARD3NL and VAP form a novel molecular tether between late endosomes and the ER. *J. Cell Sci.* **126**, 5500–12.

**Amarilio, R., Ramachandran, S., Sabanay, H. and Lev, S.** (2005). Differential regulation of endoplasmic reticulum structure through VAP-Nir protein interaction. *J. Biol. Chem.* **280**, 5934–44.

**Antonin, W., Ungricht, R. and Kutay, U.** (2011). Traversing the NPC along the pore membrane: targeting of membrane proteins to the INM. *Nucleus* **2**, 87–91.

**Arts, G. J., Kuersten, S., Romby, P., Ehresmann, B. and Mattaj, I. W.** (1998). The role of exportin-t in selective nuclear export of mature tRNAs. *EMBO J.* **17**, 7430–41.

**Aviram, N., Ast, T., Costa, E. A., Arakel, E. C., Chuartzman, S. G., Jan, C. H., Haßdenteufel, S., Dudek, J., Jung, M., Schorr, S., et al.** (2016). The SND proteins constitute an alternative targeting route to the endoplasmic reticulum. *Nature* **540**,

134–138.

**Bar, D. Z., Atkatsh, K., Tavarez, U., Erdos, M. R., Gruenbaum, Y. and Collins, F. S.** (2018). Biotinylation by antibody recognition - a method for proximity labeling. *Nat. Methods*.

**Baron, Y., Pedrioli, P. G., Tyagi, K., Johnson, C., Wood, N. T., Fountaine, D., Wightman, M. and Alexandru, G.** (2014). VAPB/ALS8 interacts with FFAT-like proteins including the p97 cofactor FAF1 and the ASNA1 ATPase. *BMC Biol.* **12**, 39.

**Behrens, T. W., Kearns, G. M., Rivard, J. J., Bernstein, H. D., Yewdell, J. W. and Staudt, L. M.** (1996). Carboxyl-terminal targeting and novel post-translational processing of JAW1, a lymphoid protein of the endoplasmic reticulum. *J. Biol. Chem.* **271**, 23528–34.

**Bengtsson, L. and Otto, H.** (2008). LUMA interacts with emerin and influences its distribution at the inner nuclear membrane. *J. Cell Sci.*

**Bengtsson, L. and Wilson, K. L.** (2004). Multiple and surprising new functions for emerin, a nuclear membrane protein. *Curr. Opin. Cell Biol.* **16**, 73–9.

**Berk, J. M., Tifft, K. E. and Wilson, K. L.** (2013a). The nuclear envelope LEM-domain protein emerin. *Nucleus* **4**, 298–314.

**Berk, J. M., Maitra, S., Dawdy, A. W., Shabanowitz, J., Hunt, D. F. and Wilson, K. L.** (2013b). O-Linked β-N-acetylglucosamine (O-GlcNAc) regulates emerin binding to barrier to autointegration factor (BAF) in a chromatin- and lamin B-enriched niche. *J. Biol. Chem.* **288**, 30192–30209.

**Berndt, U., Oellerer, S., Zhang, Y., Johnson, A. E. and Rospert, S.** (2009). A signal-anchor sequence stimulates signal recognition particle binding to ribosomes from inside the exit tunnel. *Proc. Natl. Acad. Sci. U. S. A.* **106**, 1398–403.

**Bione, S., Maestrini, E., Rivella, S., Mancini, M., Regis, S., Romeo, G. and Toniolo, D.** (1994). Identification of a novel X-linked gene responsible for Emery-Dreifuss muscular dystrophy. *Nat. Genet.* **8**, 323–7.

**Bischoff, F. R. and Görlich, D.** (1997). RanBP1 is crucial for the release of RanGTP from importin beta-related nuclear transport factors. *FEBS Lett.* **419**, 249–54.

**Bischoff, F. R. and Ponstingl, H.** (1991). Catalysis of guanine nucleotide exchange on Ran by the mitotic regulator RCC1. *Nature* **354**, 80–82.

**Bischoff, F. R., Klebe, C., Kretschmer, J., Wittinghofer, A. and Ponstingl, H.** (1994). RanGAP1 induces GTPase activity of nuclear Ras-related Ran. *Proc. Natl. Acad. Sci. U. S. A.* **91**, 2587–2591.

**Blenski, M. and Kehlenbach, R. H.** (2019). Targeting of LRRC59 to the Endoplasmic Reticulum and the Inner Nuclear Membrane. *Int. J. Mol. Sci.* **20**,.

**Boncompain, G., Divoux, S., Gareil, N., de Forges, H., Lescure, A., Latreche, L.,**

**Mercanti, V., Jollivet, F., Raposo, G. and Perez, F.** (2012). Synchronization of secretory protein traffic in populations of cells. *Nat. Methods* **9**, 493–8.

**Boni, A., Politi, A. Z., Strnad, P., Xiang, W., Hossain, M. J. and Ellenberg, J.** (2015). Live imaging and modeling of inner nuclear membrane targeting reveals its molecular requirements in mammalian cells. *J. Cell Biol.* **209**, 705–20.

**Borgese, N. and Fasana, E.** (2011). Targeting pathways of C-tail-anchored proteins. *Biochim. Biophys. Acta - Biomembr.* **1808**, 937–946.

**Borgese, N., Brambillasca, S. and Colombo, S.** (2007). How tails guide tail-anchored proteins to their destinations. *Curr. Opin. Cell Biol.* **19**, 368–75.

**Brambillasca, S., Yabal, M., Soffientini, P., Stefanovic, S., Makarow, M., Hegde, R. S. and Borgese, N.** (2005). Transmembrane topogenesis of a tail-anchored protein is modulated by membrane lipid composition. *EMBO J.* **24**, 2533–42.

**Brambillasca, S., Yabal, M., Makarow, M. and Borgese, N.** (2006). Unassisted translocation of large polypeptide domains across phospholipid bilayers. *J. Cell Biol.* **175**, 767–77.

**Branon, T. C., Bosch, J. A., Sanchez, A. D., Udeshi, N. D., Svinkina, T., Carr, S. A., Feldman, J. L., Perrimon, N. and Ting, A. Y.** (2018). Efficient proximity labeling in living cells and organisms with TurboID. *Nat. Biotechnol.* **36**, 880–887.

**Braunagel, S. C., Williamson, S. T., Saksena, S., Zhong, Z., Russell, W. K., Russell, D. H. and Summers, M. D.** (2004). Trafficking of ODV-E66 is mediated via a sorting motif and other viral proteins: facilitated trafficking to the inner nuclear membrane. *Proc. Natl. Acad. Sci. U. S. A.* **101**, 8372–7.

**Braunagel, S. C., Williamson, S. T., Ding, Q., Wu, X. and Summers, M. D.** (2007). Early sorting of inner nuclear membrane proteins is conserved. *Proc. Natl. Acad. Sci. U. S. A.* **104**, 9307–12.

**Brickner, J. H. and Walter, P.** (2004). Gene recruitment of the activated INO1 locus to the nuclear membrane. *PLoS Biol.* **2**, e342.

**Burnette, W. N.** (1981). “Western Blotting”: Electrophoretic transfer of proteins from sodium dodecyl sulfate-polyacrylamide gels to unmodified nitrocellulose and radiographic detection with antibody and radioiodinated protein A. *Anal. Biochem.* **112**, 195–203.

**Carpenter, A. E., Jones, T. R., Lamprecht, M. R., Clarke, C., Kang, I. H., Friman, O., Guertin, D. A., Chang, J. H., Lindquist, R. A., Moffat, J., et al.** (2006). CellProfiler: image analysis software for identifying and quantifying cell phenotypes. *Genome Biol.* **7**, R100.

**Casson, J., McKenna, M., Haßdenteufel, S., Aviram, N., Zimmerman, R. and High, S.** (2017). Multiple pathways facilitate the biogenesis of mammalian tail-anchored

proteins. *J. Cell Sci.* **130**, 3851–3861.

**Charneau, P., Mirambeau, G., Roux, P., Paulous, S., Buc, H. and Clavel, F.** (1994). HIV-1 reverse transcription. A termination step at the center of the genome. *J. Mol. Biol.* **241**, 651–62.

**Chen, C. and Okayama, H.** (1987). High-efficiency transformation of mammalian cells by plasmid DNA. *Mol. Cell. Biol.* **7**, 2745–2752.

**Chen, J., Zheng, X. F., Brown, E. J. and Schreiber, S. L.** (1995). Identification of an 11-kDa FKBP12-rapamycin-binding domain within the 289-kDa FKBP12-rapamycin-associated protein and characterization of a critical serine residue. *Proc. Natl. Acad. Sci. U. S. A.* **92**, 4947–51.

**Chen, H.-J., Anagnostou, G., Chai, A., Withers, J., Morris, A., Adhikaree, J., Pennetta, G. and de Belleroche, J. S.** (2010). Characterization of the properties of a novel mutation in VAPB in familial amyotrophic lateral sclerosis. *J. Biol. Chem.* **285**, 40266–81.

**Chen, T.-C., Lin, K.-T., Chen, C.-H., Lee, S.-A., Lee, P.-Y., Liu, Y.-W., Kuo, Y.-L., Wang, F.-S., Lai, J.-M. and Huang, C.-Y. F.** (2014). Using an in situ proximity ligation assay to systematically profile endogenous protein-protein interactions in a pathway network. *J. Proteome Res.* **13**, 5339–46.

**Cheng, L.-C., Baboo, S., Lindsay, C., Brusman, L., Martinez-Bartolomé, S., Tapia, O., Zhang, X., Yates, J. R. and Gerace, L.** (2019). Identification of new transmembrane proteins concentrated at the nuclear envelope using organellar proteomics of mesenchymal cells. *Nucleus* **10**, 126–143.

**Cho, I.-T., Adelmant, G., Lim, Y., Marto, J. A., Cho, G. and Golden, J. A.** (2017). Ascorbate peroxidase proximity labeling coupled with biochemical fractionation identifies promoters of endoplasmic reticulum-mitochondrial contacts. *J. Biol. Chem.* **292**, 16382–16392.

**Choi-Rhee, E., Schulman, H. and Cronan, J. E.** (2004). Promiscuous protein biotinylation by Escherichia coli biotin protein ligase. *Protein Sci.* **13**, 3043–50.

**Chojnowski, A., Sobota, R. M., Ong, P. F., Xie, W., Wong, X., Dreesen, O., Burke, B. and Stewart, C. L.** (2018). 2C-BioID: An Advanced Two Component BioID System for Precision Mapping of Protein Interactomes. *iScience* **10**, 40–52.

**Chou, K.-C. and Cai, Y.-D.** (2005). Prediction of membrane protein types by incorporating amphipathic effects. *J. Chem. Inf. Model.* **45**, 407–13.

**Colombo, S. F., Longhi, R. and Borgese, N.** (2009). The role of cytosolic proteins in the insertion of tail-anchored proteins into phospholipid bilayers. *J. Cell Sci.* **122**, 2383–92.

**Colombo, S. F., Cardani, S., Maroli, A., Vitiello, A., Soffientini, P., Crespi, A., Bram,**

**R. J., Benfante, R. and Borgese, N.** (2016). Tail-anchored protein insertion in mammals. FUNCTION AND RECIPROCAL INTERACTIONS OF THE TWO SUBUNITS OF THE TRC40 RECEPTOR. *J. Biol. Chem.* **291**, 18855.

**Cooper, S. E., Hodimont, E. and Green, C. M.** (2015). A fluorescent bimolecular complementation screen reveals MAF1, RNF7 and SETD3 as PCNA-associated proteins in human cells. *Cell Cycle* **14**, 2509–19.

**Costello, J. L., Castro, I. G., Schrader, T. A., Islinger, M. and Schrader, M.** (2017a). Peroxisomal ACBD4 interacts with VAPB and promotes ER-peroxisome associations. *Cell Cycle*.

**Costello, J. L., Castro, I. G., Hacker, C., Schrader, T. A., Metz, J., Zeuschner, D., Azadi, A. S., Godinho, L. F., Costina, V., Findeisen, P., et al.** (2017b). ACBD5 and VAPB mediate membrane associations between peroxisomes and the ER. *J. Cell Biol.* **216**, 331–342.

**Coutavas, E., Ren, M., Oppenheim, J. D., D'Eustachio, P. and Rush, M. G.** (1993). Characterization of proteins that interact with the cell-cycle regulatory protein Ran/TC4. *Nature* **366**, 585–7.

**Coy-Vergara, J., Rivera-Monroy, J., Urlaub, H., Lenz, C. and Schwappach, B.** (2019). A trap mutant reveals the physiological client spectrum of TRC40. *J. Cell Sci.* **132**, 1147–59.

**Cronshaw, J. M., Krutchinsky, A. N., Zhang, W., Chait, B. T. and Matunis, M. J.** (2002). Proteomic analysis of the mammalian nuclear pore complex. *J. Cell Biol.* **158**, 915–27.

**Cross, B. C. S., Sinning, I., Luirink, J. and High, S.** (2009). Delivering proteins for export from the cytosol. *Nat. Rev. Mol. Cell Biol.* **10**, 255–64.

**Darby, J. F., Krysztofinska, E. M., Simpson, P. J., Simon, A. C., Leznicki, P., Sriskandarajah, N., Bishop, D. S., Hale, L. R., Alfano, C., Conte, M. R., et al.** (2014). Solution structure of the SGTA dimerisation domain and investigation of its interactions with the ubiquitin-like domains of BAG6 and UBL4A. *PLoS One* **9**, e113281.

**Day, C. A., Kraft, L. J., Kang, M. and Kenworthy, A. K.** (2012). *Analysis of protein and lipid dynamics using confocal fluorescence recovery after photobleaching (FRAP).*

**De Munter, S., Görnemann, J., Derua, R., Lesage, B., Qian, J., Heroes, E., Waelkens, E., Van Eynde, A., Beullens, M. and Bollen, M.** (2017). Split-BioID: a proximity biotinylation assay for dimerization-dependent protein interactions. *FEBS Lett.* **591**, 415–424.

**De Vos, K. J., Mórotz, G. M., Stoica, R., Tudor, E. L., Lau, K.-F., Ackerley, S., Warley, A., Shaw, C. E. and Miller, C. C. J.** (2012). VAPB interacts with the mitochondrial

protein PTPIP51 to regulate calcium homeostasis. *Hum. Mol. Genet.* **21**, 1299–311.

**Dickmanns, A., Bischoff, F. R., Marshallsay, C., Lührmann, R., Ponstingl, H. and Fanning, E.** (1996). The thermolability of nuclear protein import in tsBN2 cells is suppressed by microinjected Ran-GTP or Ran-GDP, but not by RanQ69L or RanT24N. *J. Cell Sci.* **109**, 1449–1457.

**Dickmanns, A., Kehlenbach, R. H. and Fahrenkrog, B.** (2015). Nuclear Pore Complexes and Nucleocytoplasmic Transport. In *International Review of Cell and Molecular Biology*, pp. 171–233. Elsevier Ltd.

**Dittmer, T. A. and Misteli, T.** (2011). The lamin protein family. *Genome Biol.* **12**, 222.

**Dwyer, N. and Blobel, G.** (1976). A modified procedure for the isolation of a pore complex-lamina fraction from rat liver nuclei. *J. Cell Biol.* **70**, 581–91.

**Echols, N., Harrison, P., Balasubramanian, S., Luscombe, N. M., Bertone, P., Zhang, Z. and Gerstein, M.** (2002). Comprehensive analysis of amino acid and nucleotide composition in eukaryotic genomes, comparing genes and pseudogenes. *Nucleic Acids Res.* **30**, 2515–23.

**Ellenberg, J., Siggia, E. D., Moreira, J. E., Smith, C. L., Presley, J. F., Worman, H. J. and Lippincott-Schwartz, J.** (1997). Nuclear membrane dynamics and reassembly in living cells: targeting of an inner nuclear membrane protein in interphase and mitosis. *J. Cell Biol.* **138**, 1193–206.

**Ellis, J. A., Craxton, M., Yates, J. R. W. and Kendrick-Jones, J.** (1998). Aberrant intracellular targeting and cell cycle-dependent phosphorylation of emerin contribute to the Emery-Dreifuss muscular dystrophy phenotype. *J. Cell Sci.* **111 ( Pt 6**, 781–92.

**Fasana, E., Fossati, M., Ruggiano, A., Brambillasca, S., Hoogenraad, C. C., Navone, F., Francolini, M. and Borgese, N.** (2010). A VAPB mutant linked to amyotrophic lateral sclerosis generates a novel form of organized smooth endoplasmic reticulum. *FASEB J.* **24**, 1419–30.

**Favaloro, V., Spasic, M., Schwappach, B. and Dobberstein, B.** (2008). Distinct targeting pathways for the membrane insertion of tail-anchored (TA) proteins. *J. Cell Sci.* **121**, 1832–40.

**Favaloro, V., Vilardi, F., Schlecht, R., Mayer, M. P. and Dobberstein, B.** (2010). Asna1/TRC40-mediated membrane insertion of tail-anchored proteins. *J. Cell Sci.* **123**, 1522–30.

**Fazekas de St Groth, S., Webster, R. G. and Datyner, A.** (1963). Two new staining procedures for quantitative estimation of proteins on electrophoretic strips. *Biochim. Biophys. Acta* **71**, 377–91.

**Finlay, D. R., Newmeyer, D. D., Price, T. M. and Forbes, D. J.** (1987). Inhibition of in vitro nuclear transport by a lectin that binds to nuclear pores. *J. Cell Biol.* **104**, 189–

200.

**Foster, L. J., Weir, M. L., Lim, D. Y., Liu, Z., Trimble, W. S. and Klip, A.** (2000). A functional role for VAP-33 in insulin-stimulated GLUT4 traffic. *Traffic* **1**, 512–21.

**Furukawa, K., Panté, N., Aebi, U. and Gerace, L.** (1995). Cloning of a cDNA for lamina-associated polypeptide 2 (LAP2) and identification of regions that specify targeting to the nuclear envelope. *EMBO J.* **14**, 1626–36.

**Furukawa, K., Fritze, C. E. and Gerace, L.** (1998). The major nuclear envelope targeting domain of LAP2 coincides with its lamin binding region but is distinct from its chromatin interaction domain. *J. Biol. Chem.* **273**, 4213–9.

**Gardner, J. M., Smoyer, C. J., Stensrud, E. S., Alexander, R., Gogol, M., Wiegraebe, W. and Jaspersen, S. L.** (2011). Targeting of the SUN protein Mps3 to the inner nuclear membrane by the histone variant H2A.Z. *J. Cell Biol.* **193**, 489–507.

**Gerich, F. J., Funke, F., Hildebrandt, B., Fasshauer, M. and Müller, M.** (2009). H(2)O(2)-mediated modulation of cytosolic signaling and organelle function in rat hippocampus. *Pflugers Arch.* **458**, 937–52.

**Gilmore, R., Blobel, G. and Walter, P.** (1982a). Protein translocation across the endoplasmic reticulum. I. Detection in the microsomal membrane of a receptor for the signal recognition particle. *J. Cell Biol.* **95**, 463–9.

**Gilmore, R., Walter, P. and Blobel, G.** (1982b). Protein translocation across the endoplasmic reticulum. II. Isolation and characterization of the signal recognition particle receptor. *J. Cell Biol.* **95**, 470–7.

**Gingras, A. C., Abe, K. T. and Raught, B.** (2019). Getting to know the neighborhood: using proximity-dependent biotinylation to characterize protein complexes and map organelles. *Curr. Opin. Chem. Biol.* **48**, 44–54.

**Gómez-Suaga, P., Pérez-Nievas, B. G., Glennon, E. B., Lau, D. H. W., Paillusson, S., Mórotz, G. M., Calì, T., Pizzo, P., Noble, W. and Miller, C. C. J.** (2019). The VAPB-PTPIP51 endoplasmic reticulum-mitochondria tethering proteins are present in neuronal synapses and regulate synaptic activity. *Acta Neuropathol. Commun.* **7**, 35.

**Gontan, C., Güttler, T., Engelen, E., Demmers, J., Fornerod, M., Grosveld, F. G., Tibboel, D., Görlich, D., Poot, R. A. and Rottier, R. J.** (2009). Exportin 4 mediates a novel nuclear import pathway for Sox family transcription factors. *J. Cell Biol.* **185**, 27–34.

**Görlich, D. and Kutay, U.** (1999). Transport between the cell nucleus and the cytoplasm. *Annu. Rev. Cell Dev. Biol.* **15**, 607–60.

**Görlich, D., Panté, N., Kutay, U., Aebi, U. and Bischoff, F. R.** (1996). Identification of different roles for RanGDP and RanGTP in nuclear protein import. *EMBO J.* **15**, 5584–94.

**GROSS, A. J. and SIZER, I. W.** (1959). The oxidation of tyramine, tyrosine, and related compounds by peroxidase. *J. Biol. Chem.* **234**, 1611–4.

**Grossman, E., Medalia, O. and Zwerger, M.** (2012). Functional architecture of the nuclear pore complex. *Annu. Rev. Biophys.* **41**, 557–84.

**Grudnik, P., Bange, G. and Sinning, I.** (2009). Protein targeting by the signal recognition particle. *Biol. Chem.* **390**, 775–82.

**Gruenbaum, Y., Margalit, A., Goldman, R. D., Shumaker, D. K. and Wilson, K. L.** (2005). The nuclear lamina comes of age. *Nat. Rev. Mol. Cell Biol.* **6**, 21–31.

**Guna, A., Volkmar, N., Christianson, J. C. and Hegde, R. S.** (2018). The ER membrane protein complex is a transmembrane domain insertase. *Science (80-. ).*

**Han, S., Udeshi, N. D., Deerinck, T. J., Svinkina, T., Ellisman, M. H., Carr, S. a and Ting, A. Y.** (2017). Proximity Biotinylation as a Method for Mapping Proteins Associated with mtDNA in Living Cells. *Cell Chem. Biol.* **24**, 404–414.

**Han, Y., Branon, T. C., Martell, J. D., Boassa, D., Shechner, D., Ellisman, M. H. and Ting, A.** (2019). Directed Evolution of Split APEX2 Peroxidase. *ACS Chem. Biol.* **14**, 619–635.

**Harborth, J., Elbashir, S. M., Bechert, K., Tuschl, T. and Weber, K.** (2001). Identification of essential genes in cultured mammalian cells using small interfering RNAs. *J. Cell Sci.* **114**, 4557–65.

**Hassdenteufel, S., Schäuble, N., Cassella, P., Leznicki, P., Müller, A., High, S., Jung, M. and Zimmermann, R.** (2011). Ca2+-calmodulin inhibits tail-anchored protein insertion into the mammalian endoplasmic reticulum membrane. *FEBS Lett.* **585**, 3485–90.

**Haßdenteufel, S., Sicking, M., Schorr, S., Aviram, N., Fecher-Trost, C., Schuldiner, M., Jung, M., Zimmermann, R. and Lang, S.** (2017). hSnd2 protein represents an alternative targeting factor to the endoplasmic reticulum in human cells. *FEBS Lett.* **591**, 3211–3224.

**Hegde, R. S. and Keenan, R. J.** (2011). Tail-anchored membrane protein insertion into the endoplasmic reticulum. *Nat. Rev. Mol. Cell Biol.* **12**, 787–98.

**Hellemans, J., Preobrazhenska, O., Willaert, A., Debeer, P., Verdonk, P. C. M., Costa, T., Janssens, K., Menten, B., Van Roy, N., Vermeulen, S. J. T., et al.** (2004). Loss-of-function mutations in LEMD3 result in osteopoikilosis, Buschke-Ollendorff syndrome and melorheostosis. *Nat. Genet.* **36**, 1213–8.

**Hieda, M., Tachibana, T., Yokoya, F., Kose, S., Imamoto, N. and Yoneda, Y.** (1999). A monoclonal antibody to the COOH-terminal acidic portion of ran inhibits both the recycling of ran and nuclear protein import in living cells. *J. Cell Biol.* **144**, 645–655.

**Hoffmann, K., Dreger, C. K., Olins, A. L., Olins, D. E., Shultz, L. D., Lucke, B., Karl,**

**H., Kaps, R., Müller, D., Vayá, A., et al.** (2002). Mutations in the gene encoding the lamin B receptor produce an altered nuclear morphology in granulocytes (Pelger-Huët anomaly). *Nat. Genet.* **31**, 410–4.

**Holaska, J. M. and Wilson, K. L.** (2007). An emerin "proteome": purification of distinct emerin-containing complexes from HeLa cells suggests molecular basis for diverse roles including gene regulation, mRNA splicing, signaling, mechanosensing, and nuclear architecture. *Biochemistry* **46**, 8897–908.

**Hülsmann, B. B., Labokha, A. A. and Görlich, D.** (2012). The permeability of reconstituted nuclear pores provides direct evidence for the selective phase model. *Cell* **150**, 738–51.

**Hung, V., Zou, P., Rhee, H.-W., Udeshi, N. D., Cracan, V., Svinkina, T., Carr, S. A., Mootha, V. K. and Ting, A. Y.** (2014). Proteomic mapping of the human mitochondrial intermembrane space in live cells via ratiometric APEX tagging. *Mol. Cell* **55**, 332–41.

**Hung, V., Lam, S. S., Udeshi, N. D., Svinkina, T., Guzman, G., Mootha, V. K., Carr, S. A. and Ting, A. Y.** (2017). Proteomic mapping of cytosol-facing outer mitochondrial and ER membranes in living human cells by proximity biotinylation. *Elife* **6**, 1–39.

**Huttlin, E. L., Ting, L., Bruckner, R. J., Gebreab, F., Gygi, M. P., Szpyt, J., Tam, S., Zarraga, G., Colby, G., Baltier, K., et al.** (2015). The BioPlex Network: A Systematic Exploration of the Human Interactome. *Cell* **162**, 425–440.

**Izaurralde, E., Kutay, U., Von Kobbe, C., Mattaj, L. W. and Görlich, D.** (1997). The asymmetric distribution of the constituents of the Ran system is essential for transport into and out of the nucleus. *EMBO J.* **16**, 6535–6547.

**James, C., Müller, M., Goldberg, M. W., Lenz, C., Urlaub, H., Kehlenbach, R. H. and Ralph, H.** (2019). Proteomic mapping by rapamycin-dependent targeting of APEX2 identifies binding partners of VAPB at the inner nuclear membrane. *J. Biol. Chem.* **294**, 16241–16254.

**Jiang, S., Kotani, N., Ohnishi, T., Miyagawa-Yamguchi, A., Tsuda, M., Yamashita, R., Ishiura, Y. and Honke, K.** (2012). A proteomics approach to the cell-surface interactome using the enzyme-mediated activation of radical sources reaction. *Proteomics* **12**, 54–62.

**Jing, J., He, L., Sun, A., Quintana, A., Ding, Y., Ma, G., Tan, P., Liang, X., Zheng, X., Chen, L., et al.** (2015). Proteomic mapping of ER-PM junctions identifies STIMATE as a regulator of $Ca^{2+}$ influx. *Nat. Cell Biol.* **17**, 1339–47.

**Johnson, B., Leek, A. N., Solé, L., Maverick, E. E., Levine, T. P. and Tamkun, M. M.** (2018). Kv2 potassium channels form endoplasmic reticulum/plasma membrane junctions via interaction with VAPA and VAPB. *Proc. Natl. Acad. Sci. U. S. A.* **115**,

E7331–E7340.

**Kagiwada, S. and Zen, R.** (2003). Role of the yeast VAP homolog, Scs2p, in INO1 expression and phospholipid metabolism. *J. Biochem.* **133**, 515–22.

**Kagiwada, S., Hosaka, K., Murata, M., Nikawa, J. and Takatsuki, A.** (1998). The Saccharomyces cerevisiae SCS2 gene product, a homolog of a synaptobrevin-associated protein, is an integral membrane protein of the endoplasmic reticulum and is required for inositol metabolism. *J. Bacteriol.* **180**, 1700–8.

**Kalverda, B., Pickersgill, H., Shloma, V. V. and Fornerod, M.** (2010). Nucleoporins directly stimulate expression of developmental and cell-cycle genes inside the nucleoplasm. *Cell* **140**, 360–71.

**Kanekura, K., Nishimoto, I., Aiso, S. and Matsuoka, M.** (2006). Characterization of amyotrophic lateral sclerosis-linked P56S mutation of vesicle-associated membrane protein-associated protein B (VAPB/ALS8). *J. Biol. Chem.* **281**, 30223–33.

**Kanekura, K., Suzuki, H., Aiso, S. and Matsuoka, M.** (2009). ER stress and unfolded protein response in amyotrophic lateral sclerosis. *Mol. Neurobiol.* **39**, 81–9.

**Katta, S. S., Smoyer, C. J. and Jaspersen, S. L.** (2014). Destination: inner nuclear membrane. *Trends Cell Biol.* **24**, 221–9.

**Kawano, M., Kumagai, K., Nishijima, M. and Hanada, K.** (2006). Efficient trafficking of ceramide from the endoplasmic reticulum to the Golgi apparatus requires a VAMP-associated protein-interacting FFAT motif of CERT. *J. Biol. Chem.* **281**, 30279–88.

**Kehlenbach, R. H. and Gerace, L.** (2002). *Analysis of nuclear protein import and export in vitro using fluorescent cargoes.*

**Kehlenbach, R. H., Dickmanns, A. and Gerace, L.** (1998). Nucleocytoplasmic shuttling factors including Ran and CRM1 mediate nuclear export of NFAT In vitro. *J. Cell Biol.* **141**, 863–74.

**Kehlenbach, R. H., Dickmanns, A., Kehlenbach, A., Guan, T. and Gerace, L.** (1999). A role for RanBP1 in the release of CRM1 from the nuclear pore complex in a terminal step of nuclear export. *J. Cell Biol.* **145**, 645–57.

**Kim, D. I. and Roux, K. J.** (2016). Filling the Void: Proximity-Based Labeling of Proteins in Living Cells. *Trends Cell Biol.* **26**, 804–817.

**Kim, S., Leal, S. S., Ben Halevy, D., Gomes, C. M. and Lev, S.** (2010). Structural requirements for VAP-B oligomerization and their implication in amyotrophic lateral sclerosis-associated VAP-B(P56S) neurotoxicity. *J. Biol. Chem.* **285**, 13839–49.

**Kim, D. I., Birendra, K. C., Zhu, W., Motamedchaboki, K., Doye, V. and Roux, K. J.** (2014). Probing nuclear pore complex architecture with proximity-dependent biotinylation. *Proc. Natl. Acad. Sci. U. S. A.* **111**, E2453-61.

**Kim, D. I., Jensen, S. C., Noble, K. A., Kc, B., Roux, K. H., Motamedchaboki, K. and**

**Roux, K. J.** (2016). An improved smaller biotin ligase for BioID proximity labeling. *Mol. Biol. Cell* **27**, 1188–96.

**Kim, S. J., Fernandez-Martinez, J., Nudelman, I., Shi, Y., Zhang, W., Raveh, B., Herricks, T., Slaughter, B. D., Hogan, J. A., Upla, P., et al.** (2018). Integrative structure and functional anatomy of a nuclear pore complex. *Nature* **555**, 475–482.

**King, M. C., Lusk, C. P. and Blobel, G.** (2006). Karyopherin-mediated import of integral inner nuclear membrane proteins. *Nature* **442**, 1003–7.

**Kirmiz, M., Vierra, N. C., Palacio, S. and Trimmer, J. S.** (2018). Identification of VAPA and VAPB as Kv2 Channel-Interacting Proteins Defining Endoplasmic Reticulum-Plasma Membrane Junctions in Mammalian Brain Neurons. *J. Neurosci.* **38**, 7562–7584.

**Klebe, C., Wittinghofer, A., Bischoff, F. R., Ponstingl, H. and Wittinghofer, A.** (1995). Interaction of the Nuclear GTP-Binding Protein Ran with Its Regulatory Proteins RCC1 and RanGAP1. *Biochemistry* **34**, 639–47.

**Knockenhauer, K. E. and Schwartz, T. U.** (2016). The Nuclear Pore Complex as a Flexible and Dynamic Gate. *Cell* **164**, 1162–1171.

**Korfali, N., Wilkie, G. S., Swanson, S. K., Srsen, V., Batrakou, D. G., Fairley, E. A. L., Malik, P., Zuleger, N., Goncharevich, A., de Las Heras, J., et al.** (2010). The leukocyte nuclear envelope proteome varies with cell activation and contains novel transmembrane proteins that affect genome architecture. *Mol. Cell. Proteomics* **9**, 2571–85.

**Korfali, N., Wilkie, G. S., Swanson, S. K., Srsen, V., de Las Heras, J., Batrakou, D. G., Malik, P., Zuleger, N., Kerr, A. R. W., Florens, L., et al.** (2012). The nuclear envelope proteome differs notably between tissues. *Nucleus* **3**, 552–64.

**Kuijpers, M., Yu, K. Lou, Teuling, E., Akhmanova, A., Jaarsma, D. and Hoogenraad, C. C.** (2013). The ALS8 protein VAPB interacts with the ER-Golgi recycling protein YIF1A and regulates membrane delivery into dendrites. *EMBO J.* **32**, 2056–72.

**Kutay, U., Hartmann, E. and Rapoport, T. A.** (1993). A class of membrane proteins with a C-terminal anchor. *Trends Cell Biol.* **3**, 72–5.

**Kutay, U., Ahnert-Hilger, G., Hartmann, E., Wiedenmann, B. and Rapoport, T. A.** (1995). Transport route for synaptobrevin via a novel pathway of insertion into the endoplasmic reticulum membrane. *EMBO J.* **14**, 217–23.

**Kutay, U., Izaurralde, E., Bischoff, F. R., Mattaj, I. W. and Görlich, D.** (1997a). Dominant-negative mutants of importin-β block multiple pathways of import and export through the nuclear pore complex. *EMBO J.*

**Kutay, U., Bischoff, F. R., Kostka, S., Kraft, R. and Görlich, D.** (1997b). Export of importin alpha from the nucleus is mediated by a specific nuclear transport factor.

*Cell* **90**, 1061–71.

**Kutay, U., Lipowsky, G., Izaurralde, E., Bischoff, F. R., Schwarzmaier, P., Hartmann, E. and Görlich, D.** (1998). Identification of a tRNA-specific nuclear export receptor. *Mol. Cell* **1**, 359–69.

**Kyte, J. and Doolittle, R. F.** (1982). A simple method for displaying the hydropathic character of a protein. *J. Mol. Biol.* **157**, 105–32.

**Laba, J. K., Steen, A. and Veenhoff, L. M.** (2014). Traffic to the inner membrane of the nuclear envelope. *Curr. Opin. Cell Biol.* **28**, 36–45.

**Laemmli, U. K.** (1970). Cleavage of structural proteins during the assembly of the head of bacteriophage T4. *Nature* **227**, 680–5.

**Lam, S. S., Martell, J. D., Kamer, K. J., Deerinck, T. J., Ellisman, M. H., Mootha, V. K. and Ting, A. Y.** (2015). Directed evolution of APEX2 for electron microscopy and proximity labeling. *Nat. Methods* **12**, 51–4.

**Lattanzi, G., Ognibene, A., Sabatelli, P., Capanni, C., Toniolo, D., Columbaro, M., Santi, S., Riccio, M., Merlini, L., Maraldi, N. M., et al.** (2000). Emerin expression at the early stages of myogenic differentiation. *Differentiation.* **66**, 208–17.

**Lee, K. K., Haraguchi, T., Lee, R. S., Koujin, T., Hiraoka, Y. and Wilson, K. L.** (2001). Distinct functional domains in emerin bind lamin A and DNA-bridging protein BAF. *J. Cell Sci.* **114**, 4567–73.

**Lee, S.-Y., Kang, M.-G., Park, J.-S., Lee, G., Ting, A. Y. and Rhee, H.-W.** (2016). APEX Fingerprinting Reveals the Subcellular Localization of Proteins of Interest. *Cell Rep.* **15**, 1837–47.

**Lev, S., Ben Halevy, D., Peretti, D. and Dahan, N.** (2008). The VAP protein family: from cellular functions to motor neuron disease. *Trends Cell Biol.* **18**, 282–90.

**Leznicki, P., Clancy, A., Schwappach, B. and High, S.** (2010). Bat3 promotes the membrane integration of tail-anchored proteins. *J. Cell Sci.* **123**, 2170–8.

**Leznicki, P., Roebuck, Q. P., Wunderley, L., Clancy, A., Krysztofinska, E. M., Isaacson, R. L., Warwicker, J., Schwappach, B. and High, S.** (2013). The association of BAG6 with SGTA and tail-anchored proteins. *PLoS One* **8**, e59590.

**Li, X.-W., Rees, J. S., Xue, P., Zhang, H., Hamaia, S. W., Sanderson, B., Funk, P. E., Farndale, R. W., Lilley, K. S., Perrett, S., et al.** (2014). New insights into the DT40 B cell receptor cluster using a proteomic proximity labeling assay. *J. Biol. Chem.* **289**, 14434–47.

**Linstedt, A. D., Foguet, M., Renz, M., Seelig, H. P., Glick, B. S. and Hauri, H. P.** (1995). A C-terminally-anchored Golgi protein is inserted into the endoplasmic reticulum and then transported to the Golgi apparatus. *Proc. Natl. Acad. Sci. U. S. A.* **92**, 5102–5.

**Lippincott-Schwartz, J., Snapp, E. and Kenworthy, A.** (2001). Studying protein dynamics in living cells. *Nat. Rev. Mol. Cell Biol.* **2**, 444–56.

**Liu, D., Wu, X., Summers, M. D., Lee, A., Ryan, K. J. and Braunagel, S. C.** (2010). Truncated isoforms of Kap60 facilitate trafficking of Heh2 to the nuclear envelope. *Traffic* **11**, 1506–18.

**Lobingier, B. T., Hüttenhain, R., Eichel, K., Miller, K. B., Ting, A. Y., von Zastrow, M. and Krogan, N. J.** (2017). An Approach to Spatiotemporally Resolve Protein Interaction Networks in Living Cells. *Cell* **169**, 350-360.e12.

**Loewen, C. J. R. and Levine, T. P.** (2005). A highly conserved binding site in vesicle-associated membrane protein-associated protein (VAP) for the FFAT motif of lipid-binding proteins. *J. Biol. Chem.* **280**, 14097–14104.

**Loewen, C. J. R., Roy, A. and Levine, T. P.** (2003). A conserved ER targeting motif in three families of lipid binding proteins and in Opi1p binds VAP. *EMBO J.* **22**, 2025–35.

**Loewen, C. J. R., Gaspar, M. L., Jesch, S. A., Delon, C., Ktistakis, N. T., Henry, S. A. and Levine, T. P.** (2004). Phospholipid metabolism regulated by a transcription factor sensing phosphatidic acid. *Science* **304**, 1644–7.

**Lusk, C. P., Blobel, G. and King, M. C.** (2007). Highway to the inner nuclear membrane: rules for the road. *Nat. Rev. Mol. Cell Biol.* **8**, 414–20.

**Maimon, T., Elad, N., Dahan, I. and Medalia, O.** (2012). The human nuclear pore complex as revealed by cryo-electron tomography. *Structure* **20**, 998–1006.

**Mariappan, M., Li, X., Stefanovic, S., Sharma, A., Mateja, A., Keenan, R. J. and Hegde, R. S.** (2010). A ribosome-associating factor chaperones tail-anchored membrane proteins. *Nature* **466**, 1120–4.

**Martell, J. D., Deerinck, T. J., Sancak, Y., Poulos, T. L., Mootha, V. K., Sosinsky, G. E., Ellisman, M. H. and Ting, A. Y.** (2012). Engineered ascorbate peroxidase as a genetically encoded reporter for electron microscopy. *Nat. Biotechnol.* **30**, 1143–8.

**Martell, J. D., Deerinck, T. J., Lam, S. S., Ellisman, M. H. and Ting, A. Y.** (2017). Electron microscopy using the genetically encoded APEX2 tag in cultured mammalian cells. *Nat. Protoc.* **12**, 1792–1816.

**Mateja, A. and Keenan, R. J.** (2018). A structural perspective on tail-anchored protein biogenesis by the GET pathway. *Curr. Opin. Struct. Biol.* **51**, 195–202.

**Mattout-Drubezki, A. and Gruenbaum, Y.** (2003). Dynamic interactions of nuclear lamina proteins with chromatin and transcriptional machinery. *Cell. Mol. Life Sci.* **60**, 2053–63.

**Meinema, A. C., Laba, J. K., Hapsari, R. A., Otten, R., Mulder, F. A. A., Kralt, A., van den Bogaart, G., Lusk, C. P., Poolman, B. and Veenhoff, L. M.** (2011). Long

unfolded linkers facilitate membrane protein import through the nuclear pore complex. *Science* **333**, 90–3.

**Mekhail, K. and Moazed, D.** (2010). The nuclear envelope in genome organization, expression and stability. *Nat. Rev. Mol. Cell Biol.* **11**, 317–28.

**Melchior, F., Paschal, B., Evans, J. and Gerace, L.** (1993). Inhibition of nuclear protein import by nonhydrolyzable analogues of GTP and identification of the small GTPase Ran/TC4 as an essential transport factor. *J. Cell Biol.* **123**, 1649–59.

**Melchior, F., Sweet, D. J. and Gerace, L.** (1995). Analysis of Ran/TC4 function in nuclear protein import. *Methods Enzymol.* **257**, 279–91.

**Méndez-López, I. and Worman, H. J.** (2012). Inner nuclear membrane proteins: impact on human disease. *Chromosoma* **121**, 153–67.

**Mesmin, B., Antonny, B. and Drin, G.** (2013). Insights into the mechanisms of sterol transport between organelles. *Cell. Mol. Life Sci.* **70**, 3405–21.

**Mick, D. U., Rodrigues, R. B., Leib, R. D., Adams, C. M., Chien, A. S., Gygi, S. P. and Nachury, M. V.** (2015). Proteomics of Primary Cilia by Proximity Labeling. *Dev. Cell* **35**, 497–512.

**Mingot, J. M., Kostka, S., Kraft, R., Hartmann, E. and Görlich, D.** (2001). Importin 13: a novel mediator of nuclear import and export. *EMBO J.* **20**, 3685–94.

**Mock, J.-Y., Chartron, J. W., Zaslaver, M., Xu, Y., Ye, Y. and Clemons, W. M.** (2015). Bag6 complex contains a minimal tail-anchor-targeting module and a mock BAG domain. *Proc. Natl. Acad. Sci. U. S. A.* **112**, 106–11.

**Mock, J.-Y., Xu, Y., Ye, Y. and Clemons, W. M.** (2017). Structural basis for regulation of the nucleo-cytoplasmic distribution of Bag6 by TRC35. *Proc. Natl. Acad. Sci. U. S. A.* **114**, 11679–11684.

**Mohr, D., Frey, S., Fischer, T., Güttler, T. and Görlich, D.** (2009). Characterisation of the passive permeability barrier of nuclear pore complexes. *EMBO J.* **28**, 2541–53.

**Moore, M. S. and Blobel, G.** (1992). The two steps of nuclear import, targeting to the nuclear envelope and translocation through the nuclear pore, require different cytosolic factors. *Cell* **69**, 939–50.

**Mórotz, G. M., De Vos, K. J., Vagnoni, A., Ackerley, S., Shaw, C. E. and Miller, C. C. J.** (2012). Amyotrophic lateral sclerosis-associated mutant VAPBP56s perturbs calcium homeostasis to disrupt axonal transport of mitochondria. *Hum. Mol. Genet.* **21**, 1979–1988.

**Moser, B., Basílio, J., Gotzmann, J., Brachner, A. and Foisner, R.** (2020). Comparative Interactome Analysis of Emerin, MAN1 and LEM2 Reveals a Unique Role for LEM2 in Nucleotide Excision Repair. *Cells* **9**,.

**Moustaqim-Barrette, A., Lin, Y. Q., Pradhan, S., Neely, G. G., Bellen, H. J. and Tsuda,**

**H.** (2014). The amyotrophic lateral sclerosis 8 protein, VAP, is required for ER protein quality control. *Hum. Mol. Genet.* **23**, 1975–89.

**Müller, M., James, C., Lenz, C., Urlaub, H. and Kehlenbach, R. H.** (2020). Probing the Environment of Emerin by Enhanced Ascorbate Peroxidase 2 (APEX2)-Mediated Proximity Labeling. *Cells* **9**, 1–18.

**Murphy, S. E. and Levine, T. P.** (2016). VAP, a Versatile Access Point for the Endoplasmic Reticulum: Review and analysis of FFAT-like motifs in the VAPome. *Biochim. Biophys. Acta* **1861**, 952–961.

**Nachreiner, T., Esser, M., Tenten, V., Troost, D., Weis, J. and Krüttgen, A.** (2010). Novel splice variants of the amyotrophic lateral sclerosis-associated gene VAPB expressed in human tissues. *Biochem. Biophys. Res. Commun.* **394**, 703–8.

**Nakano, H., Funasaka, T., Hashizume, C. and Wong, R. W.** (2010). Nucleoporin translocated promoter region (Tpr) associates with dynein complex, preventing chromosome lagging formation during mitosis. *J. Biol. Chem.* **285**, 10841–9.

**Nili, E., Cojocaru, G. S., Kalma, Y., Ginsberg, D., Copeland, N. G., Gilbert, D. J., Jenkins, N. A., Berger, R., Shaklai, S., Amariglio, N., et al.** (2001). Nuclear membrane protein LAP2beta mediates transcriptional repression alone and together with its binding partner GCL (germ-cell-less). *J. Cell Sci.* **114**, 3297–307.

**Nishimura, Y., Hayashi, M., Inada, H. and Tanaka, T.** (1999). Molecular cloning and characterization of mammalian homologues of vesicle-associated membrane protein-associated (VAMP-associated) proteins. *Biochem. Biophys. Res. Commun.* **254**, 21–6.

**Nishimura, A. L., Mitne-Neto, M., Silva, H. C. A., Richieri-Costa, A., Middleton, S., Cascio, D., Kok, F., Oliveira, J. R. M., Gillingwater, T., Webb, J., et al.** (2004). A mutation in the vesicle-trafficking protein VAPB causes late-onset spinal muscular atrophy and amyotrophic lateral sclerosis. *Am. J. Hum. Genet.* **75**, 822–31.

**Ohba, T., Schirmer, E. C., Nishimoto, T. and Gerace, L.** (2004). Energy- and temperature-dependent transport of integral proteins to the inner nuclear membrane via the nuclear pore. *J. Cell Biol.* **167**, 1051–62.

**Ong, S.-E., Blagoev, B., Kratchmarova, I., Kristensen, D. B., Steen, H., Pandey, A. and Mann, M.** (2002). Stable isotope labeling by amino acids in cell culture, SILAC, as a simple and accurate approach to expression proteomics. *Mol. Cell. Proteomics* **1**, 376–86.

**Ostlund, C. and Worman, H. J.** (2003). Nuclear envelope proteins and neuromuscular diseases. *Muscle Nerve* **27**, 393–406.

**Ostlund, C., Ellenberg, J., Hallberg, E., Lippincott-Schwartz, J. and Worman, H. J.** (1999). Intracellular trafficking of emerin, the Emery-Dreifuss muscular dystrophy

protein. *J. Cell Sci.* **112 ( Pt 1**, 1709–19.

**Ostlund, C., Sullivan, T., Stewart, C. L. and Worman, H. J.** (2006). Dependence of diffusional mobility of integral inner nuclear membrane proteins on A-type lamins. *Biochemistry* **45**, 1374–82.

**Ott, C. M. and Lingappa, V. R.** (2002). Integral membrane protein biosynthesis: why topology is hard to predict. *J. Cell Sci.* **115**, 2003–9.

**Paek, J., Kalocsay, M., Staus, D. P., Wingler, L., Pascolutti, R., Paulo, J. A., Gygi, S. P. and Kruse, A. C.** (2017). Multidimensional Tracking of GPCR Signaling via Peroxidase-Catalyzed Proximity Labeling. *Cell* **169**, 338-349.e11.

**Paschal, B. M. and Gerace, L.** (1995). Identification of NTF2, a cytosolic factor for nuclear import that interacts with nuclear pore complex protein p62. *J. Cell Biol.* **129**, 925–37.

**Pawar, S., Ungricht, R., Tiefenboeck, P., Leroux, J.-C. and Kutay, U.** (2017). Efficient protein targeting to the inner nuclear membrane requires Atlastin-dependent maintenance of ER topology. *Elife* **6**,.

**Pedrazzini, E., Villa, A., Longhi, R., Bulbarelli, A. and Borgese, N.** (2000). Mechanism of residence of cytochrome b(5), a tail-anchored protein, in the endoplasmic reticulum. *J. Cell Biol.* **148**, 899–914.

**Pennetta, G., Hiesinger, P. R., Fabian-Fine, R., Meinertzhagen, I. A. and Bellen, H. J.** (2002). Drosophila VAP-33A directs bouton formation at neuromuscular junctions in a dosage-dependent manner. *Neuron* **35**, 291–306.

**Peretti, D., Dahan, N., Shimoni, E., Hirschberg, K. and Lev, S.** (2008). Coordinated lipid transfer between the endoplasmic reticulum and the Golgi complex requires the VAP proteins and is essential for Golgi-mediated transport. *Mol. Biol. Cell* **19**, 3871–84.

**Pfaff, J., Rivera Monroy, J., Jamieson, C., Rajanala, K., Vilardi, F., Schwappach, B. and Kehlenbach, R. H.** (2016). Emery-Dreifuss muscular dystrophy mutations impair TRC40-mediated targeting of emerin to the inner nuclear membrane. *J. Cell Sci.* **129**, 502–16.

**Powell, L. and Burke, B.** (1990). Internuclear exchange of an inner nuclear membrane protein (p55) in heterokaryons: in vivo evidence for the interaction of p55 with the nuclear lamina. *J. Cell Biol.* **111**, 2225–34.

**Rabu, C., Wipf, P., Brodsky, J. L. and High, S.** (2008). A precursor-specific role for Hsp40/Hsc70 during tail-anchored protein integration at the endoplasmic reticulum. *J. Biol. Chem.*

**Ramanathan, M., Majzoub, K., Rao, D. S., Neela, P. H., Zarnegar, B. J., Mondal, S., Roth, J. G., Gai, H., Kovalski, J. R., Siprashvili, Z., et al.** (2018). RNA-protein

interaction detection in living cells. *Nat. Methods* **15**, 207–212.

**Rapoport, T. A.** (2007). Protein translocation across the eukaryotic endoplasmic reticulum and bacterial plasma membranes. *Nature* **450**, 663–9.

**Rasala, B. A., Orjalo, A. V., Shen, Z., Briggs, S. and Forbes, D. J.** (2006). ELYS is a dual nucleoporin/kinetochore protein required for nuclear pore assembly and proper cell division. *Proc. Natl. Acad. Sci.* **103**, 17801–17806.

**Reid, D. W. and Nicchitta, C. V.** (2015). Diversity and selectivity in mRNA translation on the endoplasmic reticulum. *Nat. Rev. Mol. Cell Biol.* **16**, 221–31.

**Rexach, M. and Blobel, G.** (1995). Protein import into nuclei: association and dissociation reactions involving transport substrate, transport factors, and nucleoporins. *Cell* **83**, 683–692.

**Rhee, H.-W., Zou, P., Udeshi, N. D., Martell, J. D., Mootha, V. K., Carr, S. A. and Ting, A. Y.** (2013a). Proteomic mapping of mitochondria in living cells via spatially restricted enzymatic tagging. *Science* **339**, 1328–1331.

**Rhee, H.-W., Zou, P., Udeshi, N. D., Martell, J. D., Mootha, V. K., Carr, S. A. and Ting, A. Y.** (2013b). Proteomic mapping of mitochondria in living cells via spatially restricted enzymatic tagging. *Science* **339**, 1328–1331.

**Ribbeck, K. and Görlich, D.** (2002a). The permeability barrier of nuclear pore complexes appears to operate via hydrophobic exclusion. *EMBO J.* **21**, 2664–71.

**Ribbeck, K. and Görlich, D.** (2002b). The permeability barrier of nuclear pore complexes appears to operate via hydrophobic exclusion. *EMBO J.* **21**, 2664–71.

**Ribbeck, K., Lipowsky, G., Kent, H. M., Stewart, M. and Görlich, D.** (1998). NTF2 mediates nuclear import of Ran. *EMBO J.* **17**, 6587–98.

**Rocha, N., Kuijl, C., van der Kant, R., Janssen, L., Houben, D., Janssen, H., Zwart, W. and Neefjes, J.** (2009). Cholesterol sensor ORP1L contacts the ER protein VAP to control Rab7-RILP-p150 Glued and late endosome positioning. *J. Cell Biol.* **185**, 1209–25.

**Romanauska, A. and Köhler, A.** (2018). The Inner Nuclear Membrane Is a Metabolically Active Territory that Generates Nuclear Lipid Droplets. *Cell* **174**, 700-715.e18.

**Rothballer, A. and Kutay, U.** (2013). The diverse functional LINCs of the nuclear envelope to the cytoskeleton and chromatin. *Chromosoma* **122**, 415–29.

**Roux, K. J., Kim, D. I., Raida, M. and Burke, B.** (2012). A promiscuous biotin ligase fusion protein identifies proximal and interacting proteins in mammalian cells. *J. Cell Biol.* **196**, 801–10.

**Roux, K. J., Kim, D. I. and Burke, B.** (2013). BioID: a screen for protein-protein interactions. *Curr. Protoc. protein Sci.* **74**, 19.23.1-19.23.14.

**Saiz-Ros, N., Czapiewski, R., Epifano, I., Stevenson, A., Swanson, S., Dixon, C.,**

**Zamora, D., McElwee, M., Vijayakrishnan, S., Richardson, C., et al.** (2019). Host Vesicle Fusion Protein VAPB Contributes to the Nuclear Egress Stage of Herpes Simplex Virus Type-1 (HSV-1) Replication. *Cells* **8**, 120.

**Saksena, S., Shao, Y., Braunagel, S. C., Summers, M. D. and Johnson, A. E.** (2004). Cotranslational integration and initial sorting at the endoplasmic reticulum translocon of proteins destined for the inner nuclear membrane. *Proc. Natl. Acad. Sci. U. S. A.* **101**, 12537–42.

**Saksena, S., Summers, M. D., Burks, J. K., Johnson, A. E. and Braunagel, S. C.** (2006). Importin-alpha-16 is a translocon-associated protein involved in sorting membrane proteins to the nuclear envelope. *Nat. Struct. Mol. Biol.* **13**, 500–8.

**Salpingidou, G., Smertenko, A., Hausmanowa-Petrucewicz, I., Hussey, P. J. and Hutchison, C. J.** (2007). A novel role for the nuclear membrane protein emerin in association of the centrosome to the outer nuclear membrane. *J. Cell Biol.* **178**, 897–904.

**Sarbassov, D. D., Ali, S. M., Sengupta, S., Sheen, J.-H., Hsu, P. P., Bagley, A. F., Markhard, A. L. and Sabatini, D. M.** (2006). Prolonged rapamycin treatment inhibits mTORC2 assembly and Akt/PKB. *Mol. Cell* **22**, 159–68.

**Schirmer, E. C. and Gerace, L.** (2005). The nuclear membrane proteome: extending the envelope. *Trends Biochem. Sci.* **30**, 551–8.

**Schirmer, E. C., Florens, L., Guan, T., Yates, J. R. and Gerace, L.** (2003). Nuclear membrane proteins with potential disease links found by subtractive proteomics. *Science* **301**, 1380–2.

**Schirmer, E. C., Florens, L., Guan, T., Yates, J. R. and Gerace, L.** (2005). Identification of novel integral membrane proteins of the nuclear envelope with potential disease links using subtractive proteomics. *Novartis Found. Symp.* **264**, 63–76; discussion 76-80, 227–30.

**Schmidt, H. B. and Görlich, D.** (2016). Transport Selectivity of Nuclear Pores, Phase Separation, and Membraneless Organelles. *Trends Biochem. Sci.* **41**, 46–61.

**Schopp, I. M., Amaya Ramirez, C. C., Debeljak, J., Kreibich, E., Skribbe, M., Wild, K. and Béthune, J.** (2017). Split-BioID a conditional proteomics approach to monitor the composition of spatiotemporally defined protein complexes. *Nat. Commun.* **8**, 15690.

**Schreiber, K. H. and Kennedy, B. K.** (2013). When lamins go bad: nuclear structure and disease. *Cell* **152**, 1365–75.

**Schreiber, K. H., Ortiz, D., Academia, E. C., Anies, A. C., Liao, C.-Y. Y. and Kennedy, B. K.** (2015). Rapamycin-mediated mTORC2 inhibition is determined by the relative expression of FK506-binding proteins. *Aging Cell* **14**, 265–73.

**Schuldiner, M., Metz, J., Schmid, V., Denic, V., Rakwalska, M., Schmitt, H. D., Schwappach, B. and Weissman, J. S.** (2008). The GET complex mediates insertion of tail-anchored proteins into the ER membrane. *Cell* **134**, 634–45.

**Shao, S. and Hegde, R. S.** (2011). A calmodulin-dependent translocation pathway for small secretory proteins. *Cell* **147**, 1576–88.

**Shi, J., Lua, S., Tong, J. S. and Song, J.** (2010). Elimination of the native structure and solubility of the hVAPB MSP domain by the Pro56Ser mutation that causes amyotrophic lateral sclerosis. *Biochemistry* **49**, 3887–97.

**Shimi, T., Koujin, T., Segura-Totten, M., Wilson, K. L., Haraguchi, T. and Hiraoka, Y.** (2004). Dynamic interaction between BAF and emerin revealed by FRAP, FLIP, and FRET analyses in living HeLa cells. *J. Struct. Biol.* **147**, 31–41.

**Shimojima, M., Yuasa, S., Motoda, C., Yozu, G., Nagai, T., Ito, S., Lachmann, M., Kashimura, S., Takei, M., Kusumoto, D., et al.** (2017). Emerin plays a crucial role in nuclear invagination and in the nuclear calcium transient. *Sci. Rep.* **7**, 1–16.

**Shumaker, D. K., Lee, K. K., Tanhehco, Y. C., Craigie, R. and Wilson, K. L.** (2001). LAP2 binds to BAF.DNA complexes: requirement for the LEM domain and modulation by variable regions. *EMBO J.* **20**, 1754–64.

**Shurtleff, M. J., Itzhak, D. N., Hussmann, J. A., Schirle Oakdale, N. T., Costa, E. A., Jonikas, M., Weibezahn, J., Popova, K. D., Jan, C. H., Sinitcyn, P., et al.** (2018). The ER membrane protein complex interacts cotranslationally to enable biogenesis of multipass membrane proteins. *Elife* **7**, 1–23.

**Silbernagel, N., Walecki, M., Schäfer, M. K. H., Kessler, M., Zobeiri, M., Rinné, S., Kiper, A. K., Komadowski, M. A., Vowinkel, K. S., Wemhöner, K., et al.** (2018). The VAMP-associated protein VAPB is required for cardiac and neuronal pacemaker channel function. *FASEB J.* **32**, 6159–6173.

**Simon, D. N. and Wilson, K. L.** (2011). The nucleoskeleton as a genome-associated dynamic “network of networks”. *Nat. Rev. Mol. Cell Biol.* **12**, 695–708.

**Skehel, P. A., Martin, K. C., Kandel, E. R. and Bartsch, D.** (1995). A VAMP-binding protein from Aplysia required for neurotransmitter release. *Science (80-. ).* **269**, 1580–1583.

**Skehel, P. A., Fabian-Fine, R. and Kandel, E. R.** (2000). Mouse VAP33 is associated with the endoplasmic reticulum and microtubules. *Proc. Natl. Acad. Sci. U. S. A.* **97**, 1101–6.

**Slee, J. A. and Levine, T. P.** (2019). Systematic prediction of FFAT motifs across eukaryote proteomes identifies nucleolar and eisosome proteins with the predicted capacity to form bridges to the endoplasmic reticulum. *Contact (Thousand Oaks (Ventura County, Calif.))* **2**, 1–21.

**Smith, B. J.** (1994). SDS polyacrylamide gel electrophoresis of proteins. *Methods Mol. Biol.* **32**, 23–34.

**Smith, S. and Blobel, G.** (1993). The first membrane spanning region of the lamin B receptor is sufficient for sorting to the inner nuclear membrane. *J. Cell Biol.* **120**, 631–7.

**Snider, J., Hanif, A., Lee, M. E., Jin, K., Yu, A. R., Graham, C., Chuk, M., Damjanovic, D., Wierzbicka, M., Tang, P., et al.** (2013). Mapping the functional yeast ABC transporter interactome. *Nat. Chem. Biol.* **9**, 565–72.

**Song, J.** (2013). Why do proteins aggregate? “Intrinsically insoluble proteins” and “dark mediators” revealed by studies on “insoluble proteins” solubilized in pure water. *F1000Research* **2**, 94.

**Soullam, B. and Worman, H. J.** (1993). The amino-terminal domain of the lamin B receptor is a nuclear envelope targeting signal. *J. Cell Biol.* **120**, 1093–100.

**Soullam, B. and Worman, H. J.** (1995). Signals and structural features involved in integral membrane protein targeting to the inner nuclear membrane. *J. Cell Biol.* **130**, 15–27.

**Soussan, L., Burakov, D., Daniels, M. P., Toister-Achituv, M., Porat, A., Yarden, Y. and Elazar, Z.** (1999). ERG30, a VAP-33-related protein, functions in protein transport mediated by COPI vesicles. *J. Cell Biol.* **146**, 301–311.

**Starr, D. A. and Fridolfsson, H. N.** (2010). Interactions between nuclei and the cytoskeleton are mediated by SUN-KASH nuclear-envelope bridges. *Annu. Rev. Cell Dev. Biol.* **26**, 421–44.

**Stefanovic, S. and Hegde, R. S.** (2007). Identification of a targeting factor for posttranslational membrane protein insertion into the ER. *Cell* **128**, 1147–59.

**Stewart, C. L., Roux, K. J. and Burke, B.** (2007). Blurring the boundary: The nuclear envelope extends its reach. *Science (80-. ).* **318**, 1408–1412.

**Stoica, R., De Vos, K. J., Paillusson, S., Mueller, S., Sancho, R. M., Lau, K.-F., Vizcay-Barrena, G., Lin, W.-L., Xu, Y.-F., Lewis, J., et al.** (2014). ER-mitochondria associations are regulated by the VAPB-PTPIP51 interaction and are disrupted by ALS/FTD-associated TDP-43. *Nat. Commun.* **5**, 3996.

**Strambio-de-Castillia, C., Blobel, G. and Rout, M. P.** (1995). Isolation and characterization of nuclear envelopes from the yeast Saccharomyces. *J. Cell Biol.* **131**, 19–31.

**Sullivan, T., Escalante-Alcalde, D., Bhatt, H., Anver, M., Bhat, N., Nagashima, K., Stewart, C. L. and Burke, B.** (1999). Loss of A-type lamin expression compromises nuclear envelope integrity leading to muscular dystrophy. *J. Cell Biol.* **147**, 913–20.

**Suzuki, H., Kanekura, K., Levine, T. P., Kohno, K., Olkkonen, V. M., Aiso, S. and**

**Matsuoka, M.** (2009). ALS-linked P56S-VAPB, an aggregated loss-of-function mutant of VAPB, predisposes motor neurons to ER stress-related death by inducing aggregation of co-expressed wild-type VAPB. *J. Neurochem.* **108**, 973–985.

**Towbin, B. D., Meister, P. and Gasser, S. M.** (2009). The nuclear envelope--a scaffold for silencing? *Curr. Opin. Genet. Dev.* **19**, 180–6.

**Tran, D., Chalhoub, A., Schooley, A., Zhang, W. and Ngsee, J. K.** (2012). A mutation in VAPB that causes amyotrophic lateral sclerosis also causes a nuclear envelope defect. *J. Cell Sci.* **125**, 2831–6.

**Tsai, P.-L., Zhao, C., Turner, E. and Schlieker, C.** (2016). The Lamin B receptor is essential for cholesterol synthesis and perturbed by disease-causing mutations. *Elife* **5**, 1–26.

**Tsuchiya, Y., Hase, A., Ogawa, M., Yorifuji, H. and Arahata, K.** (1999). Distinct regions specify the nuclear membrane targeting of emerin, the responsible protein for Emery-Dreifuss muscular dystrophy. *Eur. J. Biochem.* **259**, 859–65.

**Tsuda, H., Han, S. M., Yang, Y., Tong, C., Lin, Y. Q., Mohan, K., Haueter, C., Zoghbi, A., Harati, Y., Kwan, J., et al.** (2008). The amyotrophic lateral sclerosis 8 protein VAPB is cleaved, secreted, and acts as a ligand for Eph receptors. *Cell* **133**, 963–77.

**Turgay, Y., Ungricht, R., Rothballer, A., Kiss, A., Csucs, G., Horvath, P. and Kutay, U.** (2010). A classical NLS and the SUN domain contribute to the targeting of SUN2 to the inner nuclear membrane. *EMBO J.* **29**, 2262–75.

**Tyanova, S., Temu, T., Sinitcyn, P., Carlson, A., Hein, M. Y., Geiger, T., Mann, M. and Cox, J.** (2016). The Perseus computational platform for comprehensive analysis of (prote)omics data. *Nat. Methods* **13**, 731–40.

**Ungricht, R., Klann, M., Horvath, P. and Kutay, U.** (2015). Diffusion and retention are major determinants of protein targeting to the inner nuclear membrane. *J. Cell Biol.*

**Venditti, R., Rega, L. R., Masone, M. C., Santoro, M., Polishchuk, E., Sarnataro, D., Paladino, S., D'Auria, S., Varriale, A., Olkkonen, V. M., et al.** (2019). Molecular determinants of ER-Golgi contacts identified through a new FRET-FLIM system. *J. Cell Biol.* **218**, 1055–1065.

**Vijayaraghavan, B., Figueroa, R. A., Bergqvist, C., Gupta, A. J., Sousa, P. and Hallberg, E.** (2018). RanGTPase regulates the interaction between the inner nuclear membrane proteins, Samp1 and Emerin. *Biochim. Biophys. acta. Biomembr.* **1860**, 1326–1334.

**Vilardi, F., Lorenz, H. and Dobberstein, B.** (2011). WRB is the receptor for TRC40/Asna1-mediated insertion of tail-anchored proteins into the ER membrane. *J. Cell Sci.* **124**, 1301–7.

**Vilardi, F., Stephan, M., Clancy, A., Janshoff, A. and Schwappach, B.** (2014). WRB

and CAML are necessary and sufficient to mediate tail-anchored protein targeting to the ER membrane. *PLoS One* **9**, e85033.

**Walker, A. K. and Atkin, J. D.** (2011). Stress signaling from the endoplasmic reticulum: A central player in the pathogenesis of amyotrophic lateral sclerosis. *IUBMB Life* **63**, 754–63.

**Waterham, H. R., Koster, J., Mooyer, P., Noort Gv, G. van, Kelley, R. I., Wilcox, W. R., Wanders, R. J. A., Hennekam, R. C. M. and Oosterwijk, J. C.** (2003). Autosomal recessive HEM/Greenberg skeletal dysplasia is caused by 3 beta-hydroxysterol delta 14-reductase deficiency due to mutations in the lamin B receptor gene. *Am. J. Hum. Genet.* **72**, 1013–7.

**Weis, K.** (2003). Regulating access to the genome: Nucleocytoplasmic transport throughout the cell cycle. *Cell* **112**, 441–451.

**Wild, K., Halic, M., Sinning, I. and Beckmann, R.** (2004). SRP meets the ribosome. *Nat. Struct. Mol. Biol.* **11**, 1049–53.

**Wilkie, G. S., Korfali, N., Swanson, S. K., Malik, P., Srsen, V., Batrakou, D. G., de las Heras, J., Zuleger, N., Kerr, A. R. W., Florens, L., et al.** (2011). Several novel nuclear envelope transmembrane proteins identified in skeletal muscle have cytoskeletal associations. *Mol. Cell. Proteomics* **10**, M110.003129.

**Wolff, N., Gilquin, B., Courchay, K., Callebaut, I., Worman, H. J. and Zinn-Justin, S.** (2001). Structural analysis of emerin, an inner nuclear membrane protein mutated in X-linked Emery-Dreifuss muscular dystrophy. *FEBS Lett.* **501**, 171–6.

**Worman, H. J., Yuan, J., Blobel, G. and Georgatos, S. D.** (1988). A lamin B receptor in the nuclear envelope. *Proc. Natl. Acad. Sci. U. S. A.* **85**, 8531–4.

**Wu, W., Lin, F. and Worman, H. J.** (2002). Intracellular trafficking of MAN1, an integral protein of the nuclear envelope inner membrane. *J. Cell Sci.* **115**, 1361–71.

**Xue, M., Hou, J., Wang, L., Cheng, D., Lu, J., Zheng, L. and Xu, T.** (2017). Optimizing the fragment complementation of APEX2 for detection of specific protein-protein interactions in live cells. *Sci. Rep.* **7**, 1–8.

**Yamamoto, Y. and Sakisaka, T.** (2012). Molecular Machinery for Insertion of Tail-Anchored Membrane Proteins into the Endoplasmic Reticulum Membrane in Mammalian Cells. *Mol. Cell* **48**, 387–397.

**Yip, S.-C. S.-C., Cotteret, S. and Chernoff, J.** (2012). Sumoylated protein tyrosine phosphatase 1B localizes to the inner nuclear membrane and regulates the tyrosine phosphorylation of emerin. *J. Cell Sci.* **125**, 310–6.

**Yoshida, K. and Blobel, G.** (2001). The karyopherin Kap142p/Msn5p mediates nuclear import and nuclear export of different cargo proteins. *J. Cell Biol.* **152**, 729–40.

**Zempleni, J.** (2005). Uptake, Localization, and Noncarboxylase Roles of Biotin. *Annu.*

*Rev. Nutr.* **25**, 175–196.

**Zhao, Y. G., Liu, N., Miao, G., Chen, Y., Zhao, H. and Zhang, H.** (2018). The ER Contact Proteins VAPA/B Interact with Multiple Autophagy Proteins to Modulate Autophagosome Biogenesis. *Curr. Biol.* **28**, 1234-1245.e4.

**Zuleger, N., Kelly, D. A., Richardson, A. C., Kerr, A. R. W., Goldberg, M. W., Goryachev, A. B. and Schirmer, E. C.** (2011). System analysis shows distinct mechanisms and common principles of nuclear envelope protein dynamics. *J. Cell Biol.* **193**, 109–23.

## List of figures

## List of tables

# Appendix

**Table S 1. Perseus workflow used for RAPIDS**

| Matrix number | Process | Settings |
|---|---|---|
| 1 | Load: Generic matrix upload | • **Main Column**<br>  • Ratio H/L VAPB-fwd<br>  • Ratio H/L VAPB-rev<br>  • Ratio H/L normalized VAPB-fwd<br>  • Ratio H/L normalized VAPB-rev<br>• **Numerical columns**<br>  • Intensity VAPB-fwd<br>  • Intensity VAPB-rev<br>  • Intensity<br>  • Ratio H/L count VAPB-fwd<br>  • Ratio H/L count VAPB-rev<br>  • Razor + unique peptides<br>  • Sequence coverage (%)<br>• **Categorical columns**<br>  • Only identified by site<br>  • Reverse<br>  • Potential contaminants<br>• **Text**<br>  • Protein IDs<br>  • Majority protein IDs<br>  • Protein names<br>  • Gene names |
| 2 | Filter rows based on categorical column | • **Column** Only identified by site<br>• **Values**: +<br>• **Mode:** Remove matching rows<br>• **Filter mode:** Reduce matrix |
| 3 | Filter rows based on categorical column | • **Column:** Reverse<br>• **Values**: +<br>• **Mode:** Remove matching rows<br>• **Filter mode:** Reduce matrix |
| 4 | Filter rows based on categorical column | • **Column:** Potential contaminant<br>• **Values**: +<br>• **Mode:** Remove matching rows<br>• **Filter mode:** Reduce matrix |
| 5 | Remove empty columns | |
| 6 | Transform | • **Transformation:** log2(x)<br>• **Columns**<br>  • Ratio H/L VAPB-fwd<br>  • Ratio H/L VAPB-rev<br>  • Ratio H/L normalized VAPB-fwd<br>  • Ratio H/L normalized VAPB-rev<br>  • Intensity VAPB-fwd<br>  • Intensity VAPB-rev |
| 7 | Numeric Venn diagram | • **Columns**<br>  • Ratio H/L VAPB-fwd<br>  • Ratio H/L VAPB-rev<br>  • Ratio H/L normalized VAPB-fwd<br>  • Ratio H/L normalized VAPB-rev<br>  • Intensity VAPB-fwd<br>  • Intensity VAPB-rev |

| Matrix number | Process | Settings |
|---|---|---|
| | | • Intensity<br>• Ratio H/L count VAPB-fwd<br>• Ratio H/L count VAPB-rev<br>• Razor + unique peptides<br>• Sequence coverage (%) |
| 8 | Significance B | • **Ratio columns**<br>  • Ratio H/L VAPB-fwd<br>  • Ratio H/L VAPB-rev<br>  • Ratio H/L normalized VAPB-fwd<br>  • Ratio H/L normalized VAPB-rev<br>  • Intensity VAPB-fwd<br>  • Intensity VAPB-rev<br>  • Intensity<br>  • Ratio H/L count VAPB-fwd<br>  • Ratio H/L count VAPB-rev<br>  • Razor + unique peptides<br>• **Intensity columns**<br>  • Intensity VAPB-fwd<br>  • Intensity VAPB-rev<br>  • Intensity<br>  • Ratio H/L count VAPB-fwd<br>  • Ratio H/L count VAPB-rev<br>  • Razor + unique peptides<br>  • Sequence coverage (%)<br>  • Ratio H/L normalized VAPB-fwd Significance B<br>  • Ratio H/L normalized VAPB-rev Significance B<br>• **Side:** both<br>• **Use of truncation:** Benjamini-Hochberg FDR<br>• **Threshold value:** 0.05 |
| 9 | Result of Matrix 8 | • **Main Column**<br>  • Ratio H/L VAPB-fwd<br>  • Ratio H/L VAPB-rev<br>  • Ratio H/L normalized VAPB-fwd<br>  • Ratio H/L normalized VAPB-rev<br>• **Categorical columns**<br>  • Ratio H/L normalized VAPB-fwd Significance B: +<br>  • Ratio H/L normalized VAPB-rev Significance B: +<br>• **String columns**<br>  • Protein IDs<br>  • Majority protein IDs<br>  • Protein names<br>  • Gene names<br>• **Numerical columns**<br>  • Intensity VAPB-fwd<br>  • Intensity VAPB-rev<br>  • Intensity<br>  • Ratio H/L count VAPB-fwd<br>  • Ratio H/L count VAPB-rev<br>  • Razor + unique peptides<br>  • Sequence coverage (%)<br>  • Ratio H/L normalized VAPB-fwd Significance B<br>  • Ratio H/L normalized VAPB-rev Significance B |

| Matrix number | Process | Settings |
|---|---|---|
| 10 | Scatter plot | • **Matrix access:** Columns |
| 11 | Data for export | • **Main Column**<br>  • Ratio H/L VAPB-fwd<br>  • Ratio H/L VAPB-rev<br>  • Ratio H/L normalized VAPB-fwd<br>  • Ratio H/L normalized VAPB-rev<br>• **Categorical columns**<br>  • Ratio H/L normalized VAPB-fwd Significance B: +<br>  • Ratio H/L normalized VAPB-rev Significance B: +<br>• **String columns**<br>  • Protein IDs<br>  • Majority protein IDs<br>  • Protein names<br>  • Gene names<br>• **Numerical columns**<br>  • Intensity VAPB-fwd<br>  • Intensity VAPB-rev<br>  • Intensity<br>  • Ratio H/L count VAPB-fwd<br>  • Ratio H/L count VAPB-rev<br>  • Razor + unique peptides<br>  • Sequence coverage (%)<br>  • Ratio H/L normalized VAPB-fwd Significance B<br>  • Ratio H/L normalized VAPB-rev Significance B |

**Table S 2. List of significant proteins identified for VAPB interactome at the ER by RAPIDS**

| Gene names | Protein names | Significance B | | Normalized H/L ratio ($log_2$) | |
|---|---|---|---|---|---|
| | | forward | reverse | forward | reverse |
| RMDN3 (PTPIP51) | Regulator of microtubule dynamics protein 3 | + | + | -1.01147 | 2.06309 |
| VAPB | Vesicle-associated membrane protein-associated protein B/C | + | + | -1.19496 | 1.64432 |
| WDR44 | WD repeat-containing protein 44 | + | + | -1.36606 | 1.57231 |
| CLCC1 | Chloride channel CLIC-like protein 1 | + | + | -1.27129 | 1.40577 |
| ACBD5 | Acyl-CoA-binding domain-containing protein 5 | + | + | -1.28391 | 1.22132 |
| APOL2 | Apolipoprotein L2 | + | + | -1.31592 | 1.16131 |

| Gene names | Protein names | Significance B | | Normalized H/L ratio ($log_2$) | |
|---|---|---|---|---|---|
| | | forward | reverse | forward | reverse |
| ARID4A | AT-rich interactive domain-containing protein 4A | + | + | -1.55563 | 1.12281 |
| OSBPL9 | Oxysterol-binding protein-related protein 9 | + | + | -0.70495 | 1.01364 |
| EMD | emerin | + | + | -0.85175 | 0.960734 |
| LIFR | Leukemia inhibitory factor receptor | + | + | -0.60333 | 0.955164 |
| OSBPL8 | Oxysterol-binding protein-related protein 8;Oxysterol-binding protein | + | + | -0.63356 | 0.856866 |
| BCAP31 | B-cell receptor-associated protein 31 | + | + | -0.78066 | 0.841732 |
| ESYT1 | Extended synaptotagmin-1 | + | + | -0.74289 | 0.839315 |
| TMEM43 | Transmembrane protein 43 | + | + | -0.56211 | 0.791606 |
| RTN4 | Reticulon;Reticulon-4 | + | + | -0.62704 | 0.767316 |
| SRPR | Signal recognition particle receptor subunit alpha | + | + | -0.47854 | 0.716508 |
| SRPRB | Signal recognition particle receptor subunit beta | + | + | -0.46554 | 0.700795 |
| PTPN1 | Tyrosine-protein phosphatase non-receptor type 1;Tyrosine-protein phosphatase non-receptor type | + | | -0.64780 | 0.661111 |
| GOPC | Golgi-associated PDZ and coiled-coil motif-containing protein | + | | -0.62313 | 0.657 |
| KTN1 | Kinectin | + | | -0.56109 | 0.644318 |
| HMOX2 | Heme oxygenase 2 | + | | -0.46468 | 0.596649 |
| LMAN2 | Vesicular integral-membrane protein VIP36 | + | | -0.59374 | 0.559541 |
| SUMO1 | Small ubiquitin-related modifier 1 | + | | -0.65444 | 0.556993 |
| NUP214 | Nuclear pore complex protein Nup214 | + | | -0.59268 | 0.552377 |
| FNDC3B | Fibronectin type III domain-containing protein 3B | + | | -0.85992 | 0.528171 |
| SEC24A | Protein transport protein Sec24A | + | | -0.52932 | 0.492007 |
| RANBP2 | E3 SUMO-protein ligase RanBP2 | + | | -0.56736 | 0.489646 |

| Gene names | Protein names | Significance B | | Normalized H/L ratio ($log_2$) | |
|---|---|---|---|---|---|
| | | forward | reverse | forward | reverse |
| MCCC2 | Methylcrotonoyl-CoA carboxylase beta chain, mitochondrial | + | | -0.79596 | 0.486045 |
| YIF1A | Protein YIF1A | + | | -0.82848 | 0.480265 |
| CANX | Calnexin | + | | -0.49207 | 0.465295 |
| ACSL3 | Long-chain-fatty-acid--CoA ligase 3 | + | | -0.51638 | 0.438612 |
| ITPR1 | Inositol 1,4,5-trisphosphate receptor type 1 | + | | -0.60658 | 0.420078 |
| SCFD1 | Sec1 family domain-containing protein 1 | + | | -0.60434 | 0.365245 |
| SEC23A | Protein transport protein Sec23A | + | | -0.41730 | 0.364685 |
| SCD | Acyl-CoA desaturase | + | | -0.51764 | 0.350837 |
| ARFGEF1 | Brefeldin A-inhibited guanine nucleotide-exchange protein 1 | + | | -1.16104 | 0.305795 |
| MCCC1 | Methylcrotonoyl-CoA carboxylase subunit alpha, mitochondrial | + | | -0.45379 | 0.244156 |
| ACACA | Acetyl-CoA carboxylase 1;Biotin carboxylase | + | | -0.52797 | 0.219215 |
| ACACB | Acetyl-CoA carboxylase 2;Biotin carboxylase | + | | -0.561707 | 0.145091 |
| BOLA2;BOLA2B | BolA-like protein 2 | + | | -0.530718 | 0.135666 |
| ARHGEF16 | Rho guanine nucleotide exchange factor 16 | + | | -1.28191 | 0.003746 |
| PAFAH1B3 | Platelet-activating factor acetylhydrolase IB subunit gamma | | + | -0.139236 | 1.36866 |
| XIAP | E3 ubiquitin-protein ligase XIAP | | + | -0.379676 | 1.27029 |
| TEX2 | Testis-expressed sequence 2 protein | | + | -0.449848 | 1.09518 |
| VPS13A | Vacuolar protein sorting-associated protein 13A | | + | -0.476217 | 1.0597 |
| OSBPL11 | Oxysterol-binding protein-related protein 11 | | + | -0.754821 | 1.02638 |
| DDRGK1 | DDRGK domain-containing protein 1 | | + | -0.143452 | 0.963696 |
| YIF1B | Protein YIF1B | | + | -0.676987 | 0.959622 |
| SYNE2 | Nesprin-2 | | + | -0.586709 | 0.934705 |
| ACBD3 | Golgi resident protein GCP60 | | + | -0.546161 | 0.911193 |

| Gene names | Protein names | Significance B | | Normalized H/L ratio ($log_2$) | |
|---|---|---|---|---|---|
| | | forward | reverse | forward | reverse |
| MFF | Mitochondrial fission factor | | + | -0.405528 | 0.871134 |
| OSBP | Oxysterol-binding protein 1 | | + | -0.355922 | 0.849839 |
| MTOR | Serine/threonine-protein kinase mTOR | | + | -0.202472 | 0.844064 |
| ANKLE2 | Ankyrin repeat and LEM domain-containing protein 2 | | + | -0.253859 | 0.83552 |
| ATL2 | Atlastin-2 | | + | -0.552939 | 0.791606 |
| OSBPL10 | Oxysterol-binding protein-related protein 10;Oxysterol-binding protein | | + | -0.524417 | 0.717123 |
| SACM1L | Phosphatidylinositide phosphatase SAC1 | | + | -0.222667 | 0.700884 |
| LSG1 | Large subunit GTPase 1 homolog | | + | -0.55313 | 0.690819 |
| SEC22B | Vesicle-trafficking protein SEC22b | | + | -0.3531 | 0.638862 |

**Table S 3. List of significant proteins identified for VAPB interactome at the INM by RAPIDS**

| Gene names | Protein names | Significance B | | Normalized H/L ratio ($log_2$) | |
|---|---|---|---|---|---|
| | | forward | reverse | forward | reverse |
| LMNB1 | Lamin-B1 | + | + | -1.5373 | 2.51293 |
| LMNB2 | Lamin-B2 | + | + | -1.9259 | 2.05581 |
| EMD | emerin | + | + | -1.10786 | 1.80553 |
| TOR1AIP1 | Torsin-1A-interacting protein 1 | + | + | -1.28535 | 1.72250 |
| NUP153 | Nuclear pore complex protein Nup153 | + | + | -0.89241 | 1.63987 |
| VAPB | Vesicle-associated membrane protein-associated protein B/C | + | + | -0.63206 | 1.59211 |
| LMNA | Prelamin-A/C;Lamin-A/C | + | + | -1.37097 | 1.59287 |
| AHCTF1 | Protein ELYS | + | + | -0.94652 | 1.56944 |
| TPR | Nucleoprotein TPR | + | + | -0.74460 | 1.12994 |
| TMPO | Lamina-associated polypeptide 2, isoforms beta/gamma;Thymopoi | + | + | -1.37759 | 1.35867 |

| Gene names | Protein names | Significance B | | Normalized H/L ratio ($log_2$) | |
|---|---|---|---|---|---|
| | | forward | reverse | forward | reverse |
| | etin; Thymopentin | | | | |
| APOL2 | Apolipoprotein L2 | + | | -1.32257 | 0.71061 |
| ARHA;RHOA | Transforming protein RhoA | + | | -1.30375 | 0.25398 |
| CYB5R3 | NADH-cytochrome b5 reductase; NADH-cytochrome b5 reductase 3;NADH-cytochrome b5 reductase 3 membrane-bound form;NADH-cytochrome b5 reductase 3 soluble form | + | | -0.89676 | 0.42492 |
| LAMP1 | Lysosome-associated membrane glycoprotein 1 | + | | | |
| MAD1L1 | Mitotic spindle assembly checkpoint protein MAD1 | + | | -1.20619 | 0.81434 |
| LMAN2 | Vesicular integral-membrane protein VIP36 | + | | -1.08079 | 0.44180 |
| SEC22B | Vesicle-trafficking protein SEC22b | + | | -0.68214 | 0.93997 |
| ITGB1 | Integrin beta-1 | + | | -0.75348 | 0.55070 |
| CANX | Calnexin | + | | -1.055950 | 0.60928 |
| TMX1;TXNDC | Thioredoxin-related transmembrane protein 1 | + | | -1.065883 | 1.38620 |
| RINT1 | RAD50-interacting protein 1 | | + | -0.430159 | 1.55768 |
| MTOR;FRAP1 | Serine/threonine-protein kinase mTOR | | + | -0.142194 | 2.144731 |

## Abbrevations

| | |
|---|---|
| amp | ampicillin |
| Arg | arginine |
| ATP | adenosine 5’-triphosphate |
| bp | base pair |
| $CaCl_2$ | calcium chloride |
| DAPI | 4’,6-diamino-2-phenylindole |
| DMEM | Dulbecco’s modified eagle medium |
| DMSO | dimethyl sulfoxide |
| DNA | deoxyribonucleic acid |
| dNTP | deoxyribonucleotide triphosphate |
| EDTA | ethylenediaminetetraacetic acid |
| EM | electron microscopy |
| FBS | fetal bovine serum |
| fwd | forward |
| GFP | red fluorescent protein |
| Glu | glutamine |
| GST | glutathione S-transferase |
| GTP | guanosine-5’-triphosphate |
| $H_2O_2$ | hydrogen peroxide |
| HA | hemagglutinin |
| HCl | hydrochloric acid |
| HEPES | 4-(2-hydroxyethyl)-1-piperazineethanesulfonic acid |
| His | histidine |
| HRP | horseradish peroxidase |
| IP | immune precipitation |
| kan | kanamycin |
| kb | kilo base pair |
| kDa | kilo dalton |
| LB | Luria Bertani |
| LC | liquid chromatography |
| Lys | lysine |
| M | molar |
| m/z | mass-to-charge ratio |
| MBP | maltose binding protein |

| | |
|---|---|
| mM | milli molar |
| MS | mass spectrometry |
| MWCO | molecular weight cut-off |
| NC | nitrocellulose |
| nm | nano meter |
| nM | nano molar |
| P | proline |
| PBS | phosphate buffered saline |
| PMSF | phenylmethylsulphonyl fluoride |
| Ran | Ras-related nuclear protein |
| rev | reverse |
| RIPA | radioimmunoprecipitation assay buffer |
| RNA | ribonucleic acid |
| rpm | revolutions per minute |
| S | serine |
| SDS | sodium dodecyl sulfate |
| siRNA | small interfering RNA |
| SOC | super optimal broth |
| TAE | Tris/ Acetate/ EDTA |
| tev | TEV-protease cleavage site |
| Triton X-100 | 4-oxyphenol polythoxylate |
| Tween 20 | polyoxyethylene (20) sorbitan monolaurate |
| U | unit |
| UV | ultraviolet |
| V | volt |
| w/v | weight per volume |
| ZZ | protein tag (*S. aureus* protein A IgG-binding domain) |